

UNCLASSIFIED

COASTAL ENGINEERING RESEARCH CENTER FORT BELVOIR VA F/G 8/8
COMPARISON OF NUMERICAL AND PHYSICAL HYDRAULIC MODELS, MASONBOR--ETC(U)
JUN 77 D L HARRIS, B R BODINE
CERC-GITI-6 NL

NL

1 OF 3
AD
A052795



AD A 052795

Comparison of Numerical and Physical Hydraulic Models, Masonboro Inlet, North Carolina

by

D. Lee Harris and B.R. Bodine

GITI REPORT 6



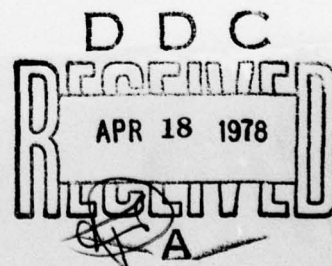
June 1977

GENERAL INVESTIGATION OF TIDAL INLETS

A Program of Research Conducted Jointly by
U.S. Army Coastal Engineering Research Center, Fort Belvoir, Virginia
U.S. Army Engineer Waterways Experiment Station, Vicksburg, Mississippi

Department of the Army
Corps of Engineers

APPROVED FOR PUBLIC RELEASE; DISTRIBUTION UNLIMITED



DDC FILE COPY

Reprint or republication of any of this material shall give appropriate credit to the U.S. Army Coastal Engineering Research Center.

Limited free distribution within the United States of single copies of this publication has been made by this Center. Additional copies are available from:

*National Technical Information Service
ATTN: Operations Division
5285 Port Royal Road
Springfield, Virginia 22151*

The findings in this report are not to be construed as an official Department of the Army position unless so designated by other authorized documents.

Cover Photo: Masonboro Inlet, North Carolina, 24 July 1974

UNCLASSIFIED

SECURITY CLASSIFICATION OF THIS PAGE (When Data Entered)

REPORT DOCUMENTATION PAGE		READ INSTRUCTIONS BEFORE COMPLETING FORM
1. REPORT NUMBER GITI Report 6	2. GOVT ACCESSION NO.	3. RECIPIENT'S CATALOG NUMBER
4. TITLE (and Subtitle) COMPARISON OF NUMERICAL AND PHYSICAL HYDRAULIC MODELS, MASONBORO INLET, NORTH CAROLINA		5. TYPE OF REPORT & PERIOD COVERED Final Report
7. AUTHOR(s) D. Lee Harris B.R. Bodine		6. PERFORMING ORG. REPORT NUMBER
9. PERFORMING ORGANIZATION NAME AND ADDRESS Department of the Army Coastal Engineering Research Center (CERRE-CO) Kingman Building, Fort Belvoir, VA 22060		8. CONTRACT OR GRANT NUMBER(s) CERC-GITI-6
11. CONTROLLING OFFICE NAME AND ADDRESS Department of the Army Coastal Engineering Research Center Kingman Building, Fort Belvoir, VA 22060		10. PROGRAM ELEMENT, PROJECT, TASK AREA & WORK UNIT NUMBERS F31019
14. MONITORING AGENCY NAME & ADDRESS (if different from Controlling Office) 12 198 p.		12. REPORT DATE Jun 77
		13. NUMBER OF PAGES 195
		15. SECURITY CLASS. (of this report) UNCLASSIFIED
		15a. DECLASSIFICATION/DOWNGRADING SCHEDULE
16. DISTRIBUTION STATEMENT (of this Report) Approved for public release; distribution unlimited.		
17. DISTRIBUTION STATEMENT (of the abstract entered in Block 20, if different from Report)		
18. SUPPLEMENTARY NOTES This report has four appendices, published as four separate volumes.		
19. KEY WORDS (Continue on reverse side if necessary and identify by block number) Masonboro Inlet, N.C. Numerical and physical hydraulic models Tidal inlets		
20. ABSTRACT (Continue on reverse side if necessary and identify by block number) Four models of Masonboro Inlet, North Carolina, have been developed in a program for assessing the value of models in investigating coastal inlet hydraulics problems. A distorted scale, fixed-bed physical model, a lumped parameter numerical model, and two two-dimensional numerical models were included in the study. → next page (continued)		

DD FORM 1 JAN 73 1473

EDITION OF 1 NOV 65 IS OBSOLETE

UNCLASSIFIED

SECURITY CLASSIFICATION OF THIS PAGE (When Data Entered)

037 050

mt

UNCLASSIFIED

SECURITY CLASSIFICATION OF THIS PAGE(When Data Entered)

cont. → Hydrodynamic equations which describe the two-dimensional flow in tidal inlets are developed in an appendix to this report. The Navier-Stokes equations are integrated vertically and time-averaged to form the governing equations for two-dimensional flow. This procedure eliminates a great deal of unnecessary detail about small-scale motions but retains terms descriptive of the interactions between small- and large-scale flow.

Equations are used to investigate the correspondence between model flows. This analysis shows that it should be possible to simulate the major aspects of tidal flow about equally well with either physical or numerical models, that physical models should be most useful for investigating the interaction of the flow of primary importance with boundary conditions or with flows of smaller scale, and that numerical models should be most useful for investigating the interaction between the flow of primary importance and larger scale or external phenomena such as the effects of storms and of the earth's rotation. The assumptions employed in the derivation of the equations used with the lumped parameter model were found to be more restrictive in applications than originally supposed. New equations are presented which display these assumptions more clearly.

→ A comparison of experimental results obtained with a physical model and calculations made with numerical models with the prototype records shows that, in general, the models simulate tidal height more satisfactorily than tidal current. Results obtained with one of the two-dimensional numerical models were much inferior to the results obtained with the other. The basic design of both two-dimensional numerical models was similar, but there were many subtle differences, indicating that a clear understanding of the modeling process is essential to success in modeling tidal flows. ↗

FOREWORD

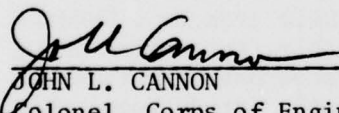
This report, prepared by the Coastal Engineering Research Center (CERC) as one in a series of reports on the Corps of Engineers' General Investigation of Tidal Inlets (GITI), concerns the evaluation of physical and numerical models of a tidal inlet performed as part of the inlet hydraulics study of the GITI. The GITI research program is under the technical surveillance of CERC and is conducted by CERC, the U.S. Army Engineer Waterways Experiment Station (WES), other Government agencies, and by private organizations.

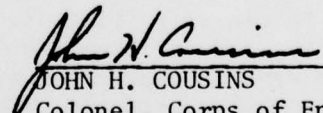
The report was prepared by D. Lee Harris and B.R. Bodine (formerly of CERC), Oceanography Branch, Research Division, CERC. C. Mason, under the general supervision of R.M. Sorensen, is responsible for CERC technical direction of the GITI. Dean Morrough P. O'Brien, Professors Robert G. Dean, Robert L. Wiegel, and Arthur T. Ippen (former member, deceased) of the Coastal Engineering Research Board were involved in the planning or review of this report.

Technical Directors of CERC and WES were T. Saville, Jr., and F.R. Brown, respectively.

Comments on this publication are invited.

Approved for publication in accordance with Public Law 166, 79th Congress, approved 31 July 1945, as supplemented by Public Law 172, 88th Congress, approved 7 November 1963.


JOHN L. CANNON
Colonel, Corps of Engineers
Commander and Director
Waterways Experiment Station


JOHN H. COUSINS
Colonel, Corps of Engineers
Commander and Director
Coastal Engineering Research Center

ACCESS: <input type="checkbox"/> 10	
NTIS	White Section <input checked="" type="checkbox"/>
DOC	Buff Section <input type="checkbox"/>
UNANNOUNCED	<input type="checkbox"/>
JUSTIFICATION	
BY	
DISTRIBUTION/AVAILABILITY CODES	
Dist.	AVAIL. AND/OR SPECIAL
A	

PREFACE

1. The Corps of Engineers, through its Civil Works program, has sponsored, over the past 23 years, research into the behavior and characteristics of tidal inlets. The Corps' interest in tidal inlet research stems from its responsibilities for navigation, beach erosion prevention and control, and flood control. Tasked with the creation and maintenance of navigable U.S. waterways, the Corps dredges millions of cubic yards of material each year from tidal inlets that connect the ocean with bays, estuaries, and lagoons. Design and construction of navigation improvements to existing tidal inlets are an important part of the work of many Corps' offices. In some cases, design and construction of new inlets are required. Development of information concerning the hydraulic characteristics of inlets is important not only for navigation and inlet stability, but also because inlets, by allowing for the ingress of storm surges and egress of flood waters, play an important role in the flushing of bays and lagoons.

2. A research program, the General Investigation of Tidal Inlets (GITI), was developed to provide quantitative data for use in design of inlets and inlet improvements. It is designed to meet the following objectives:

To determine the effects of wave action, tidal flow, and related phenomena on inlet stability and on the hydraulic, geometric, and sedimentary characteristics of tidal inlets; to develop the knowledge necessary to design effective navigation improvements, new inlets, and sand transfer systems at existing tidal inlets; to evaluate the water transfer and flushing capability of tidal inlets; and to define the processes controlling inlet stability.

3. The GITI is divided into three major study areas: (a) inlet classification, (b) inlet hydraulics, and (c) inlet dynamics.

a. Inlet Classification. The objectives of the inlet classification study are to classify inlets according to their geometry, hydraulics, and stability, and to determine the relationships that exist among the geometric and dynamic characteristics and the environmental factors that control these characteristics. The classification study keeps the general investigation closely related to real inlets and produces an important inlet data base useful in documenting the characteristics of inlets.

b. Inlet Hydraulics. The objectives of the inlet hydraulics study are to define tide-generated flow regime and water level fluctuations in the vicinity of coastal inlets and to develop techniques for predicting these phenomena. The inlet hydraulics study is divided into three areas: (1) idealized inlet model study, (2) evaluation of state-of-the-art physical and numerical models, and (3) prototype inlet hydraulics.

(1) The Idealized Inlet Model. The objectives of this model study are to determine the effect of inlet configurations and structures on discharge, head loss and velocity distribution for a number of realistic inlet shapes and tide conditions. An initial set of tests in a trapezoidal inlet was conducted between 1967 and 1970. However, in order that subsequent inlet models are more representative of real inlets, a number of "idealized" models representing various inlet morphological classes are being developed and tested. The effects of jetties and wave action on the hydraulics are included in the study.

(2) Evaluation of State-of-the-Art Modeling Techniques. The objectives of this part of the inlet hydraulics study are to determine the usefulness and reliability of existing physical and numerical modeling techniques in predicting the hydraulic characteristics of inlet-bay systems, and to determine whether simple tests, performed rapidly and economically, are useful in the evaluation of proposed inlet improvements. Masonboro Inlet, North Carolina, was selected as the prototype inlet which would be used along with hydraulic and numerical models in the evaluation of existing techniques. In September 1969 a complete set of hydraulic and bathymetric data was collected at Masonboro Inlet. Construction of the fixed-bed physical model was initiated in 1969, and extensive tests have been performed since then. In addition, three existing numerical models were applied to predict the inlet's hydraulics. Extensive field data were collected at Masonboro Inlet in August 1974 for use in evaluating the capabilities of the physical and numerical models.

(3) Prototype Inlet Hydraulics. Field studies at a number of inlets are providing information on prototype inlet-bay tidal hydraulic relationships and the effects of friction, waves, tides, and inlet morphology on these relationships.

c. Inlet Dynamics. The basic objective of the inlet dynamics study is to investigate the interactions of tidal flow, inlet configuration, and wave action at tidal inlets as a guide to improvement of inlet channels and nearby shore protection works. The study is subdivided into four specific areas: (1) model materials evaluation, (2) movable-bed modeling evaluation, (3) reanalysis of a previous inlet model study, and (4) prototype inlet studies.

(1) Model Materials Evaluation. This evaluation was initiated in 1969 to provide data on the response of movable-bed model materials to waves and flow to allow selection of the optimum bed materials for inlet models.

(2) Movable-Bed Model Evaluation. The objective of this study is to evaluate the state-of-the-art of modeling techniques, in this case movable-bed inlet modeling. Since, in many cases, movable-bed modeling is the only tool available for predicting the response of an inlet to improvements, the capabilities and limitations of these models must be established.

(3) Reanalysis of an Earlier Inlet Model Study. In 1955, a report entitled, "Preliminary Report: Laboratory Study of the Effect of an Uncontrolled Inlet on the Adjacent Beach," was published by the Beach Erosion Board (now CERC). A reanalysis of the original data is being performed to aid in planning of additional GITI efforts.

(4) Prototype Dynamics. Field and office studies of a number of inlets are providing information on the effects of physical forces and artificial improvements on inlet morphology. Of particular importance are studies to define the mechanisms of natural sand bypassing at inlets, the response of inlet navigation channels to dredging and natural forces, and the effects of inlets on adjacent beaches.

4. This report was directed toward the evaluation of the state-of-the-art of numerical and physical models and modeling techniques for tidal inlets. However, technology advanced so rapidly during the study period and the review process that a current state-of-the-art report did not result. Nevertheless, this report is believed a significant contribution toward the evaluation of current modeling techniques and will be useful to coastal engineers for several years. The evaluation was conducted by calibrating a physical model and three numerical models with data from the prototype. Since no verification data were available from the prototype, the models were not verified. However, the models were all applied to significantly different inlet hydrographic conditions and the results of the numerical models are compared with those of the physical model.

5. As an aid in model comparison and evaluation, the two-dimensional equations of motion which govern tidal flows in inlets (and many similar phenomena) are systematically derived from the Navier-Stokes equations. This mode of derivation provides a clear indication of the processes often neglected in the study of tidal flows.

6. Reports on each of the four models involved are published as separate appendixes to this report. A later report will present a comparison of new prototype observations with predictions of the physical model, and of the best numerical model for prototype conditions not used in model calibration.

CONTENTS

	Page
CONVERSION FACTORS, U.S. CUSTOMARY TO METRIC (SI)	11
SYMBOLS AND DEFINITIONS	12
I INTRODUCTION.	21
1. Historical Perspective	21
2. Types of Models.	23
3. Purpose and Scope of Hydraulic Inlet Studies	24
4. Preview of the Report.	25
II MATHEMATICAL DESCRIPTION OF TIDAL FLOWS	27
1. General.	27
2. Motions of Tidal Scale	28
3. Interpretation of the Principal Terms.	30
4. The Perturbation Terms	36
5. The Radiation Stresses	37
6. Other Secondary Terms.	38
7. Boundary Conditions.	40
III MODELING TIDAL FLOWS: PHYSICAL MODELS	40
1. General.	40
2. Physical Models for Quasi-Horizontal Flow.	41
3. Physical Models, Perturbation, and Viscous Phenomena	45
4. Boundary Conditions.	49
IV MODELING TIDAL INLETS: NUMERICAL MODELS	50
1. General.	50
2. Explicit Prediction Models	52
V A LUMPED PARAMETER MODEL.	66
1. General.	66
2. The Keulegan Lumped Parameter Model.	71
3. A Rigorous Derivation.	73
4. Summary.	84
VI MODEL CALIBRATION	84
VII COMPARISON OF MODEL RESULTS	88
1. Calibration of Models.	88
2. Comparison of Results.	90
3. Application of the Models.	115
4. Later Studies.	119
5. The Cost Factor.	143
VIII SUMMARY, CONCLUSIONS, AND RECOMMENDATIONS	143
1. Summary.	143
2. Conclusions.	145
3. Recommendations.	145
LITERATURE CITED.	147

CONTENTS--Continued

	Page
APPENDIX	
A REQUEST FOR PROPOSALS--TIDAL CALCULATIONS FOR MASONBORO INLET, N.C.	153
B A DERIVATION OF THE LONG WAVE EQUATIONS	176
C DERIVATION OF THE ONE-DIMENSIONAL OR CHANNEL EQUATIONS. .	191
TABLES	
1 Typical Inlet Parameters.	77
2 Statistical Comparison of Velocity Data	116
FIGURES	
1 Locations of tide and current observations, Masonboro Inlet . .	22
2 An example of aliasing.	55
3 Gradient of water surface over channel.	68
4 Prototype tidal data at gage 0.	89
5 Observed and predicted tides at gage 1.	91
6 Observed and predicted tides at gage 2.	92
7 Observed and predicted tides at gage 3.	93
8 Observed and predicted tides at gage 4.	94
9 Observed and predicted tides at gage 5.	95
10 Observed and predicted tides at gage 6.	96
11 Observed and predicted tides for embayment area	97
12 Prototype and predicted velocity at range 1, station N.	98
13 Prototype and predicted velocity at range 1, station C.	99
14 Prototype and predicted velocity at range 1, station S.	100
15 Prototype and predicted velocity at range 2, station N.	101
16 Prototype and predicted velocity at range 2, station C.	102
17 Prototype and predicted velocity at range 2, station S.	103

CONTENTS

FIGURES--Continued

	Page
18 Prototype and predicted velocity at range 3, station N.	104
19 Prototype and predicted velocity at range 3, station C.	105
20 Prototype and predicted velocity at range 3, station S.	106
21 Prototype and predicted velocity at range 4, station W.	107
22 Prototype and predicted velocity at range 4, station C.	108
23 Prototype and predicted velocity at range 4, station E.	109
24 Prototype and predicted velocity at range 5, station E.	110
25 Prototype and predicted velocity at range 5, station C.	111
26 Prototype and predicted velocity at range 5, station W.	112
27 Prototype and predicted mean velocity in throat of Masonboro Inlet	114
28 Mean and spring tides at Masonboro Inlet.	117
29 Hydrographic survey for Masonboro Inlet	118
30 Prejetty mean tide condition at gage 1.	120
31 Prejetty mean tide condition at gage 2.	121
32 Prejetty mean tide condition at gage 3.	122
33 Prejetty mean tide condition at gage 4.	123
34 Prejetty mean tide condition at gage 5.	124
35 Prejetty mean tide condition at gage 6.	125
36 Prejetty mean tide condition of tide in embayment area.	126
37 Tidal current velocities for prejetty and mean tide conditions at station 1N.	127
38 Tidal current velocities for prejetty and mean tide conditions at station 1C.	128
39 Tidal current velocities for prejetty and mean tide conditions at station 1S.	129

CONTENTS

FIGURES--Continued

	Page
40 Tidal current velocities for prejetty and mean tide conditions at station 2N.	130
41 Tidal current velocities for prejetty and mean tide conditions at station 2C.	131
42 Tidal current velocities for prejetty and mean tide conditions at station 2S.	132
43 Tidal current velocities for prejetty and mean tide conditions at station 3N.	133
44 Tidal current velocities for prejetty and mean tide conditions at station 3C.	134
45 Tidal current velocities for prejetty and mean tide conditions at station 3S.	135
46 Tidal current velocities for prejetty and mean tide conditions at station 4E.	136
47 Tidal current velocities for prejetty and mean tide conditions at station 4C.	137
48 Tidal current velocities for prejetty and mean tide conditions at station 4W.	138
49 Tidal current velocities for prejetty and mean tide conditions at station 5E.	139
50 Tidal current velocities for prejetty and mean tide conditions at station 5C.	140
51 Tidal current velocities for prejetty and mean tide conditions at station 5W.	141
52 Mean velocity in inlet throat, preproject condition	142

CONVERSION FACTORS, U.S. CUSTOMARY TO METRIC (SI)
UNITS OF MEASUREMENT

U.S. customary units of measurement used in this report can be converted to metric (SI) units as follows:

Multiply	by	To obtain
inches	25.4	millimeters
	2.54	centimeters
square inches	6.452	square centimeters
cubic inches	16.39	cubic centimeters
feet	30.39	centimeters
	0.3048	meters
square feet	0.0929	square meters
cubic feet	0.0283	cubic meters
yards	0.9144	meters
square yards	0.836	square meters
cubic yards	0.7646	cubic meters
miles	1.6093	kilometers
square miles	259.0	hectares
knots	1.8532	kilometers per hour
acres	0.4047	hectares
foot-pounds	1.3558	newton meters
millibars	1.0197×10^{-3}	kilograms per square centimeter
ounces	28.35	grams
pounds	453.6	grams
	0.4536	kilograms
ton, long	1.0160	metric tons
ton, short	0.9072	metric tons
degrees (angle)	0.1745	radians
Fahrenheit degrees	5/9	Celsius degrees or Kelvins ¹

¹To obtain Celsius (C) temperature readings from Fahrenheit (F) readings, use formula: $C = (5/9) (F - 32)$.

To obtain Kelvin (K) readings, use formula: $K = (5/9) (F - 32) + 273.15$.

SYMBOLS AND DEFINITIONS

A	amplitude of a sinusoidal wave
A	arbitrary grid point
A	$A(x,t) = \int_{y^1}^{y^2} D \, dy$, the cross section of an inlet channel (Sec. V)
A_B	cross-sectional area of an inlet at its junction with a bay or lagoon
A_{Bay}	area of the bay connected to the ocean by an inlet
A_c	$A_c(x,t)$, cross-sectional area of an inlet
A_n	amplitude of the n'th sinusoidal term in a Fourier expansion
A_n	cross section of the n'th inlet subchannel (Sec. V)
A_S	cross section of an inlet at its junction with the sea (Sec. V)
$A_{xx}, A_{xy}, A_{yx}, A_{yy}$	turbulent mixing coefficients in a horizontal plane
\bar{A}	$\bar{A} = \frac{1}{g(\bar{h}_B - \bar{h}_S)} \int_{x_S}^{x_B} g A \frac{\partial \bar{h}}{\partial x}$, an area characterizing an inlet
a, b, c	coefficients of the quadratic equation in standard form (Sec. V)
a_n	coefficient of the cosine term of the n'th harmonic in a Fourier expansion
B	a second arbitrary grid point
B	as a subscript, indicates that the primary variable pertains to the bay
B_n	amplitude of the n'th sinusoidal term in a second Fourier expansion
b	$b(x,t) = y_2 - y_1$, width of inlet at water surface
b_m	width of the m'th subchannel in an inlet

SYMBOLS AND DEFINITIONS--Continued

b_n	coefficient of the sine term of the n'th harmonic in a Fourier expansion
c	phase velocity of a wave
c_{max}	maximum phase velocity of a wave
D	$D(x,y,z,t)$, total depth of fluid layer
D_m	D applied to the model (Sec. III)
D_m	depth of the m'th subchannel in an inlet (Sec. V)
D_{max}	maximum value of the total depth
D_{min}	minimum value of the depth
D_p	D applied to prototype
\bar{D}	cross-section average value of D
D^*	dimensionless form of D
D'	$D - \bar{D}$
F	arbitrary function
f	$2\Omega \sin \phi$, Coriolis parameter
f_2	$2\Omega \cos \phi$, second Coriolis parameter
g	acceleration of gravity
H_b	height of the barometer column
h	$h(x,y,t)$, elevation of top of a fluid layer, usually the water surface
h	as a subscript, indicates that the variable is evaluated at the free surface of the water
h_p	h applied to the prototype
h_1	mean elevation of the water surface over a period much longer than that used in defining \bar{h} ; h_1 is generally interpreted as mean sea level
\bar{h}	mean value of h over a few wave periods
\bar{h}	as a subscript, indicates that the function is evaluated at the mean position of the free surface

SYMBOLS AND DEFINITIONS--Continued

\bar{h}'	$\bar{h} - \bar{\bar{h}}$
\bar{h}'	$\bar{h}'(x,y,t) = \bar{h} - \bar{\bar{h}}$, deviation of water surface elevation from the cross-channel average
$\bar{\bar{h}}$	$\bar{\bar{h}}(x,t) = b^{-1} \int_{y_1}^{y_2} \bar{h} dy$, average value of h across an inlet channel
$\bar{\bar{h}}_B, \bar{\bar{h}}_S$	values of $\bar{\bar{h}}$ at bay and seaward ends of an inlet
h^*	dimensionless form of h
\tilde{h}	the contribution of waves to the elevation of the water surface
i	$\sqrt{-1}$
j	arbitrary integer
K	dimensionless friction coefficient
K_e	Keulegan's coefficient of repletion
K_{HW}	Keulegan's (1967) coefficient of repletion as defined by Huval and Wintergerst (1977)
K_m	the value of K that applies to the model
K_n	friction coefficient of the n 'th subchannel in an inlet
K_p	value of K that applies to the prototype
L	length of a gravity wave or other disturbance
L_I	length of inlet
M	maximum value of m , when m is used as a running index
m	coefficient of inertia term in Keulegan's inlet equations (Sec. V)
m	a subscript indicating a running index (Sec. V)
m	a subscript to indicate that the primary variable applies to a model (Sec. III)
N	maximum value of n in summation
n	distance along a wave crest (Sec. III)

SYMBOLS AND DEFINITIONS--Continued

n	Manning's n , a dimensionless resistance coefficient
n	running index in summations
n	as a subscript indicates that the primary variable pertains to the prototype
n'	second running index
p	$p(x,y,z,t)$, pressure
p_h	pressure at the top of a fluid layer
p_z	pressure at the bottom of a fluid layer
\bar{p}	average value of p over a small volume on a time duration of a few wave periods
\bar{p}_n	time-mean pressure at the free surface of the fluid
p'	contribution of the perturbation pressure to p
\tilde{p}	contribution of wave motion to p
Q	$\bar{u}A$, inlet discharge in a one-dimensional flow
Q	$(U^2 + V^2)^{1/2}$, transport magnitude in a vertical column having unit cross-sectional area in two-dimensional flow
Q_n	discharge in the n 'th subchannel
q	horizontal velocity in the direction of s
q_{in}	flow into bay which does not pass through inlet (Sec. V)
\bar{q}_o	time-mean velocity at the outer edge of the viscous sublayer (Sec. II)
$\bar{\bar{q}}_o$	time-mean vertically averaged current velocity (Sec. II)
\tilde{q}	contribution of waves to q
\tilde{q}_z	\tilde{q} at $z = \bar{z}$
R	rainfall rate; specifically, the net excess of rainfall, runoff and bottom seepage into the basin over evaporation, and bottom seepage out of the basin
RMSD	standard deviation of prototype measurements (eq. 112)

SYMBOLS AND DEFINITIONS--Continued

RMSΔ	root-mean-square difference between two measurements (eq. 111)
R_c	closure term for the one-dimensional channel equations defined by equation (74) in Section V
R_e	v/f , radius of the inertial circle
S	as a subscript, indicates that the primary variable is to be evaluated at $x = x_s$, the inlet end nearest the sea
S_{xo}, S_{yo}	closure terms for the two-dimensional momentum equations, other than $S_{xt}, S_{yt}, S_{xv}, S_{yv}, S_{xw},$ or S_{yw}
S_{xt}, S_{yt}	closure terms representing molecular and turbulent stresses in two-dimensional momentum equations
S_{xv}, S_{yv}	closure terms arising from vertical integration for the two-dimensional momentum equations
S_{xw}, S_{yw}	closure terms arising from surface waves for the two-dimensional momentum equations
$S_{xx}, S_{xy}, S_{yx}, S_{yy}$	components of the Reynolds stress tensor due to waves (eqs. 16, 17, and 18)
s	arbitrary horizontal direction
s	distance in the direction of wave propagation
s_1	slip coefficient in the Jelesnianski (1967) bottom friction law
T	period of gravity wave; may be surface wave or tide wave
t	time
t_m	t applied to the model
t_p	t applied to the prototype
t^*	dimensionless form of t
U	$U(x,y,t) = \int_z^{\bar{h}} u dz$, transport parallel to the x -axis in a vertical column having unit cross-sectional area
U_m	U applied to the model
U_p	U applied to the prototype

SYMBOLS AND DEFINITIONS--Continued

U^*	dimensionless form of U
u, v, w	components of the total velocity parallel to the x-, y-, and z-axes
$\bar{u}, \bar{v}, \bar{w}$	elementary averages of the velocity components parallel to the x-, y-, and z-axes
u', v', w'	part of the velocity components due to turbulence
$\tilde{u}, \tilde{v}, \tilde{w}$	part of the velocity components due to surface waves
u_h, v_h	horizontal velocity components evaluated at $z = h$
\bar{u}_h, \bar{v}_h	horizontal velocity components evaluated at $z = \bar{h}$
u_Z, v_Z	horizontal velocity components evaluated at $z = Z$
\bar{u}	$\bar{u}(x,t) = A_C^{-1} \int_{y_1}^{y_2} U \, dy$, mean value of u in an inlet cross section
\bar{u}_B, \bar{u}_S	mean horizontal velocity along the inlet axis at bay and seaward ends of inlet
\bar{u}_n	mean velocity in the n'th subchannel of an inlet
u''	$u''(x,y,z,t) = u(x,y,z,t) - \bar{u}(x,t)$
u'', v''	departures of the horizontal velocity components from the vertically average values
V	$V(x,y,t) = \int_Z^{\bar{h}} v \, dz$, transport parallel to the y-axis in a vertical column having unit cross-sectional area
V_{Bay}	volume of bay
V_I	$V_I' = \int_0^t \int_{x_S}^{x_B} \int_{y_1}^{y_2} (R + E) \, dy \, dx \, (eq. 85)$
V_m	V applied to the model
V_p	V applied to the prototype
V^*	dimensionless form of V

SYMBOLS AND DEFINITIONS--Continued

V_I^I	volume of inlet
v	horizontal velocity in arbitrary direction
v_m	wind velocity for the model
v_p	wind velocity for the prototype
\bar{v}	$\bar{v}(x,t) = A_C^{-1} \int_{y_1}^{y_2} v \, dy$, mean value of v in an inlet cross section, negligibly small in most cases
w_h	vertical velocity at top of fluid layer (App. B, eq. B15)
w_Z	vertical velocity at bottom of fluid layer (App. B, eq. B14)
w_z	vertical velocity due to waves at an arbitrary value of z
w_h^I	vertical velocity at the free surface as a result of turbulence
X	arbitrary statistical function
x, y, z	principal axes in a right-handed coordinate system; z is positive upward
x_B, x_S	value of x at the bay (ocean) end of an inlet
x_m, y_m, z_m	x, y, z applied to model
x_p, y_p, z_p	x, y, z applied to prototype
x^*, y^*, z^*	dimensionless forms of x, y, z
Y	second arbitrary statistical function
y_1, y_2	values of y at opposite ends of an inlet cross section
Z	$Z(x,y,t)$, elevation of the bottom of a fluid layer
Z	as a subscript, Z indicates that the primary variable should be evaluated at $z = Z$
z_1	arbitrary value of $z < h_1$

SYMBOLS AND DEFINITIONS--Continued

α	α_m/α_p , horizontal scale ratio
α_m	dimensional factor for the horizontal dimension in a model
α_p	dimensional factor for the horizontal dimension in the prototype
α_1	arbitrary exponent
β	β_m/β_p , vertical scale ratio
β_m	dimensional factor for the vertical dimension in the model
β_p	dimensional factor for the vertical dimension in the prototype
γ	$\gamma = +1$ indicates floodtide; $\gamma = -1$ indicates ebbtide (Sec. V)
γ_m	dimensional factor for time in the model
γ_p	dimensional factor for time in the prototype
Δh	increment in height
Δs	increment of horizontal distance in any direction
Δt	increment of time
Δx	increment of distance along x-axis
δ	thickness of the viscous sublayer
η	a value of z , $\bar{h} \leq \eta \leq h$, used in an application of the mean value theorem of integral calculus
θ	arbitrary angle
θ	direction of a wave ray
θ_n	phase angle in a Fourier expansion
λ	horizontal length of an underwater slope, used only in the discussion of physical models
μ	coefficient of dynamic molecular viscosity
ν	μ/ρ , coefficient for kinematic viscosity
ν	effective viscosity coefficient in the Jelesnianski (1967) friction model

SYMBOLS AND DEFINITIONS--Continued

π	3.14159
ρ	fluid density
ρ''	$\rho'' = \rho - \bar{\rho}$
$\bar{\rho}$	$\bar{\rho} = (\bar{h} - D)^{-1} \int_Z^{\bar{h}} \rho \, dz$
$\tau_{xx}, \tau_{yx}, \tau_{zx}, \tau_{xy}, \tau_{yy}, \tau_{zy}, \tau_{xz}, \tau_{yz}, \tau_{zz}$	components of the stress tensor. The first subscript indicates the face of an elementary cube on which the stress acts; the second subscript indicates the direction in which the stress acts
$(\tau_{xx})_Z, (\tau_{zy})_Z$	stresses in a h_D at the bottom of a fluid layer parallel to the x- and y-axes
$(\tau_{xx})_h, (\tau_{zy})_h$	stresses in a horizontal plane at the upper boundary of a fluid layer parallel to the x- and y-axes
$(\bar{\tau}_{xx})_Z$	mean bottom stress at an inlet cross section
ϕ	latitude
ϕ_n	phase angle for a second Fourier expression
Ψ	angle between the x-axis and the east direction
ψ	arbitrary function
$\tilde{\psi}$	$\psi - \bar{\psi}$
$\bar{\psi}$	value of ψ averaged over a small interval of time and space
Ω	angular speed of the earth's rotation = 7.292×10^{-5} radians per second
ω	$\omega(x,y)$, weighting function for velocity along the axes of an inlet in lumped parameter model = $\bar{u}/\bar{u}_B = A_B/A_C(x)$

COMPARISON OF NUMERICAL AND PHYSICAL HYDRAULIC MODELS,
MASONBORO INLET, NORTH CAROLINA

by
D. Lee Harris
and
B.R. Bodine

I. INTRODUCTION

1. Historical Perspective.

In 1969, the Coastal Engineering Research Board (CERB) recommended that a comparative test of the accuracy of numerical models be conducted in conjunction with a distorted scale, fixed-bed model already planned for Masonboro Inlet, North Carolina. The planned fixed-bed physical model was to be used to predict changes in inlet hydraulic characteristics resulting from improvements at the inlet entrance. A bathymetric survey of the inlet was made in September 1969. Tide and current observations through one tidal period were collected on 12 September 1969 at the locations shown in Figure 1 to provide information needed for calibrating the fixed-bed model.

Implementation of the CERB recommendation was initiated in 1971 with the issuance of a Request for Proposals (bids) (App. A). In addition, the bidders were supplied with copies of the data collected in 1969 for use in calibrating the numerical models. The plan called for model calibration with the 1969 hydrographic and hydraulic data. All of the models were to be applied to November 1964 and June 1967 hydrographic data, using standard ocean tides to drive the models. The results of the application of the models to the new conditions would then be compared to evaluate the existing capability to use numerical hydraulic models to predict hydraulic conditions at coastal inlets.

After the bids were received and the work under resulting contracts was completed, it was decided that the physical model would be operated for conditions of June 1966 rather than conditions of June 1967. Since there were great differences in the hydrography for the two conditions, the hydraulic comparisons would have little meaning. Therefore, the comparisons of the numerical models with the results of the physical model for the 1967 conditions are not discussed in this report. However, results from the 1967 hydrography are included in the numerical modeling reports published as separate appendixes to this report: Chen and Hembree (1977), Huval and Wintergerst (1977), Masch, Brandes, and Reagan (1977), and Sager and Seabergh (1977). New prototype measurements made at Masonboro in 1974 were compared with results of the physical model study by Seabergh and Mason (1975). This comparison of the 1974 prototype data and numerical model results will be published in a later report.

As a result of the Request for Proposals, two two-dimensional models, constructed along the lines of Reid and Bodine (1968), and a lumped

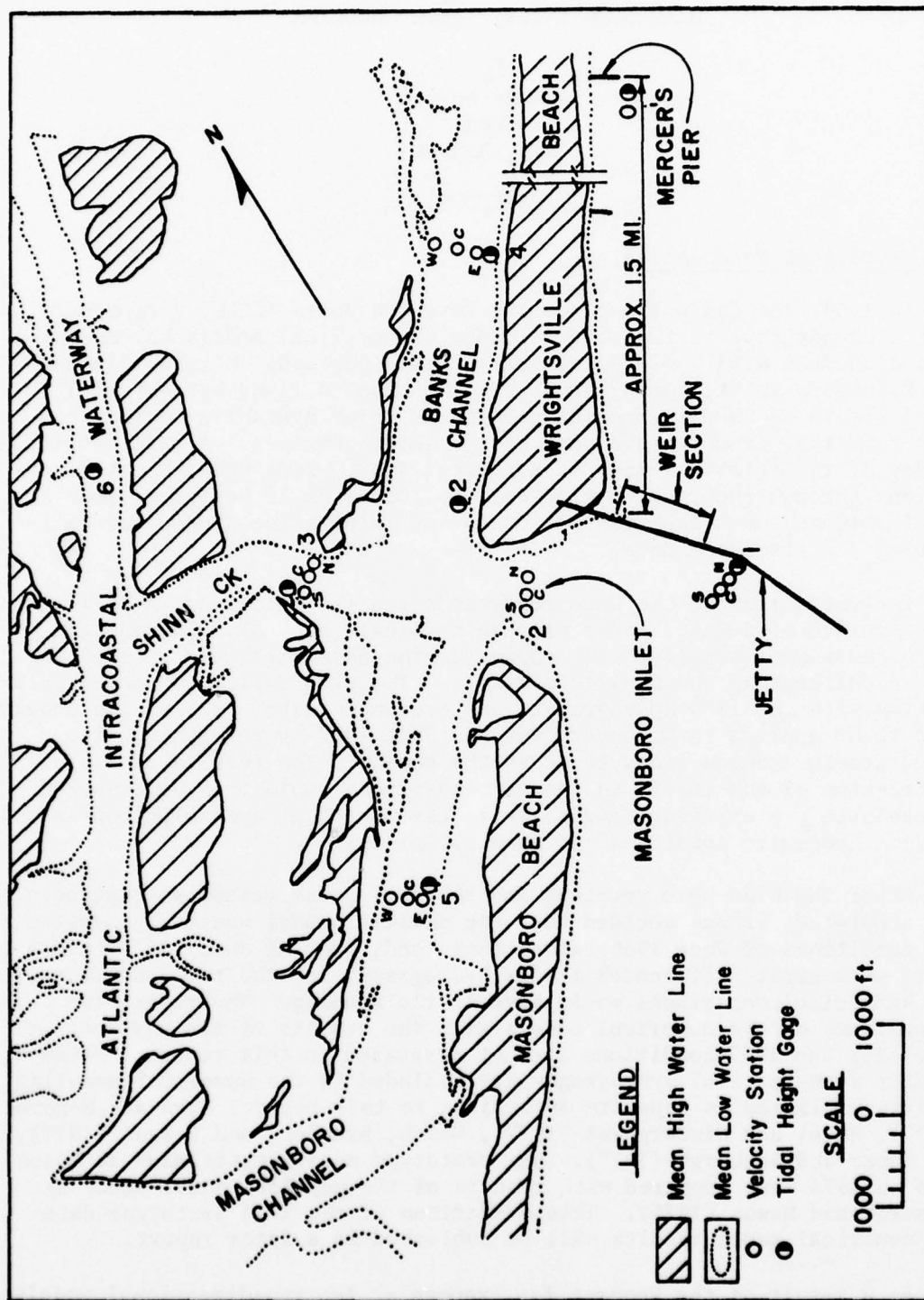


Figure 1. Locations of tide and current observations, Masonboro Inlet.

parameter model were selected from the many models proposed for study. The two-dimensional numerical models were expected to provide tidal heights and mean current estimates for one tidal cycle at each measurement location (Fig. 1). The lumped parameter model would provide only one estimated current hydrograph (a cross-sectional average at the throat of the inlet) and one estimated tide hydrograph, indicative of average conditions inside the inlet.

The use of both physical and numerical hydraulic models involves a preliminary stage or stages during which the relationships between the model and the prototype are investigated and established. Various terms have been used to describe this process; e.g., *confirmation*, *adjustment*, *verification*, and *calibration*. These terms are sometimes used interchangeably in the hydraulic model literature with definitions varying by place and time. The following definitions are used in this study:

(a) Calibration. The process where a hydraulic model is checked with prototype data and systematically adjusted to reproduce the water level and current data from corresponding prototype driving forces.

(b) Verification. The process where independent prototype data (data not used in the calibration) are used to verify that a calibrated hydraulic model produces satisfactory prototype results.

Since data from the prototype are available for only one condition (the 1969 hydrography and the September 1969 tidal height and tidal current measurements), the models used in this study could only be calibrated. It was assumed at the start of this study that more confidence could be placed in the physical model results than in the numerical model results. Therefore, a comparison of the numerical model results with the 1964 results of the physical model could be considered as verification of the numerical models.

The concept of verification of numerical models by comparison with physical models was abandoned when it was determined that one of the numerical models performed as well as the physical model in the calibration process and that physical reality is approximated differently by numerical models than by physical models.

2. Types of Models.

A model may be a (a) geometrically similar physical replica of the prototype; (b) distorted physical replica of the prototype for which appropriate corrections can be made; (c) set of mathematical equations that express the laws which govern the phenomena of interest in the prototype; or (d) physically dissimilar system governed by a similar set of equations, together with a statement of the relationships between the two systems. This study primarily discusses the consideration of distorted physical replicas of tidal inlet flow and a set of mathematical equations which describe flow within and near the inlet. However, undistorted models and electrical analogs of the flow could be used. Ishiguro (1972) reviewed the use of electrical analogs in the solution of tidal hydraulics problems.

Although physical and numerical models are different approximations of the same prototype phenomena, it is possible that each technique is superior to the other in some respects. One model might be more useful for investigating specific problems; both models might be equally satisfactory for other problems, even though each yields slightly different results.

Although laws which govern a phenomenon have not been firmly established, the design of useful physical model experiments is often possible, provided certain dimensionless parameters, formed from the most important variables associated with the phenomenon, have the same value for both model and prototype. This procedure is widely used in hydraulics, and is discussed in most literature under dimensional analysis, the Buckingham pi theorem, or the Rayleigh theorem. Dimensional analysis can be useful in the development of either distorted or undistorted physical models of tidal inlets.

3. Purpose and Scope of Hydraulic Inlet Studies.

Models of tidal inlets are constructed primarily for predicting the tidal currents and water level fluctuations in and near inlets. Predictions of the changes in the flow regime associated with dredging or construction activities are especially important. A knowledge of currents and tidal flow is needed for predicting sediment motion and the effects of currents on navigation. Predicting the effects of currents, however, is not discussed in this study.

Nearshore currents and water levels are often affected by wind and wind-generated waves as well as by astronomical tides. The modification of waves in shallow water gives rise to radiation stresses which generate nearshore currents, reduce the mean water level in the breaker zone, and increase the mean water level on the beach. Wave motions also affect the frictional effects on flows of tidal period. However, the time and space scales of tides and surface waves are so different that modeling the details of both at the same time is not feasible. A study of tidal flows requires dealing with no more than the statistical effects of the wave field. In a study of wind-generated waves, tidal elevations and tidal currents may be regarded as quasi steady-state phenomena. This is also true for most tsunamis; however, it may be necessary to consider several phases of the tide. In this study, only the possible effects of surface waves on tidal flows are considered.

Models of natural phenomena are used primarily for gathering essential data at a convenient rate and at a lower cost than would be possible with the prototype. Generally, this means a great acceleration of the time scale, associated with an increasing density of the data gathered in space. The model leads to correct predictions of prototype behavior if the laws which govern both model and prototype are identical. Models which are governed by simpler laws than the prototype can be extremely useful if these laws are nearly identical with those which govern the phenomena of interest in the prototype, and if phenomena of secondary

importance which lead to confusion at prototype scale are eliminated in the model; e.g., the elimination of wind and wind-generated waves may facilitate the study of tidal currents. The wind and wind-generated waves can always be eliminated from numerical models, and can generally be eliminated from physical models.

Although the laws which govern a natural phenomenon may be fully understood and expressible by a set of differential equations and boundary conditions, an exact solution of the equations may be difficult, and thus the construction of a physical model may be desirable. Mathematical models and dissimilar physical analogs, such as electrical analogs, are possible only to the extent that the laws which govern the phenomenon are known. When the laws which govern a physical phenomenon are understood well enough to permit a mathematical description, even physical replicas of the actual phenomena can be regarded as analog computers for solving a set of equations which govern the model. Therefore, the physical as well as the numerical models of tidal flow considered in this study are regarded as mathematical models.

4. Preview of the Report.

Equations which govern the mean flow in incompressible, nearly homogeneous fluid layers are given in Section II, along with the physical interpretation of each term. The equations are developed without ad hoc assumptions in Appendix B, and are divided into terms essential to all studies of tidal flows--descriptive terms of the mean flow which are essential to some but not all investigations, and perturbation terms that are usually neglected. It is often possible to simulate the net effects of the phenomena described by the perturbation terms with useful accuracy even though the detailed structure of the phenomena is not considered. The radiation stresses are normally neglected terms that account for the exchange of momentum between waves and currents. Sager and Seabergh (in preparation, 1977) show that the agreement between model results and prototype observations can be improved by including the wave effect in the physical model. Wave effects were not included in the original plans for the model studies and were not considered in the numerical models or the calibration of the physical model.

General considerations for modeling tidal flows and their application to distorted scale physical models with particular reference to the Masonboro Inlet model are discussed in Section III. General features of numerical models and their application to two-dimensional hydrodynamic models such as the Masonboro Inlet models are discussed in Section IV.

The material in Sections III and IV is not intended as a guide for the design and construction of either physical or numerical models, but only to provide insight for understanding the Masonboro Inlet model and other similar models. Special features of each model are described in various individual reports; however, the background information needed for a better understanding of these reports has been omitted in the description of each model. This study attempts to provide that information, including a few references to the material on the individual models.

A surprising result of this investigation (see Sec. III) is the theoretical evidence that radiation stresses can be simulated with good approximation in a distorted scale physical model. This is believed a new theoretical development. Sager and Seabergh (in preparation, 1977) report empirical evidence supporting this concept but do not provide or reference any theoretical justification. They do not claim the level of quantitative accuracy which the development in this study appears to justify.

The effects of the earth's rotation, the surface wind field, and the atmospheric pressure gradient cannot easily be modeled or satisfactorily simulated in the physical model of Masonboro Inlet or in most other physical hydraulic models. However, these phenomena are of secondary importance in the Masonboro Inlet study.

Modeling or simulating the effects of the surface wind field, the atmospheric pressure gradient, and the principal effects of the earth's rotation pose no insurmountable difficulties for numerical models. Small-scale features of the flow, with characteristic lengths of less than four- or five-grid increments, cannot be modeled with acceptable accuracy. Features of the flow with wavelengths in excess of 10 to 20 space increments can be modeled with satisfactory accuracy. Fortunately, the most important phenomenon for the Masonboro model, the astronomical tide wave, has a length in excess of 20 space increments.

In Section V, the one-dimensional equations for unstratified, incompressible flow in a channel of variable width and depth are integrated along the axis of the channel to form an equation relating flow in the ocean, inlet, and bay. The one-dimensional flow equations are developed from the two-dimensional equations in Appendix C. For some flow conditions, it is possible to combine all empirical coefficients governing the flow into a single parameter. This is the essence of the lumped parameter model introduced by Keulegan (1967). The systematic derivation given in this study facilitates an evaluation of the assumptions involved in this approach and reveals several inconsistencies that will not greatly decrease the expected accuracy of the resulting calculations for Masonboro Inlet. In applications to inlet problems in the Great Lakes where the characteristic periods are much shorter, these inconsistencies can lead to significant errors.

The calibration of both physical and mathematical models is described in Section VI. Calibration, usually a trial-and-error process, is necessary to compensate for the effect of physical processes neglected or improperly represented in the model, and the lack of precise information about the prototype.

The results obtained in the various Masonboro Inlet models are compared in Section VII; a summary with conclusions and recommendations is presented in Section VIII.

II. A MATHEMATICAL DESCRIPTION OF TIDAL FLOWS

1. General.

Tidal currents are quasi-horizontal and almost periodic with prominent components of approximately 12 and 24 hours. Tidal components with periods as short as 3 hours can be identified at some locations by a harmonic analysis of the tide records. Although the tides are affected by the earth's rotation, this effect is insignificant in many estuaries. Friction is a prominent factor in shallow areas; however, the effect of friction is negligible in deep water. Most tidal flows are adequately described by the linearized hydrodynamic equations. However, some signs of nonlinear behavior of the tides in estuaries, such as overtides and tidal bores, are not described adequately by the linearized equations.

Meteorological disturbances produce transient currents and water level disturbances with time scales which overlap those of the astronomical tides. A precise separation of the meteorological and astronomical effects on sea level and nearshore currents is never easy and is not always possible. The overlap occurs in the analysis of both empirical data and the hydrodynamic equations. Thus, any thorough study of the flow in tidal inlets and estuaries must consider both meteorological and astronomical effects. The effects of the variation of gravitational attraction of the sun and moon over a typical estuary are so small that the tides in most estuaries are adequately represented by prescribing appropriate boundary conditions in the open sea.

Many distinct hydrodynamic phenomena are associated with the tides, but not all are important at any one location. Some phenomena are prominent in parts of a problem area or for short-time periods, and insignificant in other parts of the area and at other times. Thus, any set of equations which provides a satisfactory description of a wide range of tidal problems must be fairly complete and must contain terms which can be neglected in many specific applications.

The most reliable method of formulating a dependable set of equations which satisfies the above requirements is to begin with a complete set of hydrodynamic equations which describe most fluid flows and systematically modify them to permit a ready separation of the phenomena of primary interest from phenomena of generally secondary importance.

A derivation of the long wave equations (carried out as discussed above) is given in Appendix B. An identical set of equations for the terms of primary importance has been derived directly by many authors by simply neglecting all phenomena considered of secondary importance. The most important terms have been obtained by establishing a balance of forces on a fluid element by considering only the obviously important terms. A rigorous derivation is used in this study to provide at least subjective estimates of the errors inherent in the approximating equations and to show that the errors committed in numerical and physical

modeling differ. Sometimes one type of error is more acceptable than another in solving a specific problem.

Sound waves are eliminated from the fundamental equation by assuming at the outset that the water is incompressible. The detailed structure of wind-generated waves and turbulence is eliminated from the equations without eliminating the interaction effects by averaging each important variable over a finite volume and time interval.

The practical necessity of eliminating some detail of the flow may be recognized when it is realized that all physical measurements of velocity are averages over some finite volume and time period, if only because of the physical size and finite response time of the measurement instruments. Displacements of the fluid smaller than the effective size of the instruments, and motions with time scales smaller than the response times of the instruments cannot be accurately measured. The effective averaging volume and the time interval referred to prototype scale are generally larger for physical models than for the prototype, and larger for numerical models than for physical models. Recognition of this difference is essential to the proper interpretation of the results of model studies.

Details of the vertical structure are eliminated by integrating the flow from the seabed to the free surface. Thus the horizontal velocities are replaced by total fluid fluxes, or rate of transport, and the vertical velocity is represented only by the stretching or compression of fluid layers. This mode of derivation leads to a set of equations which approximately describe both tidal flows and storm surges, and a set of remainder terms which can be used to estimate the error committed in using the approximate equations.

2. Motions of Tidal Scale.

The equations for the conservation of momentum in quasi-horizontal flow (App. B, eqs. B39 and B40) may be expressed in the form:

$$\begin{aligned} & \text{(a)} \quad \frac{\partial U}{\partial t} + \text{(b)} \quad gD \frac{\partial \bar{h}}{\partial x} + \text{(c)} \quad \left(\frac{1}{\bar{\rho}} \right) (\tau_{zx})_Z = \text{(d)} \quad \frac{1}{\bar{\rho}} (\tau_{zx}) \bar{h} - \text{(e)} \quad \frac{\partial}{\partial x} \frac{U^2}{D} - \frac{\partial}{\partial y} \frac{UV}{D} \\ & \text{(f)} \quad fV - \text{(g)} \quad \left(\frac{1}{\bar{\rho}} \right) (D) \frac{\partial \bar{p}_h}{\partial x} + S_{xt} - S_{xw} - S_{xo} - S_{xv} \quad , \end{aligned} \quad (1)$$

$$\begin{aligned} & \text{(a)} \quad \frac{\partial V}{\partial t} + \text{(b)} \quad gD \frac{\partial \bar{h}}{\partial y} + \text{(c)} \quad \frac{1}{\bar{\rho}} (\tau_{zy})_Z = \text{(d)} \quad \left(\frac{1}{\bar{\rho}} \right) (\tau_{zy}) \bar{h} - \text{(e)} \quad \frac{\partial}{\partial x} \frac{UV}{D} - \frac{\partial}{\partial y} \frac{V^2}{D} \\ & \text{(f)} \quad fU - \text{(g)} \quad \left(\frac{1}{\bar{\rho}} \right) (D) \frac{\partial \bar{p}_h}{\partial y} + S_{yt} - S_{yw} - S_{yo} - S_{yv} \quad . \end{aligned} \quad (2)$$

The two-dimensional equation of continuity (App. B, eq. B23) is:

$$\frac{\partial}{\partial t}(\bar{h} - D) + \frac{\partial}{\partial x} \bar{U} + \frac{\partial}{\partial y} \bar{V} = R + E, \quad (3)$$

where

- t = time
- x, y, z = principal axes in a right-hand coordinate system;
 z is positive-upward
- $E = - \left[\frac{\partial}{\partial x} \bar{u} \bar{h} + \frac{\partial}{\partial y} \bar{v} \bar{h} \right]$
- $\bar{U} = \int_Z^{\bar{h}} \bar{u} dz$, mean fluid transport parallel to the x-axis
- $\bar{V} = \int_Z^{\bar{h}} \bar{v} dz$, mean fluid transport parallel to the y-axis
- R = precipitation on the water surface and bottom
seepage into the basin in excess of evaporation,
and bottom seepage out of the basin
- $\bar{\rho} = \frac{1}{D} \int_Z^{\bar{h}} \rho dz$
- ρ = density
- g = acceleration of gravity
- \bar{u}, \bar{v} = mean horizontal velocity components parallel to the
x- and y-axes, where the mean is taken over a small
time and space interval
- $\bar{h} = h(x, y, t)$, mean elevation of the top of a fluid layer
above datum
- $D = D(x, y, t) = \bar{h} - Z$, total depth
- $Z = Z(x, y, t)$, mean elevation of the bottom of a fluid
layer above datum
- $f = 2\Omega \sin \phi$, Coriolis parameter

Ω	= angular speed of the earth's rotation, 7.292×10^{-5} radians per second
ϕ	= latitude
p	= $p(x,y,z,t)$, pressure within the fluid
\bar{p}_h	= pressure at the top of a fluid layer
$(\tau_{zx})_h, (\tau_{zy})_h$	= surface stresses parallel to the x-axis at the top of a fluid layer
$(\tau_{zx})_Z, (\tau_{zy})_Z$	= surface stresses parallel to the x- and y-axes at the bottom of a fluid layer
u	= $u(x,y,z,t)$ and $v = v(x,y,z,t)$, horizontal components of fluid velocities parallel to the x- and y-axes
$S_{xu}, S_{yu},$ $S_{xt}, S_{yt},$ $S_{xo}, S_{yo},$ $S_{xv}, S_{yv}; E$	= interaction between the mean flow and the perturba- tions due to waves or turbulence

The contribution of rainfall, evaporation, and seepage to the momentum equations has been omitted because these are expected to be smaller than the uncertainty in evaluating the stress terms in most applications; e.g., the inlet problems considered in this study.

Essential terms for the discussion of all two-dimensional tidal flows in shallow water are shown on the left of the equal sign in equations (1), (2), and (3). Important terms for some but not all flows of this class are shown on the right.

3. Interpretation of the Principal Terms.

The lower-case letters in parenthesis, (a) to (j), over the terms in the equations are used to identify the terms in the following discussion of their physical significance with some common approximations.

(a) $\partial U/\partial t$ and $\partial V/\partial t$. Identifies the change of the integrated flow per unit width with time. This change may result from the temporal acceleration of the mean flow or a change in thickness of the fluid layer. At least one of the two terms is important in every tidal or storm surge problem.

(b) $gD\bar{h}/\partial x$ and $gD\bar{h}/\partial y$. Describes the slope of the water surface. The pressure gradients which result from the sloping water surface are the principal driving forces for all purely tidal flows in estuaries. They are also prominent in all storm surge problems.

(c) $(\tau_{zx})_Z$ and $(\tau_{zy})_Z$. Usually interpreted as the stress of the fluid layer against the bottom boundary, but in many applications,

internal stresses are implicitly included. In most problems, the bottom boundary is the solid earth and is assumed impermeable. These terms are usually treated as the bottom friction terms. In studying stratified flow, it may be necessary to recognize two distinct fluid layers. When this is true, $(\tau_{zx})_Z$ and $(\tau_{zy})_Z$ for the upper layer may be the stress of the saline water in the lower layer on the freshwater in the upper layer.

The stress within a fluid has the dimension of the product of density and the square of the speed. In general, the magnitude of the stress terms, $(\tau_{zx})_Z$ and $(\tau_{zy})_Z$, increases with the current speed. Thus, these terms are naturally represented by the expression:

$$\left(\frac{1}{\rho}\right) \tau_{zs} = Kq^2, \quad (4)$$

where K is a dimensionless coefficient which may be a function of speed and other parameters governing the flow, q is the velocity parallel to the boundary, and the s -axis is chosen parallel to the flow. The bottom stress vector is generally assumed parallel to the velocity, q , which generally increases with distance from the nearest boundary. In specifying a horizontal surface stress, K must be a function of the distance between the boundary and the point at which q is specified. Most hydrodynamics and hydraulics textbooks show that K increases as the roughness of the surface increases.

In a study of quasi-horizontal flows, the velocity profile as a function of distance above the bottom boundary of the fluid is generally not available. Therefore, the best available approximation is usually of the form:

$$\left(\frac{1}{\rho}\right)(\tau_{zs})_Z = K|Q|\frac{Q}{D^2}, \quad (5)$$

where K decreases as the depth increases and increases as the bottom roughness increases, and $Q = (U^2 + V^2)^{1/2}$ and has the same direction as the mean flow. The stresses, $(\tau_{zx})_Z$ and $(\tau_{zy})_Z$, are the components of $(\tau_{zs})_Z$ parallel to the x - and y -axes.

The coefficient, K , may be approximated by the expression:

$$K = K_2 D^{-\alpha_2}, \quad (6)$$

where K_2 is a parameter used to characterize the bottom roughness and α_2 is an empirical parameter. Manning's investigation of expressions similar to equation (6) was summarized by Chow (1959, p. 100). Initially, α_2 was regarded as a constant less than one. Ultimately, it was decided that

$$\frac{1}{4} < \alpha_2 < \frac{1}{2}.$$

The value $1/3$ has been adopted in most studies; however, a few continue to use other values of the exponent. When the metric system is used with Manning's formulation, the bottom-stress coefficient for use in equation (5) is given by:

$$K = \frac{gn^2}{(m/s^3)^{2/3}} D^{1/3}, \quad (7a)$$

where n is a dimensionless constant which characterizes the bottom roughness. When the U.S. Customary system is used,

$$K = \frac{gn^2}{(3.2808 \text{ ft/s}^3)^{2/3}} D^{1/3}. \quad (7b)$$

The bottom roughness depends on the bottom bed forms. The bed forms in sedimentary materials vary with the current speed and the composition of the bed. In general, the effective roughness increases with the current speed to some small finite speed and decreases for higher speeds. Ludwick (1974) reported 620 measurements of the bottom-stress coefficients near the entrance to Chesapeake Bay, and found that K varied widely with the development of bed forms. In Ludwick's data, the characteristic value of K for ebb flows was about three times the characteristic value for floodflows.

Behrens, Watson, and Mason (1977) measured n in a Texas tidal inlet and also found that the bottom roughness varied with the development of bed forms, but did not find a significant difference between ebb and floodflows. Odd (1971) reported that the friction factor, K , also varied with the phase of the tide even with no change in the bottom roughness, but he does not provide any quantitative information or references to other sources where quantitative information may be found.

From the above discussion it seems that the true bottom friction depends primarily on the velocity near the bottom and the small-scale features of the flow that are not considered in detail. Several phenomena occur in nature to produce bottom stresses which cannot be described by the quadratic stress law; e.g., a finite time is required for any contribution of the surface wind to the current to be experienced at the bottom. The time required increases with increasing water depth and the direction of the bottom velocity may differ from that of the mean velocity. If the wind over a small basin continues long enough for an equilibrium slope to develop, the mean velocity may vanish and the bottom velocity may be directed opposite to the free-surface velocity. Other phenomena which lead to differences between the mean velocity and the bottom velocity are discussed later.

Thus, when equations (4) or (5) are used to evaluate the bottom stress, K should increase with increasing roughness of the bottom and decrease with increasing depth. K may also increase with increasing windspeed or wave height.

Bottom friction dissipates energy and thus contributes toward a reduction in the amplitude of the tide wave and a decrease in the phase velocity of gravity waves.

(d) $(\tau_{zx})\bar{h}$ and $(\tau_{zy})\bar{h}$. Usually interpreted as the stress in the x- and y-directions of an upper fluid layer on a lower fluid layer. When two distinct fluid layers are identified, $(\tau_{zx})\bar{h}$ and $(\tau_{zy})\bar{h}$ for the lower layer may be recognized as the stress exerted on the lower layer by the upper layer.

At a free water surface, these terms describe the friction between the wind and the water. The direct effect of the wind stress is to generate a surface current in the direction of the wind. If the movement of this current is impeded by a barrier, the current will be partially replaced by a slope of the water surface, upward in the direction of the airflow. The wind stress is an essential term in the equations for storm surge, and is generally neglected in investigations of tidal flows unless believed an essential element of the problem. However, wind usually has some effect on the water level and currents in all tidal basins. Neglecting the wind when it is a significant, though perhaps secondary factor, may lead to errors in calibrating and verifying a model for purely gravity flows.

(e) $\partial/\partial x U^2/D + \partial/\partial y UV/D$ and $\partial/\partial x UV/D + \partial/\partial y V^2/D$. May be interpreted as integrated measures of the advection of momentum or integrated measures of the inertia of the water. These terms may be important only in regions with strong velocity gradients, such as the entrances and exits of inlets, junctions of canals, flood plains, or other regions where the flow is compelled to undergo large changes in direction.

(f) fU and fV . The Coriolis terms which result from the necessity of using a coordinate frame, fixed to the rotating earth; Newton's laws of motion apply to a coordinate system fixed with respect to the stars. The Coriolis effect is discussed here in detail and documented, because the conditions under which the Coriolis effects are important are frequently misinterpreted in discussions of tidal hydraulics.

The earth's rotation can affect the water motion in several distinct ways, none of which are considered significant in typical inlets with widths of about 1 mile or less and maximum currents of about 2 meters (6.6 feet) per second or less. The Coriolis effect is measurable in some of the wider and deeper inlets, or when current speeds are exceptionally high. Coriolis acceleration is often a prominent feature of the tidal flow in the open sea adjacent to the inlet and it may have a significant effect in the bay or lagoon on the landward side of the inlet. Flow resulting from the Coriolis acceleration is often called the *inertial flow*.

The earth's rotation tends to produce an apparent rotation of the fluid toward the right in the Northern Hemisphere and toward the left in the Southern Hemisphere. The period of this rotation, called the

inertial period, is equal to $1/f$. The circle traversed by a water particle is called the *inertial circle*, its radius, R_e , is given by:

$$R_e = \frac{v}{f}, \quad (8)$$

where v is the current speed.

When the flow is generated by pressure gradients in a homogeneous fluid, as for tidal flows near the coast, the direction and magnitude of the inertial flow are nearly independent of depth. Verber (1966) reported observations of the inertial flow in Lake Michigan with currents as low as 6 centimeters (0.2 foot) per second. The radius of the corresponding inertial circle is about 586 meters (1,923 feet).

When the flow is generated by frictional stresses at the fluid boundaries, as for wind stress at the free surface and bottom friction, a finite time is required for the rotational effect to penetrate to the interior of the fluid. As a result, there is an additional rotation to the right with distance from the fluid boundary. The frictional force at the bottom is directly opposed to the bottom current which would exist in the absence of friction. These influences cause the vertically integrated flow vector, resulting from frictional forces, to be directed to the right of both the surface and bottom-stress vectors. The fluid layers affected by this rotating current are called the *Ekman boundary layers*. The thickness of the layers increases with the intensity of turbulence in the fluid. Thus, for turbulent flow in shallow water, the two boundary layers may overlap and little rotation of the currents is observed. The combined effects of the earth's rotation and fluid friction on wind-generated and tidal currents are discussed by Defant (1961; Vol. 1, Chs. 10 and 13; Vol. 2, Ch. 1) and Neuman and Pierson (1966; Ch. 8). Defant also discussed the inertial circle. Webster (1969) summarized most observations of the inertial circle published before 1968. Platzman (1963), Jelesnianski (1967, 1970), and Forristall (1974) presented schemes for including the effect of the earth's rotation on the stress vectors in storm surge computations. If this rotation is inhibited by lateral boundaries, it is replaced by an upward slope to the right of the current in the Northern Hemisphere and to the left in the Southern Hemisphere.

The magnitude of this slope can be computed from equation (2) by considering only the slope and Coriolis terms to obtain:

$$\begin{aligned} \frac{\partial h}{\partial x} &\approx \frac{fv}{gD} \\ &\approx \frac{f\bar{v}}{g}, \end{aligned} \quad (9)$$

where the y-axis is assumed to coincide with the axis of the inlet and \bar{v} is the mean velocity of the flow, parallel to the y-axis averaged in the vertical. Thus, the slope across the inlet is given by:

$$\Delta h = \left(\frac{f\bar{v}}{g} \right) \Delta x . \quad (10)$$

In applying the above considerations to Masonboro Inlet, field measurements show that the inlet is well mixed. This implies that the top and bottom Ekman layers overlap so that little rotation of the current vector with depth is expected to result from the rotation of the earth. The maximum current speeds recorded in Masonboro Inlet are about 1 meter (3.3 feet) per second. The Coriolis parameter, f , for latitude 34° is 8.155×10^{-5} per second, and the width of the inlet is 457 meters (1,500 feet). Since the radius of the inertial circle is about 12.5 kilometers (7.8 miles) or $R = v/f$, the inertial circle cannot develop. The net change in elevation across the narrow inlet, as computed by equation (10), is less than 4 millimeters (0.16 inch); however, this effect is insignificant. Reid, Vastano, and Reid (in preparation, 1977) show that bottom friction in shallow areas may overshadow the Coriolis acceleration during storms when current velocities are high, even though Coriolis acceleration and bottom friction are of the same magnitude during low flow conditions.

(g) $(1/\bar{\rho})(D) \partial \bar{p}_h / \partial \bar{x}$ and $(1/\bar{\rho})(D) \partial \bar{p}_h / \partial \bar{y}$. Describes the component of the atmospheric pressure gradient which affects the water motion. The atmospheric pressure gradient is generally neglected in studies of water motions unless believed an essential factor in the phenomena being studied. The atmospheric pressure gradient terms are generally of trivial importance in studies of tidal flows, except for hurricane-generated storm surges.

(h) $\partial(\bar{h} - Z)/\partial t$. A measure of the time rate of expansion or contraction of a fluid layer. A well-mixed estuary, such as Masonboro Inlet, can be adequately represented as a single fluid layer. In this case, \bar{h} is the elevation of the free surface and Z is the elevation of the seabed. Later in this study, Z is assumed independent of time. With this assumption, the term $\partial \bar{h} / \partial t$ in equation (3) measures the rate at which the water level is rising or falling.

(i) $\partial U / \partial x + \partial V / \partial y$. A measure of the rate at which the water is converging or diverging horizontally at any point (x, y) . The complete continuity equation (3) states that the water level must rise in an area of horizontal convergence and fall in an area of horizontal divergence. At least one of these terms is essential to all tide and storm surge models.

(j) R_o . A measure of the precipitation on the water surface and bottom seepage into the basin in excess of the evaporation and bottom seepage out of the basin. In general, R is not important in tidal

hydraulics investigations. The most prominent exception is a nearly landlocked estuary or lagoon during severe rainstorms.

4. The Perturbation Terms.

The principal terms in equations (1), (2), and (3) were derived by the vertical integration and time averaging of the Navier-Stokes equations. Deviations between the actual flows and the flows defined by vertical integration and time averaging may be defined as perturbations. Nonlinear terms in the perturbations represent the interaction between the small-scale features of the flow, such as turbulence, surface waves, and the vertical shear of the current. These phenomenon are discussed below. The turbulent stresses (App. B, eqs. B41 and B42) are:

$$S_{xt} = \int_z^{\bar{h}} \left[\left(\frac{1}{\rho} \right) \frac{\partial}{\partial x} \mu \frac{\partial \bar{u}}{\partial x} - \frac{\partial}{\partial x} \overline{(u')^2} + \left(\frac{1}{\rho} \right) \frac{\partial}{\partial y} \mu \frac{\partial \bar{u}}{\partial y} - \frac{\partial}{\partial y} \overline{u'v'} \right] dz, \quad (11)$$

$$S_{yt} = \int_z^{\bar{h}} \left[\left(\frac{1}{\rho} \right) \frac{\partial}{\partial x} \mu \frac{\partial \bar{v}}{\partial x} - \frac{\partial}{\partial x} \overline{u'v'} + \left(\frac{1}{\rho} \right) \frac{\partial}{\partial y} \mu \frac{\partial \bar{v}}{\partial y} - \frac{\partial}{\partial y} \overline{(v')^2} \right] dz. \quad (12)$$

The Reynolds stress terms, $\overline{(u')^2}$, $\overline{(v')^2}$, and $\overline{u'v'}$, are generally much larger than the terms involving molecular viscosity except in the thin viscous sublayer, never more than a few millimeters in thickness. The viscous terms can generally be neglected when discussing prototype flows. The simple form of the expression describing viscous shears can be recovered by introducing mixing coefficients defined by the relations:

$$\begin{aligned} A_{xx} &= \frac{\nu \partial \bar{u} / \partial x - \overline{(u')^2}}{\partial \bar{u} / \partial x}, & A_{yx} &= \frac{\nu \partial \bar{u} / \partial y - \overline{u'v'}}{\partial \bar{u} / \partial y}, \\ A_{xy} &= \frac{\nu \partial \bar{v} / \partial x - \overline{u'v'}}{\partial \bar{v} / \partial x}, & A_{yy} &= \frac{\nu \partial \bar{v} / \partial y - \overline{(v')^2}}{\partial \bar{v} / \partial y}. \end{aligned} \quad (13)$$

The mixing coefficients will be needed later in the discussion of numerical models.

The mixing coefficients, sometimes called macroviscosity or "eddy" coefficients, depend on the *structure of the flow field*. In contrast, the viscosity coefficient depends on the *physical properties of the fluid*. The mixing coefficients cannot be evaluated from theoretical considerations, and are usually determined empirically from measured stresses and velocity gradients, or selected subjectively to obtain an acceptable solution to a problem. Fortunately, the solution of many tidal hydraulics problems involving the mixing coefficients is not highly sensitive to the values selected.

5. The Radiation Stresses.

The earliest investigations of the effects of the Reynolds stresses due to waves on the mean flow were reported by Longuet-Higgins and Stewart (1962, 1963, 1964). The contribution of the radiation stresses to the mean transport equations as developed in Appendix B (eqs. B43 and B44) is given below in the notation of Longuet-Higgins and Stewart.

$$S_{xx} = \left(\frac{1}{\rho}\right) \left[\frac{\partial}{\partial x} S_{xxx} + \frac{\partial}{\partial y} S_{yxx} \right], \quad (14)$$

$$S_{yy} = \left(\frac{1}{\rho}\right) \left[\frac{\partial}{\partial x} S_{xyy} + \frac{\partial}{\partial y} S_{yyy} \right], \quad (15)$$

where

$$S_{xxx} = \rho \int_z^{\bar{h}} [\bar{u}^2 - \bar{w}^2] dz + \left(\frac{1}{2}\right) g \bar{h}^2, \quad (16)$$

$$S_{yx} = S_{xy} = \rho \int_z^{\bar{h}} \bar{u} \bar{v} dz, \quad (17)$$

$$S_{yy} = \rho \int_z^{\bar{h}} [\bar{v}^2 - \bar{w}^2] dz + \left(\frac{1}{2}\right) g \bar{h}^2, \quad (18)$$

where \bar{u} , \bar{v} , and \bar{w} are the components of motion due to waves, and \bar{h} is the instantaneous elevation of the free surface.

The interpretation of these stresses may be clarified by considering a train of gravity waves traveling in the s -direction, at an angle θ to the x -axis. \bar{q} is the horizontal particle velocity in the s -direction, due to the gravity waves. For these conditions,

$$\frac{\partial}{\partial x} = \cos \theta \frac{\partial}{\partial s}, \quad \frac{\partial}{\partial y} = \sin \theta \frac{\partial}{\partial s},$$

$$\bar{u} = \bar{q} \cos \theta, \quad \bar{v} = \bar{q} \sin \theta,$$

$$S_{xx} = \cos \theta \frac{\partial}{\partial s} \left[\int_z^{\bar{h}} (\bar{q}^2 - \bar{w}^2) dz + \left(\frac{1}{2}\right) g (\bar{h})^2 \right], \quad (19)$$

$$S_{yy} = \sin \theta \frac{\partial}{\partial s} \left[\int_z^{\bar{h}} (\bar{q}^2 - \bar{w}^2) dz + \left(\frac{1}{2}\right) g (\bar{h})^2 \right], \quad (20)$$

The theory of gravity waves shows that $\overline{q^2}$, $\overline{w^2}$, and $\overline{h^2}$ are proportional to A^2 where A is the amplitude of the wave. Equations (1), (2), (19), and (20) show that a decrease in wave amplitude in the direction of wave propagation is associated with an increase in the momentum of the mean flow or an upward slope of the water surface in the direction of wave propagation and vice versa.

The computed magnitude of the radiation stresses depends on the assumed wave shape. Longuet-Higgins and Stewart (1962, 1963, 1964) used the theory of infinitesimal waves to provide estimates for the radiation stress terms. James (1974a, 1974b) used cnoidal and hyperbolic wave theory to provide similar estimates.

The component of radiation stress parallel to the beach is responsible for the generation of the longshore currents, important in sediment transport. The component of radiation stress normal to the beach is responsible for wave setup; i.e., an upward tilt of the water surface from the breaker zone to the beach.

6. Other Secondary Terms.

A second-order contribution to the continuity equation resulting from wave action is given by equation (B25) in Appendix B as:

$$E = - \left[\frac{\partial}{\partial x} \widetilde{u_h h} + \frac{\partial}{\partial y} \widetilde{v_h h} \right], \quad (21)$$

where the subscript \bar{h} indicates that \widetilde{u} and \widetilde{v} are to be evaluated at $z = \bar{h}$.

This term represents the fluid transport between the trough and crest of the waves, and is analogous to the radiation stresses discussed above. The term can be significant only when the wave height is of the same order of magnitude as the water depth and is changing rapidly in space. Thus, the term may make a significant contribution to the conservation of fluid volume, but only in and near the surf zone and over shallow shoals.

A small error is made in using the product of the integrals of the horizontal velocity components in place of the integral of the products. These errors, represented by S_{xv} and S_{yv} , have the form:

$$S_{xv} = \frac{\partial}{\partial x} \int_{\bar{z}}^{\bar{h}} (u'')^2 dz + \frac{\partial}{\partial y} \int_{\bar{z}}^{\bar{h}} u''v'' dz, \quad (22)$$

$$S_{yv} = \frac{\partial}{\partial x} \int_{\bar{z}}^{\bar{h}} u''v'' dz + \frac{\partial}{\partial y} \int_{\bar{z}}^{\bar{h}} (v'')^2 dz, \quad (23)$$

where

$$u'' = u - \frac{U}{D}, \quad v'' = v - \frac{V}{D}. \quad (24)$$

The terms u'' and v'' are the deviations of the true mean velocity components, as functions of z from the vertically averaged velocity. Derivatives of these integrals will be small except in regions of relatively steep changes in bottom topography. These terms contribute toward a downward slope in the water surface or a deceleration of the flow on an upward slope and a change of opposite sign on a downward slope. Where the depth change is due to a submerged bar, the change in flow characteristics is reversible. Neglecting these terms in calculations will lead to an error in computed results near the bar, but may not have a detectable effect a short distance away.

Perturbation terms arising from products of the mean flow and perturbation variables, or from time derivatives of the perturbation variables, are given by:

$$\begin{aligned} S_{xo} = & \frac{\partial}{\partial t} \left[\overline{hu} + \overline{h^2} \frac{\partial \bar{u}}{\partial z} \right] + \frac{\partial}{\partial z} \left[\frac{\partial}{\partial x} \overline{h^2} \bar{u}^2 + \frac{\partial}{\partial y} \overline{h^2} \bar{v} \bar{u} \right] - f \left[\overline{h\bar{v}} + \overline{h^2} \frac{\partial \bar{v}}{\partial z} \right] \\ & + \overline{w_z} \frac{\partial Z}{\partial x} + \left(\frac{1}{\rho} \right) \left[\overline{h} \frac{\partial \bar{p}}{\partial x} + (\bar{h})^2 \frac{\partial}{\partial z} \frac{\partial \bar{p}_h}{\partial x} \right] + \frac{\partial}{\partial x} \overline{h^2} (\bar{u} + u'') \frac{\partial u''}{\partial z} \\ & + \frac{\partial}{\partial y} \overline{h^2} \left[(\bar{u} + u'') \frac{\partial v''}{\partial z} + (\bar{v} + v'') \frac{\partial u''}{\partial z} \right], \quad (25) \end{aligned}$$

$$\begin{aligned} S_{yc} = & \frac{\partial}{\partial t} \left[\overline{h\bar{v}} + \overline{h^2} \frac{\partial \bar{v}}{\partial z} \right] + \frac{\partial}{\partial z} \left[\frac{\partial}{\partial y} \overline{h^2} \bar{v} \bar{u} + \frac{\partial}{\partial y} \overline{h^2} \bar{v}^2 \right] \\ & + f \left[\overline{h\bar{u}} + \overline{h^2} \frac{\partial \bar{u}}{\partial z} \right] + \overline{w_z} \frac{\partial Z}{\partial y} + \left(\frac{1}{\rho} \right) \left[\overline{h} \frac{\partial \bar{p}}{\partial y} + \overline{h^2} \frac{\partial}{\partial z} \frac{\partial \bar{p}_h}{\partial y} \right] \\ & + \frac{\partial}{\partial x} \overline{h^2} \left[(\bar{u} + u'') \frac{\partial v''}{\partial z} + (\bar{v} + v'') \frac{\partial u''}{\partial z} \right] + \frac{\partial}{\partial y} \overline{h^2} (\bar{v} + v'') \frac{\partial v''}{\partial z}, \quad (26) \end{aligned}$$

where all velocity terms are evaluated at $z = \bar{h}$.

If the bottom contours do not change noticeably within a single wave period,

$$\tilde{w}_Z = \tilde{u}_Z \frac{\partial Z}{\partial x} + \tilde{v}_Z \frac{\partial Z}{\partial y}. \quad (27)$$

Thus, for a single wave train, the final term in equations (25) and (26) has the form:

$$(\tilde{q}_Z)^2 \frac{\partial Z^3}{\partial s} \cos \theta, \quad (28)$$

where \tilde{q}_z is the horizontal particle velocity near the bottom due to wave motions, $(\partial Z/\partial s)$ is the slope of the bottom in the direction of maximum slope, and θ is the angle between the direction of wave propagation and the direction of maximum slope. Mean slopes large enough to produce measurable effects cannot exist over any appreciable distance. The remaining terms in equations (25) and (26) describe interactions between surface waves and other features of the flow. These terms have not been investigated in detail, but they can make a significant contribution to the momentum balance only in a region where the wave height is a significant fraction of the mean depth. The contribution is greatest when the wave height is changing rapidly with time or distance. The conditions which favor the importance of these terms are most likely to exist in the surf zone.

7. Boundary Conditions.

In developing the two-dimensional equations of motion, it has been assumed that no fluid crosses upper and lower boundaries. The possibility of rainfall or evaporation was treated by modifying the continuity equation. The conditions of the flow at lateral boundaries must be specified before the two-dimensional equations can be solved. Three types of boundary conditions may occur when:

- (a) The flow across a fixed boundary is specified as a function of time along the boundary;
- (b) no flow occurs across parts of the boundary, but the location of the boundary varies in time, and determining the location of the boundary is part of the problem; and
- (c) the elevation of the water surface is specified as a function of time.

The application of boundary conditions is an important part of model design and is discussed in the following sections.

III. MODELING TIDAL FLOWS: PHYSICAL MODELS

1. General.

Many characteristics of tidal waterways can be simulated with useful accuracy without an exact reproduction of all the processes described previously. An advantage of modeling is the ability to eliminate some of the secondary factors from a study of phenomena of primary importance.

Physical models of tidal flows are generally constructed as small-scale, geometrically similar replicas of the prototype with the exceptions that the saltwater of the prototype (if present) is usually replaced by freshwater and the scale ratio used for the vertical dimension may differ from that used for horizontal dimensions.

Rouse and Ince (1957) reported that Reynolds in 1887 showed that for model studies which do not involve intermediate or deepwater waves, the vertical and horizontal scales for tidal flows could be selected independently but that the time scale must be a function of the vertical and horizontal space scales. When the horizontal and vertical scales are selected independently, the model is considered distorted. The undistorted model may be regarded as a special case of the distorted model in which the ratio of the vertical and horizontal scales is unity.

Some terms in the equations of motion (1), (2), and (3), e.g., gravity, cannot be scaled in the laboratory. Others, such as the rotation of the earth, the atmospheric pressure, and wind-shear forces on the water, can be modeled but only with great difficulty and expense.

These facts must be carefully considered in designing the model. Although it is impossible to properly scale a wide range of physical processes at one time, it is often possible to scale the most important processes for a given phenomenon and to simulate the effects of many secondary processes on the flows of primary importance.

Since these simulated motions do not model the prototype flow, the motions cannot be controlled correctly from theoretical considerations alone and some adjustment of the model is usually required to obtain optimum results. This adjustment process is included in model calibration.

Physical models have the distinct advantage of permitting a modeling of the boundaries of flow as accurately as desired without significantly increasing the operating cost of the model. Physical models are also useful for visually demonstrating many phenomena of potential importance.

Both physical and numerical models are useful in understanding natural phenomena. An account of the advantages and disadvantages of each model is as important an aspect of this evaluation as a comparison of the results achieved in several experiments. An examination of the principal features of each type of model is necessary to proceed further with the comparison. Physical models are discussed in this section; numerical models are discussed in Section IV.

2. Physical Models for Quasi-Horizontal Flow.

The physical model used for the study of Masonboro Inlet, like most tidal hydraulic models, is a distorted scale model.

The relation between the scaling factors for time, space, and bottom stress may be derived systematically by developing the governing equations

in dimensionless form, and then comparing the dimensional realizations of these equations for prototype and model scales. Let

$$\begin{aligned} x_p &= \alpha_p x^* & x_m &= \alpha_m x^* \\ y_p &= \alpha_p y^* & y_m &= \alpha_m y^* \\ z_p &= \beta_p z^* & z_m &= \beta_m z^* \\ t_p &= \gamma_p t^* & t_m &= \gamma_m t^* \end{aligned} \quad (29)$$

where

p = prototype

m = model

$*$ = dimensionless variable

α_p, α_m = characteristic horizontal dimensions of the prototype and model

β_p, β_m = characteristic vertical dimensions

γ_p, γ_m = characteristic time dimensions

The space and time relations in equation (29) can be combined to obtain other variables in dimensionless form, such as:

$$\begin{aligned} U_p &= \left(\frac{\alpha_p \beta_p}{\gamma_p} \right) U^* \quad , \quad V_p = \left(\frac{\alpha_p \beta_p}{\gamma_p} \right) V^* \quad , \\ D_p &= \beta_p D^* \quad , \quad h_p = \beta_p h^* \quad , \text{ etc.} \end{aligned} \quad (30)$$

Substitution from equations (29) and (30) into equation (1) yields:

$$\begin{aligned} \frac{\alpha_p \beta_p}{\gamma_p^2} \frac{\partial U^*}{\partial t^*} + \frac{\beta_p^2}{\alpha_p} g D^* \frac{\partial \bar{h}^*}{\partial x^*} + \left(\frac{1}{\bar{\rho}} \right) (\tau_{zx})_Z = \frac{1}{\bar{\rho}} (\tau_{zx})_{\bar{h}} \\ - \frac{\alpha_p \beta_p}{\gamma_p^2} \left[\frac{\partial}{\partial x^*} \frac{(U^*)^2}{D^*} + \frac{\partial}{\partial y^*} \frac{U^* V^*}{D^*} \right] \\ + \frac{\alpha_p \beta_p}{\gamma_p} f V^* - \frac{1}{\bar{\rho}} \frac{\beta_p}{\alpha_p} D^* \frac{\partial \bar{p}^*}{\partial x^*} + S_{xt} - S_{xw} - S_{xo} - S_{xv} \end{aligned} \quad (31)$$

The terms for gravity, g , and the rotation of the earth, f , are not scaled because these are not ordinarily under the control of the experimenter. The terms for stress and atmospheric pressure are not scaled in equation (31) because these have not been clearly defined in terms of the primary variables.

The terms in equation (31) for which the variables have been fully converted to dimensionless form contain the constant factors, $\alpha_p \beta_p / \gamma_p^2$ or $g \beta_p^2 / \alpha_p$. These factors can be removed from all terms specified in dimensionless form if equal; i.e., if the time scale, γ , is given by:

$$\gamma_p = \frac{\alpha_p}{\sqrt{g \beta_p}}, \quad \gamma_m = \frac{\alpha_m}{\sqrt{g \beta_m}} . \quad (32)$$

Combining equations (29) and (32) show that the transformation required to convert the horizontal velocity components to dimensionless form is:

$$u = \sqrt{g \beta_p} u^*, \quad v = \sqrt{g \beta_p} v^* . \quad (33)$$

The transformation required for horizontal transports per unit width as used in equations (1), (2), and (3) is:

$$U_p = \beta_p \sqrt{g \beta_p} U^*, \quad V_p = \beta_p \sqrt{g \beta_p} V^* . \quad (34)$$

Each term in equations (1), (2), and (3), as it applies to the prototype, can be expressed by the product of $(g \beta_p^2 / \alpha_p)$ and the corresponding term in dimensionless form. The ratio of model to prototype variables may then be determined by the ratio of the dimensional constants. In the physical model for Masonboro Inlet (App. B),

$$\alpha = \frac{1}{300}, \quad \beta = \frac{1}{60} . \quad (35)$$

Thus, for the Masonboro model, if

$$\alpha = \frac{\alpha_m}{\alpha_p}, \quad \beta = \frac{\beta_m}{\beta_p}, \quad \gamma = \alpha \beta^{-1/2} = \frac{1}{38.73},$$

$$\frac{u_m}{u_p} = \frac{v_m}{v_p} = \beta^{1/2} = \frac{1}{7.746}, \quad (36)$$

$$\frac{U_m}{U_p} = \frac{V_m}{V_p} = \beta^{3/2} = \frac{1}{464.758}, \quad (37)$$

$$\frac{w_m}{w_p} = \beta^{3/2} \alpha^{-1} = \frac{1}{1.549}. \quad (38)$$

The ratio of model boundary stresses to prototype boundary stresses is given by β^2/α . Assuming that the bottom stress can be expressed in the form:

$$(\tau_{zx})_Z = K(u_Z^2 + v_Z^2)^{1/2} u_Z = K \frac{(U^2 + V^2)^{1/2} |U|}{D^2},$$

as in equations (4) and (5) where u is scaled by equation (36), it is found that

$$\frac{K_m}{K_p} = \frac{\beta}{\alpha} = 5 \text{ for the Masonboro model.} \quad (39)$$

The stress coefficient for the bottom stress can be increased in the model to simulate the correct scaled bottom stress by increasing the bottom roughness. This technique cannot be applied at the free surface because the roughness of the free surface is determined by flow conditions and cannot be freely changed by the experimenter. If the free-surface stress is modeled, the equality of stresses must be achieved through the use of a scaling law for airflow based on the need for duplicating the surface stress. If the wind-stress coefficient is a constant, the scaling law for air velocities would be given by:

$$\frac{v_m}{v_p} = \frac{\beta}{\sqrt{\alpha}} = \frac{1}{3.464} \text{ for the Masonboro model,} \quad (40)$$

where v_m and v_p represent the wind velocity in model and prototype. In reality, modeling the surface wind stress over water is significantly more difficult than equation (40) implies, and the surface stress is generally neglected in hydraulic models. An exceptional experiment in which an effort was made to model wind stress has been reported by Shemdin (1972).

The scaling laws for the inertial terms, (e) (discussed in Sec. II), in equations (1) and (2) are automatically accounted for by the primary scaling relations. This constitutes a major advantage of physical models.

The Coriolis force terms, fV and fU , result from the rotation of the earth. The speed of the earth's rotation is not under the control of the experimenter and so the relative magnitude of this term in the model is less than in the prototype by the factor $\sqrt{\beta/\alpha} = 1/38.73$ for the Masonboro model when model and prototype are at the same latitude. This is not significant for the flow inside Masonboro Inlet where the Coriolis force is unimportant, but it can be a significant factor at some locations. The effect of a scaled Coriolis force can be simulated in the laboratory by building the model on a turntable and rotating at an appropriate speed. Experiments with rotating models have been described by Dalverney and Fontanet (1959), Valembois and Bonnefille (1959), d'Hieres (1962), and Rumer and Robson (1968). The effects of the earth's rotation have been neglected in the Masonboro model as in most other physical hydraulic models.

In discussing the scaled pressure gradients, it is convenient to express the pressure as the height of a column of water required to express the same pressure. That is,

$$p_n = \bar{\rho} g H_b, \quad (41)$$

where H_b is the height of the water column.

The term, (g) (discussed in Sec. II), described in equations (1) and (2) may be regarded as the product of the fluid depth and the atmospheric pressure gradient. Since the depth and scaling factor of the fluid column have been discussed, only the pressure gradient must be discussed here. The prototype pressure gradient is:

$$\frac{1}{\bar{\rho}} \frac{\partial p}{\partial x} = \frac{\beta_p}{\alpha_p} g \frac{\partial H_b^*}{\partial x^*}.$$

For an undistorted model, $\beta_p = \alpha_p$ would be independent of the dimensional constants, and model and prototype pressure gradients would be identical. For distorted models,

$$\left(\frac{1}{\bar{\rho}} \frac{\partial p_n}{\partial x} \right)_m \left(\frac{1}{\bar{\rho}} \frac{\partial p_n}{\partial x} \right)_p^{-1} = \frac{\beta}{\alpha} = 5 \text{ for the Masonboro model.} \quad (42)$$

The atmospheric pressure gradient is of minor importance in tidal models, and the authors are not aware of any hydraulic model studies where an effort has been made to model the atmospheric pressure gradient.

3. Perturbation and Viscous Phenomena in Physical models.

Perturbation and viscous phenomena for physical models are discussed in relation to the mathematical expressions which describe them. One set of terms due to molecular viscosity cannot be reduced sufficiently in the laboratory to permit proper scaling. Fortunately, the viscous forces are directly important only in a very thin layer near the boundaries. The direct effect of viscosity can always be neglected in the prototype. If the ratio of model depth to prototype depth is not too small, the viscous forces will also have little direct influence on model flows. The necessity of eliminating the importance of viscosity in the shallow parts of the model basin is a prime reason for using distorted scale models. Even in distorted models which include regions of tidal flats, flooded at high tide and exposed at low tide, there will be a region of advancing water at floodtide and a region of receding water at ebttide in which the viscous boundary layer may play a significant role. However, the details of the flow in this region are not of primary importance in many inlet problems.

The turbulent stresses are more important than the viscous stresses whenever the fluid layer is thicker than the viscous sublayer; this will include all of the channels and much of the tidal flat region. The

structure of turbulence in the prototype is affected by wind and surface waves as well as tidal flow and is not sufficiently understood to justify an effort at modeling or precise simulation. The calibration effort described in connection with the discussion of surface stresses is assumed to account for the simulation of the principal effects of turbulence and viscosity on the mean flow.

The radiation stresses significantly affect the mean flow only in regions where the wave heights are changing significantly in space. The greatest changes in wave height in a small space, are those due to refraction, shoaling, reflection, and friction near the coast. These stresses, unlike the turbulent stresses, are not related by simple functions of the mean flow. Hence, the effects of these stresses on the mean flow can be simulated independently from the mean flow. Sager and Seabergh (1975) and Seabergh and Mason (1975) showed that the agreement between the physical model of Masonboro Inlet and the prototype can be improved by simulating the approximate wave conditions for the period when the prototype tidal data were collected.

Although short-period surface waves cannot be modeled to scale in distorted models, it is possible to simulate with good approximation, the major effects of surface waves on the large-scale flow. The surface waves affect the large-scale flow through gradients in the radiation stresses.

It is not possible to obtain similitude for a surface wave field in a distorted scale physical model.

Keulegan (personal communication, 1976) has shown that linear wave refraction patterns can be correctly simulated, if the scaling factor used for the vertical dimension in modeling the large-scale flow is used for both horizontal and vertical dimensions when dealing with surface waves, and if the effects of reflection, friction, and diffraction can be neglected. This study shows that when these conditions are satisfied, even the nonlinear aspects of refraction and the gradient of the radiation stresses can be simulated in distorted scale models.

However, reflection and processes which depend explicitly on wavelength cannot be properly simulated in a distorted model; e.g., the effects of surface waves on harbor resonance cannot generally be investigated in distorted scale models.

To mathematically demonstrate the modeling procedures discussed above, it is convenient to begin with the equations for infinitesimal waves. The fluid motions resulting from small-amplitude gravity waves, propagating in the direction of increasing x on the surface of a fluid which is otherwise at rest, are described by the equations:

$$\tilde{h} = A \cos \left[\frac{2\pi}{L}(x - ct) \right] \quad (43)$$

$$\tilde{u} = \left(\frac{2\pi}{L}\right) cA \frac{\cosh [2\pi(z + D)/L]}{\sinh 2\pi D/L} \cos \frac{2\pi(x - ct)}{L} \quad (44)$$

$$\tilde{p} = \rho \left(\frac{2\pi}{L}\right) c^2 A \frac{\cosh [2\pi(z + D)/L]}{\sinh 2\pi D/L} \cos \frac{2\pi(x - ct)}{L} \quad (45)$$

$$\tilde{w} = \left(\frac{2\pi}{L}\right) cA \frac{\sinh [2\pi(z + D)/L]}{\sinh 2\pi D/L} \sin \frac{2\pi(x - ct)}{L} \quad (46)$$

$$c^2 = gD \frac{\tanh 2\pi D/L}{2\pi D/L} \quad (47)$$

$$L = cT \quad (48)$$

where

$2A$ = wave height, trough to crest

L = wavelength

c = phase velocity of waves, relative to the water

$D = \bar{h} - Z$ or mean depth of the water

When $D/L > 1/2$, $\tanh 2\pi D/L = 0.996$, and equation (47) may be stated with sufficient accuracy as:

$$c^2 = \frac{gL}{2\pi} \quad (49)$$

When D/L is small, e.g., $D/L < 1/20$, the function $\tanh 2\pi D/L$ may be represented by the first term in its Taylor series expansion, $2\pi D/L$, and equation (47) takes the form:

$$c^2 = gD \quad (50)$$

Equations (47) and (50) show that the phase velocity of waves decrease when propagated into water of decreasing depth. If a wave crest approaches the shore obliquely, the part of the wave crest in shallow water will travel slower than the part in deep water and the crest will bend in a direction more nearly parallel to the bottom contours. This wave refraction may lead to an increase or decrease in wave amplitude, depending on the bathymetry and concomitant currents.

Equations (47) and (50) also show that the phase velocity is a function of D/L and D . Thus, the phase velocity in the model will correspond, at every point, to the phase velocity in the prototype, but only if both D and D/L in the model correspond at every point to D and D/L in the prototype. A necessary and sufficient condition that D and D/L will correspond to the prototype values in the same manner at each point, is that L be scaled by the same factor as D . In this case, the ratio D/L is the same in both model and prototype.

The ratio, A/L , given in equations (44) and (46) for the velocity components due to waves, will be properly reproduced in the model only if A and L are scaled in the same way. It is not surprising to find that the wave amplitude must be scaled like any other vertical dimension, but this fact does provide a useful bonus.

It is well known that the phase speed in deep water is slightly greater than indicated by equation (49) by a factor which depends on the ratio $(A/L)^2$, and that the phase speed in shallow water is slightly greater than indicated by equation (50) by a factor which depends on A/D ; e.g., see Lamb (1932; Secs. 187 and 250). Dean (1974) showed that, in general, the phase speed of waves is a function of D , A/D , and A/L . Thus, when D , A , and L are scaled by the same factor, the phase speed for waves of finite amplitude is correctly simulated in the distorted wave model. Chu (1975) showed that refraction patterns can be significantly altered by the nonlinear effects due to finite amplitude waves.

The curvature of wave rays, for waves subject to refraction, is given by:

$$\frac{\partial \theta}{\partial s} = - \frac{1}{c} \frac{\partial c}{\partial n}, \quad (51)$$

where θ is the direction of the wave ray, s the distance along the wave ray, and n the distance along the wave crest. Since s and n are horizontal directions, both are scaled in the same manner and refraction patterns and wave amplitudes are properly reproduced.

Equation (50) shows that the square of the phase speed is scaled by the vertical scaling factor. Thus, the phase speed of the model wave is scaled by $\sqrt{\beta}$, which is identical with the scaling factor for currents (eq. 36). Therefore, the effects of currents, water depth, and wave amplitude on wave refraction can be simulated in a distorted scale model, provided the vertical scaling factor is used for wavelengths.

When $D/L < 1/20$, the wavelength has only a minor effect on the phase velocity of waves and it is not necessary to use the vertical scaling factor for scaling waves whenever D/L in the model is less than $1/20$. For the Masonboro model, this corresponds to a ratio of $1/100$ in the prototype.

A predictable error may occur in simulating the effect of refraction and shoaling on wave amplitudes in distorted scale models because of the partial reflection of waves by underwater topographic features.

Attempts to determine the refraction coefficients by measuring changes in wave height along a wave ray may lead to underestimates of the refraction coefficients because the increase in bottom steepness by the ratio β/α will tend to increase the reflection of wave energy by bottom features. Steep slopes are known to be more efficient reflectors of wave energy than gentle slopes. According to Kajiura (1963), the reflection coefficient

for a slope in underwater topography will be the same as that for a vertical discontinuity if $\lambda/L < 1/20$, when λ is the horizontal length of the slope, and the reflection coefficient is near zero if $\lambda/L > 1$. Ippen, Alam, and Bourodimos (1964) presented laboratory data which showed that the reflection coefficient decreases for increasing values of the ratio $2A/L$ for shallow-water waves.

More wave energy is expected to be reflected back to the open sea in the model than in the prototype, but this effect will be smaller in regions of steep waves where the wave amplitude might be expected to affect the wave refraction. Thus, refraction coefficients determined by measuring wave heights in the model may be slightly less than the refraction coefficients applicable to the prototype (the uncertainty here is due to the lack of knowledge about the effect of friction on refraction coefficients in either model or prototype). In general, changes in both wave height and wave direction are simulated with useful accuracy in the distorted scale tidal model, if both horizontal and vertical dimensions of the surface waves are scaled by the vertical scale ratio of the tidal model.

The contribution of radiation stresses to the growth of the mean current for a wave traveling in the x-direction is given by equation (16) in terms of the motions due to waves. A first approximation to the detailed description of wave motions is provided by equations (43) to (48). The component of this contribution in any other direction is given by the product of the component in the direction of wave travel and the cosine of the angle between the direction of wave travel and the desired direction.

Substitution from equations (29) and (43) to (48) into equation (16) shows that the ratio of model radiation stresses to prototype radiation stresses is given by β^2 . The horizontal gradient of the radiation stress, which interacts with the mean flow, must involve the horizontal scale of the mean flow. Thus, the ratio of the gradient of the radiation stress model to prototype is given by β^2/α . This is identical with the ratio of the surface stresses, and shows that with the exception of effects due to reflection, diffraction, and friction, the effects of radiation stresses on the mean flow are correctly simulated in distorted models, if the vertical scaling factor is used as the horizontal scaling factor for surface waves, even though similitude is not obtained for the surface wave field. In many practical cases, the effects of radiation stress on the mean flow are secondary to the effects of both friction and the pressure gradient. Most of the effects of reflection, diffraction, and friction are secondary to the effects of refraction in the modification of surface waves. Thus, the effects of radiation stress on the mean flow can, in most cases, be simulated with good approximation in distorted scale models.

4. Boundary Conditions.

Boundary conditions are easily established at fixed boundaries where no flow occurs. The movable boundary where no flow crosses the boundary may be established in physical models in a natural way. The waterline

moves up and down the beach and across tidal flats as the water level rises and falls. Complete similitude is not obtained because the viscous boundary layer can occupy a substantial part of the thin water layers, less than 2.5 centimeters (1 inch) in thickness above flat beaches and tidal flats in the model but not in the prototype. Surface tension will cause the advancing waterline to develop a prominent convex meniscus in the model but not in the prototype. These are comparatively minor shortcomings of the model and are not expected to produce a significant distortion of the flow away from the affected areas.

Riverflow above tidewater can also be reproduced without difficulty. Tidal flows in rivers or channels leave the model in an upstream direction and create a greater problem. In the physical model of Masonboro Inlet, the effects of inland tidal flows are simulated by means of reservoirs beyond the modeled part of the inlet that accept the excess water during floodtide and return it during the ebbtide. The volume and length of the reservoir and constrictions on the flow can be adjusted as part of the calibration process to improve the agreement of model and prototype tidal heights and currents. Secondary tide generators may be used to impose the boundary condition on some inland tide channels.

An inlet model must also include a small section of the ocean with artificial boundaries. The astronomical tide is simulated in physical models by adding or withdrawing water through diffusers located at the seabed near part or all of the artificial boundaries in the ocean. The waterflow is controlled to reproduce the tidal level at some designated control point which will likely produce the correct total flow through the inlet. This manner of controlling the flow through the inlet is unlikely to have much affect on the currents in the inlet and in inland channels. Generally, the tidal currents in the ocean part of the model are not properly modeled by this procedure. Evidences of eddy formation in the ocean part of the model should be checked by prototype measurements before being accepted as natural features of the flow.

IV. MODELING TIDAL INLETS: NUMERICAL MODELS

1. General.

Numerical models of tidal flows are constructed by representing the elevation of the seabed and free surface above a datum plane, the fluid transport vector or the horizontal velocity vector, and other variables of primary interest, by their numerical values at a discrete set of computation points at discrete times; i.e., the hydrodynamic variables are represented by numerical analogs at selected points in space and time. It is unnecessary to express the value of each variable at each point. Since no physical flows are involved, there is no need to scale any variable. Accounting for the rotation of the earth, atmospheric pressure gradients and prescribed wind stresses do not cause fundamental difficulty, but modeling small-scale processes can be expensive because of the great spatial resolution involved.

The time resolution required for accurate calculations is nearly always greater than needed for the solution of engineering problems, and increases as the resolution in space is increased. A reduction of the space increment by a factor of two, generally also means a reduction in the time increment by a factor of two, and for two horizontal dimensions, an increase in the number of calculations required by a factor of eight. Consequently, small-scale processes are usually simulated in operational numerical models through a parameter relating the small-scale process to a large-scale variable. The representation of friction as a constant multiplied by the square of the velocity is an example of this type of simulation.

Numerical models have the distinct advantage of permitting the elimination of unwanted processes, perhaps useful in determining the relative importance of various related phenomena.

The ability to store a numerical model in a box of punchcards or on a roll of magnetic tape when not needed may also be useful. Since some physical processes must be simulated in numerical models for economy and as the simulation is not exact modeling, calibration is required for numerical models as well as physical models.

Numerical models may be constructed along many lines, and each has advantages and disadvantages. The most common model for two-dimensional hydrodynamic problems (also the one used in both Masonboro Inlet two-dimensional numerical models) is often called a *finite-difference* model. The region of interest is covered with a rectangular grid of equally spaced points in two orthogonal directions. The computation points in this scheme are usually called "grid points" or "mesh points." The distance between grid points is usually the same value, Δs , in both directions. Computations are generally made for constant increments in time, Δt . A variety of numerical models suitable for the study of two-dimensional problems in hydrodynamics was discussed by Roache (1972). Reduced but constant values of both Δs and Δt may be used in some subregions of the basin to provide greater detail.

Natural basins are seldom represented accurately in terms of the rectangular grids preferred for numerical models. Curvilinear boundaries are often represented by line segments and many right-angle corners. Each of these corners becomes the source of false disturbances which may propagate throughout the system. In spite of the disturbances growing from the false corners, useful information has been obtained from models using "stair-step" boundaries.

Jelesnianski (1976) and Wanstrath, et al. (1976) worked with coordination transformations which permit some curvilinear boundaries and unequal space increments to be mapped onto rectangles with constant space increments without significant error. These transformations permit improved representation of the boundary conditions and improved resolution of physical processes where it is most needed.

Approximations of the governing differential equations by the method of finite differences may be solved explicitly or implicitly. Explicit models are based on prediction equations which express the future state of each variable explicitly as functions of present or past values of the same and other variables. Implicit models are based on the simultaneous solution of equations relating past, present, and future states of the variables. Each solution is discussed later in this section.

An alternative model for two-dimensional modeling of hydrodynamic phenomena, called a *finite-element* model, is gaining popularity. For many situations, the finite-element approach permits greater freedom in varying spatial resolution to satisfy the need for detail and an accurate representation of the boundary conditions. The finite-element technique has been discussed by Zienkecwicz (1971), Connor (1972), and Wang and Connor (1975). The finite-element technique has not been used in any of the Masonboro studies reviewed in this report. Hinwood and Wallis (1975a, 1975b) provided a classification scheme for numerical models of tidal waters, along with a concise review of 141 reports on numerical models of tidal basins. Discussions of this report have been provided by Abraham and Karelse (1976) and Abbott (1976).

2. Explicit Prediction Models.

When the differential expressions in the motion equations (1), (2), and (3) are represented by the differences between the appropriate variables at neighboring grid points at the same or nearby times, predictions may be made for a designated grid point "A" at time $t + \Delta t$, in terms of conditions at the same and neighboring grid points at times t and $t - \Delta t$. Each grid point may be considered in turn, by systematically considering each grid point in each row. This procedure, which was used in both two-dimensional models of Masonboro Inlet, produces an *explicit prediction model*.

Explicit prediction models have been found to be useful tools in solving the two-dimensional problems of meteorology and oceanography, and should be equally useful in coastal engineering if the lessons learned by hydrodynamicists in other disciplines are fully utilized.

Some difficulties and pitfalls are inherent in the numerical modeling art. One success may lead to excessive confidence and misuse of the technique, or one failure may lead to distrust of a useful but misunderstood tool.

The best known pitfall in the use of explicit prediction numerical models is the development of computational instability when $\Delta t/\Delta s$ is too large. Computational instability, which makes its presence known by a growth in the mechanical energy as computed by the model when no corresponding growth of energy is expected in the prototype flow, may also arise from the nonlinear terms in the equations or from the boundary conditions.

Other difficulties are associated with the development, in the model, of spurious waves which have no counterpart in the prototype, and a ratio of phase speed in the numerical model to phase speed in the prototype which is less than unity. Both of these difficulties are most serious when the ratio of $L/\Delta s$ is small, where L is the wavelength of the disturbance.

Round-off error which is due to the calculations made with a finite number of significant digits, may become significant after some large, but finite number of time steps.

Serious growth of errors due to any of these causes can often be avoided by additional programing, and misinterpretation of the errors that occur can also be avoided by understanding the nature and cause of the errors. Therefore, each of these difficulties is discussed here in detail to indicate probable trouble areas and the possible need for corrective procedures, not to teach construction of perfect numerical models. The computational stability problem has been discussed by Haltner (1971, Chs. 5 and 12) in an introductory text in numerical weather prediction for meteorologists.

The following discussion of computational problems is designed to permit the engineer to exercise some qualitative judgment about results obtained with numerical models in general and explicit prediction tidal hydraulic models in particular.

a. Fourier Series Representation. Any function which is specified only for $2N$ discrete values of x can be expressed without loss of accuracy as:

$$\psi(x) = \sum_{n=0}^N a_n \cos \left(\frac{2\pi n \Delta x}{2N \Delta x} \right) + b_n \sin \left(\frac{2\pi n \Delta x}{2N \Delta x} \right), \quad (52)$$

where $x = n \Delta x$, and a_n and b_n are constants which can be determined from the tabulated data by standard techniques. This expression yields $N + 1$ values of a_n , and $N - 1$ values of b_n . Values for b_0 and b_N are not needed because $\sin (2\pi n \Delta x / 2N \Delta x)$ vanishes for $n = 0$ and $n = N$. Equation (52) may be rewritten as:

$$\psi(nox) = \sum_{n=0}^N A_n \cos \left(\frac{n\pi}{N} - \phi_n \right), \quad n = 0, 1, 2, \dots, N, \quad (53)$$

where

$$A_n^2 = a_n^2 + b_n^2$$

$$\phi_n = \tan^{-1} \frac{b_n}{a_n}.$$

Equation (53) shows that $\psi(x)$ is fully described by the mean value and harmonics of the interval $2N\Delta x$. Thus no perturbation in $\psi(x)$ with a characteristic length less than $2\Delta x$ can be identified in the available data. Any perturbation with a wavelength $(2 - \epsilon)\Delta x$, where $\epsilon < 2$, which does exist in $\psi(x)$, will appear in the tabulated data to have a wavelength of $(2 + \epsilon)\Delta x$ (Fig. 2). In the figure, wavelengths shorter than $2\Delta x$ appear in the plotted data as having a longer wavelength. This is known as a *long wave alias*.

In many two-dimensional models, it is possible for waves to be organized along a diagonal of the computational grid squares. These waves can be recognized in the computations only by projections on the computational lines. Consequently, a wavelength of $2\Delta s$ traveling along a diagonal will appear to have a wavelength of $\sqrt{2}\Delta s$, and will be aliased into a wavelength of $[2 + (2 - \sqrt{2})]\Delta s = 2.586\Delta s$. The length used for the space averaging, needed to separate the tidal scale flow from perturbations (discussed in Sec. 2 and App. B), must exceed $2\sqrt{2}\Delta s$. However, the critical length may be different in some models.

An early explanation of computational instability in explicit finite-difference numerical models, although not entirely rigorous but provides much insight and nearly always leads to the correct conclusion, is based on the concept that in any physical system it is possible for conditions at any designated point A to be affected by events at a second point B, in the time interval required for energy to travel from B to A by the fastest wave which the physical system permits. This principle also applies to explicit finite-difference numerical computation models where the term "physical system" is replaced by "numerical model." Correct predictions cannot be expected from a prediction equation which does not include all of the information which can affect the outcome of the prediction. This means that the time interval, Δt , involved in a prediction must not exceed the time required for the fastest wave to travel from the boundary of the influence region, to the point for which the prediction is made. For physical models the outer limit of the influence region will coincide with the circle of radius, r , centered on A, where

$$r = \Delta t c_{max} ,$$

and c_{max} is the speed of the fastest wave which the system can support. For one-dimensional numerical models the extreme limits of the influence region are given by:

$$x = A \pm \Delta t c_{max} .$$

In numerical finite-difference models, it is generally convenient to use the constant space increment, Δs , for both horizontal directions. This procedure was followed in both of the modes involved in this study. Thus, for one-dimensional numerical models the time increment, Δt , must not exceed $\Delta s/c_{max}$. When two-dimensional numerical models are considered, it is necessary to recognize the possibility of plane waves traveling

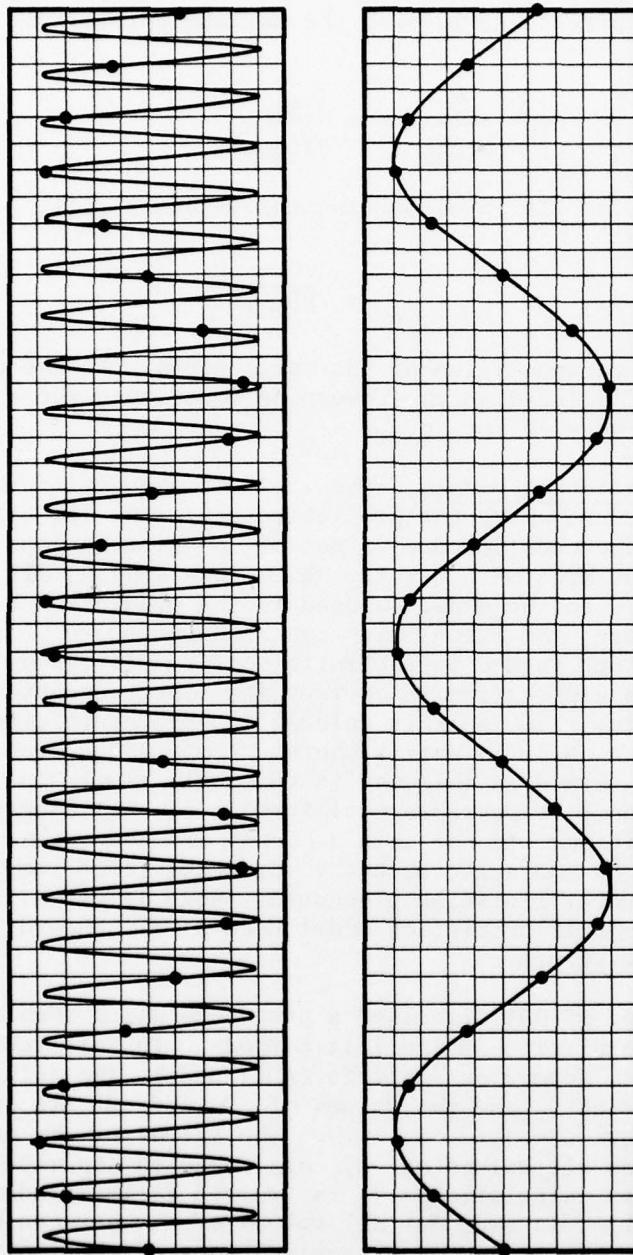


Figure 2. An example of aliasing. When the values of the function represented by the upper curve are known only at the large dots, as in a tabulation with an interval of this size, the values are indistinguishable from a similar tabulation of the function represented by the lower curve.

along a diagonal of the computation matrix. In this case, a wave front which coincides with one diagonal of the computational square will generally travel to the nearest computational point on the other diagonal, at a distance of $(1/2) \sqrt{2} \Delta s$ in a time interval Δt . For explicit two-dimensional, finite-difference models, the maximum permissible value of Δt is given by:

$$\Delta t \leq \frac{\sqrt{2}}{2c_{max}} \Delta s = \frac{\Delta s}{\sqrt{2}c_{max}} .$$

For tidal hydraulics models involving incompressible fluids, c_{max} is generally given by:

$$c_{max} = \sqrt{gD_{max}} , \quad (55)$$

where D_{max} is the maximum value of the total depth. If the compressibility of water was included in the governing equations, the speed of sound would have to be used for c_{max} .

b. Implicit Prediction Models. The implicit prediction model is an alternative procedure where the prediction equations for all variables at all grid points are considered as a set of N simultaneous equations in N unknown values at time, $t + \Delta t$. With this scheme, all of the information available to the model is used in the prediction for each grid point. Therefore, the calculation can be expected to be unconditionally stable without regard to the ratio $\Delta t/\Delta s$. It can be shown rigorously that this expectation is correct for linear equations with constant coefficients. The implicit calculation procedure results in an equation involving an N by N matrix where N may range from 1,000 to 10,000. The matrix formed in this way is unusually simple and is generally of the tridiagonal or pentadiagonal form; i.e., all elements more than one or two positions off the main diagonal are zero. The solution is usually obtained by iterative methods. Sielecki (1968) reported an investigation of several iteration procedures, none of which led to an economy over the explicit prediction model used as a standard in an investigation of storm surges.

Roache (1972, pp. 87-95) discussed a procedure which combined some advantages of both explicit and implicit methods. In this technique, called an *alternating direction implicit* (ADI) model, the values of h are computed at $t = n\Delta t$, and the values of U and V are computed for $t = (n + 1/2)\Delta t$, where $n = 1, 2, 3, \dots$. The values of h and U for future times, and for all values of x , are computed separately for each value of y . In this calculation, V is treated as independent of time. An implicit calculation is made for all values of x between boundaries at that value of y . Two independent applications of the implicit integration procedure will be made if, for that value of y , there is an obstruction to the flow, as by an island, with water on both sides. When all calculations for U are completed, the operation is repeated for V and h , assuming that U is independent of time, and considering each

value of x as one or more independent problems. This procedure permits the use of longer time steps for a given space increment and may be used to reduce the cost for a given space resolution, or to provide more resolution in space at a fixed cost. In general, this procedure provides less resolution in time and less accuracy for identical space resolution.

The loss in time resolution and accuracy is trivial in many applications but significant in others. No models of this type were included in the Masonboro Inlet comparison project, but Butler and Raney (1976) apply this procedure to the Masonboro data. They report acceptable results with time steps 30 times longer than would be permissible with a purely explicit model and reduction in running time by a factor of 15.

Leendertse (1967, 1970) has been a leading advocate of implicit and hybrid models in the solution of hydrodynamical problems of the coastal region. He has cited the unconditional stability of the solutions, demonstrated for linearized equations as the reasons for this preference. However, Weare (1976) showed that the nonlinear terms used by Leendertse in his numerical model but not in his computational stability test, can lead to instability in many practical applications. The destabilizing effects of nonlinear terms in the prediction equations are discussed later. Leendertse and Liu (1975b) stated that an explicit prediction scheme was used in their latest model. Butler and Raney (1976) acknowledge the tendency for nonlinear instability in their model and reduce the growth of the instability by the use of numerical filters which selectively dampen the short-period oscillations which make the greatest contribution to the growth of instability.

Sobey (1970) compared four finite-difference schemes widely used in the analysis of tidal flows in the coastal region and showed that each underestimates the phase speed of the waves. The extent of the underestimation decreases with decreasing values of the ratio $\Delta s/L$, where L is the wavelength. Haltner (1971, Ch. 6) showed that the simple numerical schemes that are most satisfactory in other respects generally underestimate the phase speed. Even the sign of the phase speed may be reversed in some models when $L = 2\Delta s$, but the error is small when $L > 20\Delta s$. Schemes which give excessive phase speeds can be developed. Roache (1972) discussed a scheme in which a correct mean phase speed is maintained by alternating between procedures which underestimate or overestimate the phase speed.

Haltner (1971, Ch. 6) showed that some simple computational schemes, which are otherwise satisfactory, generally yield two wavelike solutions: (a) The physical mode which corresponded to the prototype wave, and (b) the computation mode which moved in the opposite direction to the prototype wave and changed phase with each time step. Computational modes are not present in all models; however, when present, the wave amplitude required to satisfy initial conditions is divided between the two modes. The computational mode may be dominant when $L = 2\Delta s$. Relative amplitude of the computational mode decreases for longer waves. The computational mode may be negligibly small for $L > 10\Delta s$.

If the product of $\psi(x)$ and $F(x)$ appears in the modeling equations, $\psi(x)$ may be expressed as in equation (53), and $F(x)$ may be expressed as:

$$F(x) = \sum_{n'=0}^N B_{n'} \cos \left(\frac{n' \pi}{N - \theta_{n'}} \right). \quad (56)$$

The product, $\psi(x) F(x)$, may be expressed as:

$$\psi(x) F(x) = \sum_{n=0}^N \sum_{n'=0}^N A_n B_{n'} \cos \left(\frac{n \pi}{N - \phi_n} \right) \cos \left(\frac{n' \pi}{N - \theta_{n'}} \right), \quad (57)$$

$$n, n' = 0, 1, 2, 3, \dots N.$$

A well-known trigonometry identity may be used to transform equation (57) into

$$\begin{aligned} \psi(x) F(x) = \left(\frac{1}{2} \right) \sum_{n=0}^N \sum_{n'=0}^N A_n B_{n'} \left\{ \cos \left[\frac{(n - n') \pi}{N - (\phi_n - \theta_{n'})} \right] \right. \\ \left. + \cos \left[\frac{(n + n') \pi}{N - (\phi_n + \theta_{n'})} \right] \right\}. \quad (58) \end{aligned}$$

All terms of the type $(n - n') \pi / N$ may be expressed in the form $j \pi / N$, where $j \leq N$. Thus, each of these terms corresponds to a harmonic of the computation region which is adequately represented by the model. When the terms involving $n + n'$ are expressed in the same manner, j may exceed N , if either n or n' exceeds $N/2$. Equation (58) describes a flow of momentum from the perturbations of largest size into perturbations of both greater and shorter wavelengths. This is a natural process which is not well described by the numerical models. Perturbations with wavelengths greater than $2\Delta s$ can be properly represented on the computational grid; perturbations with wavelengths less than $2\Delta s$ cannot be properly represented and will be aliased, so that they appear with wavelengths longer than $2\Delta s$. The error arising in this manner in a single time step is generally small, and many time steps may be required for a significant error to develop; however, errors from this process may ultimately destroy the validity of the solution. This growth of errors may be reduced by the use of digital filters designed to reduce or eliminate all irregularities with wavelengths of $4\Delta s$ or less from the data before forming products. More elaborate filtering procedures are required for long prediction times than for short prediction times.

Round-off error first appears in the least significant digit of the numbers representing any of the variables. The occurrence of round-off error is basically random. Thus, sign changes are frequent, the wavelengths and periods are short. Wavelengths of $2\Delta s$ and periods of $2\Delta t$

are most common. Round-off errors grow if the computation scheme is in any way unstable. The growth may be exponential with the number of time steps. With modern computers having a word length of 32 bits or more, several hundred, or sometimes several thousand time steps are usually required before round-off error becomes significant. Round-off error can generally be reduced by increasing the word length used in the calculations. The growth of round-off error will ultimately overcome the effect of a straightforward reduction of the space increment, Δx , in improving the accuracy of the calculations, especially when minicomputers with short word lengths are used. However, large numbers of calculations are generally cheaper on modern computers with long computational word lengths, so the difficulty here may be more a matter of convenience than economics and can often be solved by using a computer with a longer computational word. The total cost of the computation will increase when increased accuracy is obtained solely by a reduction in the grid increment.

Finite-difference equations are formed by using finite differences to approximate the differentials which appear in the governing differential equations. The error resulting from this approximation is called the *truncation error*, and can be estimated as shown below. In forming an expression for $\partial y / \partial x$, at $x = n\Delta x$, y is expanded as a Taylor series around $n\Delta x$. Thus,

$$y(n\Delta x + \Delta x) = y(n\Delta x) + y'(n\Delta x) \Delta x + \left(\frac{1}{2}\right) y''(n\Delta x) \Delta x^2 + \dots$$

By rearranging terms,

$$\left. \frac{\partial y}{\partial x} \right|_{n\Delta x} = \frac{y(n\Delta x + \Delta x) - y(n\Delta x)}{\Delta x} + \epsilon_1,$$

where

$$|\epsilon_1| = \left. \frac{1}{2} \frac{\partial^2 y}{\partial x^2} \right|_{n\Delta x} \Delta x + \dots$$

The above equation is of first order because it depends on the first power of Δx . An approximation which is accurate to second order, e.g., the error depends on the second power of Δx , may be formed by combining expansions for $y(n\Delta x \pm \Delta x)$ to obtain:

$$\left. \frac{\partial y}{\partial x} \right|_{n\Delta x} = \frac{y(n\Delta x + \Delta x) - y(n\Delta x - \Delta x)}{2\Delta x} + \epsilon_2,$$

where

$$|\epsilon_2| = \left. \frac{1}{3} \frac{\partial^3 y}{\partial x^3} \right|_{n\Delta x} \Delta x^2.$$

Higher ordered approximations may be derived by considering more values of y and eliminating more derivatives from the resulting expansions. By assuming that y has the form,

$$y = \cos \left(\frac{2\pi m}{L} \right) x ,$$

higher ordered approximations can be shown to give better estimates of the derivatives when the wavelength is long relative to the interval used in defining the derivatives. However, for the shortest waves supported by the system, the use of higher ordered approximations may lead to less accurate estimations of the derivatives than low-ordered approximations.

c. Error Control. Numerical models contain many sources of errors. Nearly all originate with small-scale perturbations that cannot be resolved on the computational grid, or with the smallest perturbations that can occur in the grid. The probability of significant errors from any source, other than round off, can be reduced by reducing the space increment, Δs , to obtain a better resolution of the phenomena being studied. Increasing the resolution will increase the number of time steps required, thus increasing the cost of the calculation and increasing the probability that round-off error will become significant.

The probability of significant error may also be reduced by removing the small-scale phenomena from the governing equations and the boundary and initial conditions at the beginning of the calculation. Since the product of two variables may contain perturbations of smaller scale than either variable, the stability of the calculations can often be improved through the use of smoothing or filtering operations at various times during the calculations. Even when errors cannot be entirely eliminated, it may be helpful to know that the large-scale features are more nearly correct than small-scale perturbations. Small-scale errors due to faulty boundary conditions are often no more than 2 or 3 Δs in length; therefore, since the phase speed in the numerical model is an increasing function of $\Delta s/L$, the errors only slowly propagate into the interior of the computation region. Thus, the solution tends to be more reliable near the center of the computation region, and least reliable near boundaries where the true boundary condition may be unknown, or not properly represented on the computational grid. The Masonboro Inlet numerical models have been used only for a study of tide propagation into the inlet-bay system. The length of the tide wave is many times the length of the basin considered.

Initially, the flow variables contained no short wave perturbations. The phase speed of tide wave in the model should have been within 1 to 2 percent of the prototype speed. Although the computational mode does not appear in any of the models used in this study, the success of the model in reproducing tidal flow should not lead to an assumption, without further examination, that the same models will provide satisfactory solutions for a study of harbor oscillations, where prominent oscillations with

short wavelengths when compared to the entire basin may occur, although both phenomena are governed by the same differential equations. With extended operation of the tidal cycle in the Masonboro model, the solution can be expected to deteriorate due to nonlinear interaction of the tide with small features of the basin. The model should perform better in bays with more regular coastlines and which are larger relative to the space step employed. Thus, the model may perform better when applied to Galveston Bay, Apalachicola Bay or the North Carolina sounds than when applied to Masonboro Inlet.

d. Selection of Terms for Numerical Modeling and Representation. Even if the numerical modeling was accomplished in an ideal manner, the model could give incorrect results if important physical processes are omitted, or improperly represented in finite-difference form. The importance of various physical processes was discussed in Section II. Difficulties in modeling or simulating these processes in numerical models are discussed below.

Nonlinear numerical models always require more computer time than linear models with the same resolution, although in some cases the increase may be small. Adding nonlinear terms to a linear numerical model always increases the probability of computational instability. There is a distinct advantage in linearizing the governing equations unless a significant reduction in error can be expected to result from including the nonlinear terms. Specification of the conditions and procedures which justify linearization in numerical models is an essential purpose of this discussion.

The first term in equation (1), $\partial U / \partial t$, is clearly linear and requires no additional discussion.

The second term in equation (1) may be rewritten as:

$$gD \frac{\partial \bar{h}}{\partial x} = g(h_1 - Z) \left[1 + \frac{\bar{h} - h_1}{h_1 - Z} \right] \frac{\partial \bar{h}}{\partial x}, \quad (59)$$

where h_1 is the mean sea level (MSL) or mean water level over an interval much longer than any prominent period of the phenomena being modeled. The product,

$$\left[\frac{(\bar{h} - h_1)}{(h_1 - Z)} \right] \frac{\partial \bar{h}}{\partial x}, \quad (60)$$

is quadratic in \bar{h} . If $(\bar{h} - h_1) \ll (h_1 - Z)$ everywhere, neglecting the quadratic term will not lead to serious error. Neglecting this term may be desirable if $(\bar{h} - h_1) < (h_1 - Z)$ everywhere and much less at all but a few isolated points, or much less everywhere but the line of grid points nearest the shore. The quadratic term in \bar{h} is sometimes neglected in the study of tidal flow within fixed boundaries. Neglecting the quadratic

term when $(\bar{h} - h_1)$ and $(h_1 - Z)$ are of the same order of magnitude over any substantial area of the basin may lead to significant error.

The quadratic term cannot be neglected in models where boundaries move inland with rising water. This nonlinear term is included in both Masonboro models because it is necessary to account for the flooding of tidal flats in the model.

The bottom stress, term (c) in Section II, must be explicitly stated as input information from an external source or simulated as a clearly defined function of the physical variables in numerical models. The technique of implicit simulation by adding artificial roughness to the boundaries used with physical models is not available.

The usual procedure is to express the bottom stress as:

$$(\tau_{zx})_Z = K|q|^2 \cos \theta, \quad (61)$$

where q is the magnitude of the vertically averaged velocity, θ the angle between the velocity and the x -axis, and K a coefficient assumed to depend on bottom roughness. The bottom stress is often expressed in the algebraically equivalent form of equation (4). In early models, K was taken as a constant throughout the model. This saved computer space and was a convenient choice while developing the more important aspects of the model. In general, the calculations are not very sensitive to the value of K . In many other models developed for modern computers where storage space is not a premium, K has been treated as a function of position; i.e., a different value of K may be used for each grid point. The coefficient, K , may be taken initially as a decreasing function of depth and later modified on a point by point basis as needed for model calibration. Masch, Brandes, and Reagan (1977) follow this procedure in a model of Masonboro Inlet.

Reid (1957) analyzed channel flows subject to wind action, and showed that the value of K when used as in equation (4), is a function of wind stress as well as bottom roughness. Harris (1967) reported that Reid's formulation of the bottom friction term gives better predictions for hurricane storm surges on the open coast than could be obtained with the form of equation (61). This formulation is nonlinear and tends to produce a growth of small-scale perturbations with the associated aliasing problems if the running time for the model is large, unless eliminated by the application of a smoothing operation. Many investigators, e.g., Dronkers (1964), introduced heuristically derived linear friction laws when working with equations that were otherwise linear. However, the quadratic friction law does not have a rigorous justification, (see Sec. II).

Jelesnianski (1967) expanded on a development by Platzman (1963) to show that a linear friction law could be derived for geophysical flows in a more rigorous manner than that used in deriving the more widely used quadratic law, and that the application of this law permitted a significant improvement in hurricane storm surge predictions along the open coast over those obtained with Reid's (1957) friction law.

Jelesnianski, in developing his friction law, recognized that bottom friction is a result of a vertical diffusion of momentum, and that diffusion requires finite time, more time being required for greater depths. Because of the earth's rotation during the diffusion time, the stress vector at the bottom is not generally parallel to the mean flow. However, for short-time periods and shallow water, the bottom-stress vector is nearly parallel to the mean flow. In general, the velocity does not vanish outside the viscous boundary layer near the bottom.

The bottom stress in Jelesnianski's model is expressed as:

$$\left. \frac{\nu \partial(u + iv)}{\partial z} \right|_{z=Z} = s_\ell (u + iv) \Big|_{z=Z}, \quad (62)$$

where

ν = effective viscosity coefficient

u, v = velocity components

i = $\sqrt{-1}$

s_ℓ = slip coefficient

Thus, the Jelesnianski friction law is linear in the flow values but requires two coefficients. Jelesnianski (1967) reported that the solution is less sensitive to the exact values of the coefficients ν and s_ℓ , than it is to the exact value of K when equation (4) or (61) is used to simulate the bottom stress term. Forristall (1974) extended the analytical path of Platzman (1963) and Jelesnianski (1967) to provide a model for computing the vertical profile of the horizontal currents at selected locations without the expense of using a three-dimensional grid.

The stress at the free surface is normally attributed to the wind and must be supplied explicitly to the computer routine used for the calculations of water motions. The application of an arbitrary wind-stress field to the numerical model does not cause any difficulty unless the wind-stress field contains small-scale features that cannot be properly represented at the grid scale used. Wind stress was considered by Masch, Brandes, and Reagan (1977) in the model of Masonboro Inlet. The ability to impose a wind-stress field on the equations of motion for waterflow is a prime reason for adopting numerical models for the study of coastal phenomena.

Wind stress is a secondary aspect of most inlet problems and a consideration of wind-stress effects was not part of the specifications for the Masonboro Inlet study. Therefore, the problems of developing the wind-stress field from the available meteorological data are not discussed in this study.

In physical models the advective terms, (e) of Section II,

$$\frac{\partial}{\partial x} \frac{U^2}{D} + \frac{\partial}{\partial y} \frac{UV}{D},$$

are always treated implicitly without any special attention by the experimenter. However, the terms appear in numerical models only if they are explicitly expressed. These nonlinear terms may be improperly represented in numerical models unless an effort is made to eliminate the generation of perturbations too small for proper representation on the calculation grid. The physical importance of these terms was discussed in Section II, and must be included if omission is likely to produce a significant error. The terms were included in the most successful of the Masonboro models (Masch, Brandes, and Reagan, 1977), but were expressed approximately as:

$$\frac{U}{D} \frac{\partial U}{\partial x} + \frac{V}{D} \frac{\partial U}{\partial y}.$$

Butler and Raney (1976) and others also used these incomplete forms, but the advective terms were omitted by Chen and Hembree (1977). The representation of the advective terms in the form used by Masch, Brandes, and Reagan would represent an improvement over their omission in some but not all practical conditions. This problem requires more study for a definitive evaluation.

Three effects of the earth's rotation (Coriolis acceleration) on tidal flows were discussed under term (e) in Section II, 3. The most important effect in modeling flows of tidal period is the continual acceleration of the current to the right of the existing current direction in the Northern Hemisphere and to the left in the Southern Hemisphere which can be reproduced in numerical models without great difficulty. This feature is included in all large-scale numerical weather models. The effect of Coriolis acceleration in producing a rotation of the mean current with increasing depth and the effect of Coriolis acceleration turbulent stress have been successfully modeled by Platzman (1963), Jelesnianski (1967), and Forristall (1974). The authors are not aware of any experiments in which the generation of the inertial circle was simulated as an incidental feature of the calculation of tidal or storm surge flows. It is assumed that effects of the inertial circle on the mean flow cannot be simulated by means of parameters and mean flow variables unless the averaging period extends over many days.

The possibility of including the atmospheric pressure gradient effect (term (g) in Sec. II, 3) in a straightforward manner is a minor, but sometimes significant advantage of numerical models of water motions in the coastal zone. When atmospheric pressure is considered, the essential information must be explicitly supplied as input data. The atmospheric pressure gradient acts as a correction to the surface slope term. When pressure information is available, it may be treated in the same manner as the slope term with regard to linearization.

Each term in equation (2) is analogous to a corresponding term in equation (1) and all terms in equation (3) are well specified and linear. Thus, no additional discussion of the principal terms is required. In numerical models, as in physical models, it is impossible to treat the perturbation processes explicitly; however, simulation of the most important effects of the small-scale processes on the large-scale flow is often practical.

Turbulent stresses act to smooth irregularities and eliminate sharp gradients in the prototype flow. Smoothing operators accomplish the same effect in numerical models. In many cases, the large-scale flow is not highly sensitive to the amount of smoothing involved. Occasionally, it is necessary to increase the amount of smoothing in some part of the model to obtain a good reproduction of the flow. Overland and Myers (1976) reported on a one-dimensional model of the Cape Fear River, North Carolina, in which the horizontal current over the tidal flats was related to the flow in the main channel through an eddy viscosity term in a form which is equivalent to writing equation (11) as:

$$S_{xt} = A_{yx} \frac{\partial \bar{u}}{\partial y} . \quad (63)$$

Leendertse and Liu (1975a) described a three-dimensional numerical model in which the stress terms are represented by horizontal and vertical eddy-stress coefficients of the type described by equation (13).

The radiation stresses are generally considered in investigations of wave-generated currents. Numerical models which combine calculations of wave refraction and radiation stresses for the calculation of nearshore currents have been reported by several investigators, e.g., Noda, et al. (1974). Liu and Mei (1975) considered refraction diffraction and radiation stresses near a breakwater. No numerical model is known in which the effect of waves on tidal currents in an estuary has been considered.

e. Boundary Conditions. Boundary conditions are easily applied for fixed boundaries with zero flow normal to the boundary in both physical and numerical models. Movable boundaries are more difficult to treat in numerical models than in physical models. Most aspects of the numerical modeling of geophysical hydrodynamic phenomena have been extensively treated by meteorologists interested in numerical weather prediction, or other scientists interested in basic research. Numerical modeling of boundaries which change in location due to tidal fluctuations is an exception. The only treatment used in the Masonboro model studies as part of the General Investigation of Tidal Inlets (GITI) is the procedure reported by Reid and Bodine (1968). Modifications of this procedure were used in both two-dimensional models of Masonboro Inlet. The boundary location in the numerical model is allowed to change discontinuously by the distance Δs in either direction, as the water rises above or falls below designated critical values which depend on the elevation of the land surface surrounding a grid point. No theoretical evaluations of this procedure are known. The scheme is described by Masch, Brandes, and Reagan (1977).

Riverflows above tidewater cause no great difficulties in either physical or numerical models. Tidal flows in rivers or channels leaving the model in an upstream direction cause difficulties in both numerical and physical models. The method of treating these inland tidal boundaries adopted for the physical model could have been applied in the numerical models, but this would have required detailed calculation of the water motions in the fictional reservoirs and in the tidal channels and would have been more expensive for the numerical than for the physical models. Masch, Brandes, and Reagan (1977) simulate tidal records at the internal water boundaries in the form of amplitude and phase changes applied to the open ocean tide. Chen and Hembree (1977) simulate these internal boundaries by extrapolation from the interior of the computation region. The relative merits of the two basic expressions which can be used for open water boundaries were discussed by Reid (1975) and Forristall (1975). It appears that no available procedure for dealing with open water boundaries in numerical models is ideal; however, the procedure used by Masch, Brandes, and Reagan (1977) may be preferable to that used by Chen and Hembree (1977).

Both numerical and physical models of inlets require artificial boundaries around a small part of the ocean. In both models the information required for controlling the flow is provided by specifying the tidal height, as a function of time, at a specified point. Currents in the numerical models are controlled by the slope of the water surface near the artificial boundary. Masch, Brandes, and Reagan (1977) and Chen and Hembree (1977) use different expressions for this purpose. The expressions by Reid (1975) and Forristall (1975) applied to the tidal channels and to the open water conditions in the ocean.

Controlling the currents by the computed slope of the water surface in numerical models is less restrictive than the procedure used for physical models, since tidal currents parallel to the shore can develop. Cotidal charts, which give the relative phase of the tide over an entire ocean basin, generally show that the tide wave travels parallel to the shore, indicating that tidal currents should have a component parallel to the shore. However, the cotidal chart by Defant (1961) showed that much of the U.S. Atlantic coast is an exception, and that tidal currents parallel to the shore are not expected near Masonboro. Thus, the possibility of predicting tidal currents parallel to the shore is not as important for Masonboro Inlet as for other inlets, or as important for tidal problems as for storm surge models.

V. A LUMPED PARAMETER MODEL

1. General.

The design engineer or researcher frequently needs a simple model to get a "first look" at inlet hydraulics. The model should be easy to use, inexpensive, require a minimum number of input parameters, and give

reasonable results quickly. As in other mathematical or physical models, this model is optimized by adjusting the input data to simulate known conditions.

A mathematical model for tidal inlets, designed to meet these criteria, is the "lumped parameter inlet model" proposed by Keulegan (1967). In the lumped parameter model, all coefficients which could be adjusted to improve model performance were combined into a single parameter.

The original development was based on the consideration of a minimum number of terms which might possibly provide useful results for the simplest cases, and a recognition that the bottom roughness could not be determined accurately without a detailed investigation. Manning's n may be uncertain by a factor of two. Thus, many secondary terms may be neglected without a significant increase in the uncertainty of the calculations.

The Keulegan model has led to satisfactory resolution of many inlet problems. In other applications, the results obtained with the Keulegan model have been unsatisfactory. The model has been extended by Huval and Wintergerst (1977) and others by adding new terms to permit extension of the model to general conditions.

The equations by Keulegan to describe the model and the definition sketch (Fig. 1 in Keulegan, 1967) are inconsistent.

Physical insight for the dominant control of tidal flows in many inlets may be gained by a revision of the definition sketch shown in Figure 3(a).

The original figure in Keulegan (1967) identified only two points in a horizontal plane: the boundary between the sea and the inlet, x_2 , and the boundary between the bay and the inlet, x_1 . The figure and equations by Keulegan seem to imply that the pressure gradient from x_2 to x_1 is responsible for the acceleration required to produce the inflow velocity at x_2 during floodtide, and that the pressure gradient from x_1 to x_2 is responsible for the acceleration required to produce the inflow velocity at x_1 during ebbtide. However, this is not physically possible.

If two additional positions, x_0 and x_3 , are postulated (Fig. 3,b), a lower slope from x_3 to x_2 (Keulegan's ΔH_1) can produce the acceleration required to generate the flood currents, and the slope between x_2 and x_1 (Keulegan's ΔH_2) could exactly balance the friction and kinetic energy terms as he has postulated. To apply the same logic on ebbtide, it is necessary to assume that the acceleration required for the ebb current is generated by the slope from x_0 to x_1 (Fig. 3,c). This approach is excellent for presenting the concept that in many inlets, the slope through the inlet is approximately balanced by friction within the inlet, and in many situations will permit a simple and useful first approximation to inlet flows.

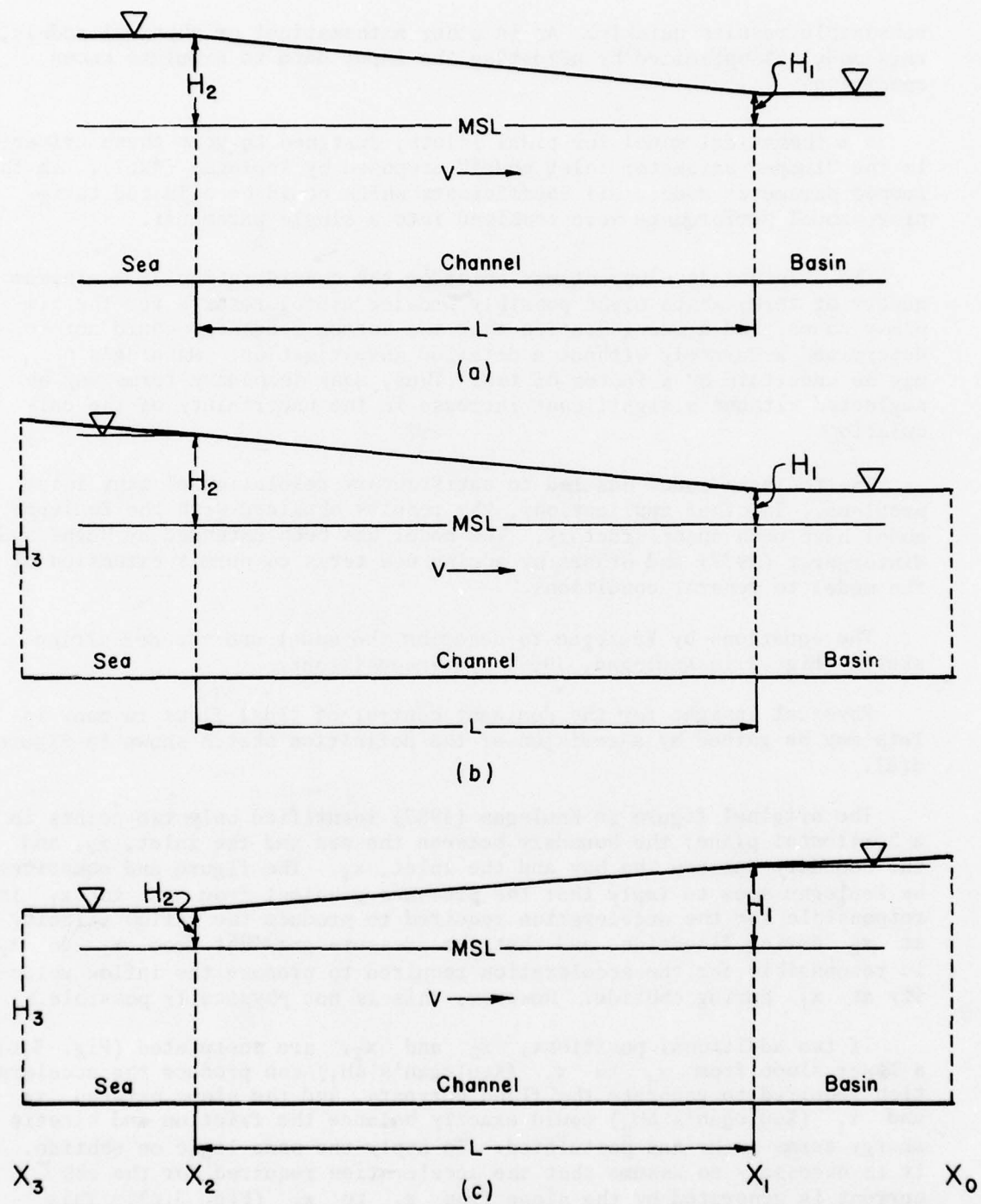


Figure 3. Gradient of water surface over channel: (a) as presented by Keulegan (1967), (b) as modified floodflow conditions, and (c) as modified ebb flow conditions.

However, this interpretation does not provide a satisfactory approach to generating improvements to the first approximation, since it does not permit a straightforward application of the equation for the conservation of energy, momentum, and mass.

If the purpose of the model is quantitative calculations, the figure appears to be correctly drawn and the equations appear to be missing several terms which are negligibly small in many practical applications, but important in others. Most of the material in this section was developed on this assumption.

A more rigorous development than that originally employed, which clearly shows the implicit assumptions used by Keulegan (1967) and by Huval and Wintergerst (1977) may be developed by integrating the one-dimensional equations of motion from the open sea to the bay or lagoon. This approach discloses the terms omitted in the original equations. In many applications these terms do not have a significant effect on the calculated results, but are important in others. The one-dimensional equations of motion are developed in Appendix C by integrating the two-dimensional equations of motion with respect to y from one side of a channel, $y_1(x)$, to the other side of the channel, $y_2(x)$.

The resulting equations (B13) and (B14) in Appendix B may be stated as:

$$\frac{\partial \bar{u}}{\partial t} + \frac{1}{2} \frac{\partial \bar{u}^2}{\partial x} + g \frac{\partial \bar{h}}{\partial x} + \frac{1}{A_c} \int_{y_1}^{y_2} (\tau_{zx})_Z dy = \frac{1}{A_c} \left[R_c - \bar{u} \int_{y_1}^{y_2} (R + E) dy \right], \quad (64)$$

$$\frac{\partial \bar{D}}{\partial t} + \frac{\partial \bar{D} \bar{u}}{\partial x} = b^{-1} \int_{y_1}^{y_2} (R + E) dy - \frac{\bar{D}}{b} \left[\frac{\partial b}{\partial t} + \bar{u} \frac{\partial b}{\partial x} \right], \quad (65)$$

where

$$A_c(x, t) = \int_{y_1}^{y_2} D dy$$

is the cross-sectional area of the inlet at position x along the channel at time, t ,

$$\bar{u}(x, t) = A_c^{-1} \int_{y_1}^{y_2} U dy = A_c^{-1} \int_{y_1}^{y_2} \int_{\bar{z}}^{\bar{h}} u dz dy.$$

Thus, $u(x,t)$ is the average of $u(x,y,z,t)$ in that cross section,

$$R_c = - \frac{\partial}{\partial x} \int_{y_1}^{y_2} [\bar{D}(u'')^2 + 2\bar{u}D''u'' + D''(u'')^2] dy \\ - \int_{y_1}^{y_2} D'' \frac{\partial h''}{\partial x} dy + \frac{1}{\bar{\rho}} \left[b(\overline{\tau_{zx}})_h - A_c \frac{\partial \bar{p}_h}{\partial x} \right],$$

$$u''(x,y,z,t) = u(x,y,z,t) - \bar{u}(x,t),$$

$$\bar{h}(x) = b^{-1} \int_{y_1}^{y_2} \bar{h}(x,y) dy,$$

$$D = \frac{A_c}{b},$$

$$\bar{h}'(x,t) = \bar{h} - \bar{h},$$

$$D'(x,y,t) = D - \bar{D},$$

and

$$b(x) = y_2 - y_1 \text{ width of channel.}$$

R_c contains all terms which appear when the one-dimensional momentum equation is derived, without approximation, from the three-dimensional equations, but which are generally neglected in the one-dimensional momentum equation.

The right-hand sides of equations (64) and (65) are closure terms, normally neglected in dealing with the one-dimensional equations of motion. These terms are generally small and are given primarily for completeness, but several of the terms can be locally significant. The physical processes which the terms represent were discussed in Section II. None of the terms were considered in the lumped parameter models of Keulegan (1967) and Huval and Wintergerst (1977).

In most applications, the displacement of the free surface is assumed infinitesimal with respect to the total depth, and the elevation of the channel bottom is assumed independent of time. When these assumptions are made, the continuity equation (65) takes the familiar form:

$$\frac{\partial \bar{h}}{\partial t} + \frac{\partial}{\partial x} D \bar{u} = 0. \quad (66)$$

2. The Keulegan Lumped Parameter Model.

The basic concept of the lumped parameter model introduced by Keulegan (1967) may be obtained by neglecting the right side of equation (64), assuming that A_c is independent of x and integrating the resulting equation from the open sea, $x = x_S$, to the bay, $x = x_B$, and rearranging terms to obtain:

$$\frac{1}{2}[\bar{u}_B^2 - \bar{u}_S^2] + g[\bar{h}_B - \bar{h}_S] + \int_{x_S}^{x_B} \frac{1}{A_c} \int_{y_1}^{y_2} (\tau_{zx})_Z dy dx = - \int_{x_S}^{x_B} \frac{\partial \bar{u}}{\partial t} . \quad (67)$$

Keulegan made the assumption, consistent with equations (4) and (5), that,

$$(\tau_{zx})_Z = \frac{K|U|U}{\bar{D}^2} , \quad (68)$$

and implicitly assumed that the right side of equation (67) could be neglected.

Substitution from equation (68) into equation (67) yields:

$$g[\bar{h}_S - \bar{h}_B] = \left(\frac{1}{2}\right)[\bar{u}_B^2 - \bar{u}_S^2] + \int_{x_S}^{x_B} \left[\frac{1}{A_c} \int_{y_1}^{y_2} \frac{K|U|U}{\bar{D}^2} dy \right] dx . \quad (69)$$

Keulegan (1967) evaluated \bar{u}_S^2 , not at the same value of x , as used for the tide height \bar{h}_S , but so far at sea that a zero value could be assumed. He implicitly assumed that the flow was uniform throughout the channel. Thus, the velocity, U/\bar{D} , is given by \bar{u}_B . Thus, Keulegan's basic equation takes the form:

$$g[\bar{h}_S - \bar{h}_B] = \frac{1}{2}\bar{u}_B^2 + \frac{\gamma K(x_B - x_S)}{\bar{D}} \bar{u}_B^2 . \quad (70)$$

The two terms involving the square of the speed were combined to give:

$$[\bar{h}_S - \bar{h}_B] = \gamma \left[\frac{2K(x_B - x_S)}{\bar{D}} + m \right] \frac{\bar{u}_B^2}{2g} , \quad (71)$$

where m is a coefficient related to the velocity profile and is taken as unity in most applications, $\gamma = +1$ for floodflow, and $\gamma = -1$ for ebb flow. Note that $\gamma(\bar{h}_S - \bar{h}_B) = |\bar{h}_S - \bar{h}_B|$, and $\gamma^2 = 1$.

Equation (71) contains two deviations from a rigorous derivation, both resulting from the integration of the term $\partial/\partial x \bar{u}^2$. A rigorous derivation of equation (67) requires that the term representing the advection of momentum, $\partial \bar{u}^2/\partial x$, be integrated over the same domain as the pressure gradient term, $\partial \bar{h}/\partial x$, so that the gain in kinetic energy associated with the head loss resulting from the slope of the water surface is realized. By evaluating the water level at opposite ends of the inlet and the kinetic energy in the open sea, where $\bar{u} = 0$, and at the bay end of the inlet, Keulegan overestimated the gain in kinetic energy as a result of the head loss within the inlet. The first term, \bar{u}_B^2 in equation (70), represents kinetic energy, a positive scalar without regard to the direction of current flow. The second term represents the bottom stress, a vector which changes sign with changes in the direction of flow. When these are combined, as in equation (71), the kinetic energy is incorrectly assigned a negative value during ebb flow. The kinetic energy term is often much smaller than the friction term and has only a trivial affect on the solution when $2K(x_2 - x_1)/D \gg m$; i.e., when the length of the inlet is several hundred times the effective depth. This condition is satisfied by most real inlets.

Keulegan assumed Manning's formulation of the bottom friction law where $K \propto D^{-1/3}$. Since this assumption is not critical to the basic discussion of this section, K is left in the general form, $K = K(x, y)$, without considering the reason for variability.

To eliminate the velocity \bar{u}_B from equation (71), Keulegan assumed that water enters and leaves the bay only through the inlet, the area of the bay is independent of time, and the phase of the tide in the bay is independent of position to justify the expressions:

$$\begin{aligned} \frac{\partial V_{Bay}}{\partial t} &= \bar{u}_B A_B \\ &= A_{Bay} \frac{\partial \bar{h}_B}{\partial t}, \end{aligned}$$

or

$$\frac{\partial \bar{h}_B}{\partial t} = \frac{A_B}{A_{Bay}} \bar{u}_B, \quad (72)$$

where V_{Bay} and A_{Bay} are the volume and surface area of the bay. These assumptions are rarely satisfied exactly, but may be approximated with useful accuracy in many inlets.

Elimination of \bar{u} between equations (71) and (72) yields:

$$\frac{\partial \bar{h}_B}{\partial t} = \gamma K_e \left[2g|\bar{h}_S - \bar{h}_B| \right]^{1/2}, \quad (73)$$

where

$$K_e = \frac{A_B}{A_{Bay}} \left[\frac{\bar{D}}{2K(x_B - x_S) + m\bar{D}} \right]^{1/2} \quad (74)$$

K_e is Keulegan's coefficient of repletion, and apart from a few changes in notation, equations (73) and (74) correspond to equations 12 and 13 in Keulegan (1967). All five empirical parameters A_B , A_{Bay} , \bar{D} , K , and $(x_B - x_S)$ are lumped into the single parameter, K_e . If sufficient records of \bar{h}_S and \bar{h}_B are available and the theory holds, K_e can be defined in a least squares sense by standard statistical procedures. If the various assumptions and approximations used in the derivation of equation (74) are approximately valid, it should be possible to obtain a good approximation of K_e from measurements obtained from a hydrographic chart.

For many practical problems, the assumptions leading up to equations (73) and (74) are too restrictive to justify much confidence in a direct application of the Keulegan lumped parameter model. The principal need for a lumped parameter approach is to provide a method for estimating tidal flows in small or dredged inlets where observations of tides are unavailable.

Huval and Wintergerst (1977) propose a relaxation of Keulegan's (1967) assumptions by heuristic extensions of his basic equations.

The differences between the equations used and those found in a rigorous derivation were not identified and eliminated; new errors were introduced. To display these errors, their importance should be estimated, and to find a satisfactory solution, it is perhaps necessary to eliminate the assumption of a constant cross section, independent of x , and retain the closure terms. The one-dimensional transport equation is more convenient for this purpose than the mean flow equation (64). The transport equation C10 in Appendix C, has the form:

$$\frac{\partial}{\partial t} A_c \bar{u} + \frac{\partial}{\partial x} A_c \bar{u}^2 + g A_c \frac{\partial \bar{h}}{\partial x} + \int_{y_1}^{y_2} (\tau_{zx})_Z dy = R_c, \quad (75)$$

where $A_c = A_c(x)$ = cross section of inlet.

3. A Rigorous Derivation.

The integral of equation (75) may be stated as:

$$\int_{x_S}^{x_B} \left[\frac{\partial}{\partial x} A_c \bar{u}^2 + g A_c \frac{\partial \bar{h}}{\partial x} + \int_{y_1}^{y_2} (\tau_{zx})_Z dy \right] dx = \int_{x_S}^{x_B} \left[R_c - \frac{\partial}{\partial t} A_c \bar{u} \right] dx. \quad (76)$$

Terms neglected by Keulegan (1967) are on the right in equation (76). The first term in this equation may be readily integrated to obtain:

$$\int_{x_S}^{x_B} \frac{\partial}{\partial x} A_C \bar{u}^2 dx = (A_C \bar{u}^2)_{x_B} - (A_C \bar{u}^2)_{x_S} . \quad (77)$$

If either of the factors, A_C or $\partial \bar{h} / \partial x$ of the second term in equation (76), is nearly constant, the integral of this term may be approximated as:

$$\int_{x_S}^{x_B} g A_C \frac{\partial \bar{h}}{\partial x} dx = g (\bar{h}_B - \bar{h}_S) \bar{A}_C , \quad (78)$$

where \bar{A}_C is a representative cross-sectional area for the entire inlet. Equation (78) is the definition of \bar{A}_C . The slope of the water surface, $\partial \bar{h} / \partial y$, may be nearly constant whenever the phase change in the inlet is small; i.e., when

$$(x_B - x_S) \ll [g D_{min}]^{1/2} T , \quad (79)$$

where D_{min} is the minimum value of \bar{D} in the inlet, and T is the period of the tide wave. The variability of A_C can be determined from a hydrographic chart or a hydrographic survey.

Equation (4) may be used to obtain the integral of the stress term in the form:

$$\int_{x_S}^{x_B} \int_{y_1}^{y_2} (\tau_{zx})_Z dy dx = \gamma \bar{u}_B^2 \int_{x_S}^{x_B} \int_{y_1}^{y_2} K \omega^2(x, y) dy dx , \quad (80)$$

where

$$\omega(x, y) = \frac{[U/D]}{\bar{u}_B} = \frac{\bar{u}}{\bar{u}_B} . \quad (81)$$

The stress coefficient, K , may be a function of x , y , and t .

Substitution from equations (77), (78), and (80) into equation (76) yields:

$$\begin{aligned} & A_B \bar{u}_B^2 - A_S \bar{u}_S^2 + g (\bar{h}_B - \bar{h}_S) \bar{A}_C + \gamma \bar{u}_B^2 \int_{x_S}^{x_B} \int_{y_1}^{y_2} K \omega^2 dy dx \\ & = \int_{x_S}^{x_B} \left[R_C - \frac{\partial}{\partial t} A_C \bar{u} \right] dx . \end{aligned} \quad (82)$$

The continuity equation for the one-dimensional equations of motion is derived in Appendix C, equation (C9) as:

$$\frac{\partial A_C}{\partial t} + \frac{\partial}{\partial x} A_C \bar{u} = \int_{y_1}^{y_2} (R + E) dy . \quad (83)$$

Equation (75) may be readily integrated along the inlet to obtain:

$$\int_{x_S}^{x_B} \frac{\partial A_C}{\partial t} dx + A_B \bar{u}_B - A_S \bar{u}_S = \int_{x_S}^{x_B} \int_{y_1}^{y_2} (R + E) dy dx . \quad (84)$$

The first term in equation (84) may be simplified by noting that

$$\int_{x_S}^{x_B} A_C dx = V_I' , \quad (85)$$

where V_I' is the volume of the inlet. Thus, the integrated continuity equation for the inlet may be expressed as:

$$\frac{\partial V_I'}{\partial t} = A_S \bar{u}_S - A_B \bar{u}_B + \int_{x_S}^{x_B} \int_{y_1}^{y_2} (R + E) dy dx . \quad (86)$$

When the phase change within the inlet is small, the volume, as a function of height, may be computed from hydrographic and topographic data; thus, if $\bar{h}_S(t)$ is a known function, and the phase change within the inlet is small, $V_I'(t)$ may be determined.

Equation (86) may be solved for \bar{u}_S in the form:

$$\bar{u}_S = \frac{A_B}{A_S} \bar{u}_B + \frac{1}{A_S} \frac{\partial V_I'}{\partial t} , \quad (87)$$

where

$$\frac{\partial V_I'}{\partial t} = \frac{\partial V_I'}{\partial t} - \int_{x_S}^{x_B} \int_{y_1}^{y_2} (R + E) dy dx . \quad (88)$$

The term, $\partial V_I'/\partial t$, represents the contribution of tidal flow to the local time derivative of the inlet volume. The term, $\partial V_I'/\partial t$, is the complete local time derivative of the inlet volume. The integral of the net precipitation, $(R + E)$, over the area of the inlet is

the net contribution of precipitation, evaporation, and overbank flow to the volume change of the inlet. Most of the time this term is much smaller than the volume change of the inlet due to the tidal range and can be neglected in most cases. An exception may occur during intense rainstorms, over inlets with small tidal ranges. In most cases, $\partial V_I / \partial t$ is an adequate estimate of the total time derivative of the inlet volume.

Substitution from equation (87) into equation (82) and a slight rearrangement of terms in equation (70) yield:

$$\begin{aligned} & \left[\gamma \int_{x_S}^{x_B} \int_{y_1}^{y_2} K \omega^2 dy dx + A_B \left(\frac{1 - A_B}{A_S} \right) \right] \bar{u}_B^2 \\ & - \gamma \left[\frac{A_B}{A_S} \frac{\partial V_I}{\partial t} \right] \bar{u}_B \\ & - \left[\bar{A}_g (\bar{h}_S - \bar{h}_B) + \frac{1}{A_S} \left(\frac{\partial V_I}{\partial t} \right)^2 + \int_{x_S}^{x_B} \left[R_c - \frac{\partial}{\partial t} A_c \bar{u} \right] dx \right] = 0 . \quad (89) \end{aligned}$$

Equation (89) is the complete form of the momentum equation approximated by equation (70). It is a quadratic equation for \bar{u}_B , and the solution may be given in the standard form:

$$\bar{u}_B = \frac{-b \pm \sqrt{b^2 - 4ac}}{2a} , \quad (90)$$

where

$$a = \gamma \int_{x_S}^{x_B} \int_{y_1}^{y_2} K \omega^2 dy dx + A_B \left(\frac{1 - A_B}{A_S} \right)$$

$$b = - \gamma \left[\left(\frac{A_B}{A_S} \right) \frac{\partial V_I}{\partial t} \right] ,$$

$$c = - \left[\bar{A}_g (\bar{h}_S - \bar{h}_B) + A_S^{-1} \left(\frac{\partial V_I}{\partial t} \right)^2 + \int_{x_S}^{x_B} \left[R_c - \frac{\partial}{\partial t} A_c \bar{u} \right] dx \right]$$

It is necessary to neglect the second term of a , b , and the last two terms of c to obtain Keulegan's (1967) equation. The second term in a vanishes for a uniform channel cross section as assumed by Keulegan but the other terms are always real even though they may be small relative to the uncertainty in the friction term. Consideration of typical values for each term in equation (90) is useful to provide perspective for neglecting minor terms, remembering that the initial estimate for Manning's n may easily be in error by 50 percent. Consequently, K is uncertain by

a factor of two. The parameters in Table 1 may be taken as typical of many inlets in North America. In an order of magnitude analysis, integrals may be replaced by the product of their ranges and typical values of the integrands. Differentials may be replaced by average or maximum values.

Table 1. Typical inlet parameters.

Parameters	Symbols	Values
Depth	D	3 m
Width	b	300 m
Cross-sectional area	$D\bar{b}$	$9 \times 10^2 \text{ m}^2$
Length	L_I	2,000 m
Surface area	bL_I	$6 \times 10^5 \text{ m}^2$
Tidal range	$2\bar{h}$	1 m
Volume of tidal change	$2\bar{h}bL_I$	$6 \times 10^5 \text{ m}^3$
Tidal period	T	12.4 hr
Average rate of inlet volume change	$\partial V_I / \partial t$	$26.67 \text{ m}^3/\text{s}$
Peak velocity	$ \bar{u}_B _{max}$	1 m/s
Manning's n	n	0.025
K	$n^2 D^{-1/3}$	4.33×10^{-4}
	ω	1.0
Acceleration of gravity	g	10 m/s^2
	A_B/A_S	0.9
	$\bar{h} - \bar{h}_B$	0.1 m

Substitution for most terms in equation (90) yields:

$$a = \gamma(6 \times 10^5)(4.33 \times 10^{-4}) \pm 9 \times 10^2 \times 10^{-1} \\ = 260 \gamma \pm 90$$

$$b = 9 \times 10^{-1} \times 26.67 \\ = 24$$

$$c = 9 \times 10^{2+1}(\bar{h}_S - \bar{h}_B) + 1.1 \times 10^{-3} \times 7.11^1 \times 10^2 \\ + 2 \times 10^3 \times [R_c - 8 \times 10^{-4}] \\ = 9 \times 10^2 + 7.9 \times 10^{-1} - 1.6 + 2 \times 10^3 R_c$$

It is difficult to assign meaningful typical values to R_c . Generally, this term is small in relation to the first term in c, but R_c may be the largest single term in equation (90) when a strong wind is blowing parallel to the inlet axis. The wave setup term, S_{ω} , can be

large when large waves are breaking in the inlet, and negligibly small at other times. Other terms may also become significant in special circumstances.

Substitution of numerical values into equation (89) shows that for the assumed conditions, $\partial V_I / \partial t$ and $\partial / \partial x (A_C u)$ can be neglected without serious error, even when average absolute values are considered. Since these are alternating terms, the actual net value of the errors rising from neglect is generally small. The second term of a vanishes for inlets of uniform cross section as assumed by Keulegan (1967). When the cross section of the inlet is variable, the second term can be significant, and for short inlets, the second term may be dominant. Inlet dimensions vary widely, and values for the particular inlet being considered should be substituted into equations (89) and (90) to determine which terms can be neglected in particular cases.

Thus, with good approximation, \bar{u}_B may be written as:

$$\bar{u}_B = \gamma \left[\frac{\bar{A}_g |\bar{h}_S - \bar{h}_B|}{\int_{x_S}^{x_B} \int_{y_1}^{y_2} K \omega^2 dy dx + \gamma A_B (1 - A_B/A_S)} \right]^{1/2} . \quad (91)$$

The first form of equation (72) may be generalized to account for inflow to the bay from precipitation, overbank flow, and rivers by:

$$\frac{\partial V_{Bay}}{\partial t} = \bar{u}_B A_{Bay} + q_{in} , \quad (92)$$

where q_{in} is the net contribution from rivers, overbank flow, and precipitation, etc. This yields an expression for $\partial \bar{h}_B / \partial t$ in the form:

$$\frac{\partial \bar{h}_B}{\partial t} = \frac{A_B}{A_{Bay}} \bar{u}_B + \frac{q_{in}}{A_{Bay}} . \quad (93)$$

Equation (91) can be used to eliminate \bar{u}_B from equation (93) to obtain:

$$\frac{\partial \bar{h}_B}{\partial t} = \frac{\gamma A_B}{A_{Bay}} \left[\frac{\bar{A}_g |\bar{h}_S - \bar{h}_B|}{\int_{x_S}^{x_B} \int_{y_1}^{y_2} K \omega^2 dy dx + \gamma A_B (1 - A_B/A_S)} \right]^{1/2} + \frac{q_{in}}{A_{Bay}} \quad (94)$$

or

$$\frac{\partial \bar{h}_B}{\partial t} = \gamma K_e [2g |\bar{h}_S - \bar{h}_B|]^{1/2} + \frac{q_{in}}{A_{Bay}} , \quad (95)$$

where

$$K_e = \frac{A_B}{A_{Bay}} \left[\frac{\bar{A}}{\int_{x_S}^{x_B} \int_{y_1}^{y_2} K \omega^2 dy dx + \gamma A_B (1 - A_B/A_S)} \right]^{1/2} \quad (96)$$

When q_{in} is neglected, equation (95) is identical with equation (73). Thus equation (95) is a generalization of equation (73) which permits water to reach the bay without going through the inlet. When $\omega = \text{unity}$, and both K and A are a constant, equation (96) reduces to the form of equation (74) where m is neglected. Thus, equations (95) and (96) are generalizations of equations (73) and (74).

Huval and Wintergerst (1977) propose a heuristic generalization of Keulegan's (1967) model for application to inlets of irregular shape, as partitioning the inlet into several parallel channels, and the channels into cells, with the goal of obtaining nearly uniform values of depth, roughness, velocity, and cross-sectional area in each cell. They recognize that these conditions cannot, in general, be satisfied exactly; however, no guidance is provided to determine how well these conditions can or must be satisfied to justify the use of the proposed model.

A systematic approach to the Huval and Wintergerst model leads to an alternate expression of comparable simplicity which does not require such stringent assumptions. Moreover, the alternate expression can be converted into the form given by Huval and Wintergerst only if all their assumptions are completely satisfied.

A rigorous derivation could begin with the numerical integration of equation (C1) in Appendix C. However, the principal concern here is the extension of Keulegan's basic equation (70). Thus, the derivation can begin with a generalization of equation (70), based on equation (69).

It will be assumed that an inlet can be partitioned into a number of subchannels and that within each subchannel, the depth, roughness, and velocity are nearly constant for each value of x . In general, these variables, including the width, within each subchannel may be arbitrary, and all four may vary with x . The first step in this derivation is to rewrite the last term in equation (69) as:

$$\int_{x_S}^{x_B} \frac{1}{A_c} \int_{y_1}^{y_2} \frac{K|U|U}{D^2} dy dx = \gamma \int_{x_S}^{x_B} \frac{1}{A_c} \int_{y_1}^{y_2} K \bar{u}^2 dy dx \quad (97)$$

In equation (95), y_1 and y_2 are taken as the limits of the sub-channel. With the aid of equation (97) and, in conformity with Keulegan (1967), the assumption that \bar{u}_S^2 can be neglected, an alternative form of equation (70) is obtained:

$$g[\bar{h}_S - \bar{h}_B] = \gamma \int_{x_S}^{x_B} \frac{K_m \bar{u}^2 b_m}{A_m} dx . \quad (98)$$

The subscript m is used to designate the m 'th subchannel.

The inertia term, arising from $\partial \bar{u}^2 / \partial x$, has been omitted as explained above. The integration of equation (98) across the inlet is accomplished by adding the solutions for all subchannels to obtain:

$$\bar{u}_B^2 \sum_{m=1}^M \int_{x_S}^{x_B} \frac{K_m \omega_m^2 b_m}{A_m} dx = M \gamma g (\bar{h}_S - \bar{h}_B) . \quad (99)$$

Equation (81) has been used to factor \bar{u}_B^2 from the integral. If \bar{u}_B is taken as the average velocity across the entire inlet, equation (99) may be solved to obtain:

$$\bar{u}_B = \gamma \left[\frac{M g |\bar{h}_S - \bar{h}_B|}{\sum_{m=1}^M \int_{x_S}^{x_B} K_m \omega_m^2 / \bar{D}_m dx} \right]^{1/2} , \quad (100)$$

where

$$\sum_{m=1}^M b_m = b , \quad (101)$$

and, as in equation (91), the inertial term has been neglected. Substitution from equation (100) into equation (93) yields equation (95), with K_e given by:

$$K_e = \frac{B}{A B a y} \left[\frac{M}{\sum_{m=1}^M \int_{x_S}^{x_B} K_m \omega_m^2 / \bar{D}_m dx} \right]^{1/2} . \quad (102)$$

In equations (96) and (102), the major problem is to determine the values of $\omega_m(x)$. Practical procedures are developed and several applications of the procedures are given by Seelig, Harris, and Herchenroder (in preparation, 1977). The other parameters can generally be measured or estimated from available charts.

The solution of Huval and Wintergerst (1977) may be obtained from equation (99) by setting all values of

$$\frac{K_m \omega_m^2 b_1}{A_m} = \frac{K_1 \omega_1^2}{\bar{D}_1}, \quad (103)$$

so that equation (99) may be rewritten as:

$$M \bar{u}_B^2 \int_{x_S}^{x_B} \frac{K_1 \omega_1^2}{\bar{D}_1} dx = \gamma g M (\bar{h}_S - \bar{h}_B). \quad (104)$$

If $K\omega^2/D$ is the same function of x in each channel, equation (98) may be applied separately to each channel. The model of Huval and Wintergerst is based on the implicit assumption that equation (98) can be applied separately to each of the parallel channels.

Huval and Wintergerst (1977) defined the quantity, ω , by postulating that the total flow in each subchannel would be constant for all x . By using this assumption, the total flow, Q , is given by:

$$Q = \sum_{m=1}^M Q_m, \quad (105)$$

where

$$Q_m(x) = A_m(x) \bar{u}_m(x),$$

and

$$A_B = \sum_{m=1}^M B_m(A_B)_m,$$

substitution from equation (81) shows that

$$\omega_m(x) = \frac{\bar{u}_m(x)}{\bar{u}_B} = \frac{Q_m/A_m(x)}{\bar{u}_B}. \quad (106)$$

Factoring equation (104) by M , substituting from equation (106) for ω_m , and rearranging terms in equation (99) will obtain:

$$Q_m = \gamma \left[\frac{g|\bar{h}_S - \bar{h}_B|}{\int_{x_S}^{x_B} K_m dx / \bar{D}_m A_m^2(x)} \right]^{1/2} . \quad (107)$$

Summing all Q_m to obtain the total transport, noting that $A_B \bar{u}_B = Q$, and substituting the sum of all Q_m into equation (72) yield:

$$K_e = K_{HW} = \frac{1}{A_{Bay}} \sum_{m=1}^M \left[\frac{1}{\int_{x_S}^{x_B} K_1 dx / \bar{D} A_1^2(x)} \right]^{1/2} , \quad (108)$$

where the subscript, HW , is used to indicate the form developed by Huval and Wintergerst.

The conditions required to justify equation (108) show that this equation is equal to equation (102). All terms in the denominator of the bracketed terms in equation (108) are independent of y and the total cross section is the sum of the cross sections of the individual channels. If A_1 is also independent of x , the summation in equation (108) yields:

$$K_{HW} = \frac{A_B}{A_{Bay}} \left[\frac{1}{\int_{x_S}^{x_B} K_1 dx / \bar{D}} \right]^{1/2} , \quad (109)$$

For the conditions required to justify equation (108), i.e., A_1 is constant and K_1 and \bar{D} are independent of y , all terms in the denominator of the bracketed term in equation (102) are also constant, and the total width of the inlet is equal to the sum of the widths of the channels. Thus, for these conditions, equation (102) may be written as:

$$K_e = \frac{A_B}{A_{Bay}} \left[\frac{1}{\int_{x_S}^{x_B} K_1 dx / \bar{D}} \right]^{1/2} , \quad (110)$$

where

$$\frac{A_{1B}^2}{A_1^2}(x) = \omega_1^2 = 1 .$$

The general validity of the lumped parameter model of Keulegan (1967) has been established for the following conditions:

- (a) All flow into the bay passes through the inlet.
- (b) Surface area of inlet and bay is independent of time.
- (c) Cross-sectional area of inlet is independent of x .
- (d) Phase change of the tide within inlet and bay is small.
- (e) The friction effect is much larger than the effect of momentum advection; e.g., $2K(x_B - x_S) \gg \bar{D}$.

This latter condition is required to ensure that the error in treating the terms arising from the term $\partial \bar{u}^2 / \partial x$ does not become significant.

Huval and Wintergerst (1977) successfully relax the following conditions:

- (a) Full relaxation.
- (b) Area of inlet and bay may change as linear or quadratic functions of \bar{h} . This is sufficiently generalized for most practical cases.
- (c) The requirement for a channel cross section independent of x is generalized as follows:
 - (1) The inlet is partitioned into several channels of equal width. The width may change with distance along the inlet axis, but the cross section in each channel is as nearly independent of x as possible.
 - (2) The transport in each channel is constant along its length. This is equivalent to the specification that the subchannel boundaries be streamlines.
 - (3) The factor, $K_m \omega_m^2 / \bar{D}_m$, has the same value in each channel for each value of x .

Condition (c) is unlikely to be satisfied even approximately unless the inlet is approximately symmetric to the centerline. Conditions (d) and (e) for the Keulegan (1967) model are retained in the model of Huval and Wintergerst (1977).

Both models become invalid whenever strong winds blow parallel to the inlet axes and when large waves break in the inlet. There may be special but unusual circumstances when either of the models fails because one or more other processes grouped under the term R_o become important.

4. Summary.

Equations of motion for the vertically and cross-channel integrated flow in a channel of variable cross section have been derived in Appendix C in a manner which explicitly identifies the assumptions generally made in adopting one-dimensional equations of motion. These equations have been further integrated along the channel in this section to provide a differential equation for the tidal height in the ocean and the inlet geometry. The work was motivated by the inlet studies of Keulegan (1967) and Huval and Wintergerst (1977).

This study has shown that the inertia terms appear to have been improperly treated by Keulegan (1967); however, these terms are of trivial importance in some inlets and may have little affect on the flow.

Huval and Wintergerst attempt to generalize Keulegan's treatment by relaxing some of his restrictions, without going back to a complete set of equations as a starting point. A thorough analysis of the problem has shown that Huval and Wintergerst found a singular solution of the problem which is nearly as restrictive as that presented by Keulegan. The new derivation in this study produced a solution of the same level of complexity which agrees with Huval and Wintergerst whenever their solution is valid, and which is valid for a much wider range of conditions. The new solution has not been developed here for practical application, but is accomplished in Seelig, Harris, and Herchenroder (in preparation, 1977).

VI. MODEL CALIBRATION

Both the numerical and physical models used for the study of coastal hydrodynamics are designed to reproduce, as reliably as possible, the primary flow phenomena being investigated, and to approximate or simulate indirectly the effects of secondary phenomena. The optimum design simulation and approximation procedures cannot be determined or evaluated solely on the basis of theory. Thus, a process of experimental adjustment and evaluation of the model must be carried out before it can be used with confidence for either engineering or scientific studies. This process has been termed *confirmation*, *adjustment*, *verification*, or *calibration* by various investigators. In this study, calibration is used to describe the process where a physical or numerical model of hydraulics phenomena is checked with prototype data and systematically adjusted to reproduce desired prototype data from corresponding prototype driving forces. Verification is restricted to the process where independent prototype data (data not used in the calibration) are used to verify that a calibrated hydraulics model reproduces prototype observations with satisfactory accuracy.

Models of coastal phenomena can be useful without being completely accurate. Hudson, et al. (in preparation, 1977, pp. 3-5) stated that all models of estuaries have one characteristic in common: that is that they cannot be completely accurate simulations of all the complex phenomena inherent in tidal waterways...."

American Society of Civil Engineers (1942) reported "That the necessity for the trial-and-error process of model verification arises from the inability of the experimenter to design and construct his model so as to insure the attainment of dynamic similitude." The previous quotation (Hudson, et al., in preparation, 1977) showed that this need is still much in evidence.

American Society of Civil Engineers (1942) and Hudson, et al. (in preparation, 1977) give lengthy descriptions of the procedures used for the adjustment of physical models. Durham, Greer, and Whalin (1976) and Whalin, Perry, and Durham (in preparation, 1977) discuss a calibration procedure based on the harmonic analysis of tidal records for a period of about 15 days which appears to be an improvement on traditional procedures. The field data collection program at Masonboro Inlet was too restricted to support this approach. Odd (1971) surveyed the problem in less detail for one-dimensional mathematical models. The four appendices to this report present specific examples of model calibration. This section does not furnish a guide to model calibration, but provides the reader with an understanding of the physical and mathematical need for calibration and with background information needed for the assessment of the calibration procedures for the four Masonboro Inlet models.

The imperfections in hydraulics models that lead to the requirement for calibration result in part from the lack of precise information about the prototype and in part from distortion or total neglect in the model of processes that are of secondary but significant importance in the prototype.

Friction is generally the most important of the distorted physical processes. The process of model adjustment for improving the calibration of model to prototype is often discussed as if the only important problem is to secure the proper value of bottom friction everywhere in the model.

Friction has two important affects on the prototype flow. Turbulence, generated by friction, serves to mix adjacent fluid elements, thus smoothing out large-scale gradients of momentum and dispersing any substance mixed with the water. Turbulence also increases the frequency of locally intense gradients in the flow, thereby increasing the conversion of kinetic energy to heat by molecular viscosity. These two effects of turbulence and one other effect are important in the physical model. By increasing the generation of turbulence near the bottom, friction decreases the thickness of the viscous boundary layer, and the thickness of the fluid layer in which molecular viscosity exerts a direct control over the velocity profile in the fluid.

The bottom stresses must be increased by a factor equal to the distortion ratio, β/α , to be correctly represented in distorted scale physical models (see Sec. III). Hudson, et al. (in preparation, 1977) derived the same correction factor by a different procedure.

Internal friction, as described by all nine components of the turbulent stress tensor (App. B, eq. B13), can contribute to fluid mixing and

the dissipation of energy. When no special effort is made to represent any one of these terms in the model, whether physical or numerical, the missing processes are assumed to be lumped with the bottom stresses in the model. Although not always clearly expressed, this principle is often used in the adjustment of physical models. The most frequently used procedure at the U.S. Army Engineer Waterways Experiment Station (WES), Vicksburg, Mississippi, is to embed small metal strips into the concrete bottom of fixed-bed models and to bend or remove the strips later as required to obtain a satisfactory level of turbulence during the model calibration procedure. This procedure and others are described by Sager and Seabergh (1977).

However, according to Hudson, et al., (in preparation, 1977), it is not always possible to achieve sufficient mixing of fluid elements by these techniques, and oscillating fans may be directed toward the water surface to increase the intensity of turbulence in the water. Small electrical vortex generators similar to kitchen mixers are used in some European laboratories for the same purpose.

The geometry of the inland tide reservoirs (see Sec. III), may be changed to improve the calibration of the physical model. Sometimes it is necessary to deepen a noncritical part of the basin or to constrict the flow somewhere in the model more than strict geometric similitude would prescribe, to duplicate some important features of the prototype flow in the model.

Reproduction of water levels is more easily achieved than the reproduction of currents in both physical and mathematical models. Hudson, et al. (in preparation, 1977) recommended that acceptable calibration of water levels through one or more tidal cycles be obtained before attempting to adjust the model for the reproduction of currents.

Model adjustments which are not determined by theoretical considerations leave something to be desired, but are often considered necessary. A model that cannot reproduce recorded events acceptably cannot be depended on to predict future events. The final stage of calibration for many models appears to be a trial-and-error procedure.

Numerical hydraulic models have not been in use as long as physical models. Consequently, the techniques for adjustment during the calibration process are not well developed. In general, the development has followed along the lines previously used with physical models. Some techniques, however, are more conveniently applied to one type of model or the other.

The concept of considering all adjustments of the model as changes in the bottom stress has carried over from physical modeling. In numerical models, the stress can easily be expressed in the form of equations (4) or (5) with a constant stress coefficient. Also, an initial estimated stress coefficient which may vary with position, can easily be changed by a constant factor or a constant increment. Since this type of stress

law or change in the stress law is difficult to achieve in a physical model, it is used more often with numerical models. Reid and Bodine (1968) used a constant stress coefficient for the entire model of Galveston Bay, but varied the value between repeated calculations to obtain optimum agreement between model and prototype. Chiu, van de Kreeke, and Dean (1970) also experimented with constant values for K during each calibration and selected the value which optimized agreement between model and prototype for later experiments. Masch, Brandes, and Reagan (1977) chose initial values of K which varied with water depth, and later adjusted some values on a point by point basis to optimize the agreement. Chen and Hembree (1977) intended to follow a similar procedure; their computer program has a provision for reading in an initial estimate of friction factors. However, the input friction factors are not included with the program listing, and no numerical values or descriptive logic are provided. Thus, it is impossible to determine from the material submitted, how the bottom stress was actually treated in this numerical model.

Odd (1971) reviewed the problem of representing bottom friction in one-dimensional numerical tidal models and concluded that empirical resistance functions, such as the Chezy and Manning formulas, provided an inadequate description of frictional resistance in shallow estuaries with an appreciable tidal range. The reasons for this opinion are not presented with enough details for application to two-dimensional models.

Reid and Bodine (1968) treated the overtopping of previously dry grid points by imposing a simulated weir and supplying both weir elevations and coefficients for each case. Thus, additional constants become available for adjustment during the calibration process. Simulated weirs could be used to impose a reduction in the cross section of flow to compensate for the difficulty in representing channels with widths less than Δs , or channels which could not otherwise be properly represented within the selected network of grid points. Procedures similar to those used by Reid and Bodine (1968) were applied in both of the Masonboro Inlet two-dimensional numerical models.

None of the reports cited describe the processes used in deciding how roughness elements should be distributed in a physical model, or how quantitative coefficients should be selected in numerical models to efficiently improve the agreement between model and prototype. Therefore, model calibration by both physical and numerical models remains a trial-and-error process.

Adjustment of a model to optimize agreement between the model and prototype for known events, and verification to measure the degree of success achieved, are necessary steps. A model cannot be depended on to reproduce future events with greater accuracy than the model has displayed in reproducing known events. However, there is no guarantee that the prediction of future events will achieve the degree of success displayed in calibration even when the model is not modified. Any substantial modification of the model is likely to change the calibration.

The reliability of both physical and numerical models for predicting the effects of changed conditions will be greatly increased when the process of adjustment is changed from an art to a science.

VII. COMPARISON OF MODEL RESULTS

The performance of each model used in the Masonboro Inlet study for simulating tidal-induced water motions is discussed in this section. The inlet modeling study consisted of two phases: (a) Calibration of the models to 1969 basin geometry and to given 1969 velocity and tidal data, and (b) application of the models to Masonboro Inlet for basin geometry, corresponding to prejetty (1964) conditions. In the first phase, the effectiveness of each model in reproducing water motions is shown by comparing the tides and velocities predicted in the models to the tides and velocities observed in the 1969 prototype; in the second phase, the results obtained with the mathematical models are compared with the tides and velocities measured in the physical model for 1964 conditions.

1. Calibration of Models.

Basic data for calibrating the models to Masonboro Inlet were from basin geometry collected during September and October 1969, and from tidal excitations and current velocities collected on 12 September 1969. Basin geometry data, including both hydrography and topography, were taken from a chart (scale of 1 inch to 500 feet) with 2-foot (0.61 meter) contours representing the hydrography below the mean low water (MLW) Beaufort Datum, or 1.88 feet (0.51 meter) below the National Geodetic Vertical Datum (formally called the 1929 Mean Sea Level Datum) elevations for describing the ground elevations above the local mean high water (MHW) Beaufort Datum. Selection of the physical limits of water motions at specific locations was reproduced.

Tide and current velocity data were collected at several locations. For the period 0300 to 2100 hours, eastern standard time (e.s.t.), continuous tidal information was recorded by seven tide gages. Concurrently, from about 0600 to 2100 hours, e.s.t., current velocities were measured and recorded at 15 stations. Locations of the tide gages and velocity measurement stations are shown in Figure 1; three velocity measurement stations were used to measure the velocities in a particular channel cross section. Measurements were taken at each station at three levels in the vertical, 1 foot above the bottom, middepth, and 1 foot below the free surface.

Tides recorded on 12 September 1969 at gage 0, located on Mercer's Pier on the oceanside of Wrightsville Beach and about 15 miles from Masonboro Inlet (Fig. 1), provided the basic input to all models. The data recorded at gage 0 (Fig. 4) indicates that the tide for this location is nearly sinusoidal in shape and has a semidiurnal period of about 12.5 hours.

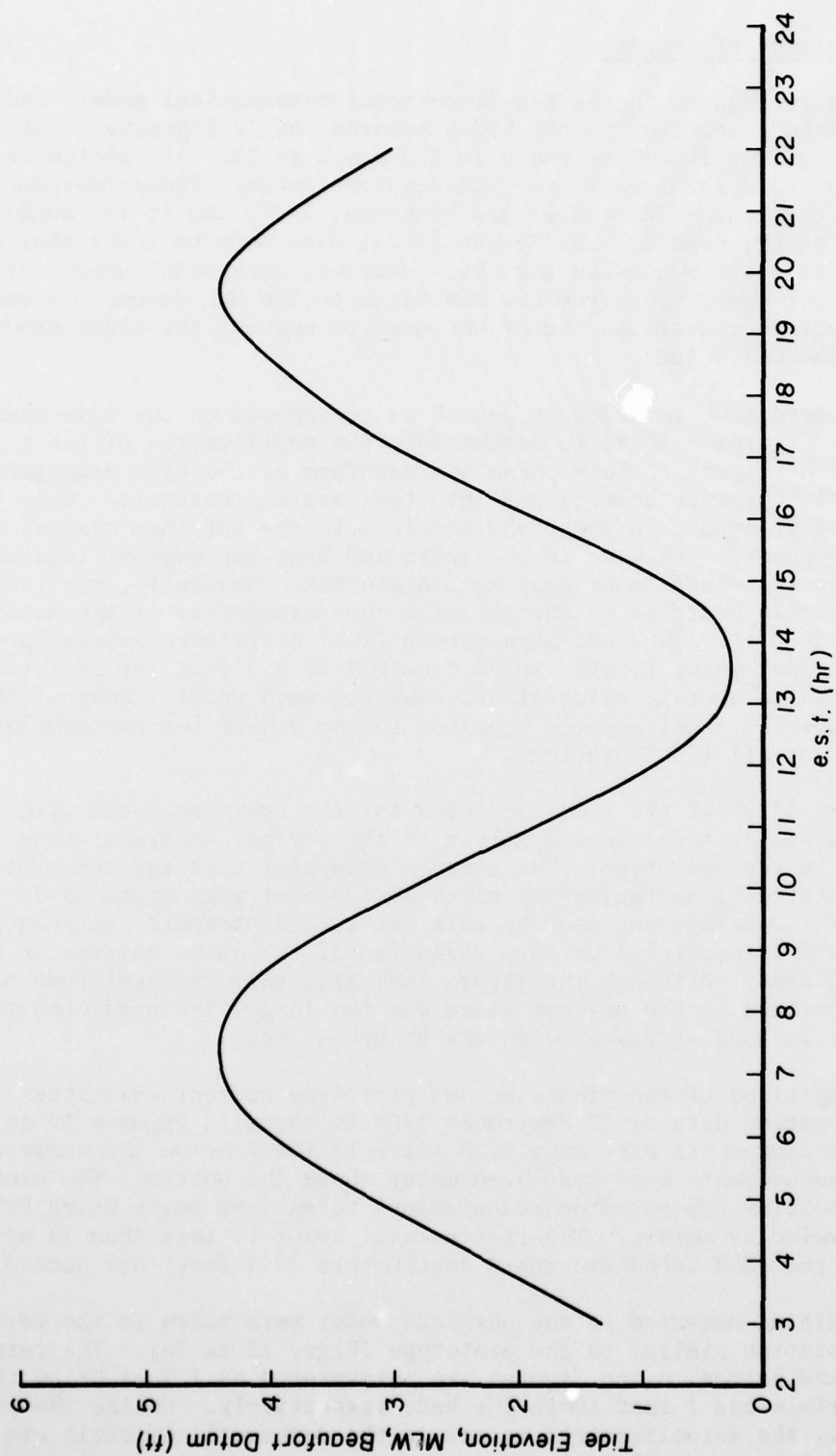


Figure 4. Prototype tidal data at gage 0, 12 September 1969.

2. Comparison of Results.

Tides reproduced in the two-dimensional mathematical models and physical model in comparison to the tides recorded on 12 September 1969 at the various gage locations are shown in Figures 5 to 10. All plotted tidal elevations were referred to the MLW Beaufort Datum. Tides reproduced in both the physical model (Sager and Seabergh, 1977) and in the numerical model by Masch, Brandes, and Reagan (1977) used a datum level that was intended to correspond with the MSL. However, each model used a different constant for converting from the MLW datum to the MSL datum. In each case, the respective conversion factor was used to convert the tidal elevations back to the MLW datum.

The ocean tide recorded at gage 0 is superposed on the tide hydrographs in Figures 5 to 10 to demonstrate the modification of the tidal curves with respect to both phase and waveform as the tide propagates through the entrance channel and into the back-bay channels. Only a slight change occurs in phase and waveform in the entrance channel (Fig. 5). As expected, the wave in the inlet and back-bay channel lags more in phase, and the waveform becomes more distorted. Generally, the tide wave is not greatly modified by the physical characteristics of the Masonboro Inlet study area. The root-mean-square (rms) difference between prototype and model water levels varied from 0.1 to 0.3 foot for individual gages, with an overall value of 0.2 foot for each model. None of the models appeared significantly superior to the others for reproducing the tides at all tidal stations.

Figure 11 shows the tide predicted for the embayment area with the lumped parameter model in comparison to the average embayment tide observed in the prototype. The average embayment tide for the prototype was calculated by averaging the tides observed at gage stations 3, 4, and 5. This average was used because the lumped parameter mathematical model can only predict a uniform variation of the water surface in the embayment area. Although the figure indicates that the amplitude of the tide calculated at the maximum stage was too large, the predicted tide is generally in good agreement with the observed tide.

A comparison of the predicted and prototype current velocities for the calibration data of 12 September 1969 is shown in Figures 12 to 26. Surface measurements were made 0.30 meter (1 foot) below the surface; bottom measurements were made 0.30 meter above the bottom. The prototype velocities are based on measurements taken from boats using Price cuptype velocity meters. The instrumental error is less than 10 percent when the recorded speed exceeds 3 centimeters (0.1 foot) per second.

Velocities measured in the physical model were taken in the vertical at each station similar to the prototype (Figs. 12 to 26). The terms *surface* and *bottom* in the figures are interpreted as 1 foot below the water surface and 1 foot above the bed, respectively. Unlike the physical model, the velocities calculated in the mathematical models are vertically averaged velocities.

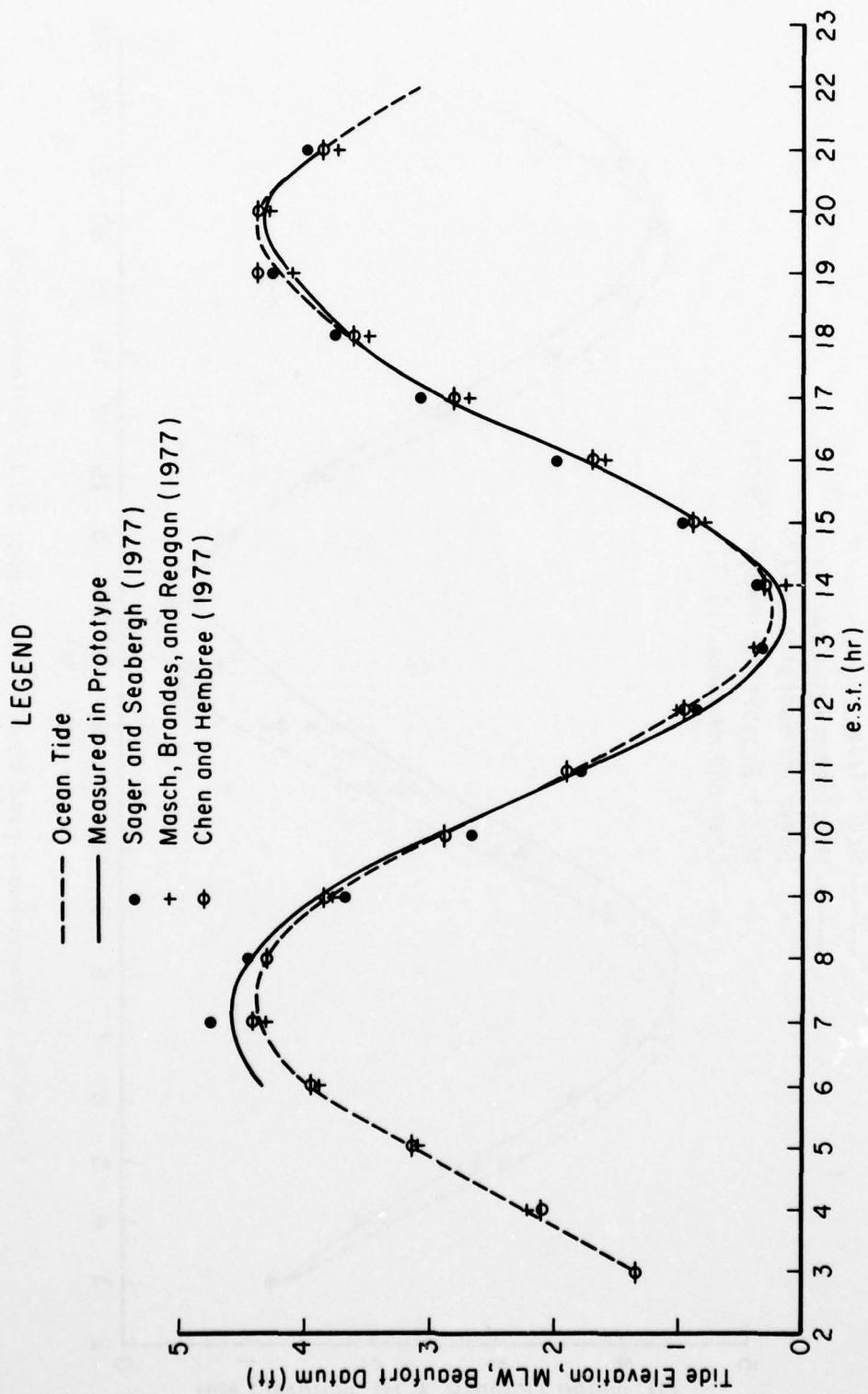


Figure 5. Observed and predicted tides at gage 1, 12 September 1969.

LEGEND

- Ocean Tide
- Measured in Prototype
- Sager and Seabergh (1977)
- + Masch, Brandes, and Reagan (1977)
- ⊖ Chen and Hembree (1977)

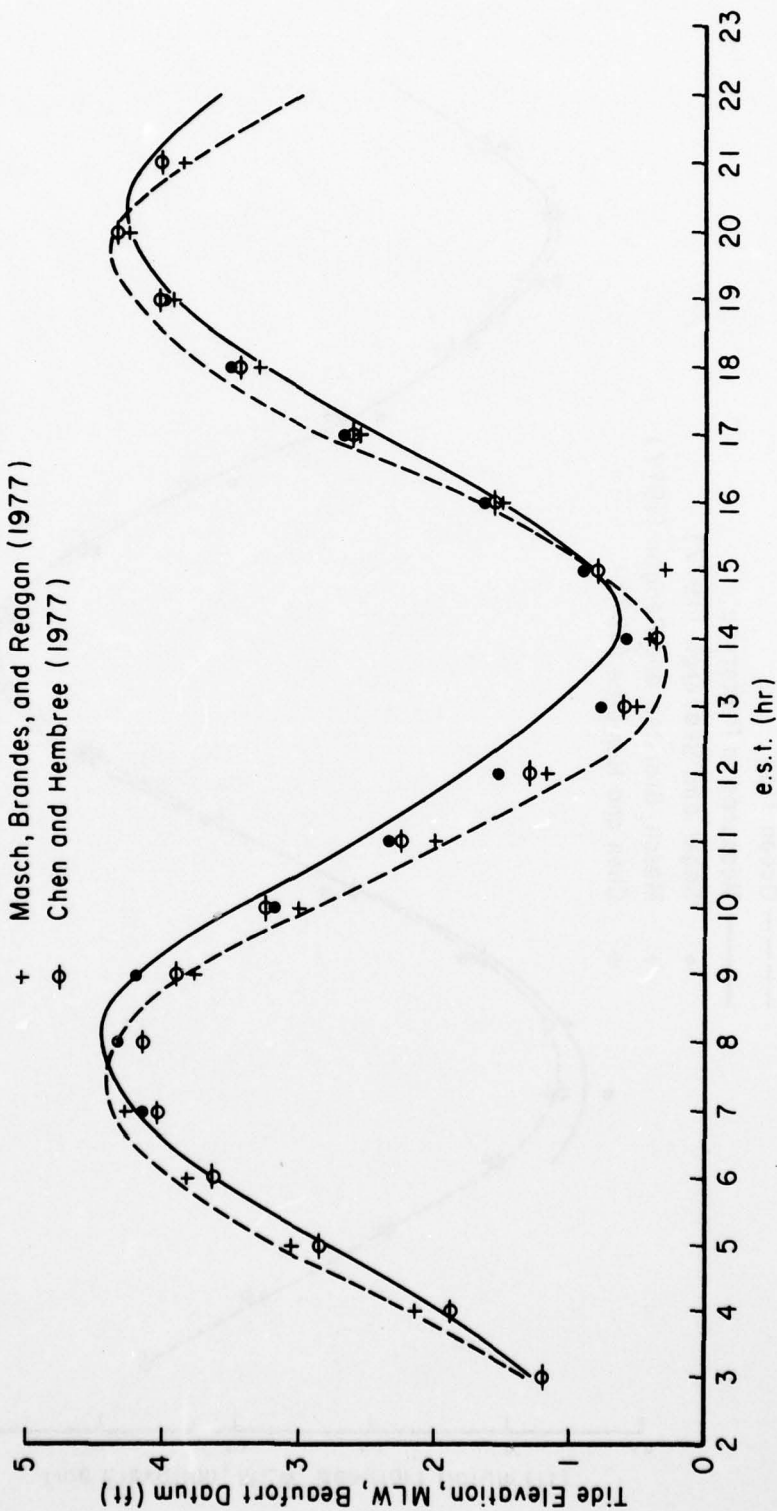


Figure 6. Observed and predicted tides at gage 2, 12 September 1969.

LEGEND

- Ocean Tide
- Measured in Prototype
- Sager and Seabergh (1977)
- + Masch, Brandes, and Reagan (1977)
- ⊖ Chen and Hembree (1977)

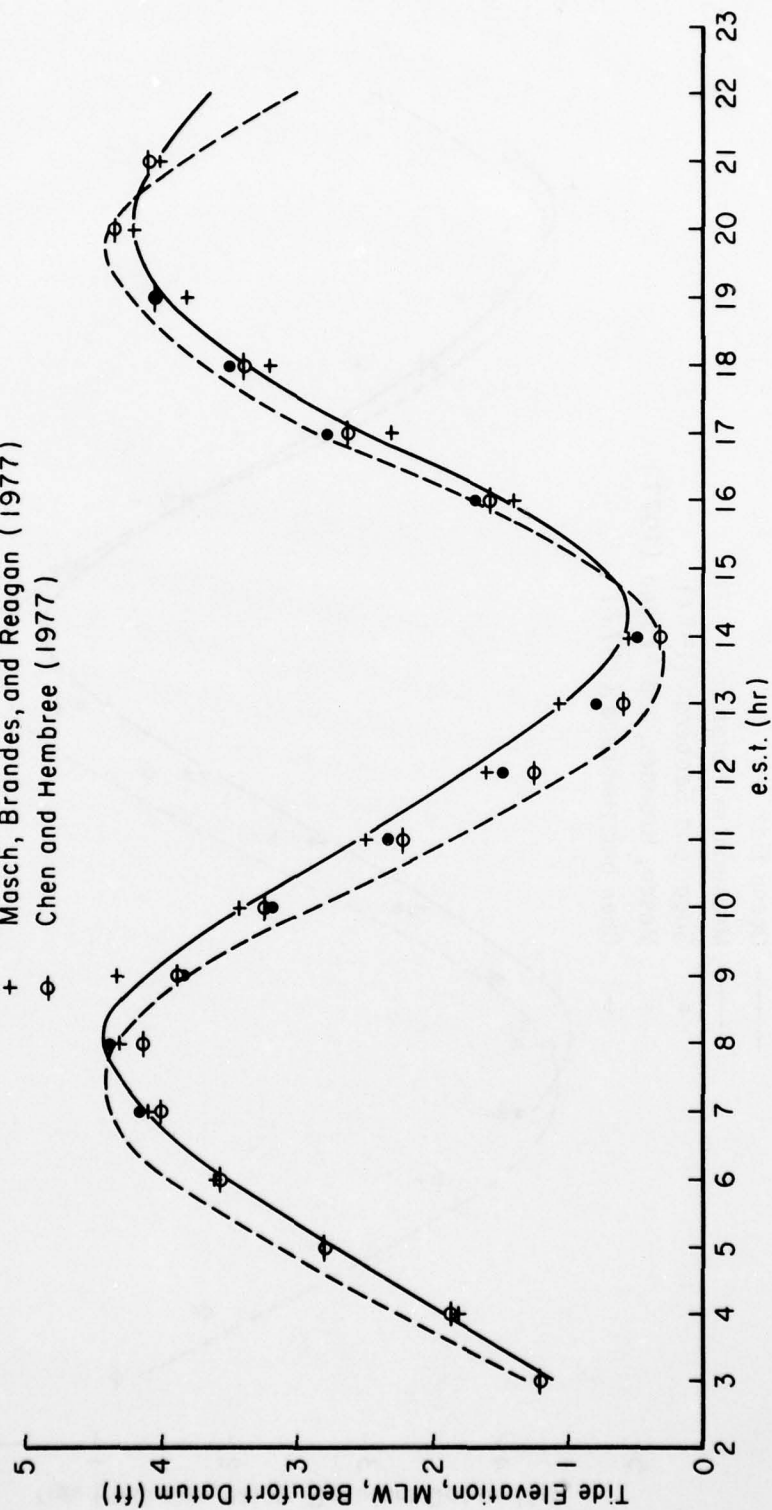


Figure 7. Observed and predicted tides at gage 3, 12 September 1969.

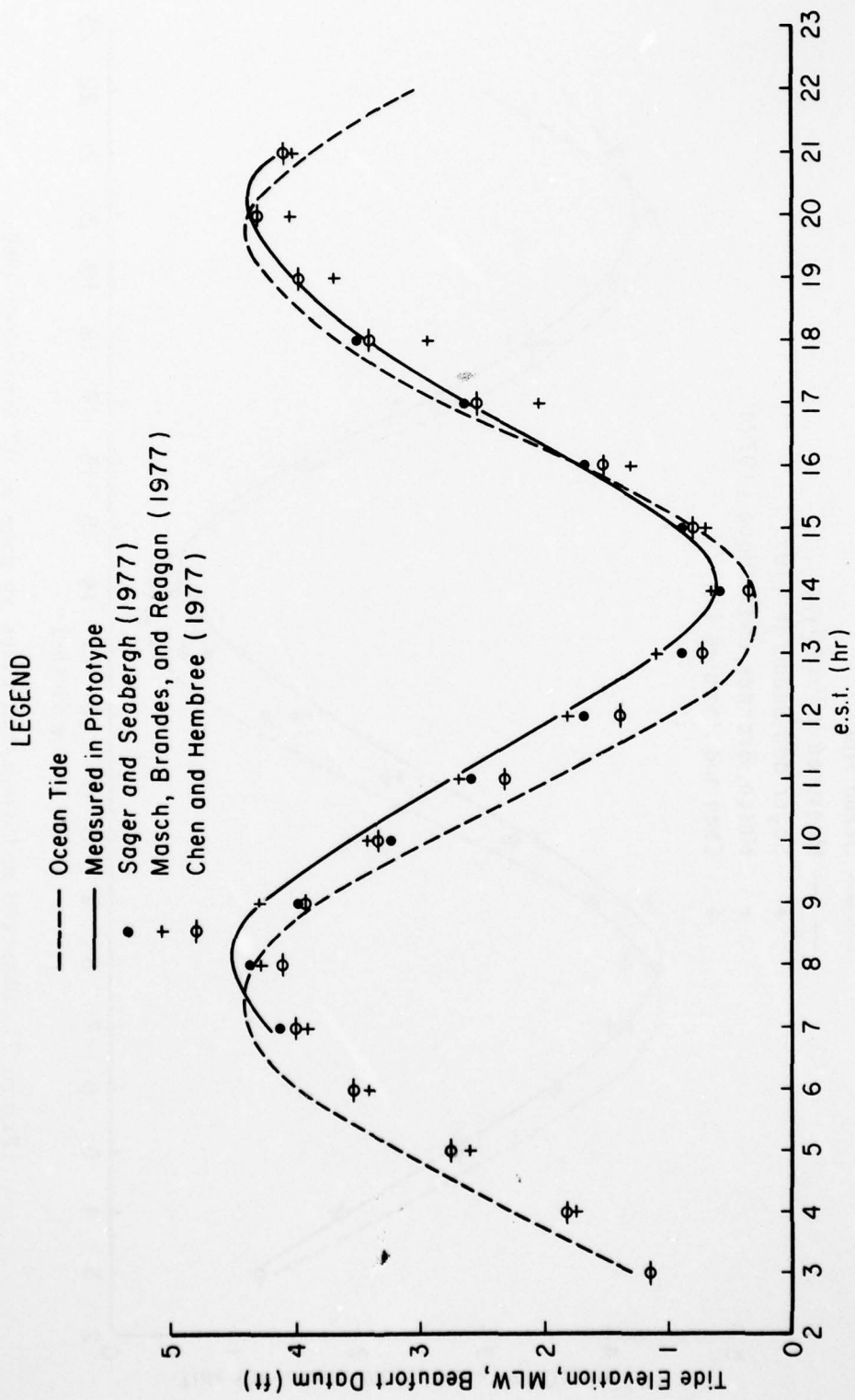


Figure 8. Observed and predicted tides at gage 4, 12 September 1969.

AD-A052 795

COASTAL ENGINEERING RESEARCH CENTER FORT BELVOIR VA
COMPARISON OF NUMERICAL AND PHYSICAL HYDRAULIC MODELS, MASONBOR--ETC(U)
JUN 77 D L HARRIS, B R BODINE
CERC-6ITI-6

F/G 8/8

UNCLASSIFIED

NL

2 OF 3

AD A052795



LEGEND

- Ocean Tide
- Measured in Prototype
- Sager and Seabergh (1977)
- + Masch, Brandes, and Reagan (1977)
- ⊖ Chen and Hembree (1977)

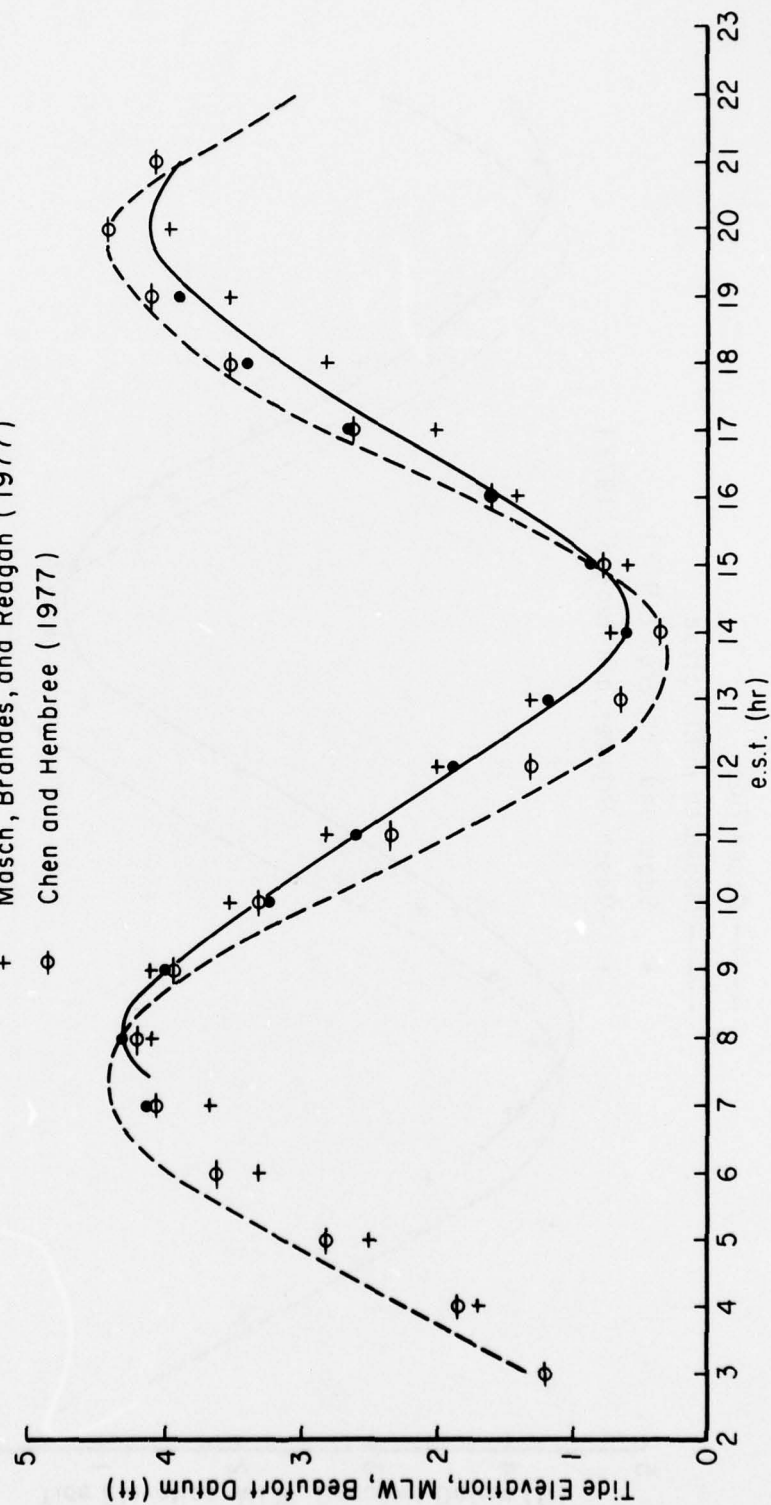


Figure 9. Observed and predicted tides at gage 5, 12 September 1969.

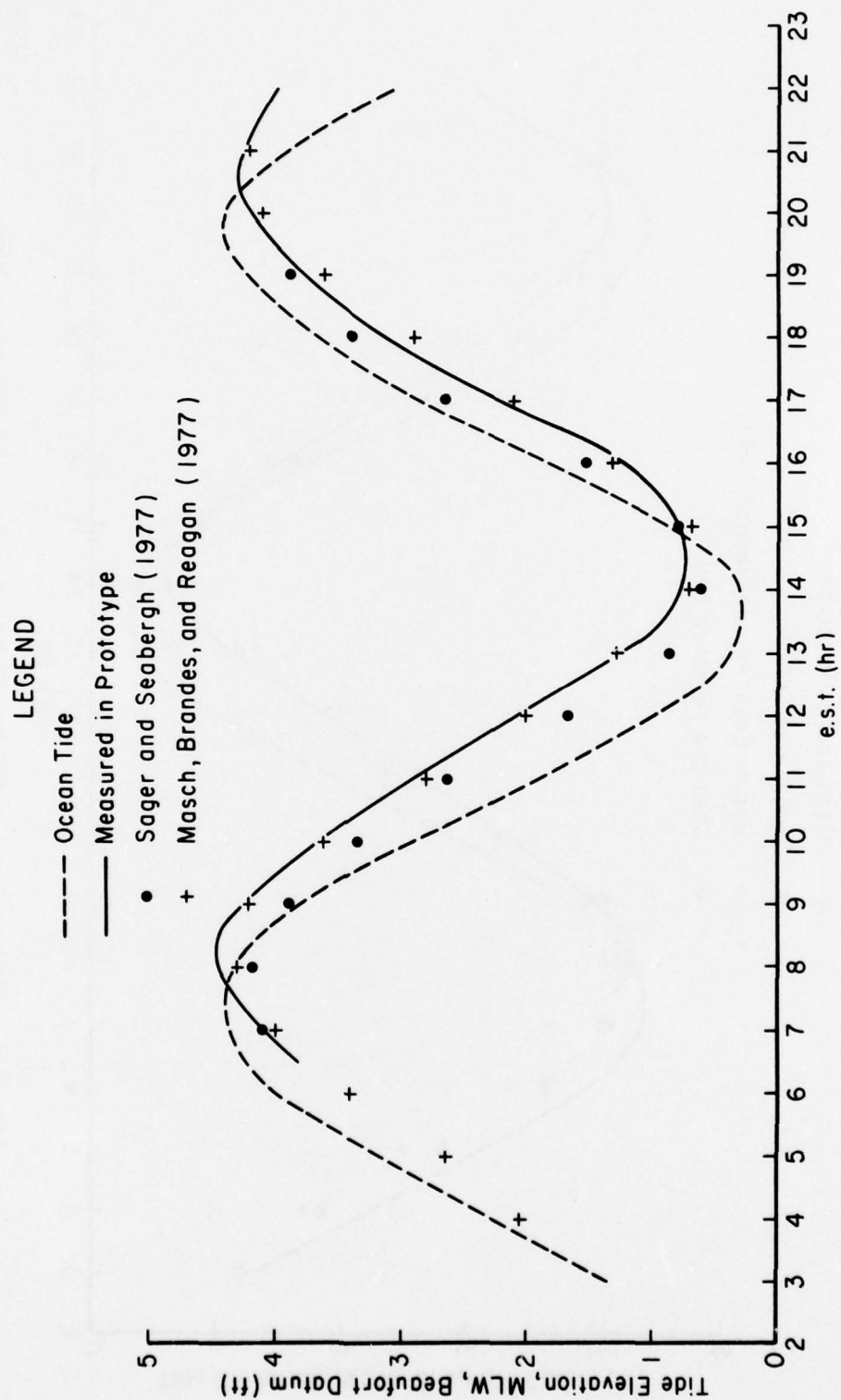


Figure 10. Observed and predicted tides at gage 6, 12 September 1969.

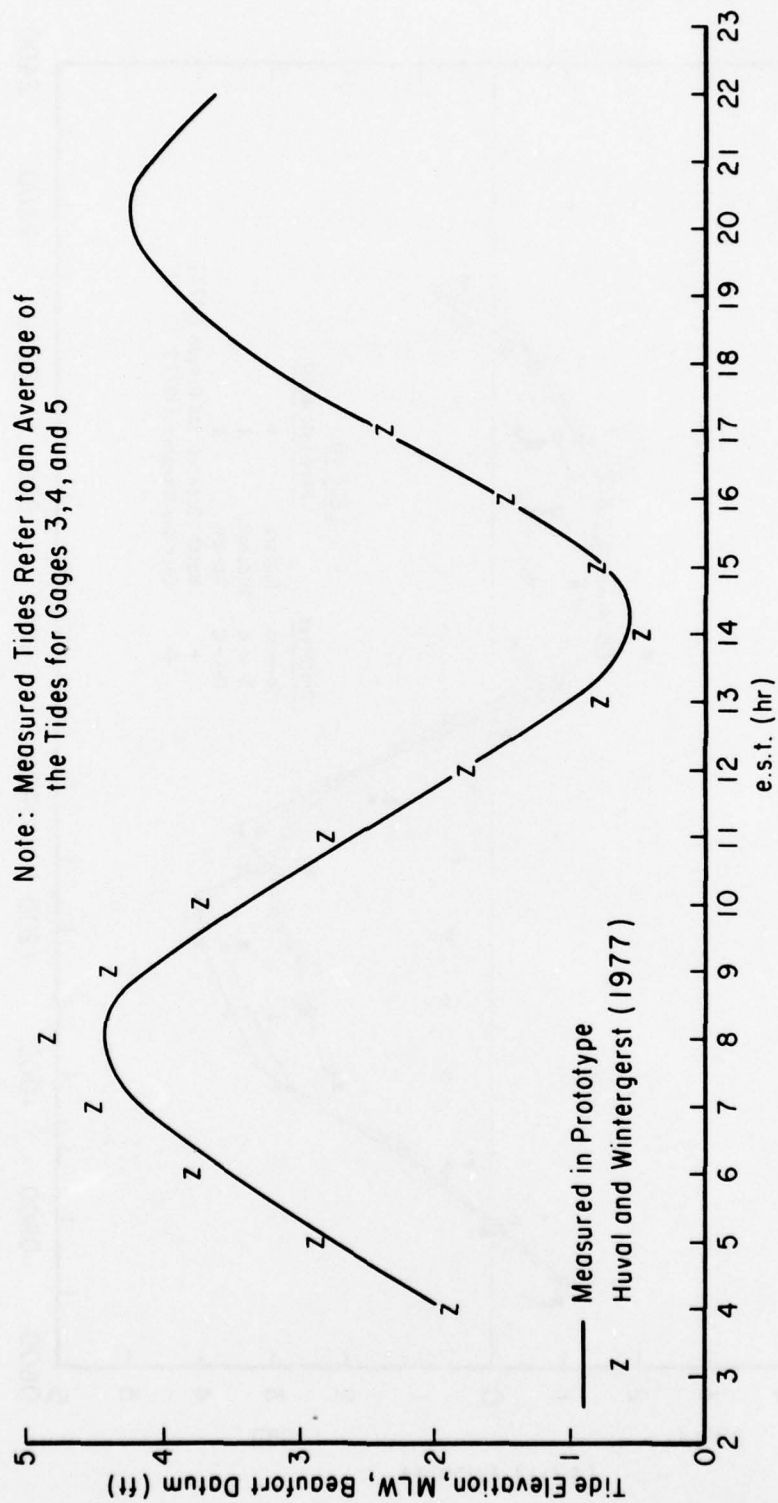


Figure 11. Observed and predicted tides for embayment area.

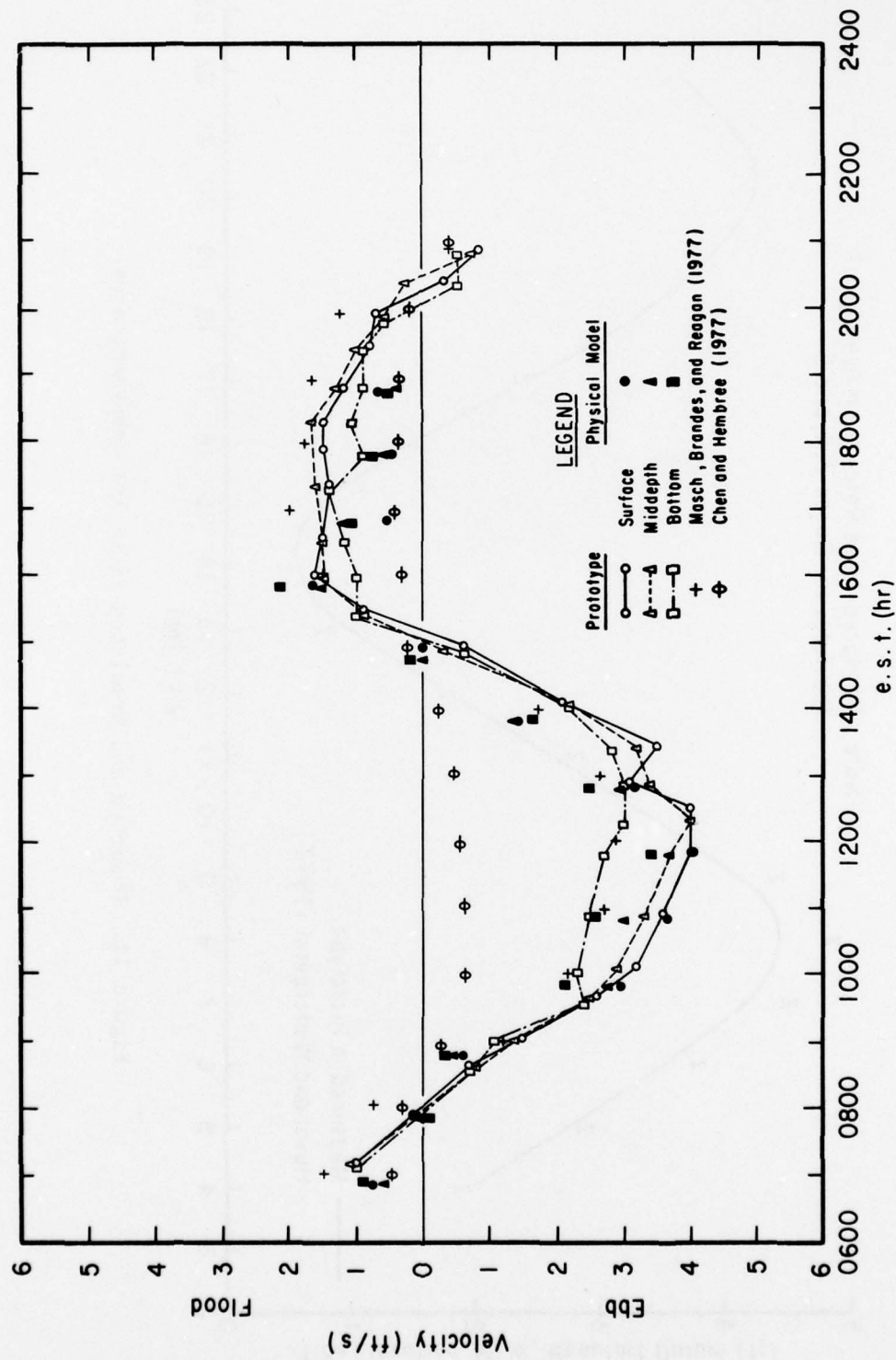


Figure 12. Prototype and predicted velocity for Masonboro Inlet at range 1, station N (north), 12 September 1969.

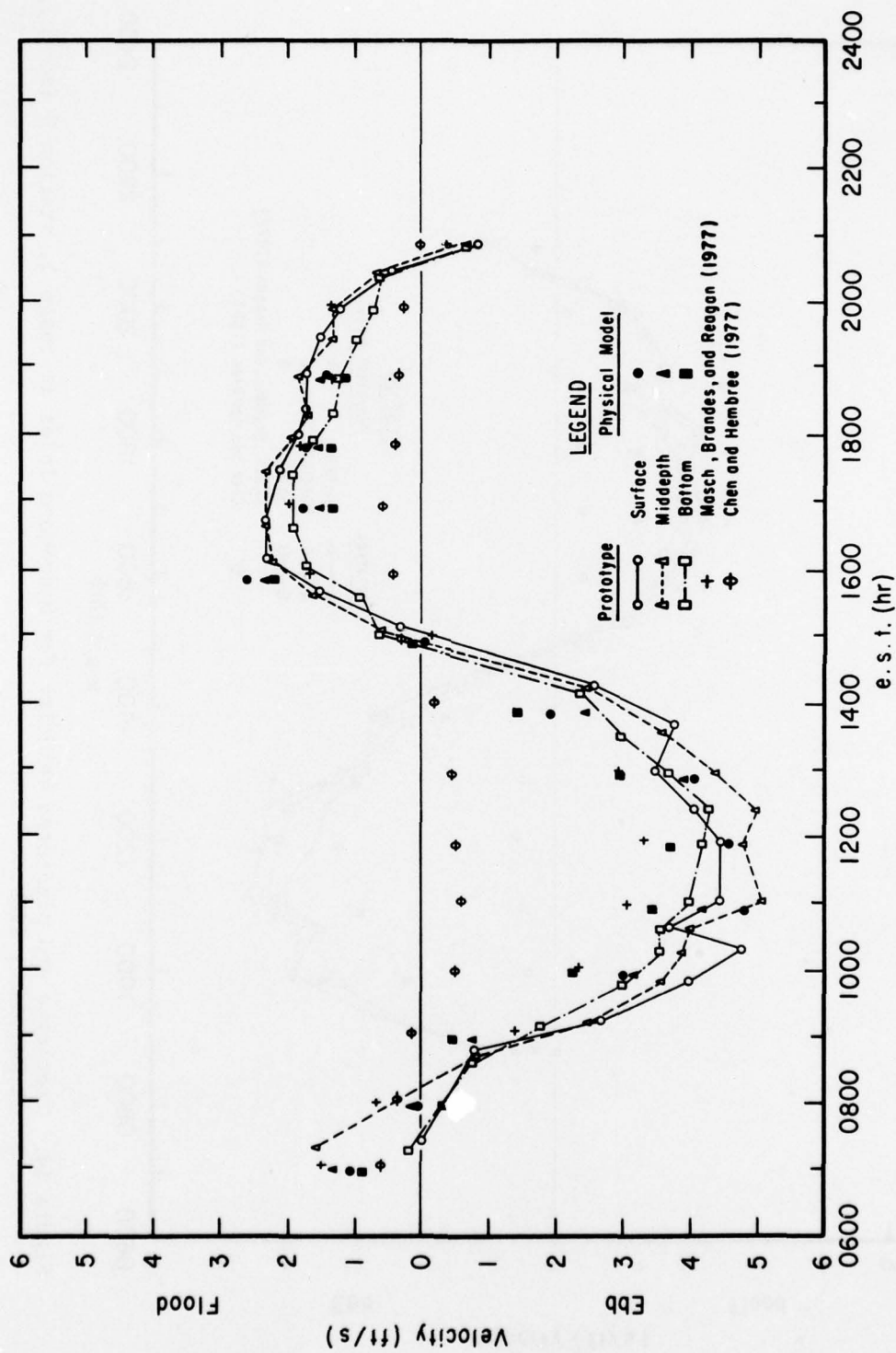


Figure 13. Prototype and predicted velocity for Masonboro Inlet at range 1, station C (center), 12 September 1969.

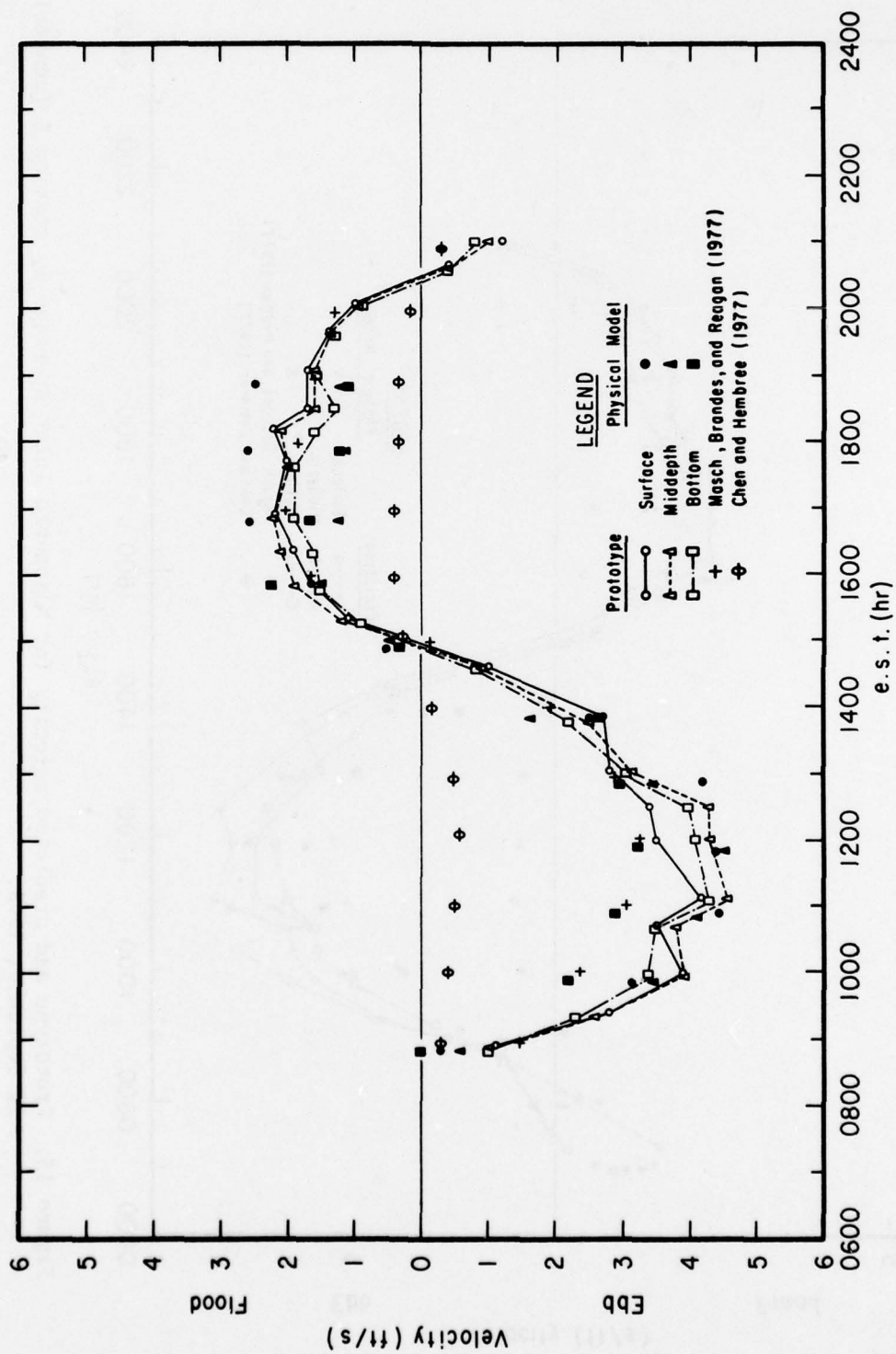


Figure 14. Prototype and predicted velocity for Masonboro Inlet at range 1, station S (south), 12 September 1969.

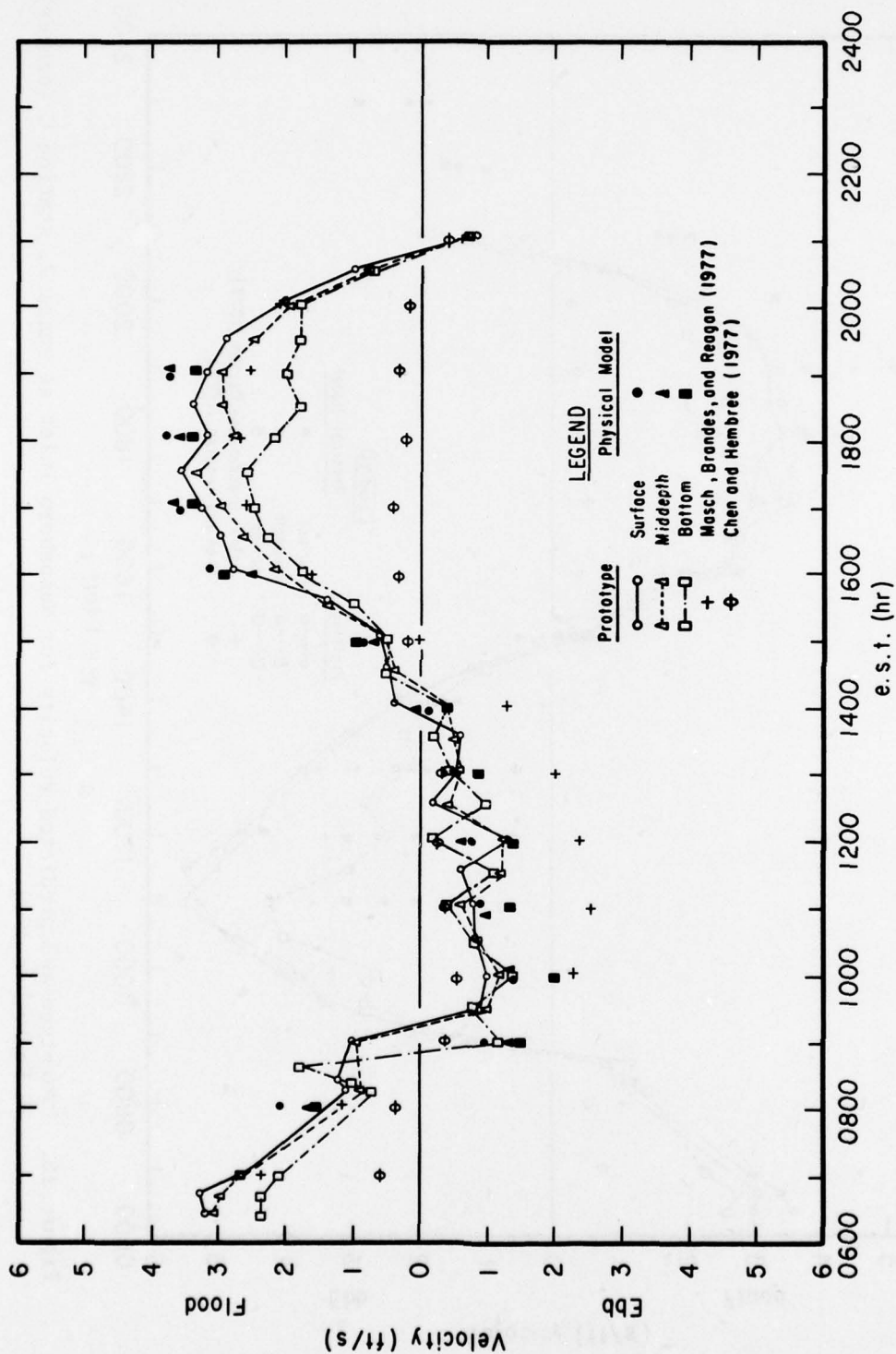


Figure 15. Prototype and predicted velocity for Masonboro Inlet at range 2, station N (north), 12 September 1969.

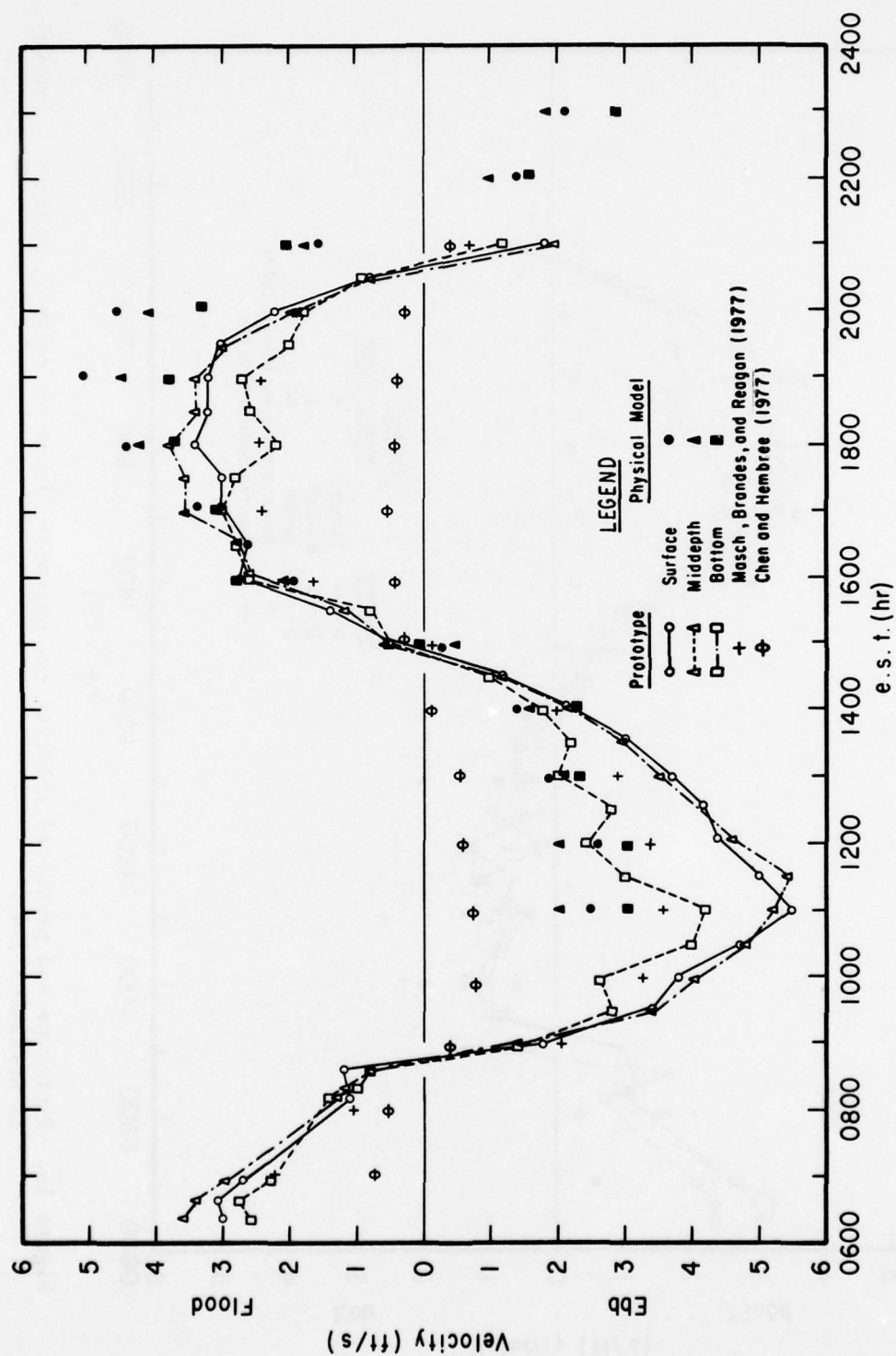


Figure 16. Prototype and predicted velocity for Masonboro Inlet at range 2, station C (center), 12 September 1969.

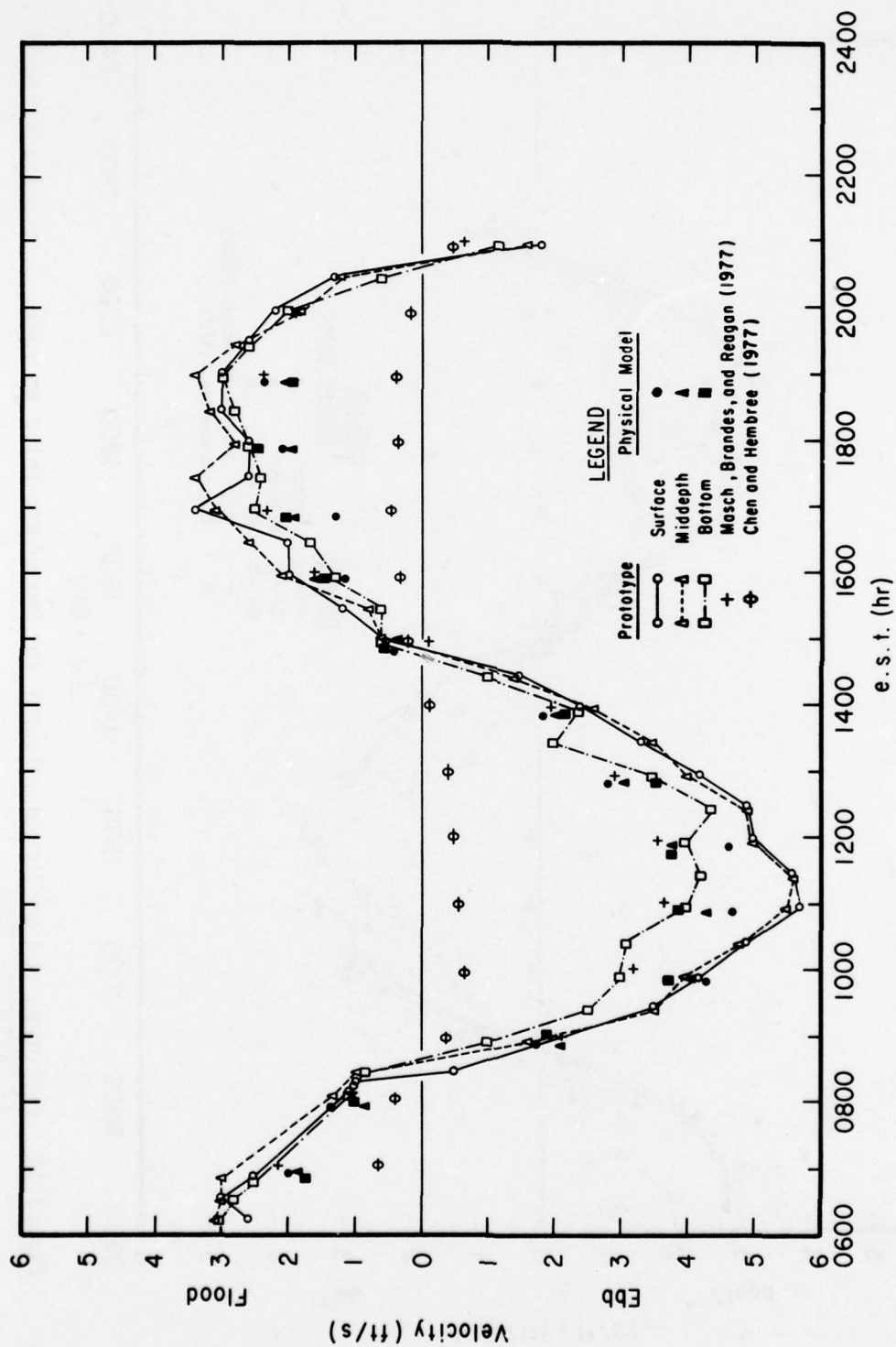


Figure 17. Prototype and predicted velocity for Masonboro Inlet at range 2, station S (south), 12 September 1969.

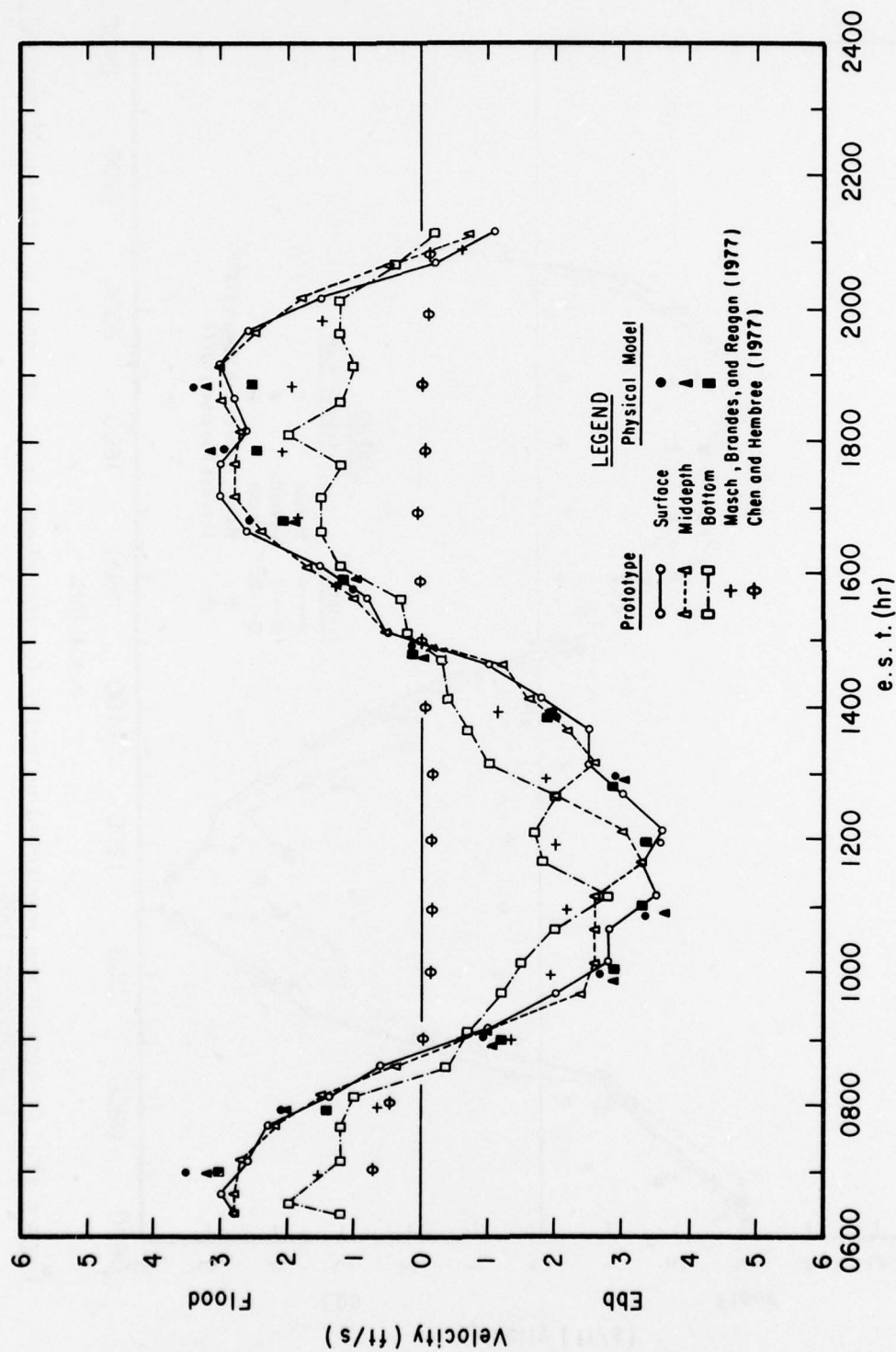


Figure 18. Prototype and predicted velocity for Masonboro Inlet at range 3, station N (north), 12 September 1969.

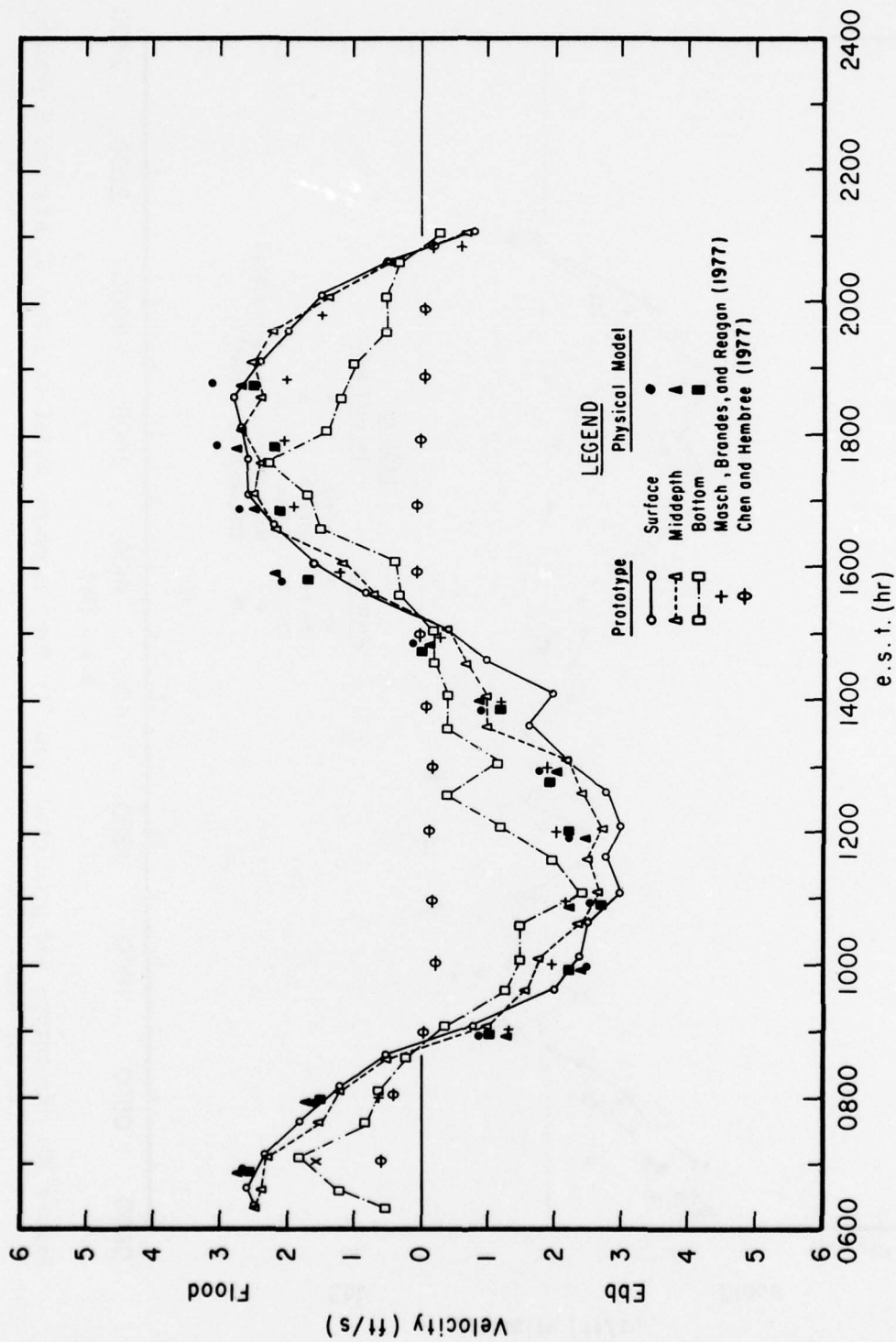


Figure 19. Prototype and predicted velocity for Masonboro Inlet at range 3, station C (center), 12 September 1969.

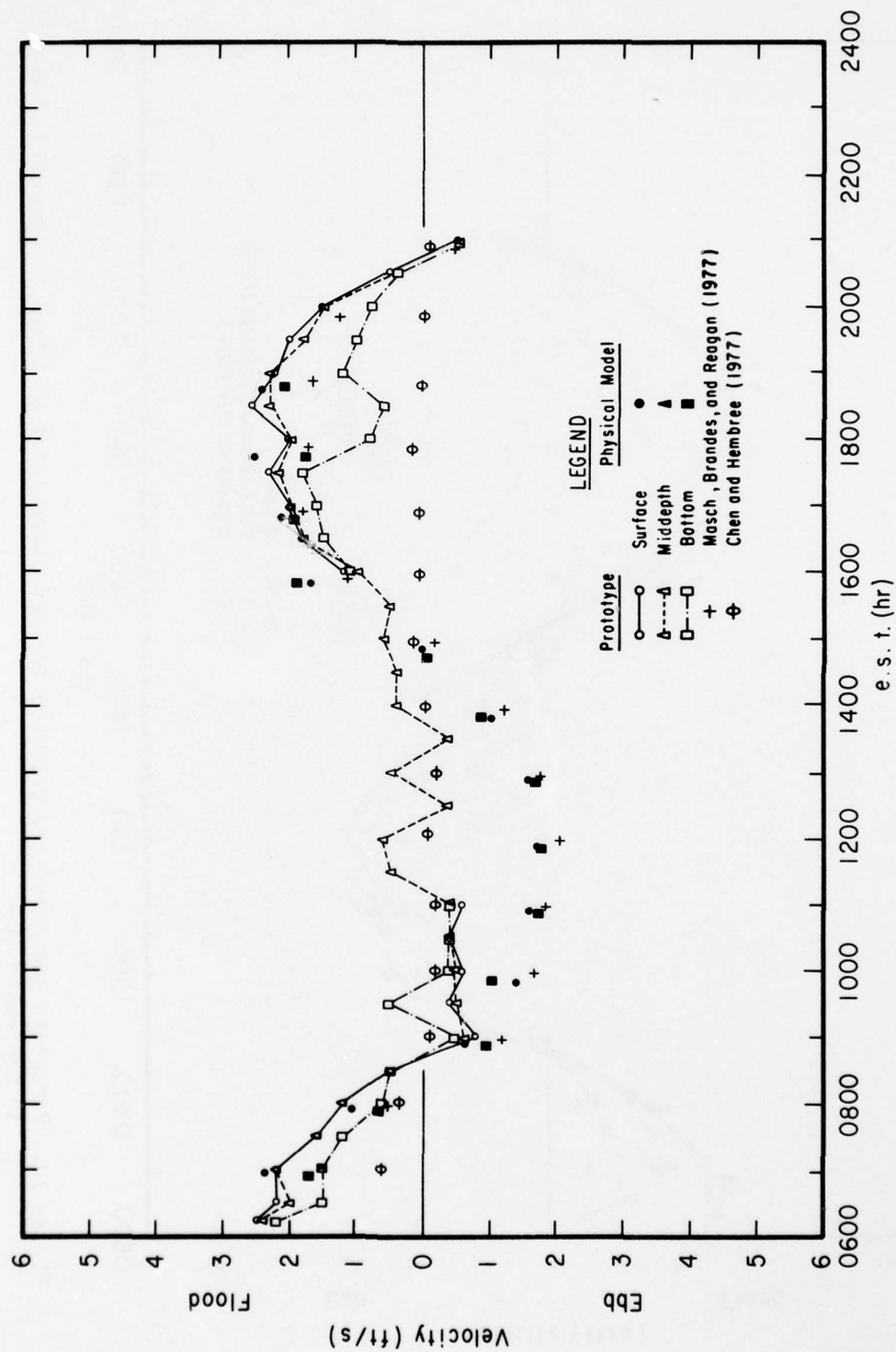


Figure 20. Prototype and predicted velocity for Masonboro Inlet at range 3, station S (south), 12 September 1969.

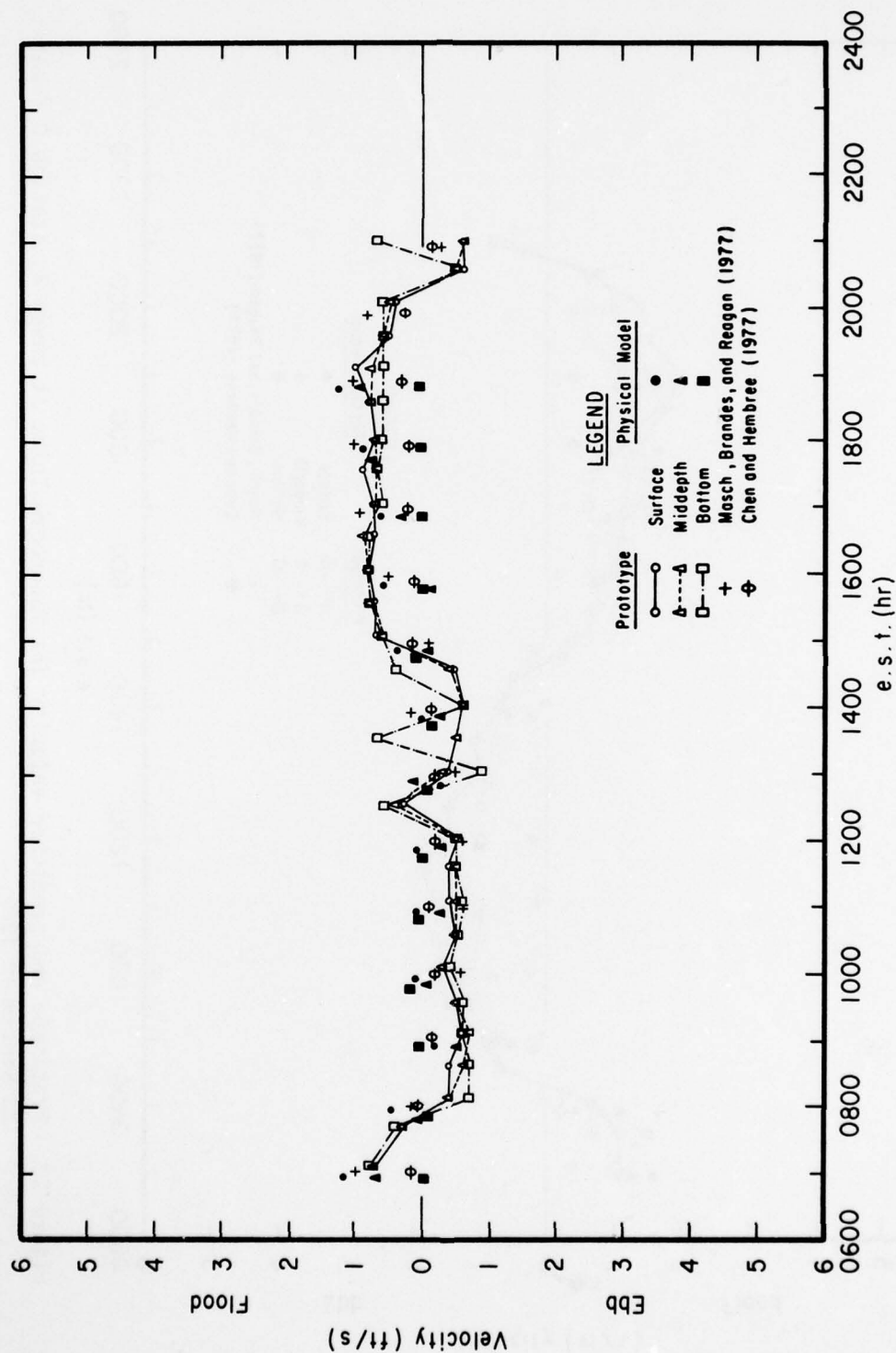


Figure 21. Prototype and predicted velocity for Masonboro Inlet at range 4, station W (west), 12 September 1969.

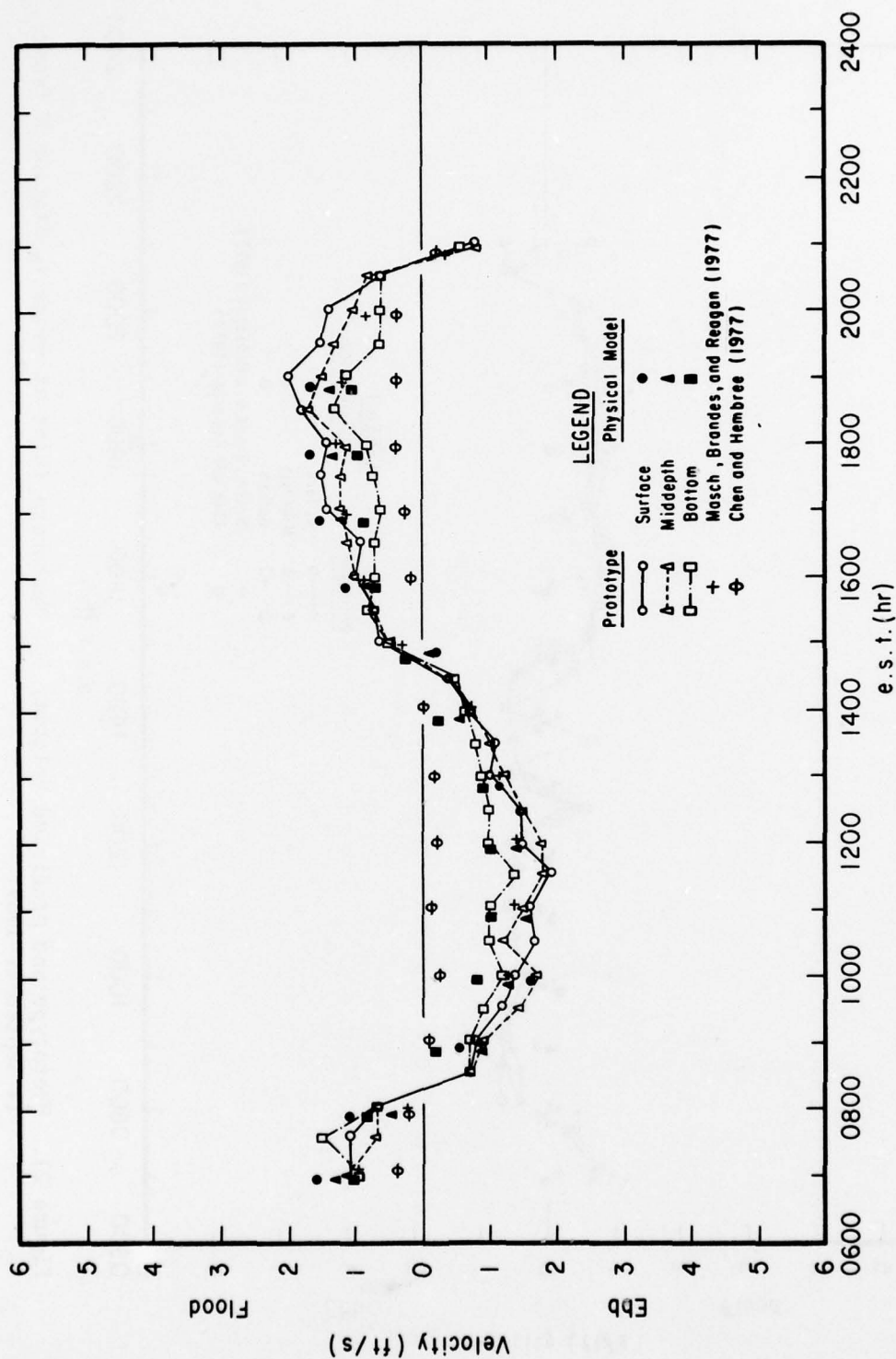


Figure 22. Prototype and predicted velocity for Masonboro Inlet at range 4, station C (center), 12 September 1969.

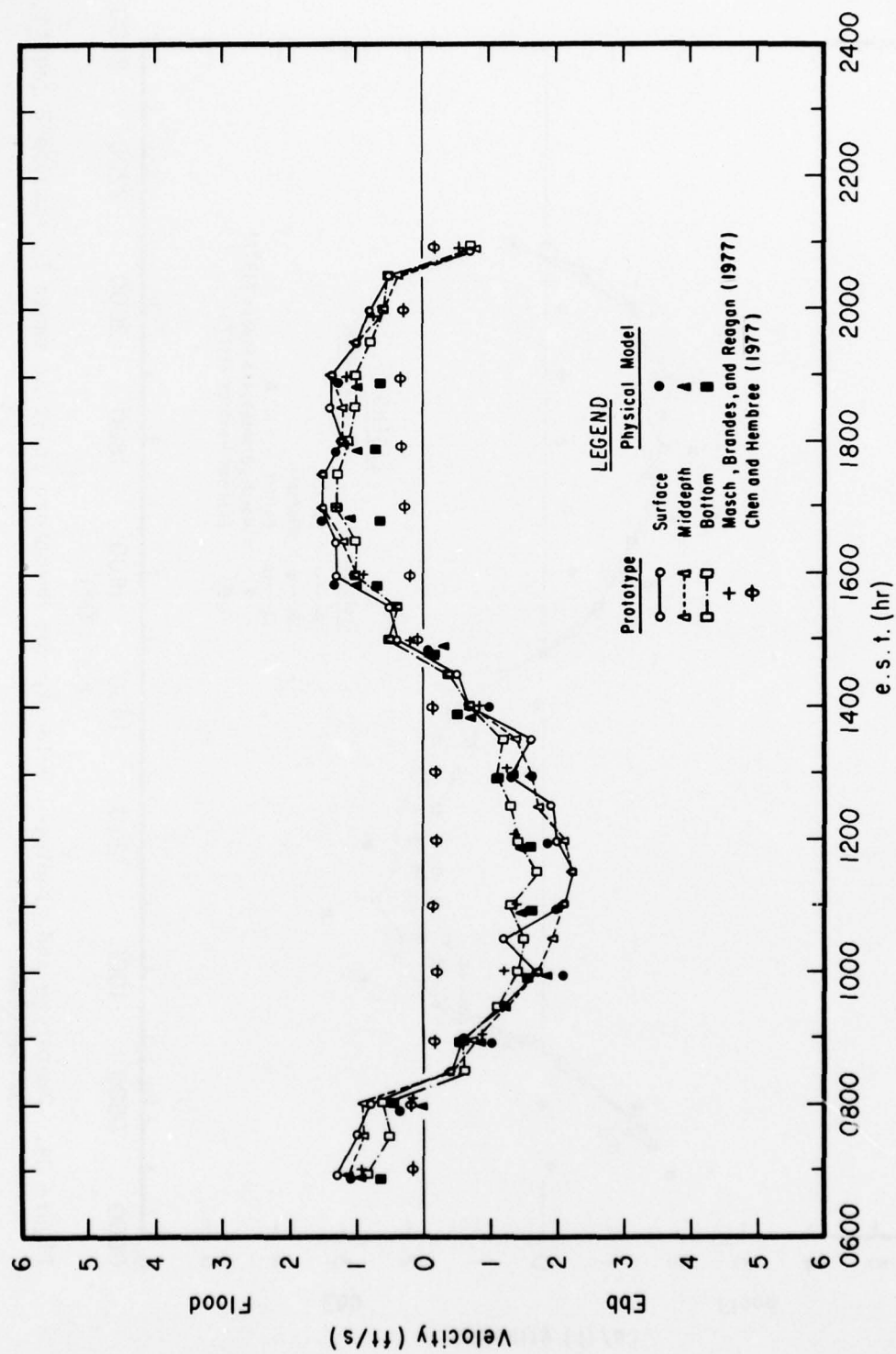


Figure 23. Prototype and predicted velocity for Masonboro Inlet at range 4, station E (east), 12 September 1969.

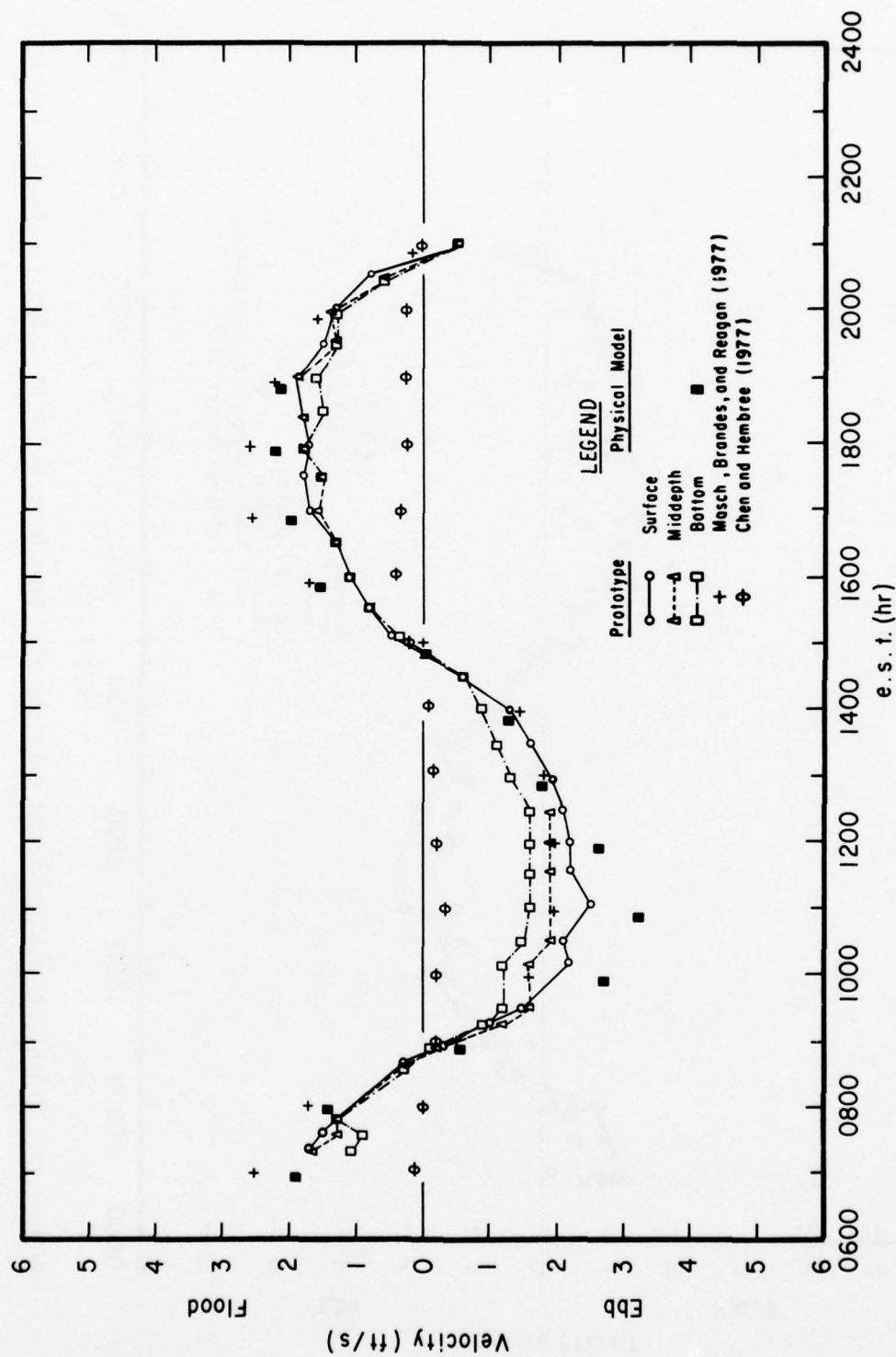


Figure 24. Prototype and predicted velocity for Masonboro Inlet at range 5, station E (east), 12 September 1969.

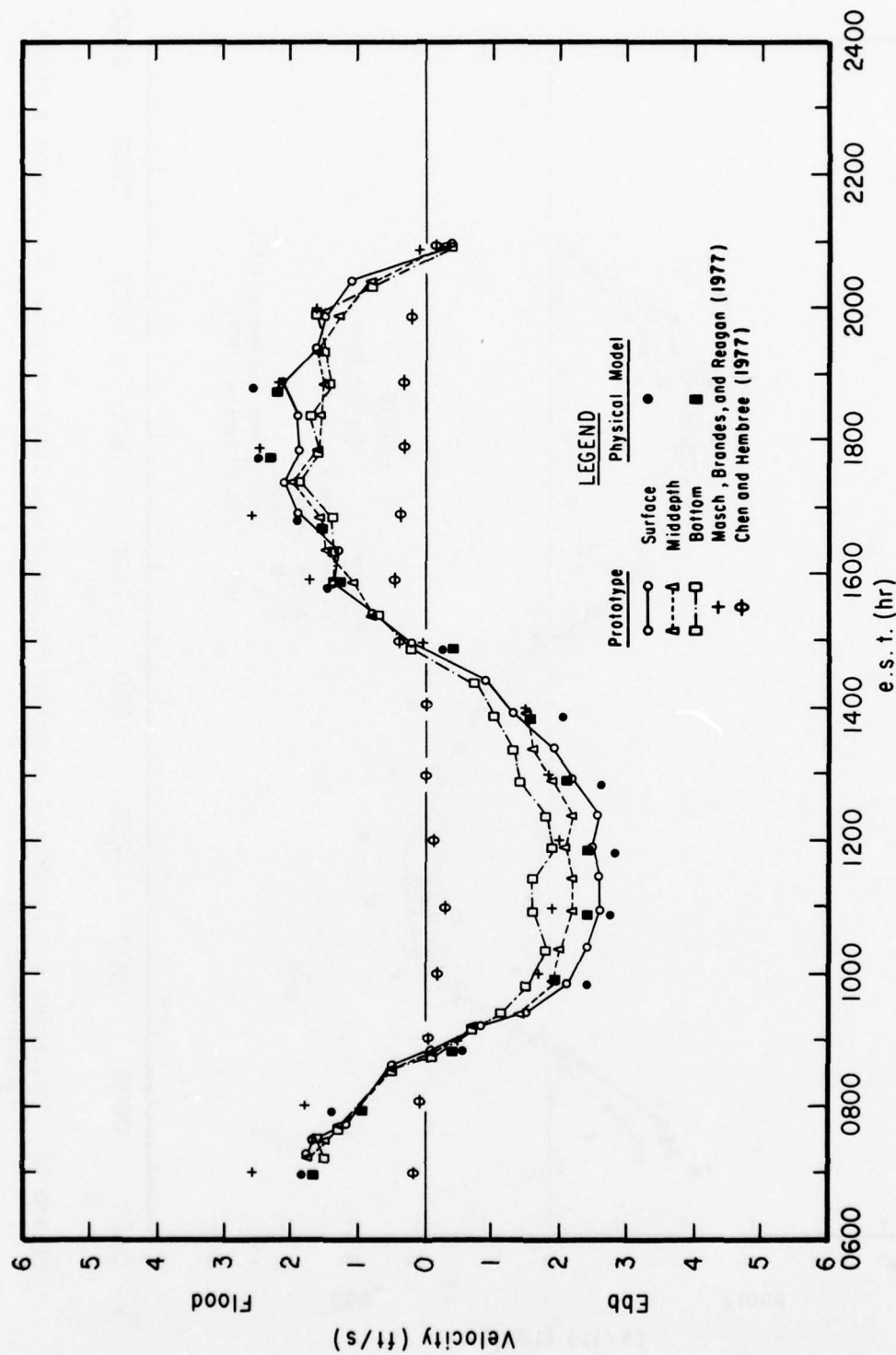


Figure 25. Prototype and predicted velocity for Masonboro Inlet at range 5, station C (center), 12 September 1969.

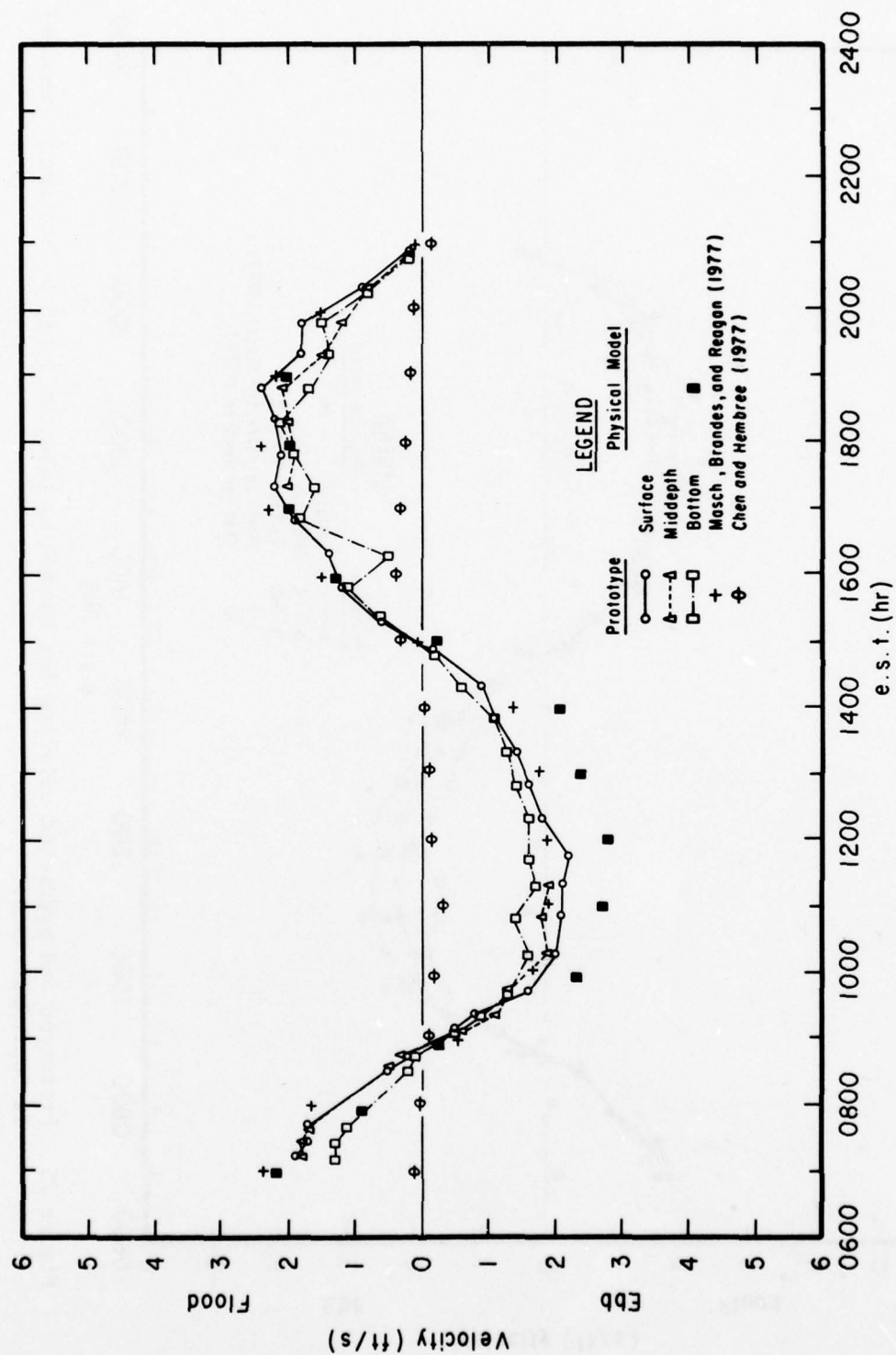


Figure 26. Prototype and predicted velocity for Masonboro Inlet at range 5, station W (west), 12 September 1969.

The velocity curves (Figs. 12 to 26) show that Chen and Hembree (1977) were unable to achieve a good velocity verification. Although the phasing was in fairly good agreement with observations, the magnitude of the flood and ebb velocities was generally poor with respect to the prototype velocities. However, both Sager and Seabergh (1977) and Masch, Brandes, and Reagan (1977) obtained a better velocity verification.

The lumped parameter mathematical model, because of its formulation, can predict only the mean velocities in the throat of the inlet. To show how well this model was calibrated to prototype conditions, reduction of the velocities measured in the inlet to mean velocities was necessary. To obtain mean velocities for the inlet from the measurements, all nine measurements for the three velocity stations were averaged. A simple average was used to determine both the predicted and prototype mean velocities. A comparison of the inlet velocities reproduced in the lumped parameter model and the mean prototype velocities is shown in Figure 27. The figure also shows the mean velocities determined by Masch, Brandes, and Reagan (1977) and Sager and Seabergh (1977). Results are not shown in Chen and Hembree (1977) because of the poor velocity reproductions.

Both the physical and numerical models by Masch, Brandes, and Reagan simulated the prototype velocities at all stations more satisfactorily than the model by Chen and Hembree (see Figs. 12 to 26). However, it is difficult to determine whether the physical model or the numerical model by Masch, Brandes, and Reagan gave the best overall reproduction. A systematic procedure for making this determination is to compare the rms difference between prototype velocities and the velocities obtained from the models.

To carry out such an analysis, the prototype and simulated velocities were tabulated hourly for each station. Velocities measured in the physical model and prototype were converted to vertically averaged velocities to agree with the velocities reproduced in the numerical model. These conversions were made by taking a simple average of the velocities, usually given at three levels in the vertical, for a given time level. The root-mean-square velocity difference ($RMS\Delta$) was determined for each station in both models. The $RMS\Delta$ is defined by:

$$RMS\Delta = \left[\frac{1}{N} \sum (Y - X)^2 \right]^{1/2}, \quad (111)$$

where Y is the model velocity, X is the prototype velocity for the same observation time, and N is the number of variables compared. The $RMS\Delta$'s were normalized by division by the mean-square value of the prototype measurement $RMSP$, defined by:

$$RMSP = \left[\frac{1}{N} \sum X^2 \right]^{1/2}. \quad (112)$$

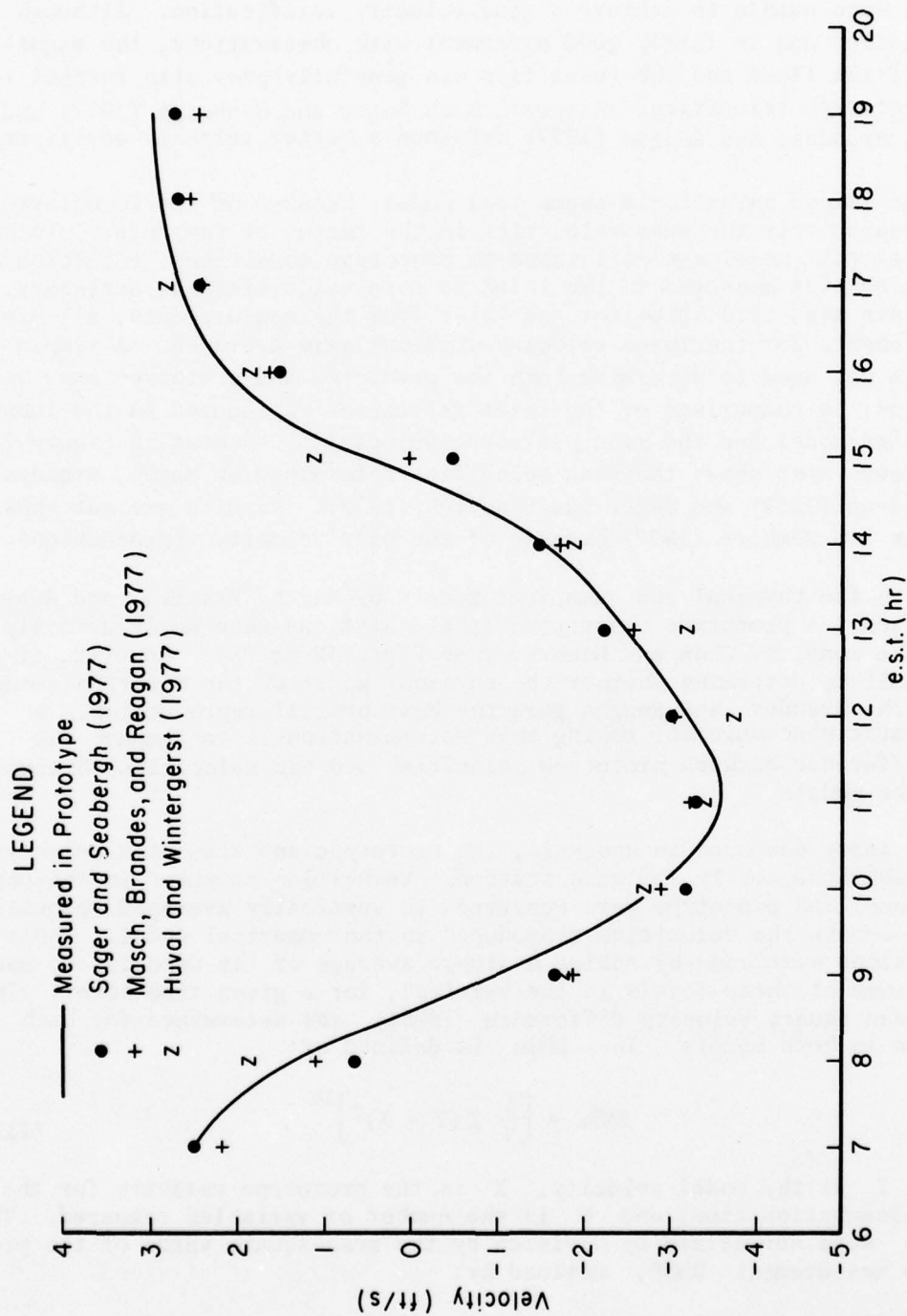


Figure 27. Prototype and predicted mean velocity in throat of Masonboro Inlet.

The results of this analysis for each velocity station are shown in Table 2. The last two columns in the table give the relative normalized variations, $N(RMS\Delta/RMSP)^2$, for the physical and Masch, Brandes, and Reagan (1977) models. A comparison of the values in the columns implies that velocities are reproduced more satisfactorily at some stations in the physical model and at other stations in the model of Masch, Brandes, and Reagan. If each of the last two columns in Table 2 is summed and divided by the sum of N , the overall normalized mean squares are found. The square root of the normalized mean squares is simply the normalized root mean squares, $RMS\Delta/RMSP$. By carrying out these calculations, it is found that $RMS\Delta/RMSP = 0.355$ for the physical model and 0.299 for the model by Masch, Brandes, and Reagan. If those stations are omitted when velocity data were missing at some levels in the vertical in the physical model, then $RMS\Delta/RMSP = 0.313$ in the physical model and 0.300 in the model by Masch, Brandes, and Reagan. Since only slight differences in the overall rms deviations were found, it is impossible to conclude that either model reproduced the velocities more satisfactorily than the other because of possible errors in reading the velocities from curves and only a limited set of data was used in the analysis. In general, both models performed about equally well in reproducing the velocities. However, it should not be assumed that the best possible calibrator was obtained for any of the models.

3. Application of the Models.

The second phase of the modeling study was applying the calibrated models of Masonboro Inlet to calculations for periods where the geometry of the system was substantially different from that for the 1969 conditions. Preproject conditions (1964) when Masonboro Inlet was in a natural state were selected.

Because tides or velocities were not available for the preproject conditions, idealized mean and spring tides characteristic of the Masonboro Inlet area were used for excitation of the models. The idealized tidal curves are shown in Figure 28.

Application of the models to Masonboro Inlet for the preproject conditions was made primarily to obtain additional insight on the performance of numerical models. If the initial calibration of the physical model had been significantly better than either numerical model, and if the divergence between physical and numerical models had increased significantly for the preproject conditions, the assumption would be that neither of the numerical models considered would be reliable for application to any condition other than that used in the initial calibration. Due to the small differences between the idealized mean and spring tides, the comparison of the modeling result is shown only for the mean tide conditions (Fig. 28). Information was furnished for modifying the models to reflect the hydrography corresponding to the November 1964 preproject conditions (Fig. 29).

Table 2. Statistical comparison of velocity data (ft/s).

Sta.	N	Physical		MBR ¹		Physical		MBR		Prototype		Physical		MBR		Physical		MBR	
		RMSΔ	RMSΔ	RMSΔ	N(RMSΔ) ²	RMSΔ	RMSΔ	RMSΔ	N(RMSΔ) ²	RMSΔ	RMSΔ	RMSΔ	RMSΔ	RMSΔ	N(RMSΔ) ²	RMSΔ	RMSΔ	RMSΔ	N(RMSΔ) ²
1 N	13	0.580	0.293	4.376	1.114	1.967	3.869	0.295	0.149	1.131	0.288	0.288	0.288	0.288	0.288	0.288	0.288	0.288	0.288
1 C	13	0.492	0.568	3.148	4.197	2.494	6.222	0.197	0.228	0.506	0.674	0.674	0.674	0.674	0.674	0.674	0.674	0.674	0.674
1 S	11	0.510	0.506	2.859	2.816	2.445	5.979	0.209	0.207	0.478	0.471	0.471	0.471	0.471	0.471	0.471	0.471	0.471	0.471
2 N	13	0.642	0.040	5.365	5.328	1.486	2.208	0.432	0.431	2.430	2.413	2.413	2.413	2.413	2.413	2.413	2.413	2.413	2.413
2 C	13	0.317	0.620	1.307	5.002	2.876	8.272	0.110	0.216	0.158	0.605	0.605	0.605	0.605	0.605	0.605	0.605	0.605	0.605
2 S	13	0.621	0.725	5.008	6.825	3.044	9.264	0.204	0.238	0.541	0.737	0.737	0.737	0.737	0.737	0.737	0.737	0.737	0.737
3 N	13	0.563	0.818	4.122	8.696	2.044	4.179	0.275	0.400	0.986	2.081	2.081	2.081	2.081	2.081	2.081	2.081	2.081	2.081
3 C	13	0.433	0.332	2.441	1.434	1.822	3.318	0.238	0.182	0.736	0.432	0.432	0.432	0.432	0.432	0.432	0.432	0.432	0.432
3 S	8	0.455 ²	0.435	1.654 ²	1.515	0.963	0.966	0.487 ²	0.452	1.712 ²	1.568	1.568	1.568	1.568	1.568	1.568	1.568	1.568	1.568
4 W	13	0.431	0.344	2.418	1.539	0.627	0.393	0.687	0.549	6.153	3.916	3.916	3.916	3.916	3.916	3.916	3.916	3.916	3.916
4 C	13	0.186	0.179	0.447	0.414	1.121	1.256	0.166	0.160	0.356	0.330	0.330	0.330	0.330	0.330	0.330	0.330	0.330	0.330
4 E	13	0.199	0.294	0.516	1.122	1.242	1.544	0.160	0.237	0.334	0.727	0.727	0.727	0.727	0.727	0.727	0.727	0.727	0.727
5 W	7	0.689 ³	0.302	3.319 ³	0.641	1.592	2.536	0.499 ³	0.190	1.737 ³	0.253	0.253	0.253	0.253	0.253	0.253	0.253	0.253	0.253
5 C	13	0.331 ²	0.411	1.439 ²	2.195	1.593	2.541	0.207 ²	0.258	0.563 ²	0.864	0.864	0.864	0.864	0.864	0.864	0.864	0.864	0.864
5 E	7	0.802 ³	0.374	4.709 ³	0.979	1.588	2.522	0.578 ³	0.236	2.336 ³	0.388	0.388	0.388	0.388	0.388	0.388	0.388	0.388	0.388

¹Masch, Brandes, and Reagan (1977)

²No middepth velocities recorded.

³No surface or middepth velocities recorded.

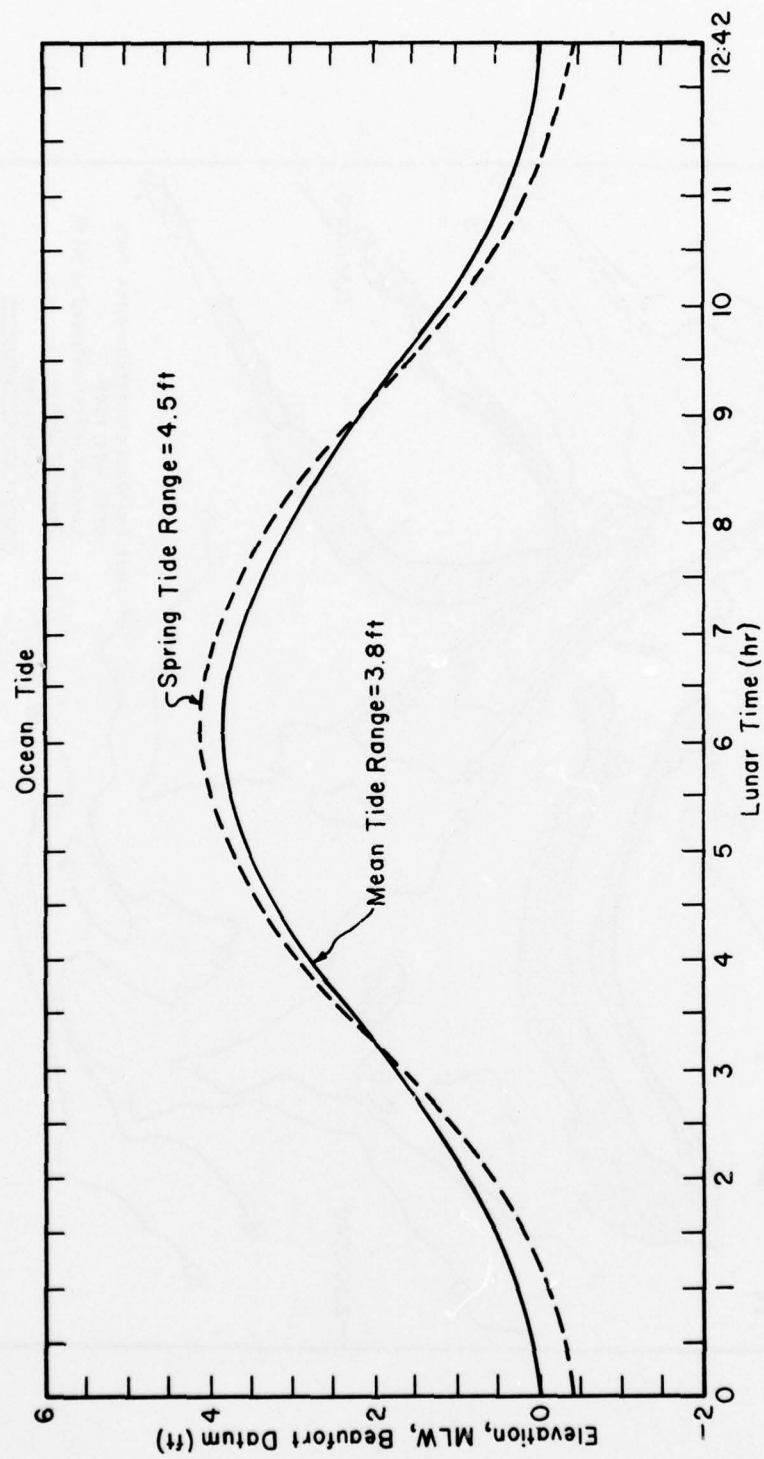
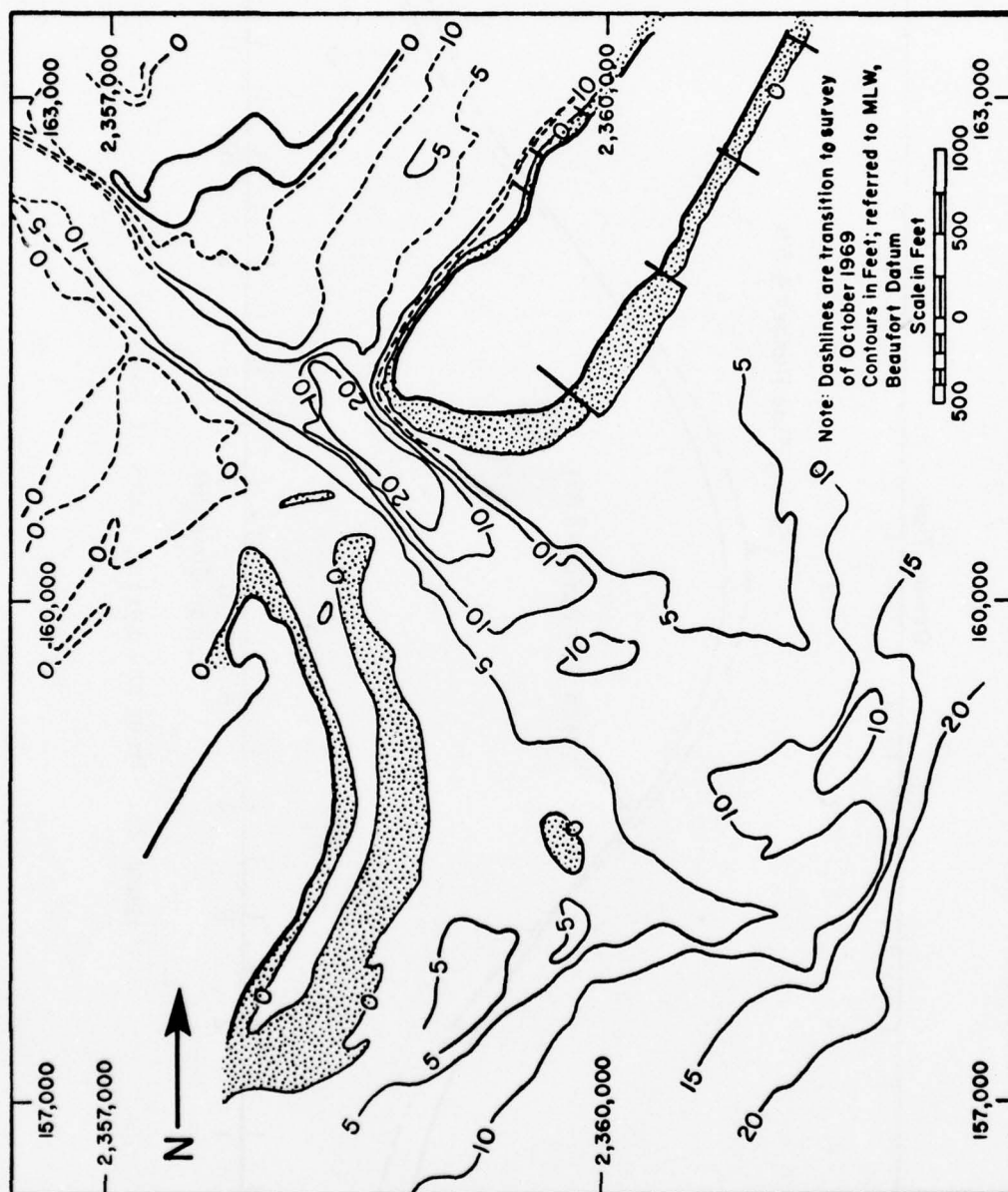


Figure 28. Mean and spring tides at Masonboro Inlet.



The variations in water surface elevations predicted by all three two-dimensional models are shown by hydrographs in Figures 30 to 35. These hydrographs show that, in general, the tides simulated by the two-dimensional mathematical models were in reasonable agreement with those simulated in the physical model. However, about a $\frac{1}{2}$ -hour phase lag occurs in the tides predicted by Masch, Brandes, and Reagan (1977) relative to the predictions by the physical model at gage 6. Chen and Hembree (1977) did not calculate the tide for this location. Since the tides calculated by Masch, Brandes, and Reagan matched the prototype observations at station 6 better than the tides observed in the physical model, the numerical model possibly provided a better approximation than the physical models on the tides at this station.

Figure 36 shows the uniform embayment water level elevations calculated by the lumped parameter model in comparison to the average embayment elevations reproduced in the physical model; the lumped parameter model is in good agreement with the physical model in reproduction of tides for the preproject conditions.

Predicted tidal current velocities for all three models are shown in Figures 37 to 51. The agreement between the physical model and the numerical model by Masch, Brandes, and Reagan is again much better than the agreement between either of these models and the model by Chen and Hembree. However, there are significant differences between the physical model and the numerical model by Masch, Brandes, and Reagan. Stronger ebb current velocities were computed by Masch, Brandes, and Reagan at station 3C (Fig. 44); smaller ebb current velocities were computed by this model at stations 4E, 4W, 5C, and 5W (Figs. 46 and 48 to 51). Why these deviations occurred or which prediction is more correct, is unknown.

The velocities computed by the lumped parameter method (Huval and Wintergerst, 1977) are compared to average velocities in the inlet as predicted by both the physical model (Sager and Seabergh, 1977) and the numerical model (Masch, Brandes, and Reagan, 1977) (Fig. 52).

4. Later Studies.

A new hydrographic survey of Masonboro Inlet was made in July 1974. The physical model of the inlet was remodeled to the 1974 bathymetry and the measurements described above were repeated. The rms differences between model and prototype and two other measures of goodness of calibration were computed. The results are given by Seabergh and Mason (1975). A report covering both physical and numerical models will be published later under the GITI program. The rms differences were slightly larger than in calibration tests, as would be expected when no effort was made to force the model. The rms differences for stations 1 and 2 (which should be most affected by waves in the ocean part of the model) were clearly reduced when waves were added to the model.

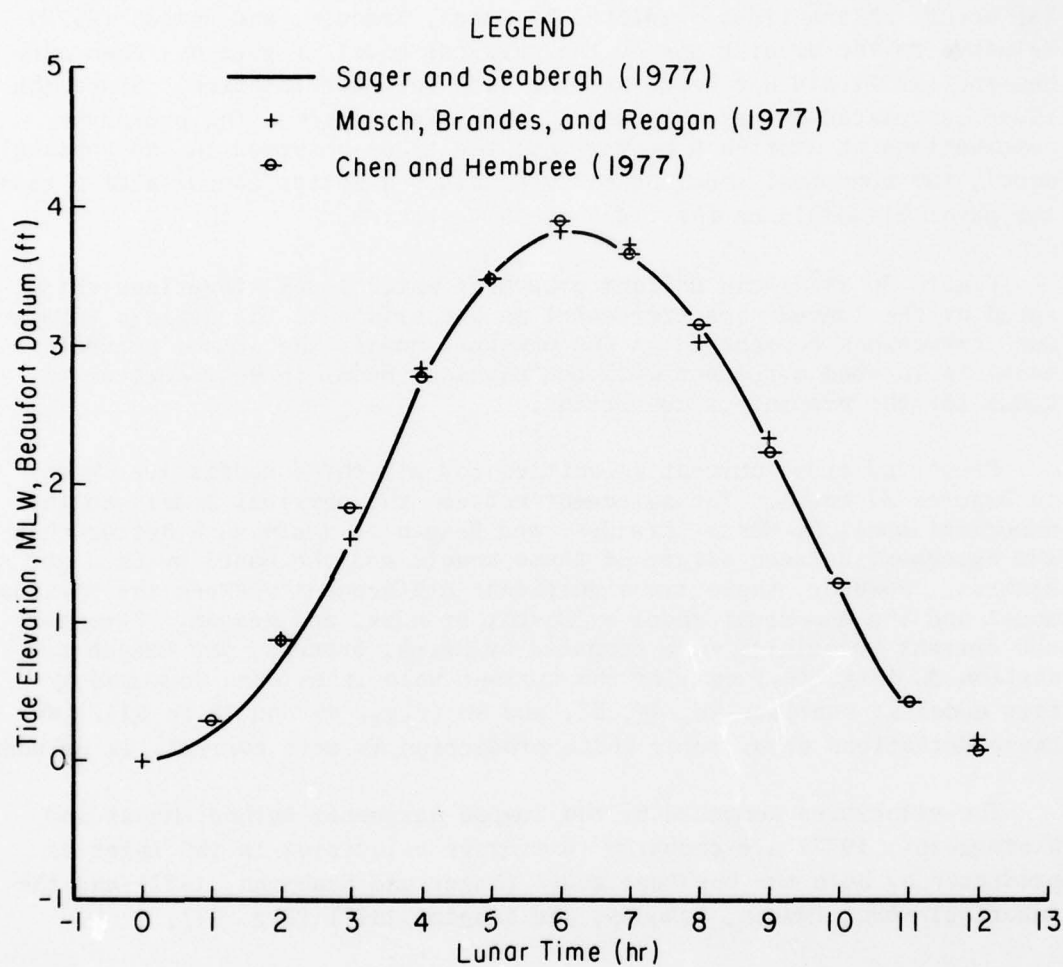


Figure 30. Prejetty (1964) mean tide condition at gage 1.

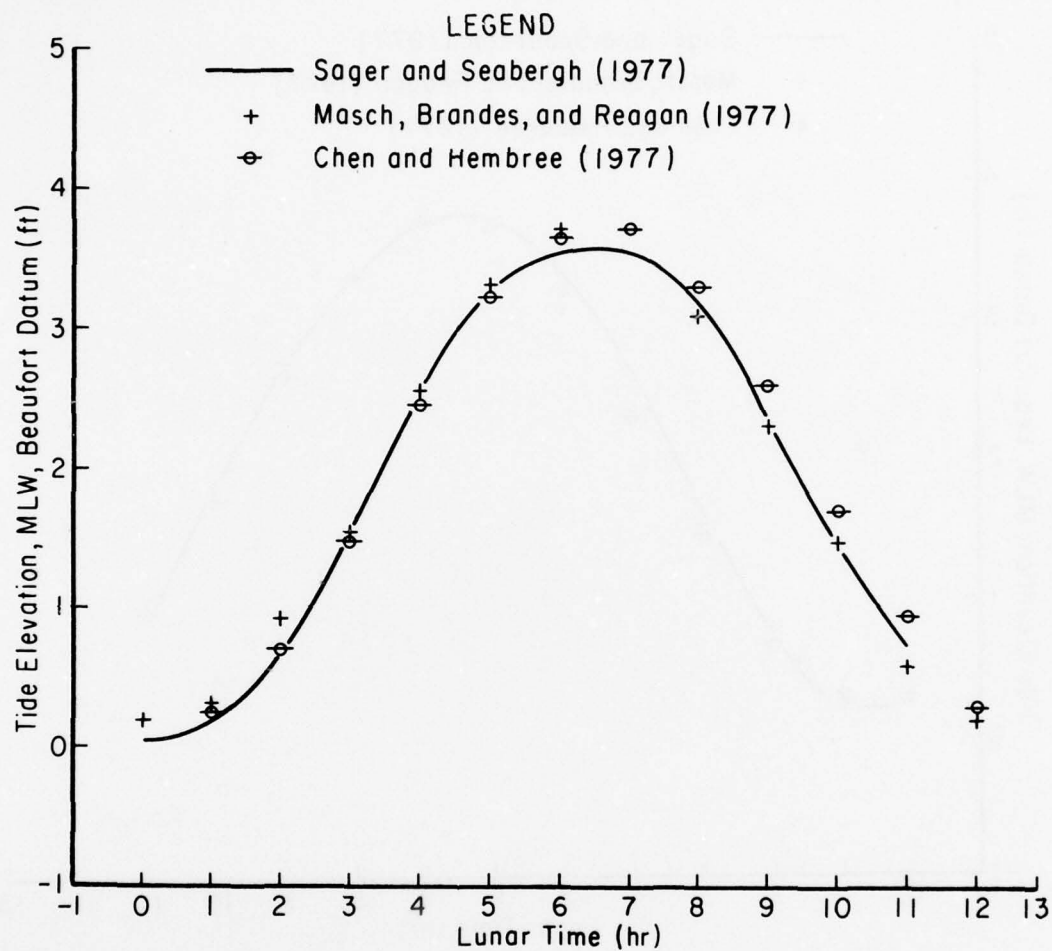


Figure 31. Prejetty (1964) mean tide condition at gage 2.

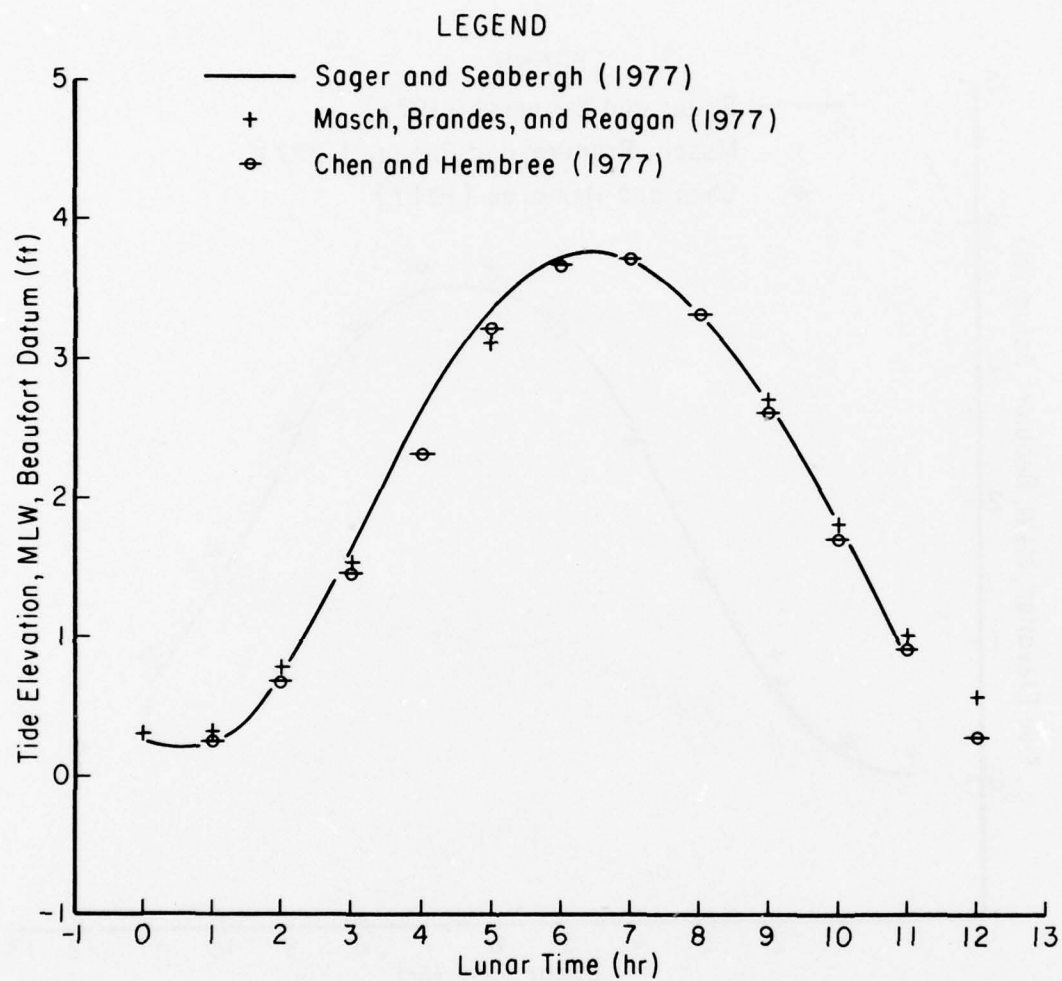


Figure 32. Prejetty (1964) mean tide condition at gage 3.

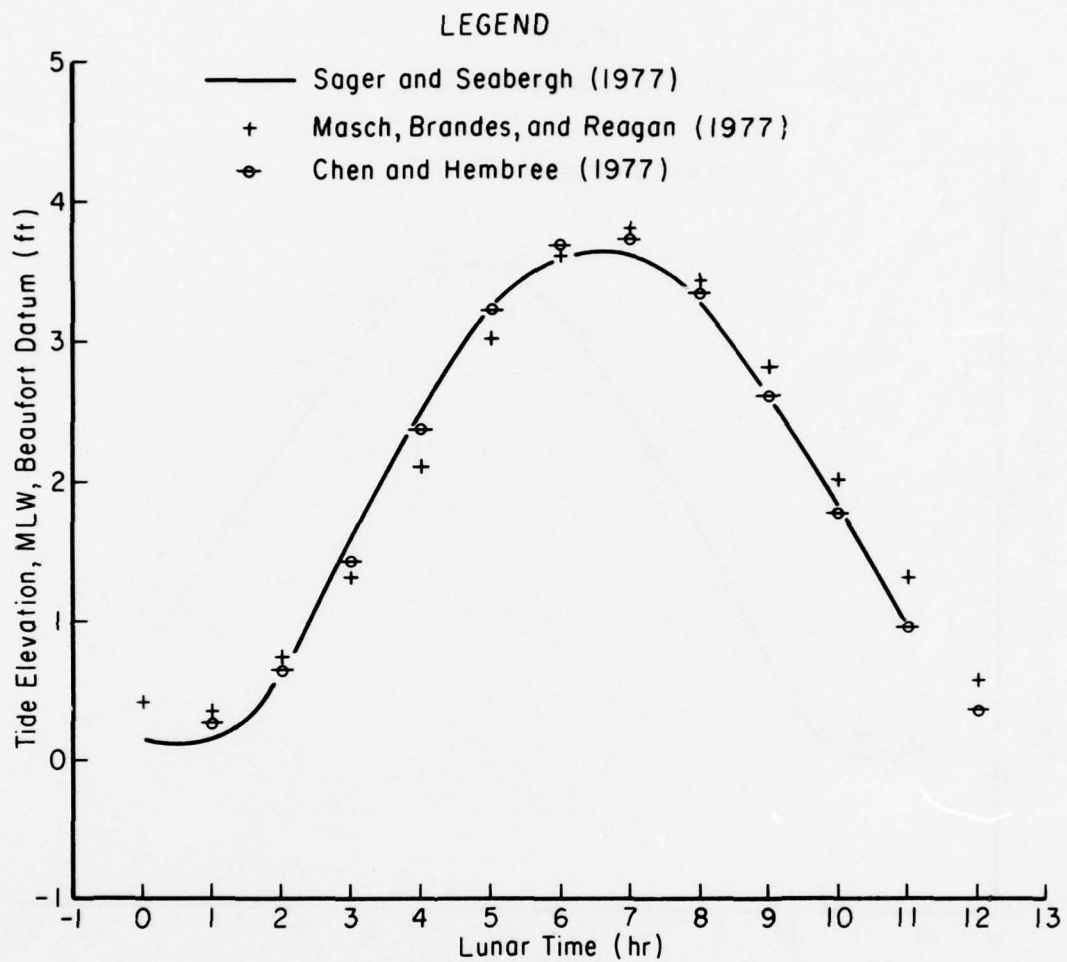


Figure 33. Prejetty (1964) mean tide condition at gage 4.

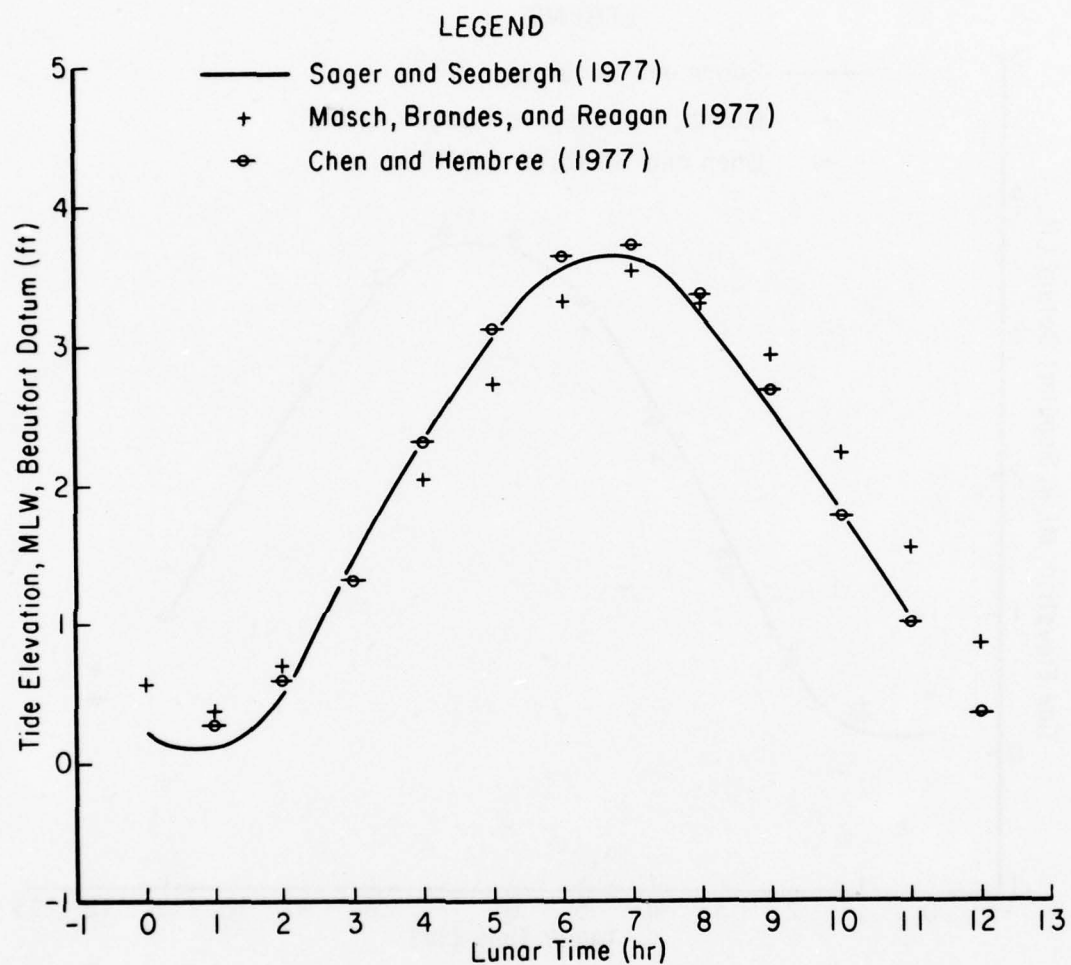


Figure 34. Prejetty (1964) mean tide condition at gage 5.

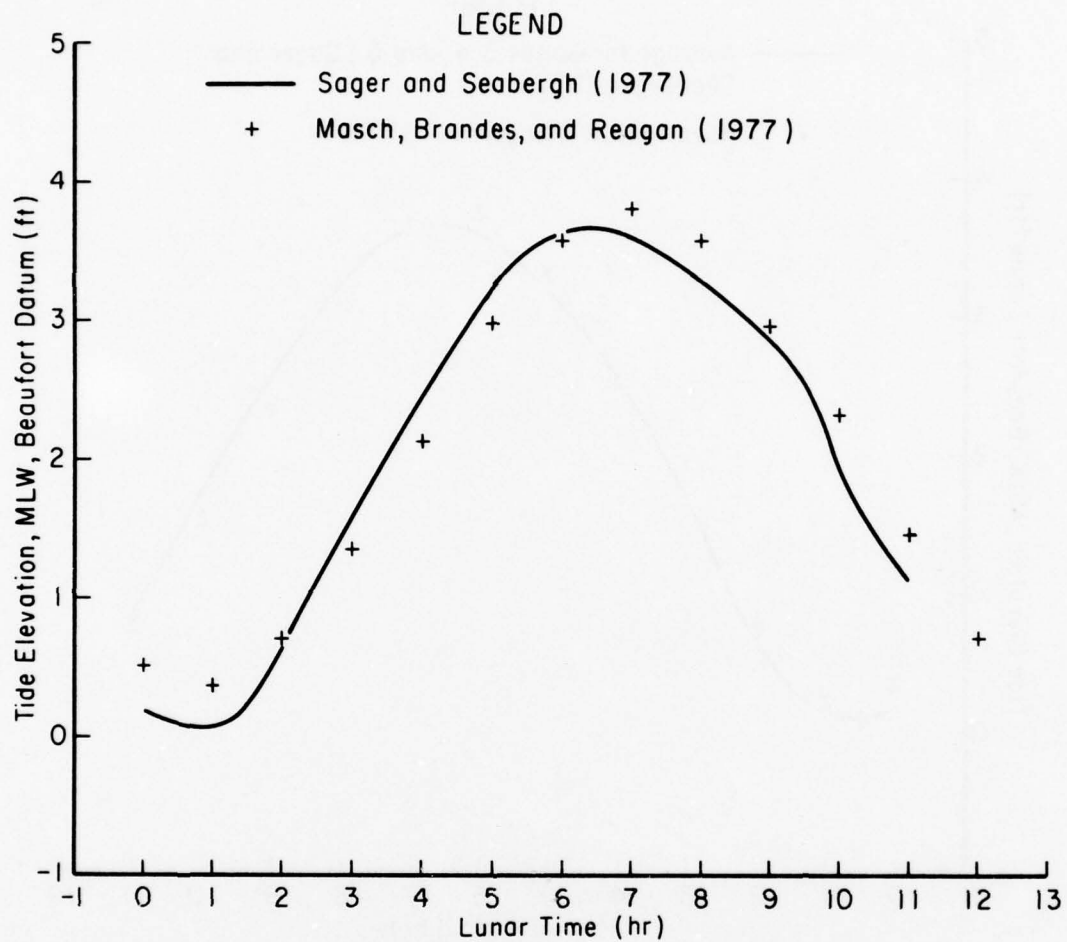


Figure 35. Prejetty (1964) mean tide condition at gage 6.

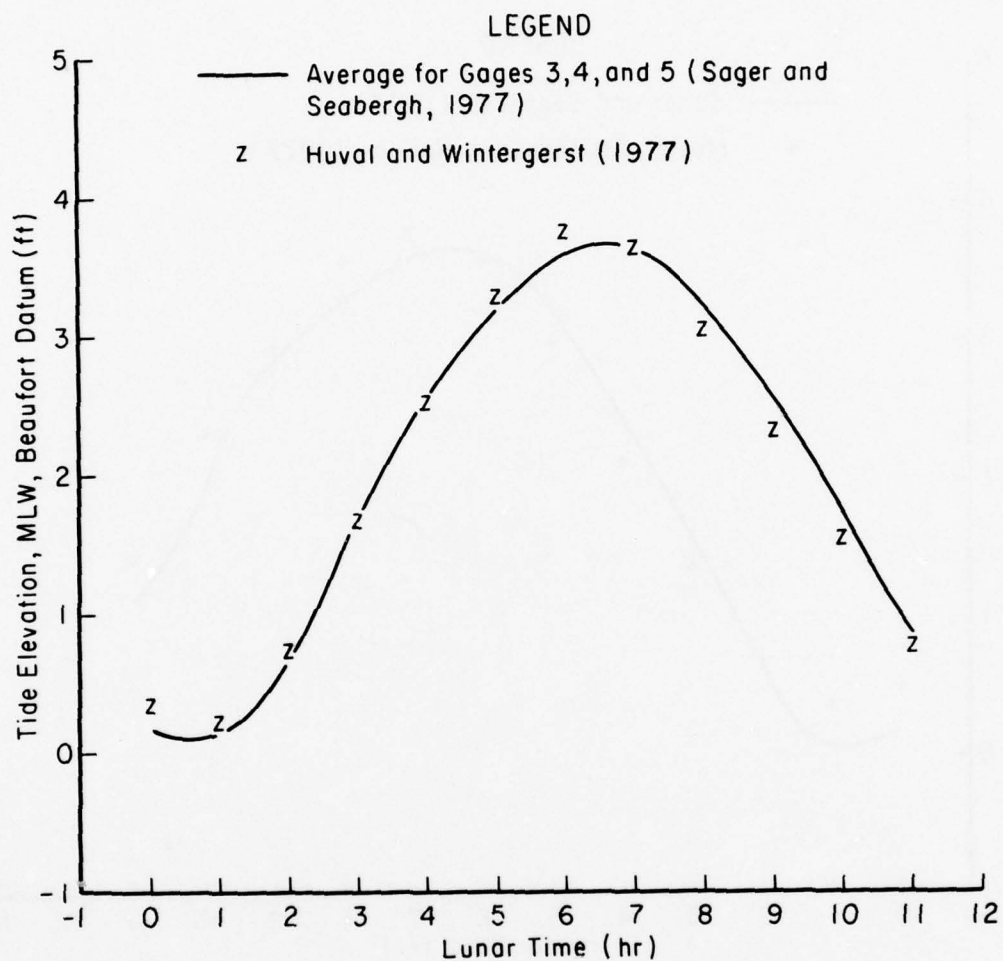


Figure 36. Prejetty (1964) mean tide condition of tide in embayment area.

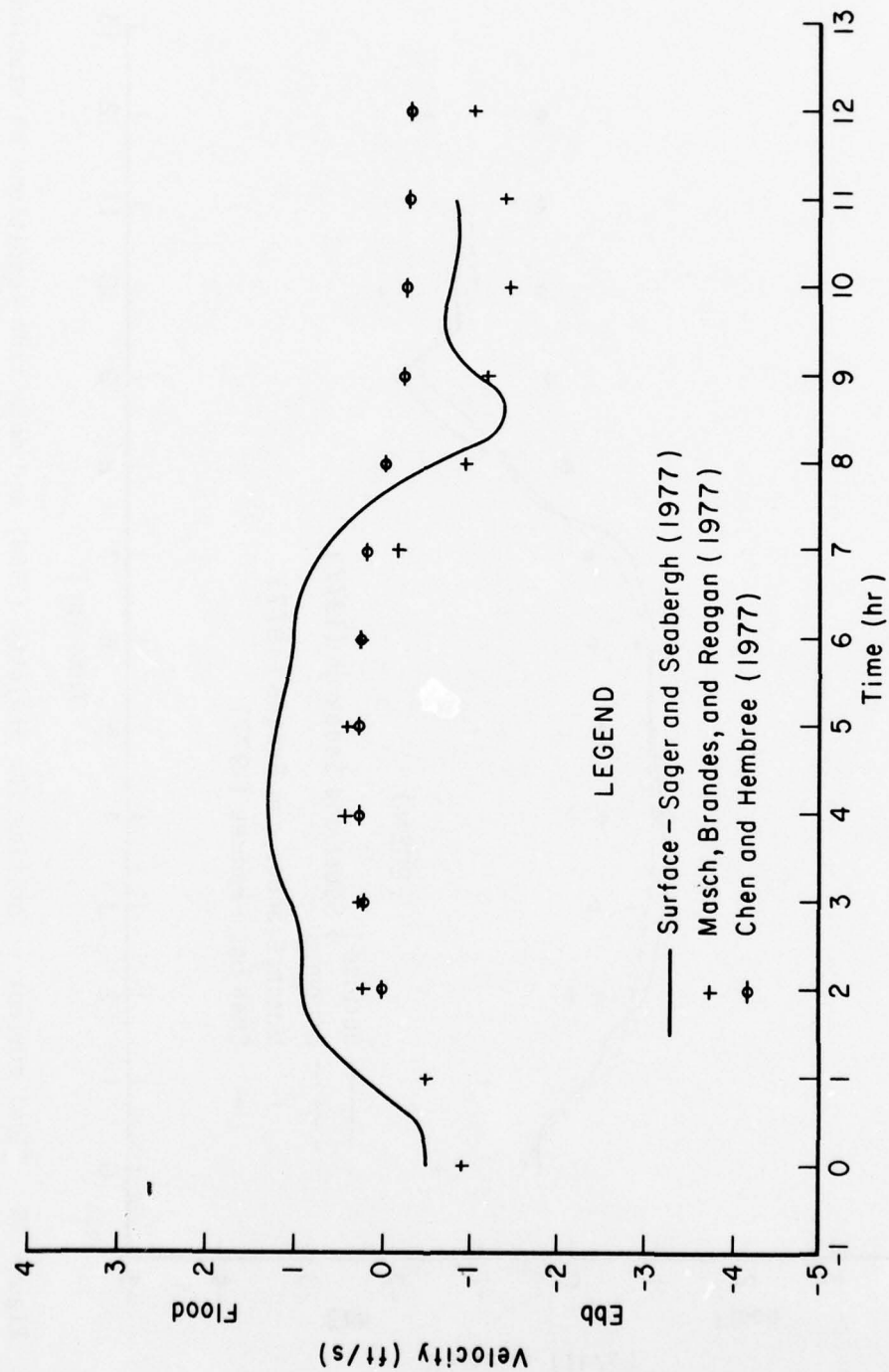


Figure 37. Tidal current velocities for prejetty (1964) and mean tide conditions at station 1N.

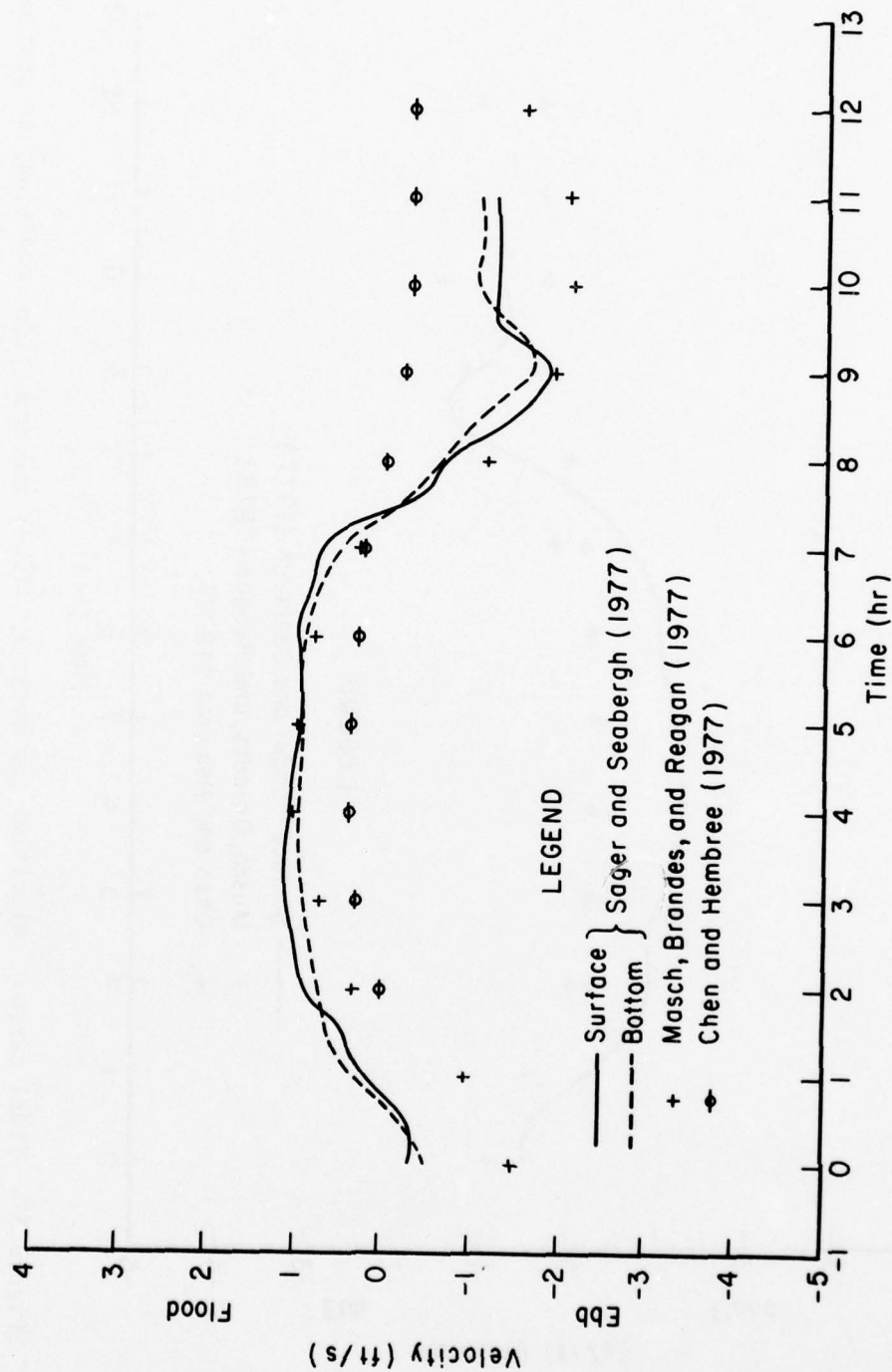


Figure 38. Tidal current velocities for prejetty (1964) and mean tide conditions at station 1C.

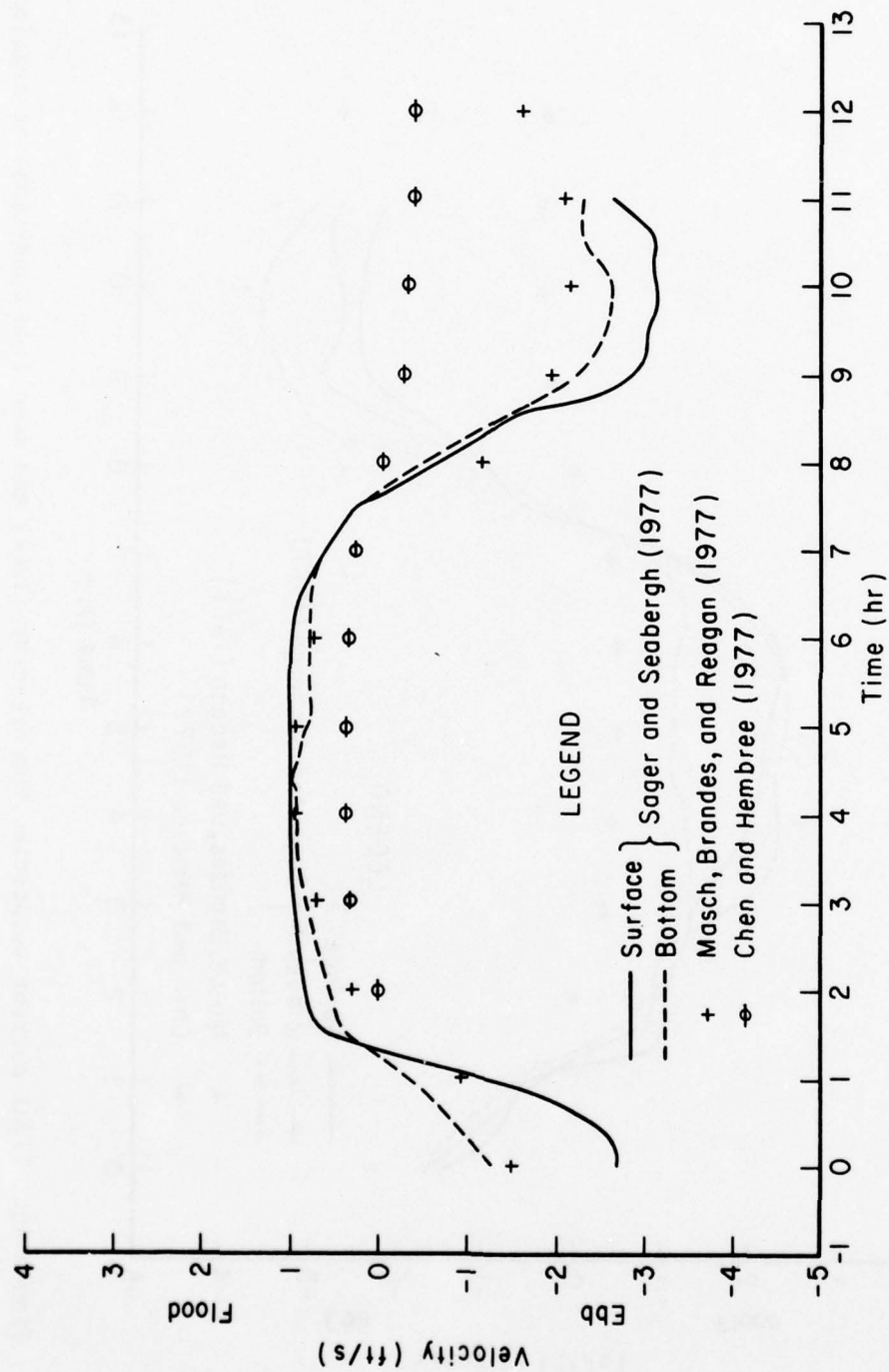


Figure 39. Tidal current velocities for prejetty (1964) and mean tide conditions at station 1S.

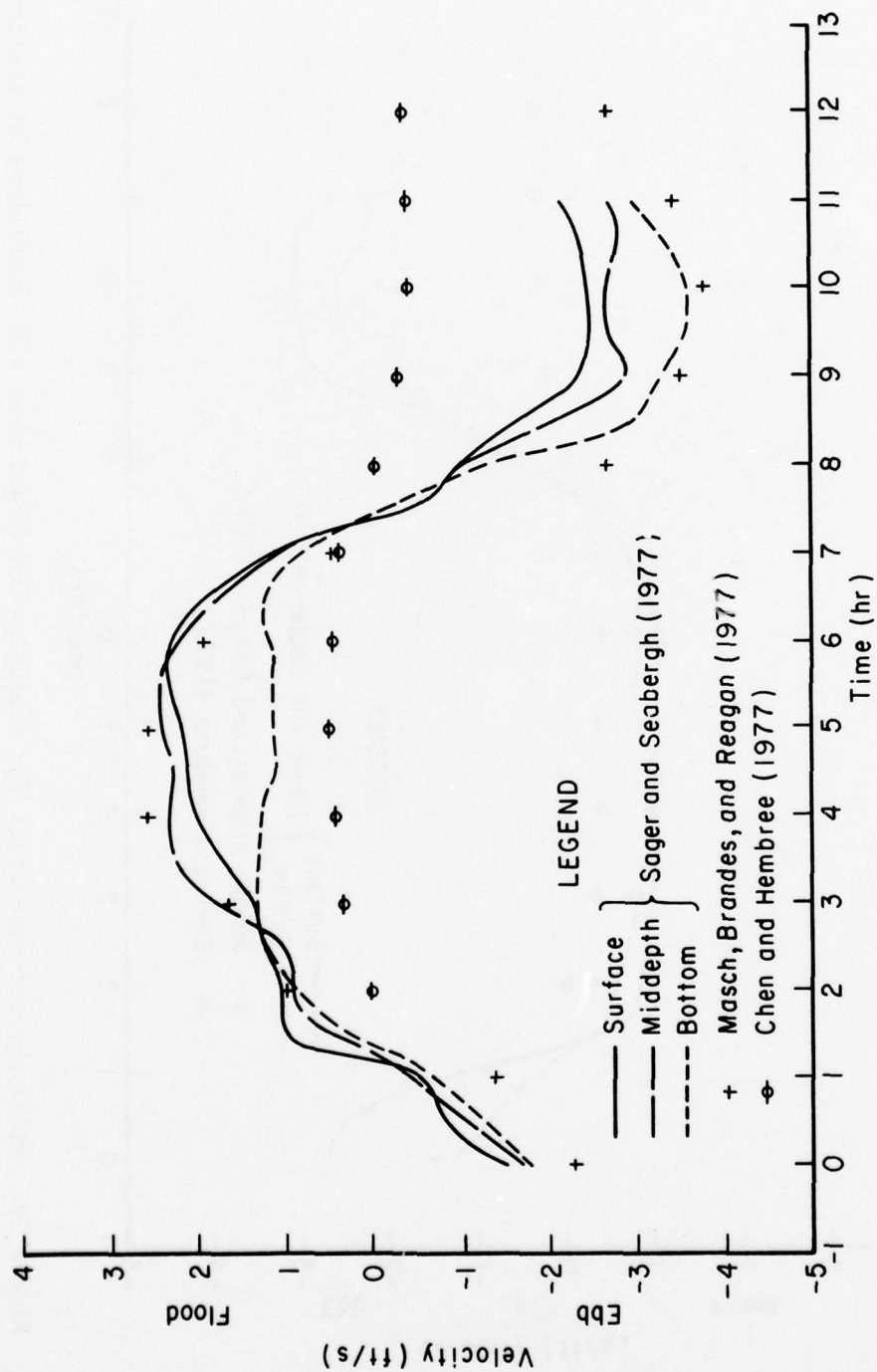


Figure 40. Tidal current velocities for prejetty (1964) and mean tide conditions at station 2N.

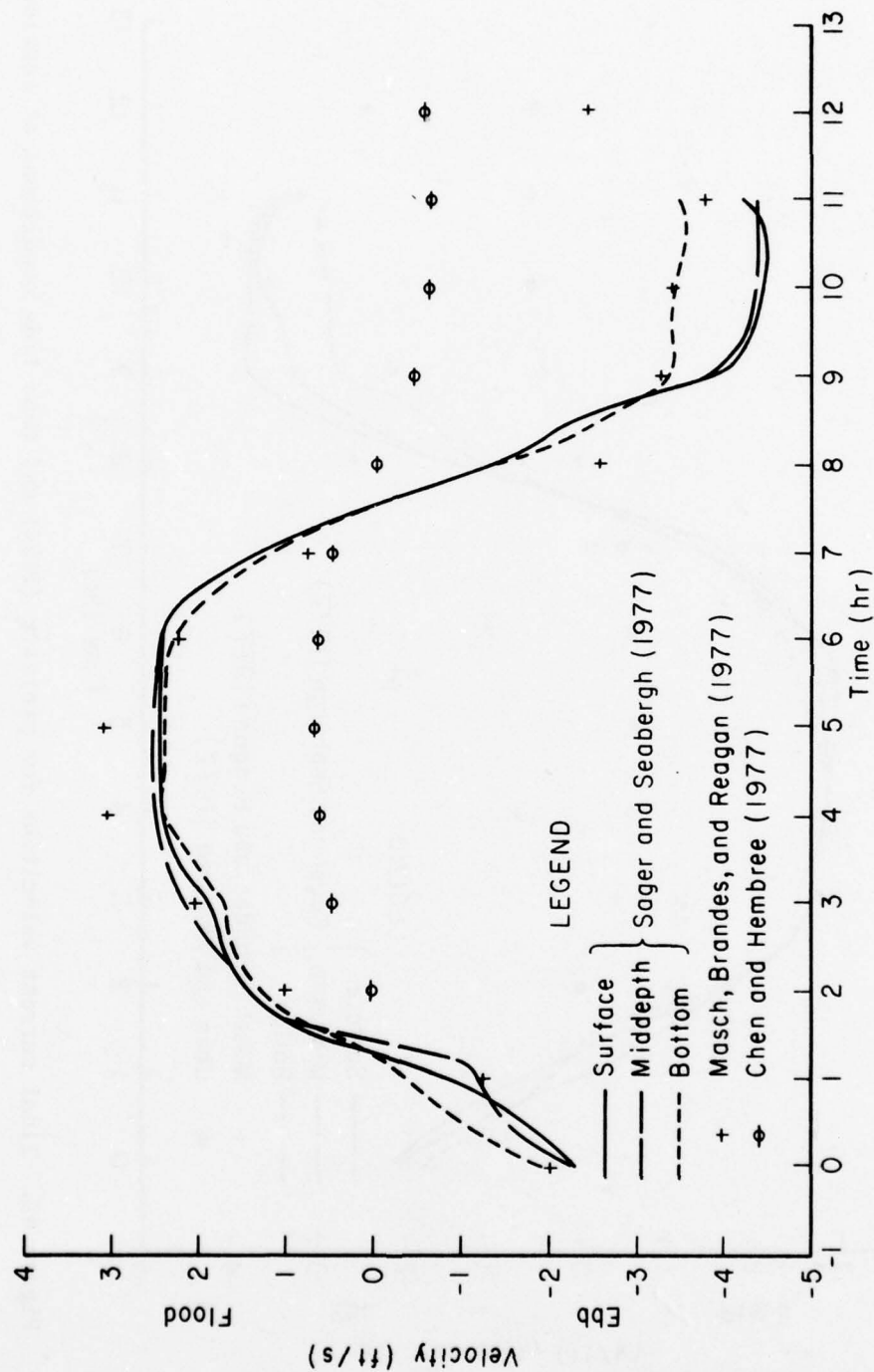


Figure 41. Tidal current velocities for prejetty (1964) and mean tide conditions at station 2C.

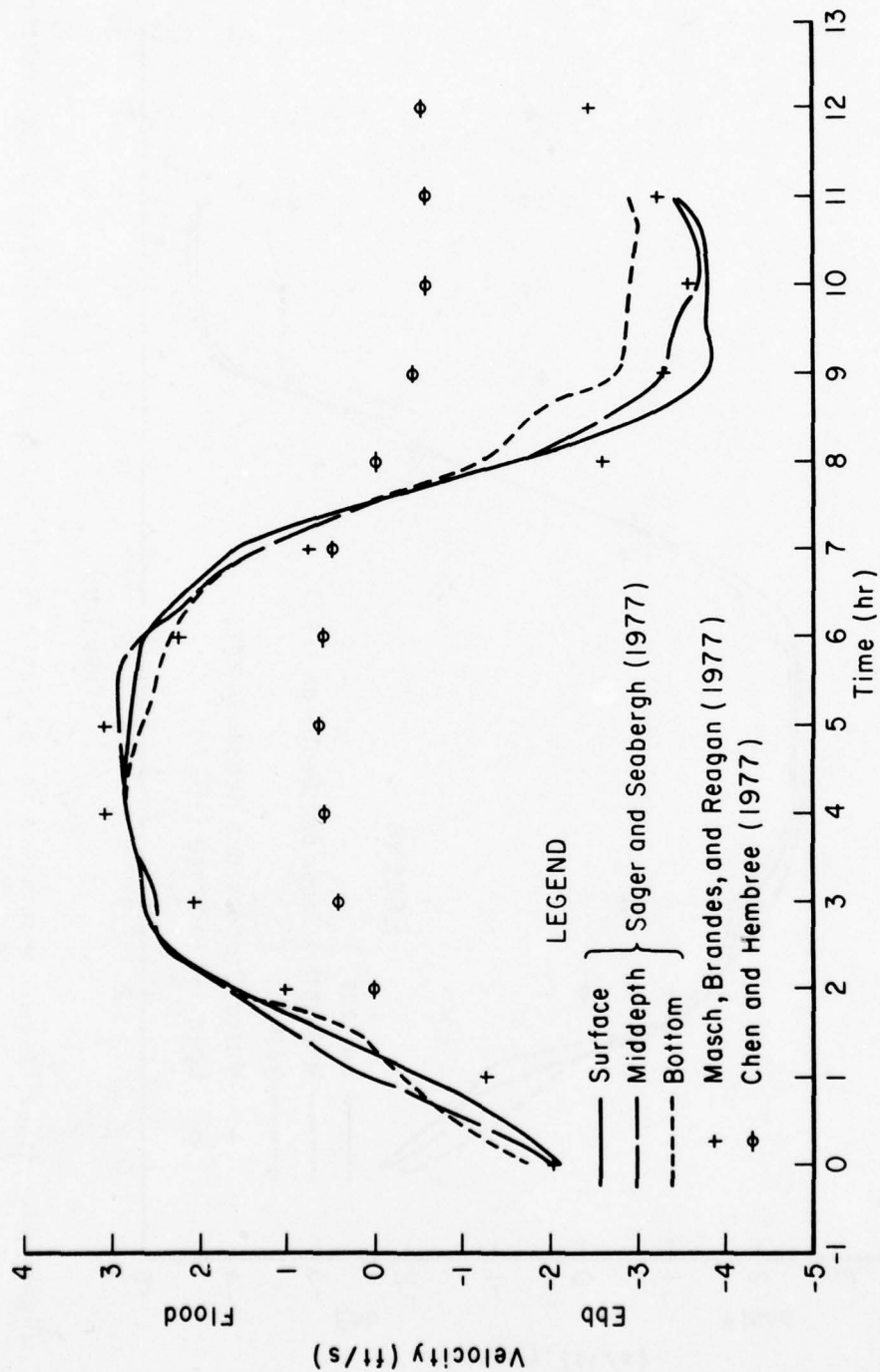


Figure 42. Tidal current velocities for prejetty (1964) and mean tide conditions at station 2S.

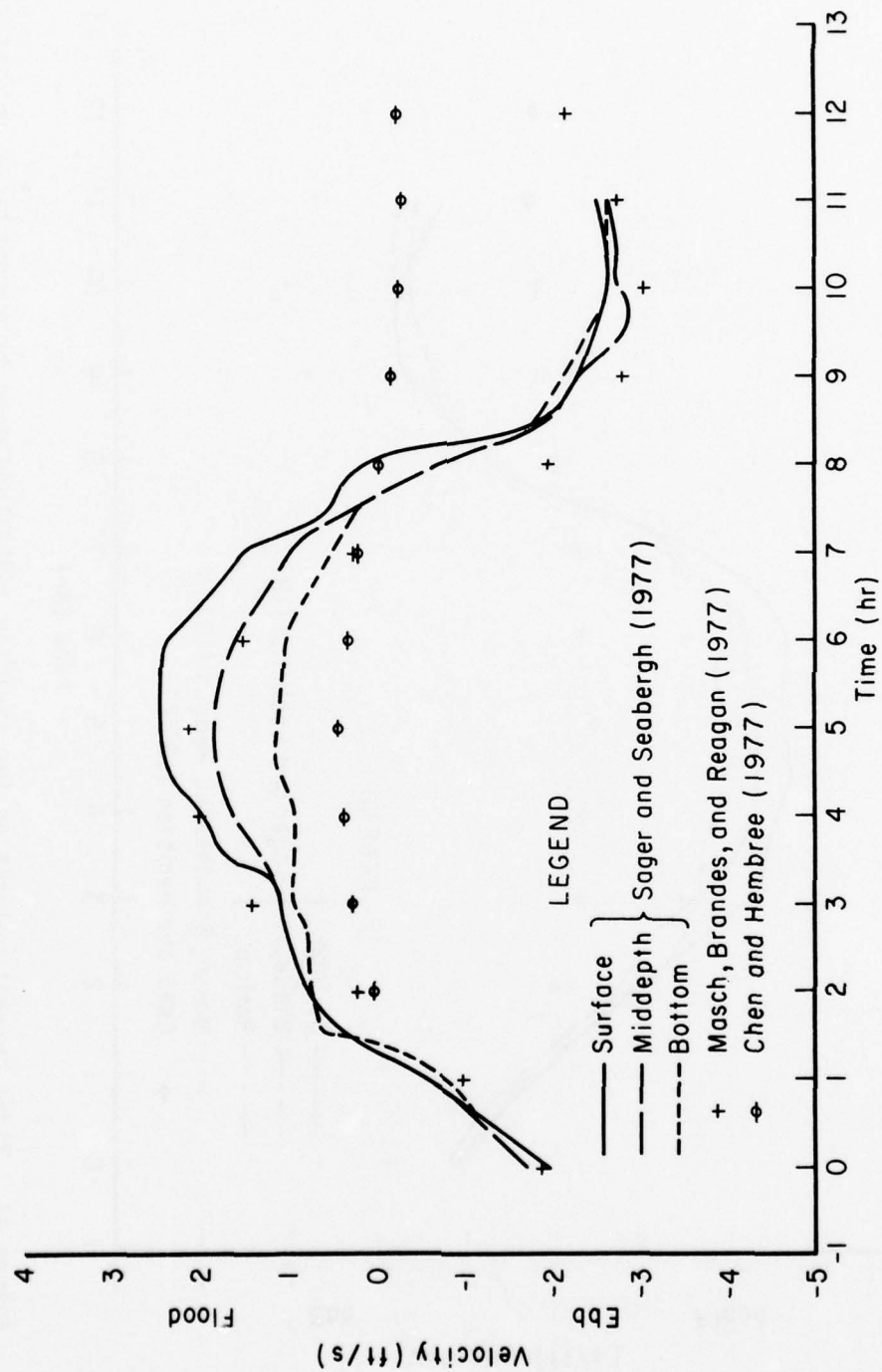


Figure 43. Tidal current velocities for prejetty (1964) and mean tide conditions at station 3N.

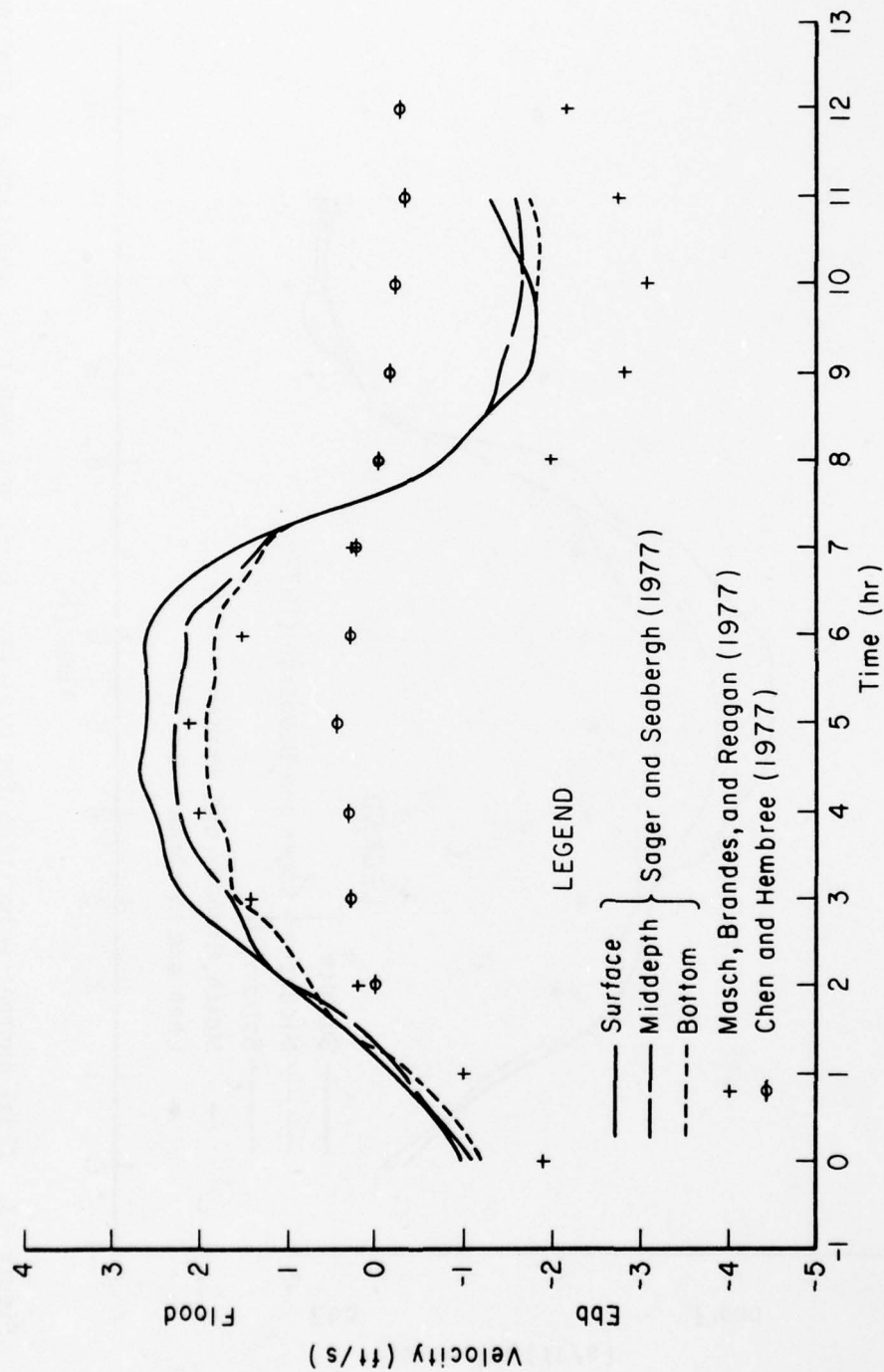


Figure 44. Tidal current velocities for prejetty (1964) and mean tide conditions at station 3C.

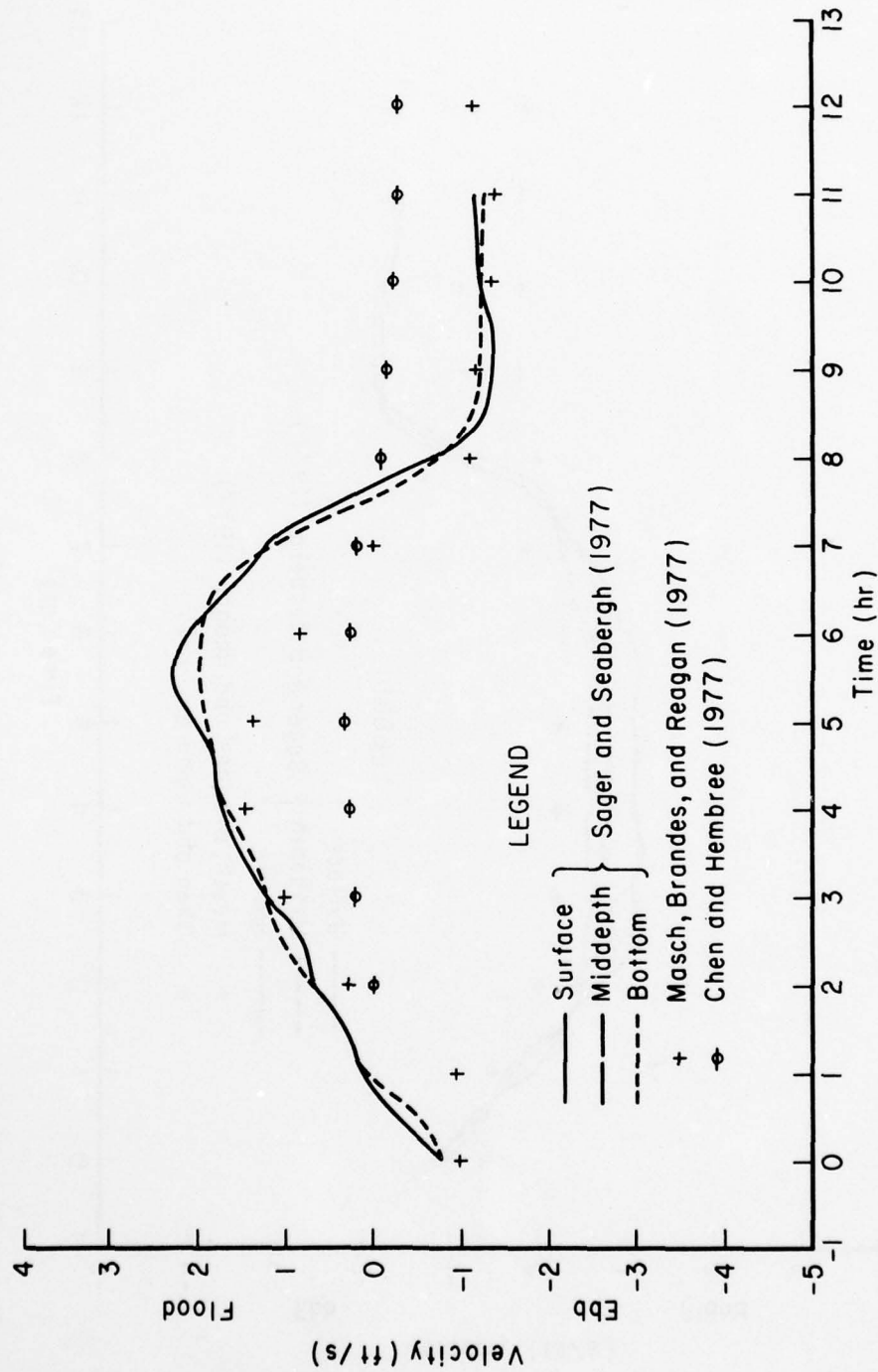


Figure 45. Tidal current velocities for prejetty (1964) and mean tide conditions at station 3S.

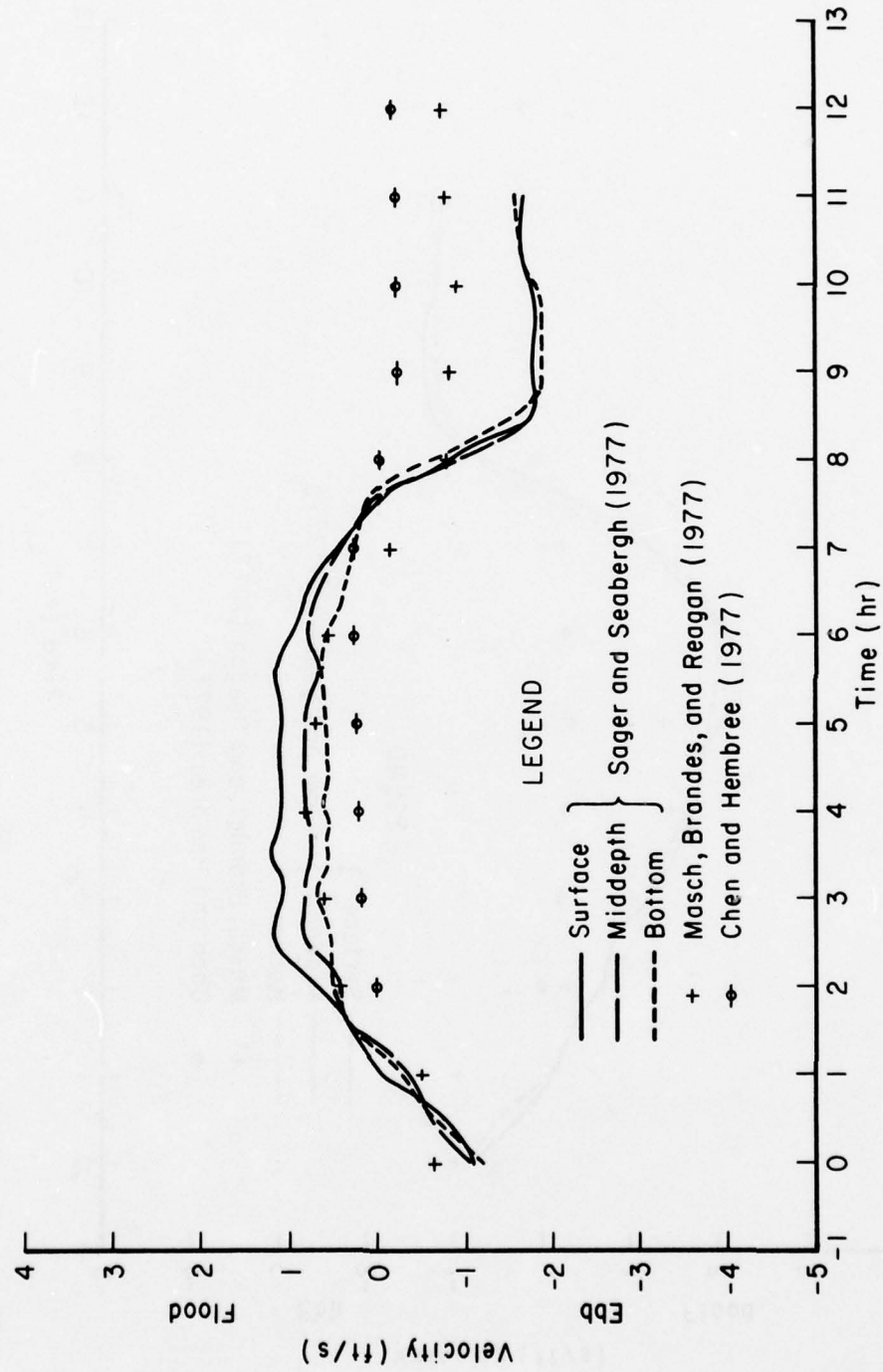


Figure 46. Tidal current velocities for prejetty (1964) and mean tide conditions at station 4E.

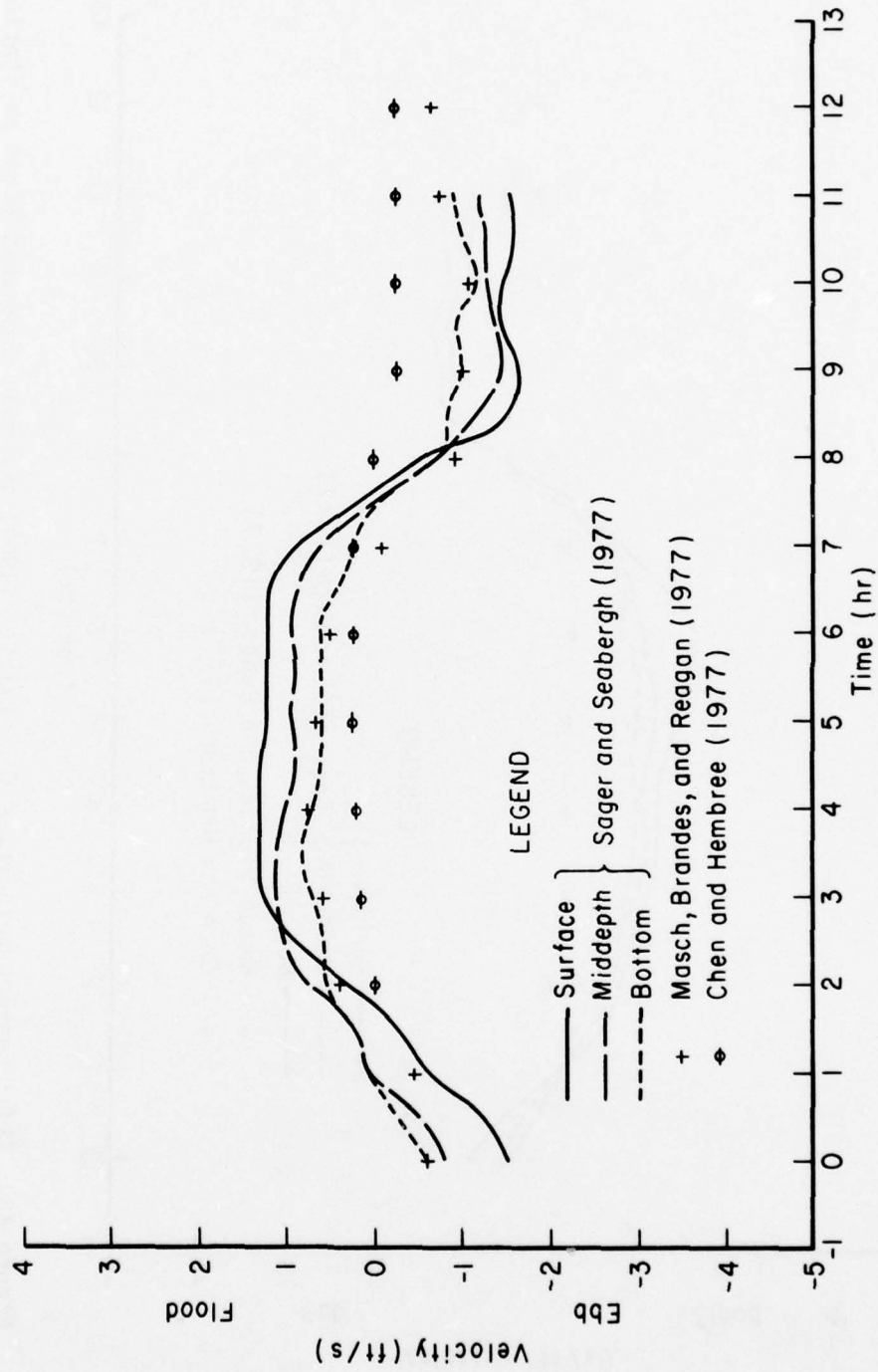


Figure 47. Tidal current velocities for prejetty (1964) and mean tide conditions at station 4C.

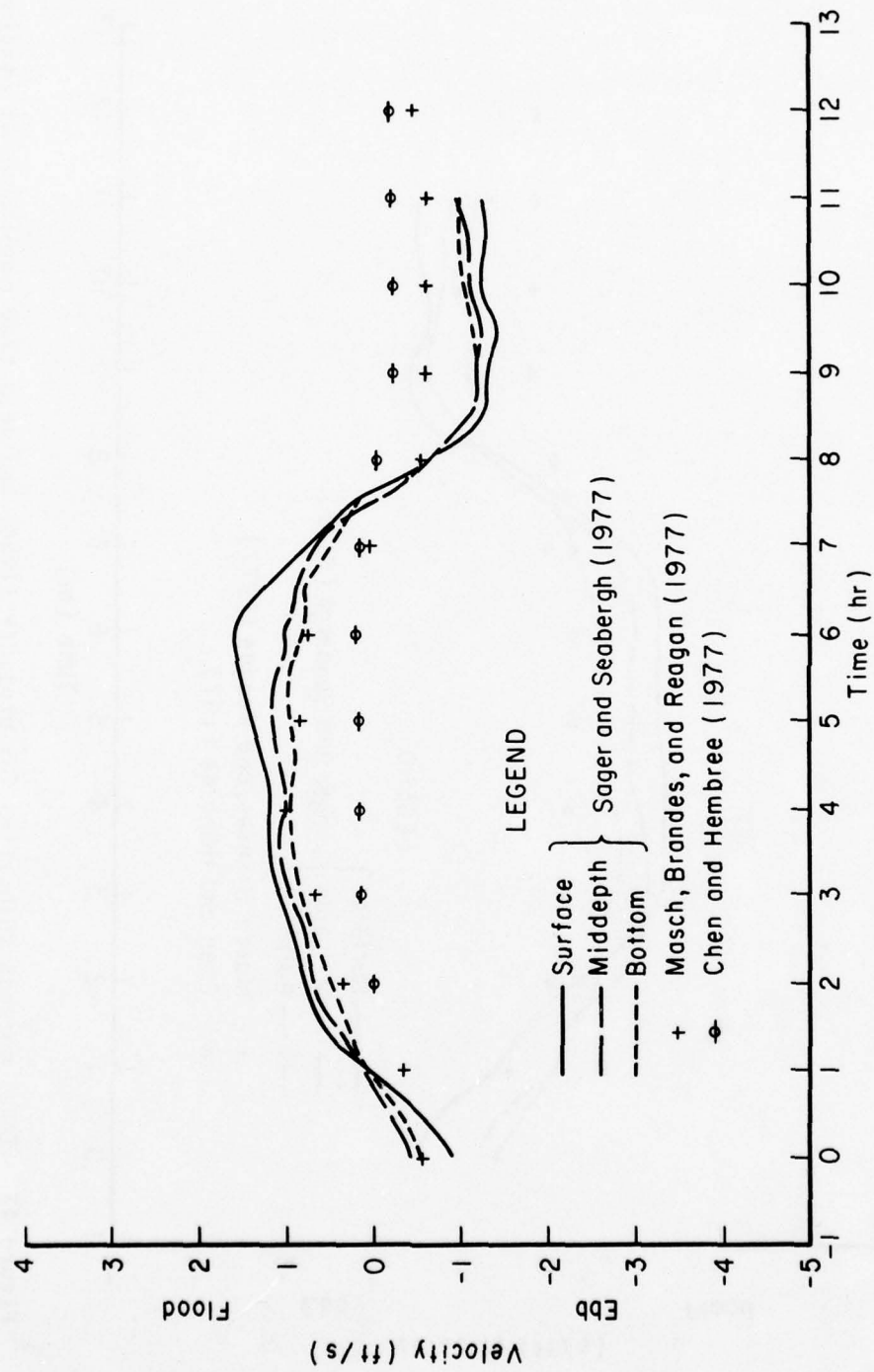


Figure 48. Tidal current velocities for prejetty (1964) and mean tide conditions at station 4W.

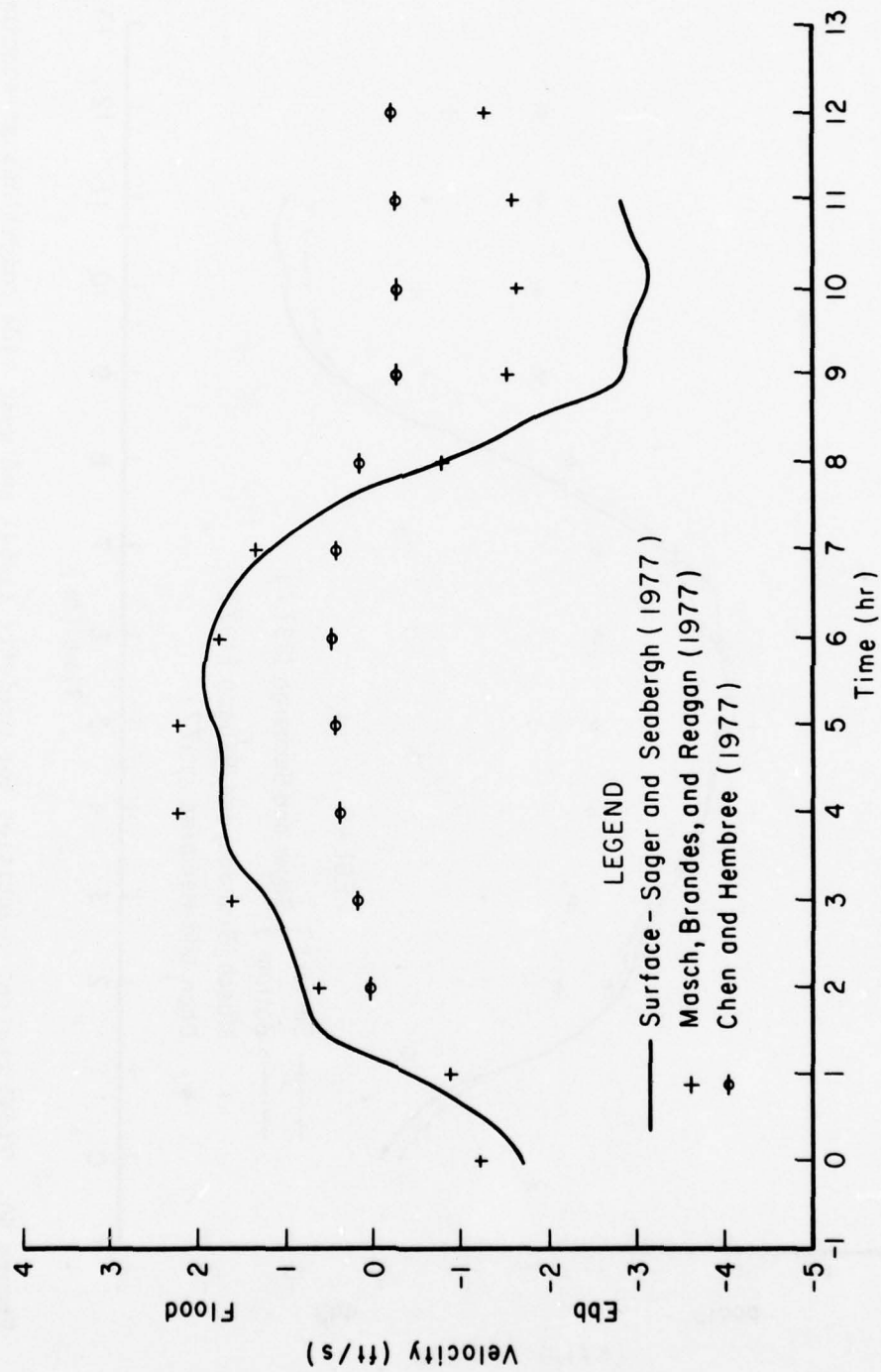


Figure 49. Tidal current velocities for prejetty (1964) and mean tide conditions at station SE.

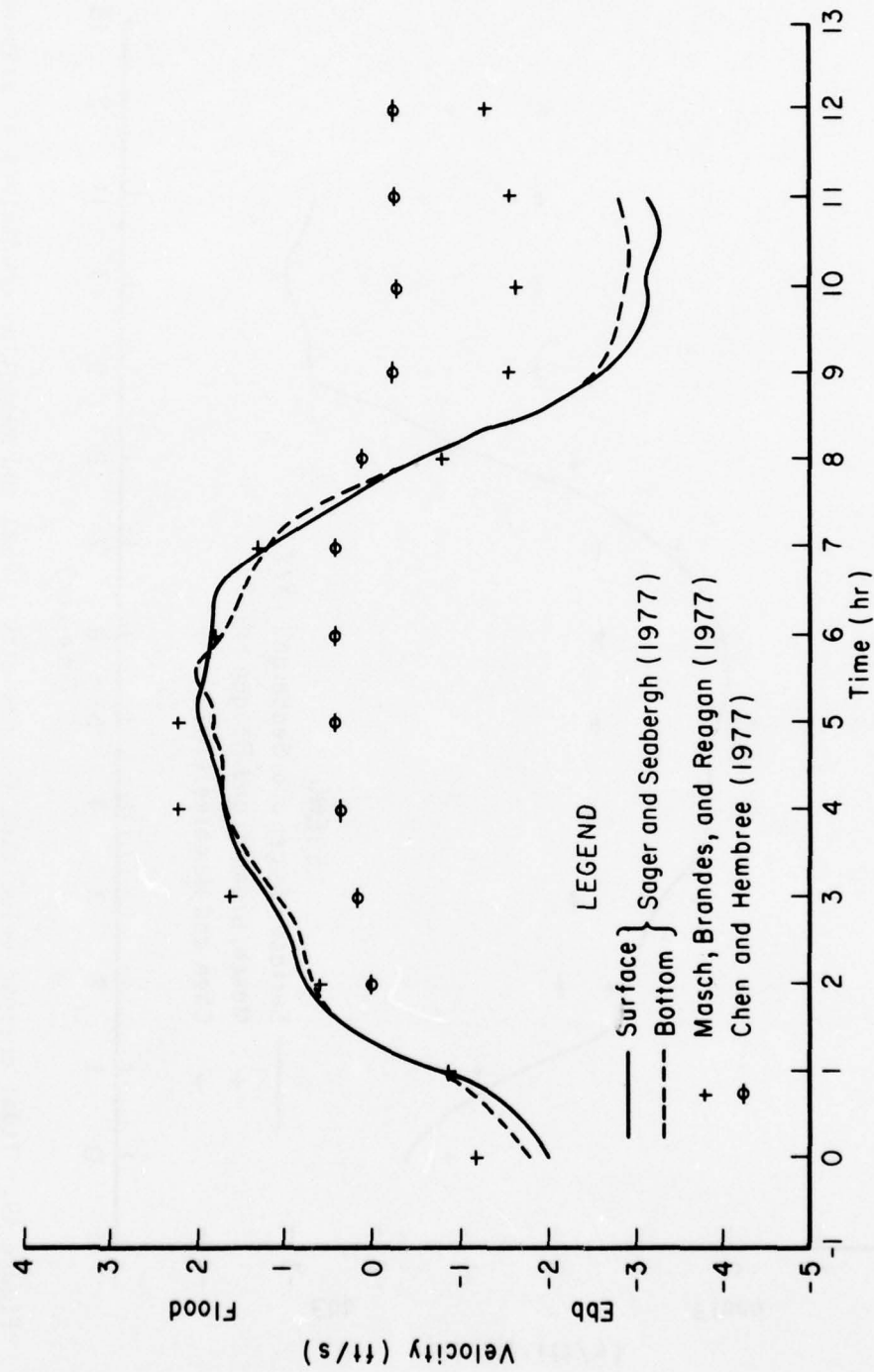


Figure 50. Tidal current velocities for prejetty (1964) and mean tide conditions at station 5C.

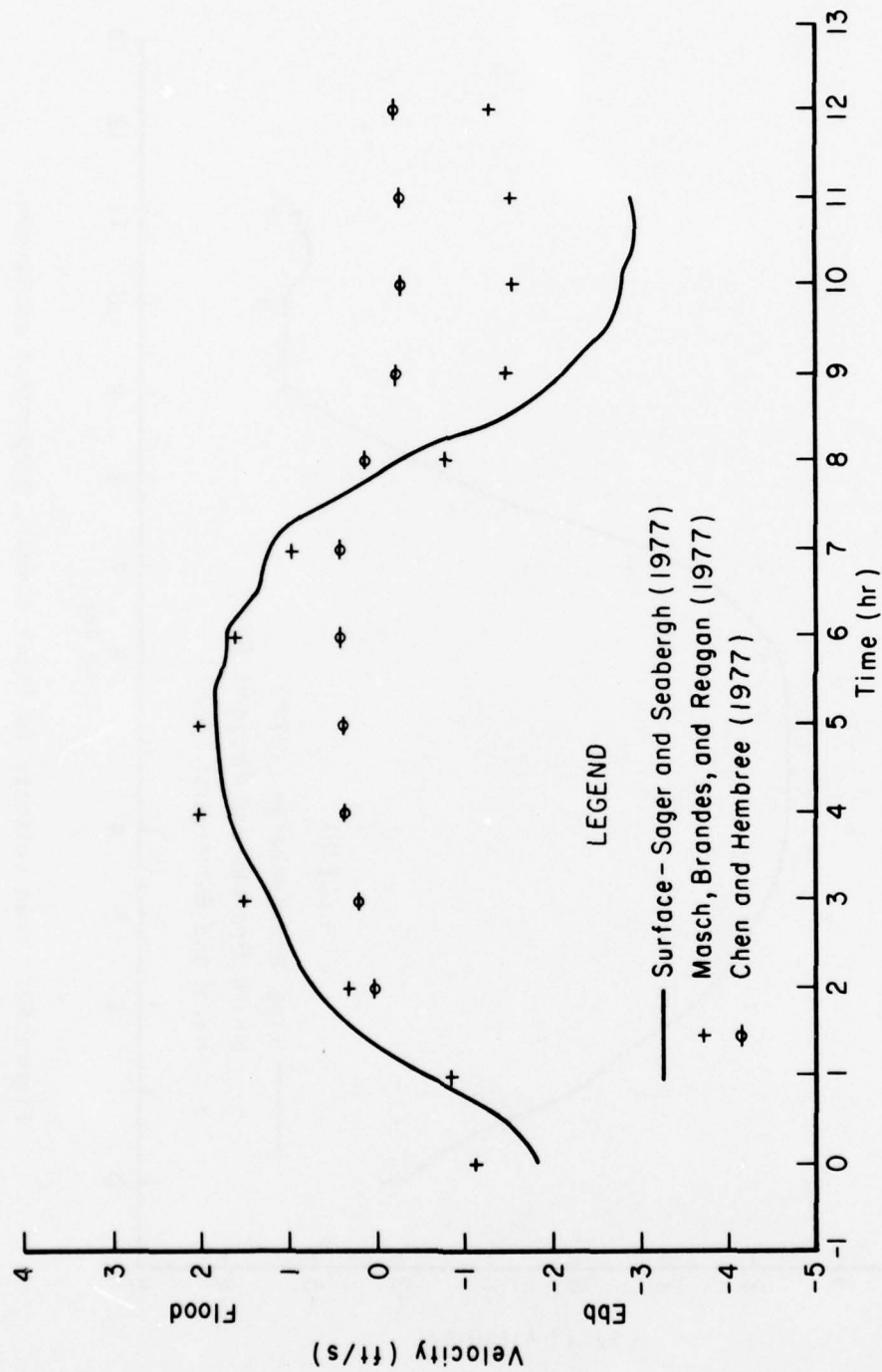


Figure 51. Tidal current velocities for prejetty (1964) and mean tide conditions at station 5W.

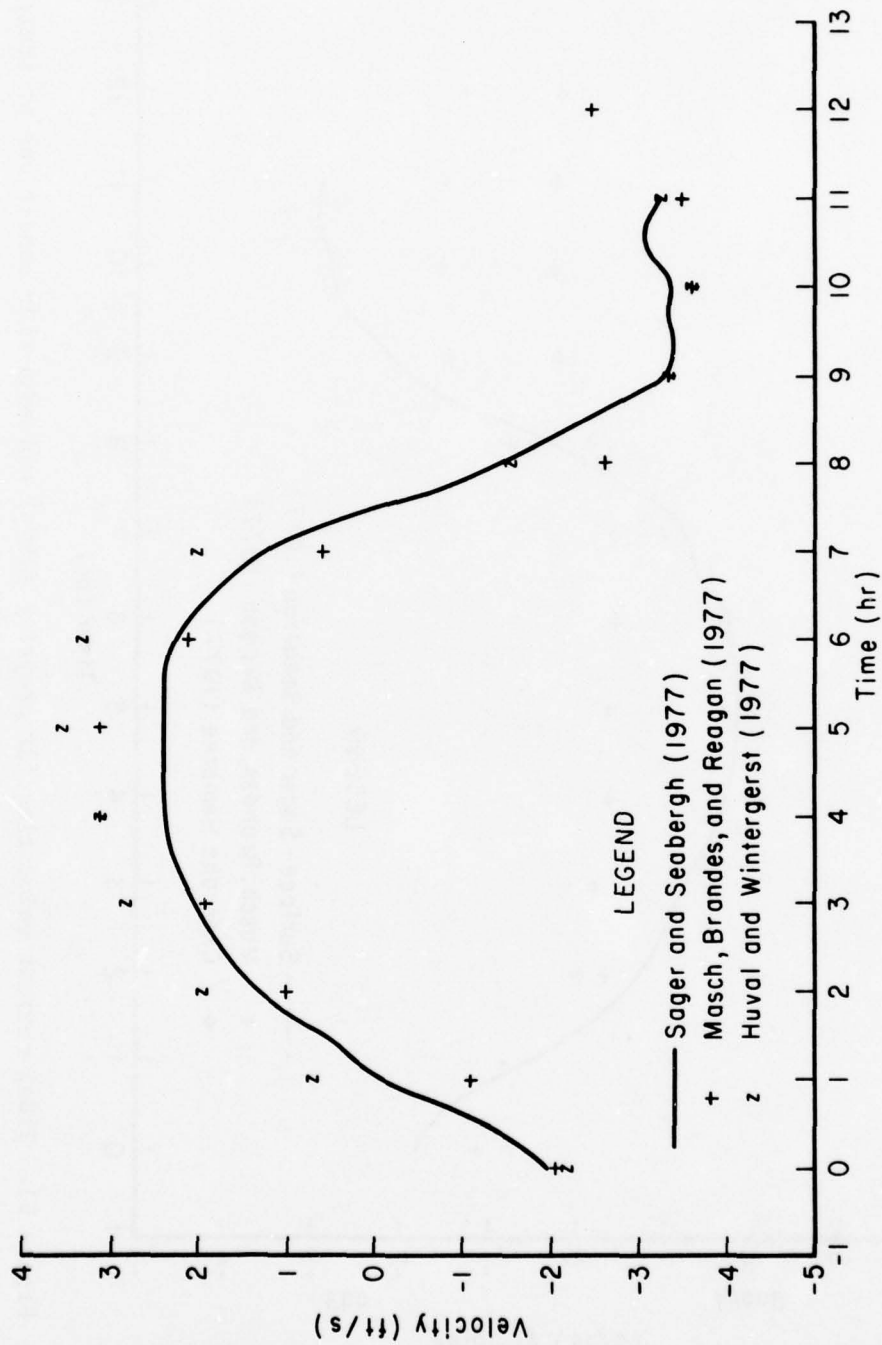


Figure 52. Mean velocity in inlet throat, preproject condition.

5. The Cost Factor.

The solution of many engineering problems is based not only on the reliability of the estimate but also the cost and efforts involved. The costs incurred in conducting each of the model studies for Masonboro Inlet are as follows:

The lumped parameter mathematical model-----	\$ 5,000
(Huval and Wintergerst, 1977)	
Mathematical model-----	23,400
(Chen and Hembree, 1977)	
Mathematical model-----	46,035
(Masch, Brandes, and Reagan, 1977).	
Physical model-----	\$225,000
(Sager and Seabergh, 1977)	

The cost for the physical model represents an estimate, since the physical model was used to conduct other studies which were not a part of the comparison of numerical and physical models. This shows that there may be a substantial difference in costs of carrying out tidal studies with the various modeling techniques. However, this discussion does not cover all aspects of the costs. Physical models are more suited for some problems than the presently available numerical models. Conversely, numerical models are superior to physical models for some purposes. Numerical models are newer than the physical models, and the numerical technology is advancing faster. A judicious combination of physical and numerical models will likely soon become the most economical approach.

VIII. SUMMARY, CONCLUSION, AND RECOMMENDATIONS

1. Summary.

To evaluate the state-of-the-art modeling techniques for tidal inlets, a physical model, a lumped parameter model, and two two-dimensional numerical models of Masonboro Inlet were commissioned. All four models were adjusted to the hydrography of September 1969, and later used to predict the flow with prejetty (1964) bathymetry. The lumped parameter model could predict only the average flow in the inlet and the average tide for the basin at the landward end of the inlet. The other three models yielded estimates of both tide and current at several locations in the experimental basin. All models yielded tide hydrographs of substantially the same quality. The physical model and the two-dimensional numerical model developed by Masch, Brandes, and Reagan (1977) yielded estimates of currents of substantially equal quality. The lumped parameter model agreed reasonably well with the average measured currents and inland tides of 1969, and with the predictions obtained with the physical and numerical models by Masch, Brandes, and Reagan for the 1964 bathymetry. The second numerical model by Chen and Hembree (1977) gave poor reproduction of the measured currents of 1969, and did not agree well with the predictions of the other three models for the 1964 bathymetry.

To extend the comparison of physical and numerical models, the two-dimensional shallow-water hydrodynamic equations were derived from the Navier-Stokes equations in Appendix B. Terms describing the interaction of horizontal flows with flows that are not necessarily horizontal were retained. The physical interpretation of each term and the conditions under which each term can make a significant contribution to the mean horizontal flow were discussed in Section II.

The design of physical models, interpreted as analog computers, and the extent to which the physical models can reproduce or simulate the processes described by the governing equations were discussed in Section III. This led to the surprising conclusion that the effects of radiation stresses, due to wind-generated waves, on the tidal flow can be simulated with useful accuracy in a distorted scale physical model. Sager and Seabergh (in preparation, 1977) independently show that the agreement between the Masonboro Inlet model and the prototype could be improved by simulating the effect of waves on the tidal flow. This study was not a part of the initial plan of investigation and the contribution of waves was not included in the comparison results by any of the models. It has been shown in this study (Sec. III) that the physical model could not simulate the effects of the earth's rotation, the atmospheric pressure gradient, or the wind stress; however, none of these effects were of great importance in Masonboro Inlet. The friction coefficient in the distorted scale Masonboro Inlet model must be five times as great as the bottom roughness in the prototype to correctly simulate the bottom-stress term.

A brief review of the literature on the numerical solution of the two-dimensional hydrodynamic equations indicates that the phase speed of waves computed by most numerical models, including the two models used for Masonboro Inlet, is less than the true speed. The ratio of the computed speed to the true speed increases with the ratio of wavelength to the space increment ($L/\Delta S$). Small-scale phenomena with characteristic lengths less than four-space increments ($4\Delta S$) are poorly reproduced in numerical models. The effects of the earth's rotation, atmospheric pressure gradients, and surface wind stresses can be adequately simulated in numerical models with little difficulty.

The two-dimensional equations of motion were integrated in a cross-channel direction to form one-dimensional channel equations. These in turn were integrated along the channel axis to form a zero dimension or a lumped parameter model of an inlet. This mode of derivation, where the simplest equation is derived by systematically simplifying the most complete equations, revealed several discrepancies with the derivation of the lumped parameter model discussed in this report.

In some practical calculations, these mathematical errors do not lead to any significant error in calculated tidal heights and currents; in others, the errors may invalidate the technique. Procedures for determining the situation when the original technique is valid, and for extending the technique when needed, are given.

Both physical and numerical models need to be calibrated for the phenomena of interest because it is impossible (in any one model) to correctly model or simulate all hydrodynamic phenomena of interest in tidal waterways. Minor adjustments to even a well-designed model are generally made during model calibration to improve the agreement between model and prototype for known events. Although a few guidelines have been established for the adjustment procedure, adjustment is usually a trial-and-error process.

2. Conclusions.

Both physical and numerical models of inlets, when well designed and properly used, can provide quantitative predictions of useful accuracy for hydrodynamic phenomena. No model can provide complete accuracy for all phenomena of interest. In general, the physical model can provide more reliable predictions than the numerical model for the effect of small-scale phenomena; e.g., turbulence and waves on the phenomena of tidal scale. However, the numerical model can provide more reliable predictions than physical models for the effects of the earth's rotation, wind stress, and atmospheric pressure gradients.

The lumped parameter model developed by Keulegan (1967) and many extensions of this model, including the model by Huval and Wintergerst (1977), contain discrepancies with the rigorous development presented in this report. This model yields respectable predictions for Masonboro Inlet in spite of the discrepancies with the rigorous development presented here, because the processes incorrectly described in the model are of only minor importance in the Masonboro Inlet.

The proper design or modification of models and the interpretation of results from both physical and numerical models require a great deal of specialized information and training not usually included in the training or experience of engineers or other physical scientists. This is especially true for numerical models which have only recently become common, and new insights are gained almost every year. The application of models to engineering studies by engineers without recent training or experience in this field, is unlikely to produce optimal results and the results can be misleading.

When a numerical model capable of providing the needed information with only minor modification is available, the model can generally be used more economically than a physical model and can be more easily stored for future use.

3. Recommendations.

a. A systematic program should be established for exploring the artifacts of numerical modeling of tidal hydraulics problems, developing solutions for such difficulties as the reduced speeds of short waves and evaluating the relative merits of alternative procedures. The experiences of meteorologists can serve as guides for this activity, and many of the

results obtained can be used with little change. The boundary conditions needed for coastal models are different from those used in meteorology; therefore, improved techniques are needed most in the field of boundary conditions and movable boundaries.

b. Reports of modeling experiments should include candid discussions of the specific efforts to improve model-prototype calibration so that data are developed which will permit a systematic optimization of model performance.

c. Each modeling effort involving either physical or numerical models should include at least one active team member with previous training and experience in using the same type of model.

d. Observations of wave direction, height, period or spectra, and local winds should be included with hydrographic surveys in planning data collection for either physical or numerical models. The data collection program should include observations of tidal heights or tidal currents at all tidal boundaries including any tidewater channels which leave the model in an inland direction. Tidal observations for model calibration and verification should be continued for at least 1 lunar month.

e. A lumped parameter model based on the corrected equations should be evaluated for possible field use.

LITERATURE CITED

- ABBOTT, M.B., "Review of Models of Tidal Waters," a discussion, *Journal of the Hydraulics Division*, Vol. 102, Aug. 1976, pp. 1145-1148.
- ABRAHAM, G., and KARELSE, M., "Classification of Models of Tidal Waters and Review of Models of Tidal Waters," a discussion, *Journal of the Hydraulics Division*, Vol. 102, June 1976, pp. 808-811.
- AMERICAN SOCIETY OF CIVIL ENGINEERS "Hydraulic Models," ASCE Manuals on Engineering Practice, No. 25, prepared by the Committee of the Hydraulics Division on Hydraulic Research, adopted 23 July 1942, New York, 1942.
- BEHRENS, E.W., WATSON, R.L., and MASON, C., "Hydraulics and Dynamics of New Corpus Christi Pass, Texas, A Case History, 1972-1973," GITI Report 8, U.S. Army, Corps of Engineers, Coastal Engineering Research Center, Fort Belvoir, Va., and U.S. Army Engineer Waterways Experiment Station, Vicksburg, Miss., Jan. 1977.
- BUTLER, H.L., and RANEY, D.C., "Finite Difference Schemes for Simulation Flow in an Inlet-Wetlands System," *Proceedings of the 1976 Army Numerical Analysis and Computers Conference*, ARO Report 76-3, U.S. Army Research Office, Research Triangle Park, N.C., 1976, pp. 393-411.
- CHEN, R.M., and HEMBREE, L.A., "Numerical Simulation of Hydrodynamics (TRACOR)," App. 3, GITI Report 6, *Comparison of Numerical and Physical Models, Masonboro Inlet, North Carolina*, U.S. Army, Corps of Engineers, Coastal Engineering Research Center, Fort Belvoir, Va., and U.S. Army Engineer Waterways Experiment Station, Vicksburg, Miss., June 1977.
- CHIU, T.Y., VAN DE KREEKE, J., and DEAN, R.G., "Residence Times of Waters Behind Barrier Islands," Technical Report No. 7, Department of Coastal and Oceanographic Engineering, University of Florida, Gainesville, Fla., 1970.
- CHOW, V.T., *Open-Channel Hydraulics*, McGraw-Hill, New York, 1959.
- CHU, H.L., "Numerical Model for Wave Refraction by Finite Amplitude Wave Theories," *Symposium on Modeling Techniques, Modeling 75*, Vol. II, 1975, pp. 1082-1100.
- CONNOR, J.J., "A Survey of Finite Element Methods in Continuum Mechanics," *Proceedings of the Variational Methods in Engineering*, Sept. 1972.
- DALVERNEY, J., and FONTANET, F., "Realisation de Plaque Tournantes Plaque de Grenoble," *La Houille Blanche*, Vol. 14, No. 5, Aug. 1959, pp. 598-606.

- DEAN, R.G., "Evaluation and Development of Water Wave Theories for Engineering Application," Special Report No. 1, Vol. I, Presentation of Research Results, Stock No. 008-022-00083, Vol. II, Tabulation of Dimensionless Stream Function Theory Variables, Stock No. 008-022-00084, U.S. Government Printing Office, Washington, D.C., Nov. 1974.
- DEFANT, A., *Physical Oceanography*, Pergamon Press, Oxford, Vols. 1 and 2, 1961.
- d'HIERES, G.C., "Reglages et Exploitation de la plaque tournante de Grenoble," *La Houille Blanche*, Vol. 17, No. 2, Mar.-Apr. 1962, pp. 244-254.
- DRONKERS, J.J., *Tidal Computations in Rivers and Coastal Waters*, North Holland, Amsterdam, Wiley and Sons, New York, 1964.
- DURHAM, D.L., GREER, H.C., III, and WHALIN, R.W., "Automated Control, Data Acquisition, and Analyses for Hydraulic Models of Tidal Inlets," *Proceedings of the 1976 Army Numerical Analysis and Computers Conference*, ARO Report 76-3, U.S. Army Research Office, Research Triangle Park, N.C., 1976, pp. 223-248.
- FORRISTALL, G.Z., "Three-Dimensional Structure of Storm-Generated Currents," *Journal of Geophysical Research*, Vol. 79, No. 18, June 1974, pp. 2721-2729.
- FORRISTALL, G.Z., "Three-Dimensional Structure of Storm-Generated Currents," reply to comment by R.O. Reid, *Journal of Geophysical Research*, Vol. 80, No. 9, Mar. 1975, pp. 1186-1187.
- FORTAK, H.G., "Concerning the General Vertically Averaged Hydrodynamic Equations with Respect to Basic Storm Surge Equations," Report No. 51, National Hurricane Research Project, Apr. 1962.
- HALTNER, G.J., *Numerical Weather Prediction*, Wiley and Sons, New York, 1971.
- HARRIS, D.L., "A Critical Survey of the Storm Surge Protection Problems," *Symposium on Tsunami and Storm Surges*, The 11th Pacific Science Congress, 1967, pp. 47-65.
- HINWOOD, J.B., and WALLIS, I.G., "Classification of Models of Tidal Waters," *Journal of the Hydraulics Division*, Vol. 101, Oct. 1975a, pp. 1315-1331.
- HINWOOD, J.B., and WALLIS, I.G., "Review of Tidal Waters," *Journal of the Hydraulics Division*, Vol. 101, Nov. 1975b, pp. 1405-1421.
- HUDSON, R.Y., et al., "Coastal Hydraulic Models," U.S. Army, Corps of Engineers, Coastal Engineering Research Center, Fort Belvoir, Va. (in preparation, 1977).

- HUVAL, C.J., and WINTERGERST, G.L., "Simplified Numerical (Lumped Parameter) Simulation," App. 4, GITI Report 6, *Comparison of Numerical and Physical Hydraulic Models, Masonboro Inlet, North Carolina*, U.S. Army, Corps of Engineers, Coastal Engineering Research Center, Fort Belvoir, Va., and U.S. Army Engineer Waterways Experiment Station, Vicksburg, Miss., June 1977.
- IPPEN, A.T., ALAM, M.Z., and BOUODIMOS, E.L., "Wave Reflection and Transmission in Channels of Gradually Varying Depth," Hydraulics Laboratory Report No. 72, R64-31, School of Engineering, Massachusetts Institute of Technology, Cambridge, Mass., 1964.
- ISHIGURO, S., "Electronic Analogues In Oceanography," *Oceanography and Marine Biology*, Annual Review, George Allen and Unwin Ltd., London, Vol. 10, 1972, pp. 17-96.
- JAMES, I.D., "Non-Linear Waves in the Nearshore Regions: Shoaling and Set-up," *Estuarine and Coastal Marine Science*, Vol. 2, No. 3, July 1974a, pp. 207-234.
- JAMES, I.D., "A Non-linear Theory of Longshore Currents," *Estuarine and Coastal Marine Science*, Vol. 2, No. 3, July 1974b, pp. 235-249.
- JELESNIANSKI, C.P., "Numerical Computations of Storm Surges with Bottom Stress," *Monthly Weather Review*, Vol. 95, No. 11, Nov. 1967, pp. 740-756.
- JELESNIANSKI, C.P., "Bottom Stress Time-History in Linearized Equations of Motion for Storm Surges," *Monthly Weather Review*, Vol. 98, No. 6, June 1970, pp. 462-478.
- JELESNIANSKI, C.P., "A Sheared Coordinate System for Storm Surge Equations of Motion with a Mildly Curved Coast," Technical Memorandum NWS TDL-61, National Oceanic and Atmospheric Administration, Rockville, Md., July 1976.
- KAJIURA, K., "On The Partial Reflection of Water Waves Passing Over A Bottom of Variable Depth," *Proceedings of the Tsunami Meeting*, The 10th Pacific Science Congress, July 1963, pp. 206-230.
- KEULEGAN, G.W., "Tidal Flow In Entrances, Water-Level Fluctuations of Basins in Communication with Seas," Technical Bulletin No. 14, Committee on Tidal Hydraulics, U.S. Army, Corps of Engineers, Vicksburg, Miss., July 1967.
- LAMB, H., *Hydrodynamics*, 6th ed., Dover, New York, 1932.
- LEENDERTSE, J.J., "Aspects of a Computational Model for Long Period Water Waves Propagation," Memo. No. RM-5294 PR, The Rand Corporation, N.Y., 1967.

- LEENDERTSE, J.J., "A Water-Quality Simulation Model for Well-Mixed Estuaries and Coastal Seas," RM-6230-RC, *Principles of Computation*, Vol. I, The Rand Corporation, Santa Monica, Calif., 1970.
- LEENDERTSE, J.J., and LIU, S.-K., "A Three-Dimensional Model for Estuaries and Coastal Seas: Volume 11, Aspects of Computation," R-1764-OWRT, prepared for the Office of Water Research and Technology, The Rand Corporation, Santa Monica, Calif., June 1975a.
- LEENDERTSE, J.J., and LIU, S.-K., "Modeling of Three-Dimensional Flows in Estuaries," *Symposium on Modeling Techniques, Modeling 75*, Vol. I, 1975b.
- LIU, P.L.F., and MEI, C.C., "Effects of A Breakwater on Nearshore Currents Due to Breaking Waves," TM-57, U.S. Army, Corps of Engineers, Coastal Engineering Research Center, Fort Belvoir, Va., Nov. 1975.
- LONGUET-HIGGINS, M.S., and STEWART, R.W., "Radiation Stress and Mass Transport in Gravity Waves, with Application to Surf Beats," *Journal of Fluid Mechanics*, Vol. 13, 1962, pp. 481-504.
- LONGUET-HIGGINS, M.S., and STEWART, R.W., "A Note On Wave Set-Up," *Journal of Marine Research*, Vol. 21, 1963, pp. 4-10.
- LONGUET-HIGGINS, M.S., and STEWART, R.W., "Radiation Stresses in Water Waves; A Physical Discussion, With Applications," *Deep-Sea Research*, Vol. 11, No. 4, Aug. 1964, pp. 529-562.
- LUDWICK, J.C., "Variations in Boundary Drag Coefficient in the Tidal Entrance to Chesapeake Bay, Virginia," Technical Report No. 19, Institute of Oceanography, Old Dominion University, Norfolk, Va., Aug. 1974.
- MASCH, F.D., BRANDES, R.J., and REAGAN, J.D., "Numerical Simulation of Hydrodynamics (WRE)," App. 2, GITI Report 6, *Comparison of Numerical and Physical Models, Masonboro Inlet, North Carolina*, U.S. Army, Corps of Engineers, Coastal Engineering Research Center, Fort Belvoir, Va., and U.S. Army Engineer Waterways Experiment Station, Vicksburg, Miss., June 1977.
- NEUMAN, G., and PIERSON, W.J., Jr., *Principles of Physical Oceanography*, Prentice-Hall, Englewood Cliffs, N.J., 1966.
- NODA, E.K., et al., "Nearshore Circulations under Sea Breeze Conditions and Wave-Current Interactions in The Surf Zone," Technical Report No. 4, Tetra Tech No. TC-149-4, Tetra Tech, Inc., Pasadena, Calif., Feb. 1974.
- ODD, N.V.M., "Practical Application of Mathematical Model Techniques to Predict Effects of Engineering Works on Tidal Flow in Estuaries with a Large Tidal Range," *Proceedings of the Institution of Civil Engineers*, Vol. 50, Dec. 1971, pp. 507-519.

OVERLAND, J.E., and MYERS, V.A., "A Model of Hurricane Tide in Cape Fear Estuary," *Journal of Waterways, Harbors, and Coastal Engineering Division*, Vol. 102, No. WW4, Nov. 1976, pp. 407-424.

PLATZMAN, G.W., "The Dynamical Prediction of Wind Tides on Lake Erie," *Meteorological Monographs*, Vol. 4, No. 26, Sept. 1963.

REID, R.O., "Modification of the Quadratic Bottom-Stress Law for Turbulent Channel Flow in the Presence of Surface Wind-Stress," TM-93, U.S. Army, Corps of Engineers, Beach Erosion Board, Washington, D.C., Feb. 1957.

REID, R.O., Comment on "Three-Dimensional Structure of Storm-Generated Currents," *Journal of Geophysical Research*, Vol. 80, No. 9, Mar. 1975, pp. 1184-1185.

REID, R.O., and BODINE, B.R., "Numerical Model for Storm Surges in Galveston Bay," *Journal of the Waterways and Harbors Divisions*, Vol. 94, No. WW1, Feb. 1968, pp. 33-57.

REID, R.O., VASTANO, A.C., and REID, T.J., "Development of Surge II Program with Application to the Sabine-Calcasieu Area for Carla and Design Hurricanes," CSI Study 74-5, U.S. Army Engineer District, Galveston, Galveston, Tex. (in preparation, 1977).

ROACHE, P.J., *Computational Fluid Dynamics*, Hermosa Publishers, Albuquerque, N. Mex., 1972.

ROUSE, H., and INCE, S., *History of Hydraulics*, 1st ed., Dover, New York, 1957.

RUMMER, R.R., and ROBSON, L., "Circulation Studies in a Rotating Model of Lake Erie," *Proceedings of the 11th Conference on Great Lakes Research*, 1968, pp. 487-495.

SAGER, R.A., and SEABERGH, W.C., "Modeling Sediment Movement for Masonboro Inlet," *Symposium on Modeling Techniques, Modeling 75*, Vol. I, 1975, p. 274.

SAGER, R.A., and SEABERGH, W.C., "Fixed-Bed Hydraulic Model Results," App. 1, GITI Report 6, *Comparison of Numerical and Physical Models, Masonboro Inlet, North Carolina*, U.S. Army, Corps of Engineers, Coastal Engineering Research Center, Fort Belvoir, Va., and U.S. Army Engineer Waterways Experiment Station, Vicksburg, Miss., June 1977.

SAGER, R.A., and SEABERGH, W.C., "Physical Model Simulation of the Hydraulics of Masonboro Inlet, North Carolina," GITI Report, U.S. Army, Corps of Engineers, Coastal Engineering Research Center, Fort Belvoir, Va., and U.S. Army Engineer Waterways Experiment Station, Vicksburg, Miss. (in preparation, 1977).

- SEABERGH, W.C., and MASON, C., "Masonboro Inlet Fixed-Bed Model Evaluation," *Symposium on Modeling Techniques, Modeling 75*, Vol. I, 1975, p. 294.
- SEELIG, W.N., HARRIS, D.L., and HERCHENRODER, B.E., "A Spatially Integrated Numerical Model of Inlet Hydraulics," GITI Report 14, U.S. Army, Corps of Engineers, Coastal Engineering Research Center, Fort Belvoir, Va., and U.S. Army Engineer Waterways Experiment Station, Vicksburg, Miss. (in preparation, 1977).
- SHEMDIN, O.H., "Modeling of Wind Over Water," Paper No. OTC 1515, *Offshore Technology Conference*, Vol. I, 1972, pp. 35-42.
- SIELECKI, A., "An Energy-Conserving Difference Scheme for the Storm Surge Equations," *Monthly Weather Review*, Vol. 96, No. 3, Mar. 1968, pp. 150-156.
- SOBEY, R.J., "Finite Difference Schemes Compared for Wave-Deformation Characteristics in Mathematical Modeling of Two-Dimensional Long Wave Propagation," TM-32, U.S. Army, Corps of Engineers, Coastal Engineering Research Center, Washington, D.C., Oct. 1970.
- VALEMBOIS, J., and BONNEFILLE, R., "Etude de l'action de la force de Coriolis," *La Houille Blanche*, Vol. 14, No. 5, Aug. 1959, pp. 568-585.
- VERBER, J.L., "Inertial Currents in the Great Lakes," *Proceedings of the Ninth Conference on Great Lakes Research*, 1966, pp. 375-379.
- WANG, J.D., and CONNOR, J.J., "Mathematical Modeling of Near Coastal Circulation," Report No. MITSG 75-13, Massachusetts Institute of Technology, Cambridge, Mass., Apr. 1975.
- WANSTRATH, J.J., et al., "Storm Surge Simulation in Transformed Coordinates," TR 76-3, U.S. Army, Corps of Engineers, Coastal Engineering Research Center, Fort Belvoir, Va., Nov. 1976.
- WEARE, T.J., "Instability in Tidal Flow Computational Schemes," *Journal of the Hydraulics Division*, Vol. 102, No. HY 5, May 1976, pp. 569-580.
- WEBSTER, F., "Observations of Inertial-Period Motions in the Deep Sea," *Reviews of Geophysics*, Vol. 6, No. 4, Nov. 1969, pp. 473-490.
- WHALIN, R.W., PERRY, F.C., and DURHAM, D.L., "Model Verification for Tidal Constituents," *Proceedings of the 15th Coastal Engineering Conference* (in preparation, 1977).
- ZIENKEWICZ, O.C., *The Finite Element Method in Engineering Sciences*, McGraw-Hill, New York, 1971.

APPENDIX A

Request for Proposals

TIDAL CALCULATIONS FOR MASONBORO INLET, N. C.

Introduction

Masonboro Inlet, North Carolina, has been selected for extensive field, physical model, and mathematical model investigations as a "typical" inlet problem area. As a basic part of the investigation, the effectiveness of both mathematic and physical models in predicting tidal heights and current velocities for selected prototype conditions is to be determined. A physical fixed-bed model of Masonboro Inlet has been constructed and verified using the data of Inclosure 1. Further tests will be conducted to arrive at the tidal heights and current velocities in November 1964 and June 1967 using the inlet hydrography and jetty placement of those dates. Concurrently, it is desired to obtain predictions using existing mathematical model procedures for the same hydrographic conditions to be tested on the physical model. The work of Earl I. Brown (1) and G. H. Keulegan (2) is to be considered as well as other appropriate approaches.

Purpose

The purpose of this study is to evaluate the degree to which mathematical models can be used to predict quantitatively the hydrodynamics (other than sediment movement) of flow through tidal inlets. This will be done by computing flows through a specific inlet, Masonboro Inlet, for which actual flow conditions are known.

The Prototype

Masonboro Inlet is located along the North Carolina coast north of the mouth of the Cape Fear River (see USC&GS Chart No. 1235). Inclosure 2 is the portion of this chart showing the inlet area. The inlet-bay is an intricate complex of channels, overflow regions, and marshland.

Work Statement

The study is to consist of the calibration and application of a previously selected lumped or discretized (one-dimensional or two-dimensional) mathematical model to predict the water surface time-history and current velocities of Masonboro Inlet for two specific hydrographic conditions. Basically, the study will include: (a) adaptation of the previously selected (at the proposal stage) model to Masonboro Inlet; (b) adjustment of the model to allow reproduction of the prototype tides and currents of 12 September 1969 as shown by Inclosure 1; (c) prediction of the tides and currents for the additional hydrographic conditions of the inlet as shown by Inclosures 4 and 5 for an idealized mean and spring

tide in the ocean (see Inclosure 6); and (d) preparation of a final report describing in detail all significant phases of the study.

Methodology

The proposals to be submitted in response to the request are to consider each of the following possible approaches separately:

1. Lumped approach (Keulegan)
2. Discretized approach (one-dimensional)
3. Discretized approach (two-dimensional)

Proposals may be submitted on any one, any two, or all of these approaches as long as the portion on each method is kept completely separate so that the proposal for each separate method may be accepted or rejected on its own merits. Details of the first method are given in references (1) and (2). The second method may be any existing model such as that developed by Reid and Bodine (3) or Leendertse (4). The lumped model will be used to determine tidal response of the inner connecting channels and velocities within the inlet due to a given ocean tide. The one-dimensional model will be used to predict water surface time-histories, the tidal prism, and the maximum mean (average) velocity in the inlet channel and interior channels. The two-dimensional model will be used to predict variation of water surface elevations and current velocities with time in the ocean approach, the inlet, and the interior channels.

Mathematical Model Confirmation

The appropriate topographic and field data are attached as Inclosure 1. Inclosure 3 shows the location of the seven ocean tide and five current velocity stations. The mathematical model will be applied to Masonboro Inlet using given ocean tide and steady state or other initial conditions. The model will be adjusted and confirmed to the 1969 bottom survey and to given 1969 velocity and tide data (Inclosure 1).

Mathematical Model Application

The developed model will be applied to Masonboro Inlet under the following conditions:

1. Preproject undeveloped inlet conditions--predict tides, tidal prism, and currents for November 1964 survey data (Inclosure 4) at locations shown in Inclosure 3.
2. Modified inlet and north jetty--predict tides, tidal prism, and currents for June 1967 survey data (Inclosure 5) at locations shown in Inclosure 3.

Report Preparation

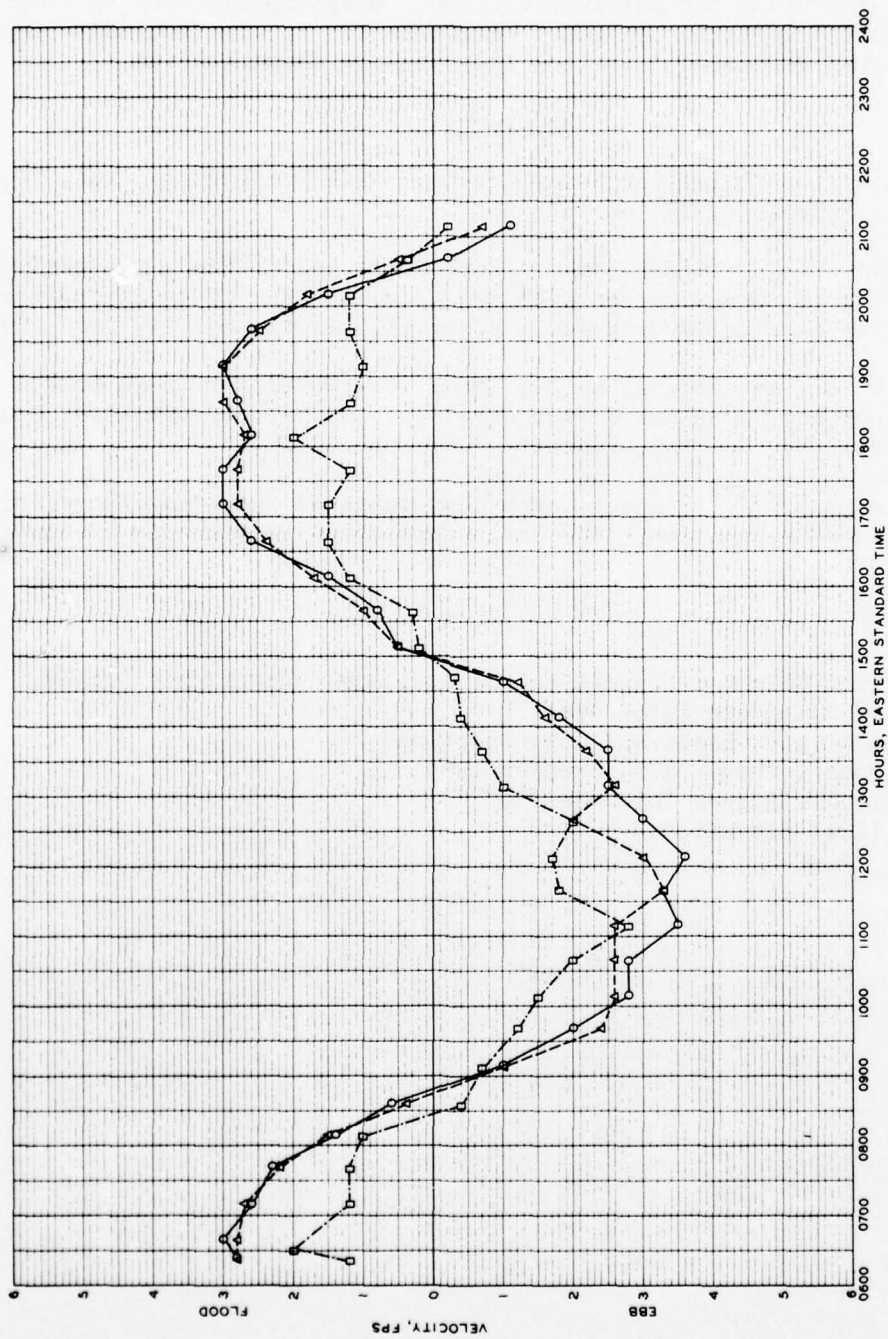
A final report will be written on the investigation, including results, suggestions for mathematical model usage appropriate to other inlets, and a description of model development. It will include a copy of the program deck with a listing and adequate documentation.

References

1. Brown, E. I., "Inlets on Sandy Coasts," ASCE Proceedings, Vol. 54, Part I, February 1928, pp. 508-553.
2. Keulegan, G. H., "Tidal Flow in Entrances: Water-Land Fluctuations of Basins in Communication with Seas," U. S. Army Corps of Engineers, Committee on Tidal Hydraulics, Technical Bulletin No. 14, July 1967.
3. Reid, R. O., and Bodine, B. R., "Numerical Model for Storm Surges in Galveston Bay," Journal of the Waterways and Harbors Division, Proc., ASCE, Vol. 94, No. WW1, February 1968, pp. 33-57.
4. Leendertse, J. J., "Aspects of a Computational Model for Long-Period Water-Wave Propagation," The Rand Corporation, Memorandum RM-5294-PR, May 1967.

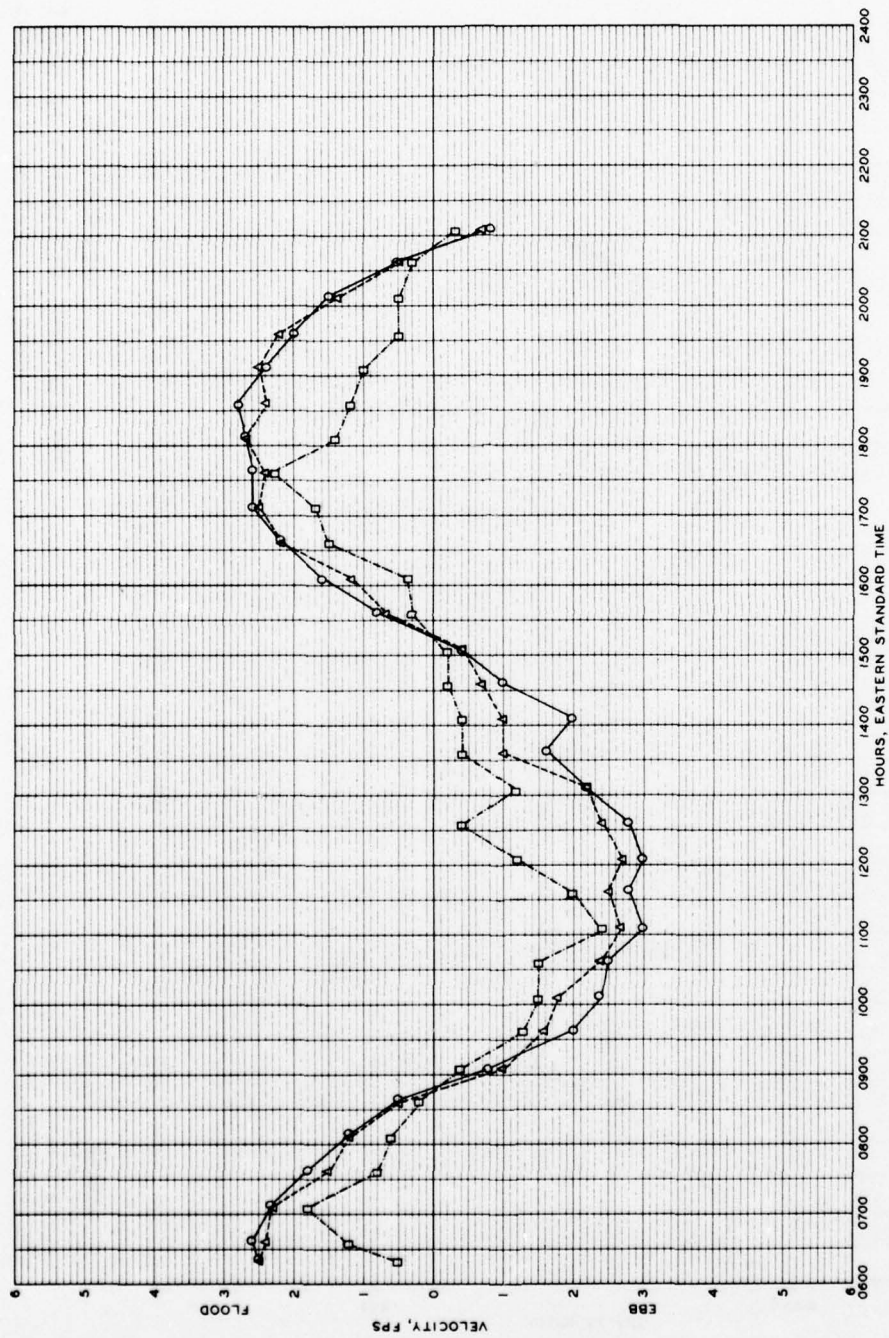
Inclosures

1. 1969 Tidal Heights, Current Velocities, and Hydrographic Survey
2. Chart of Masonboro Inlet Area
3. Masonboro Inlet Range and Gage Locations
4. Hydrographic Survey for November 1964
5. Hydrographic Survey for June 1967
6. Ocean Tidal Elevations



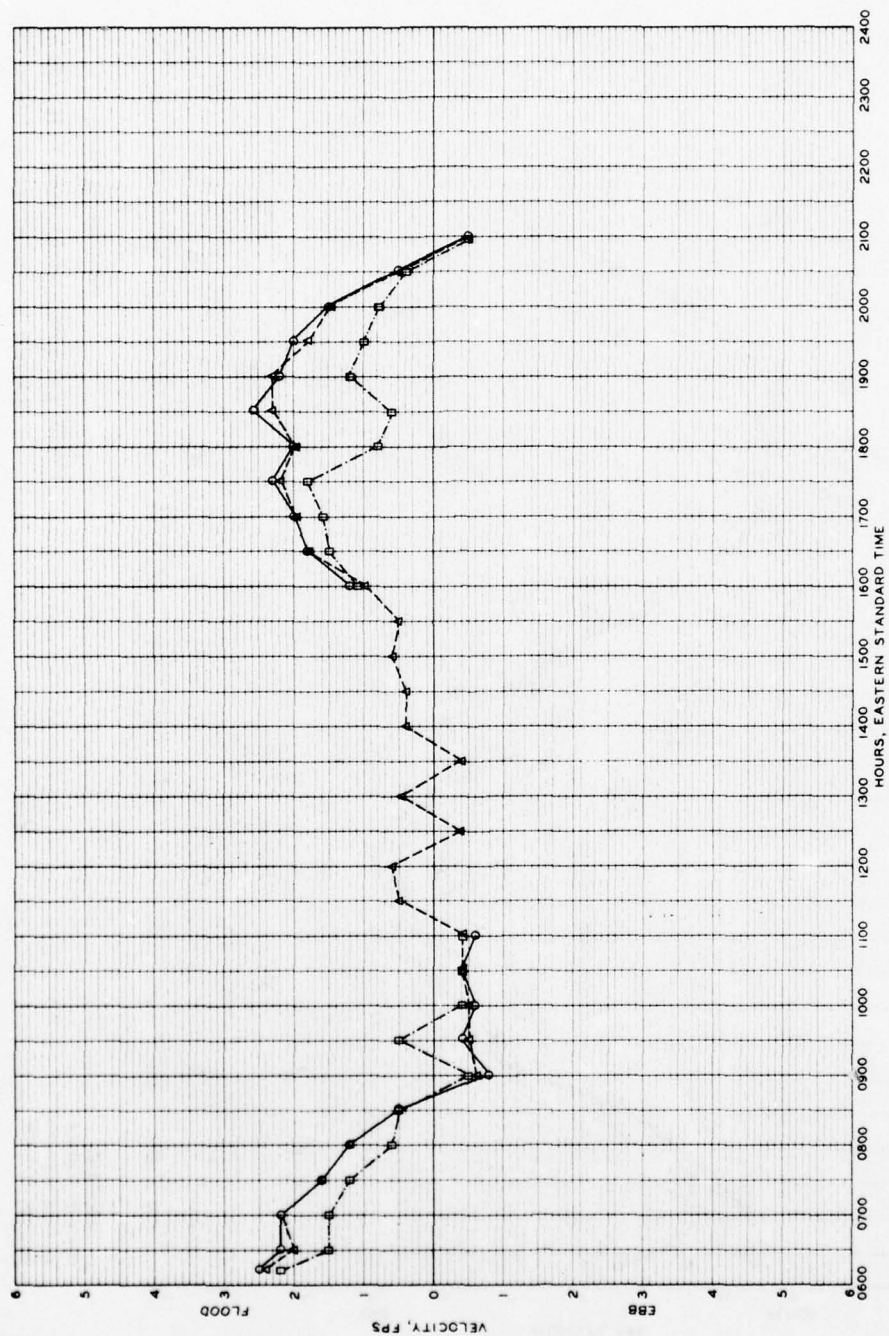
MASONBORO INLET
 PROTOTYPE VELOCITY 12 SEPT 1969
 RANGE 3 - STATION N (NORTH)

Incl 1 to App. A, p. 1 of 15 pp.



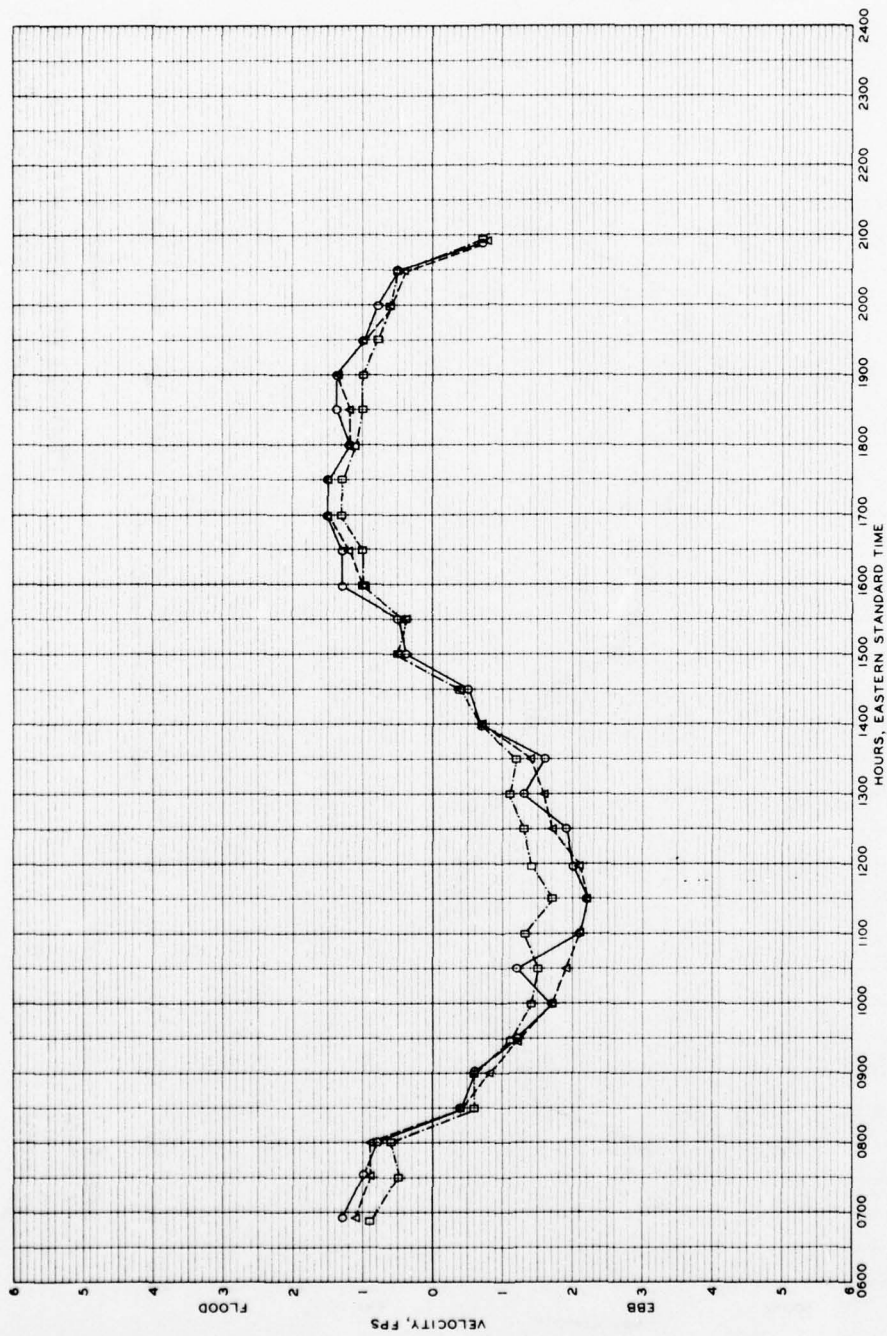
MASONBORO INLET
 PROTOTYPE VELOCITY 12 SEPT 1969
 RANGE 3 - STATION C (CENTER)

Incl 1 to App. A, p. 2 of 15 pp.



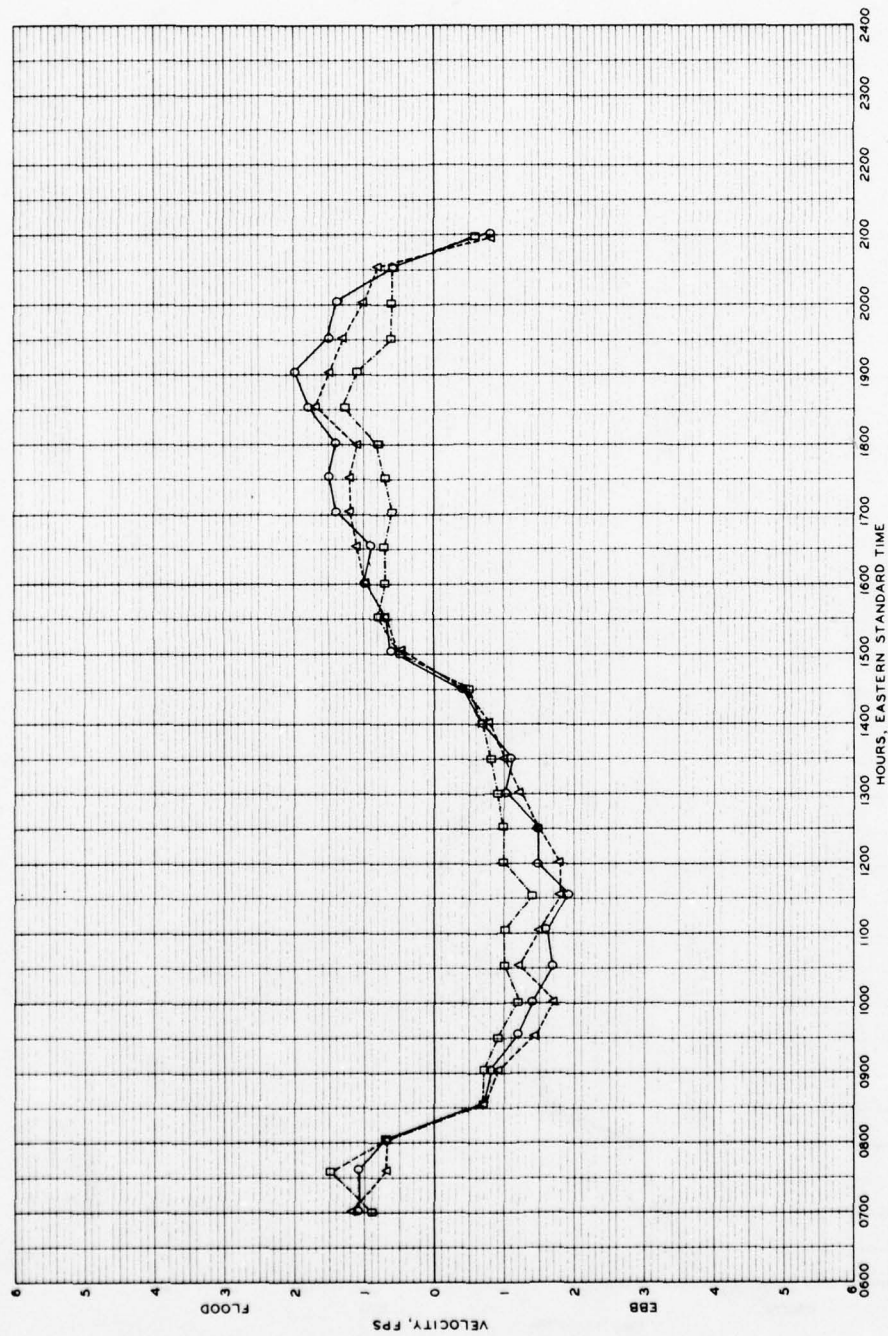
MASONBORO INLET
 PROTOTYPE VELOCITY 12 SEPT 1969
 RANGE 3 - STATION S (SOUTH)

Incl 1 to App. A, p. 3 of 15 pp.



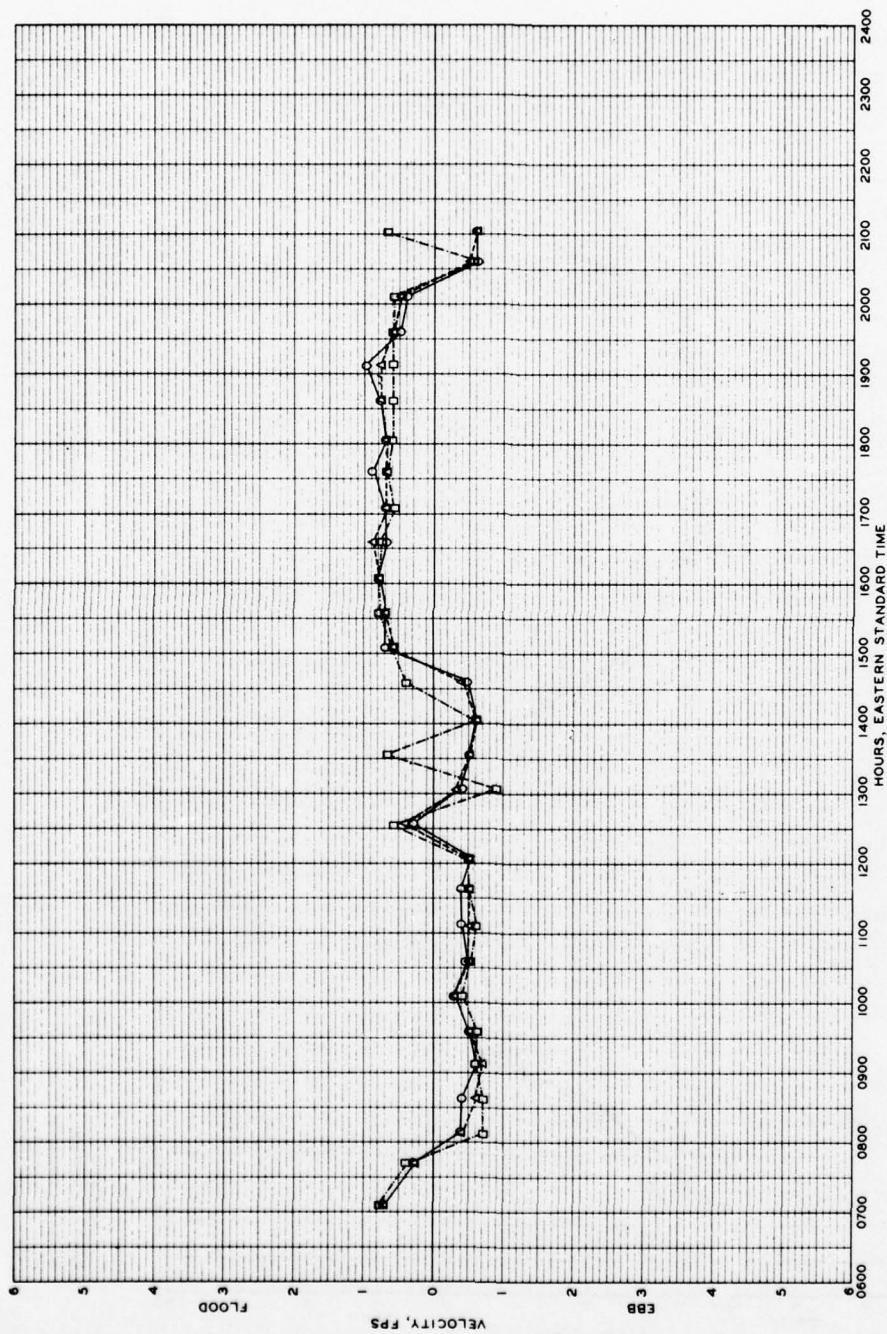
MASONBORO INLET
 PROTOTYPE VELOCITY 12 SEPT 1969
 RANGE 4 - STATION E (EAST)

Incl 1 to App. A, p. 4 of 15 pp.



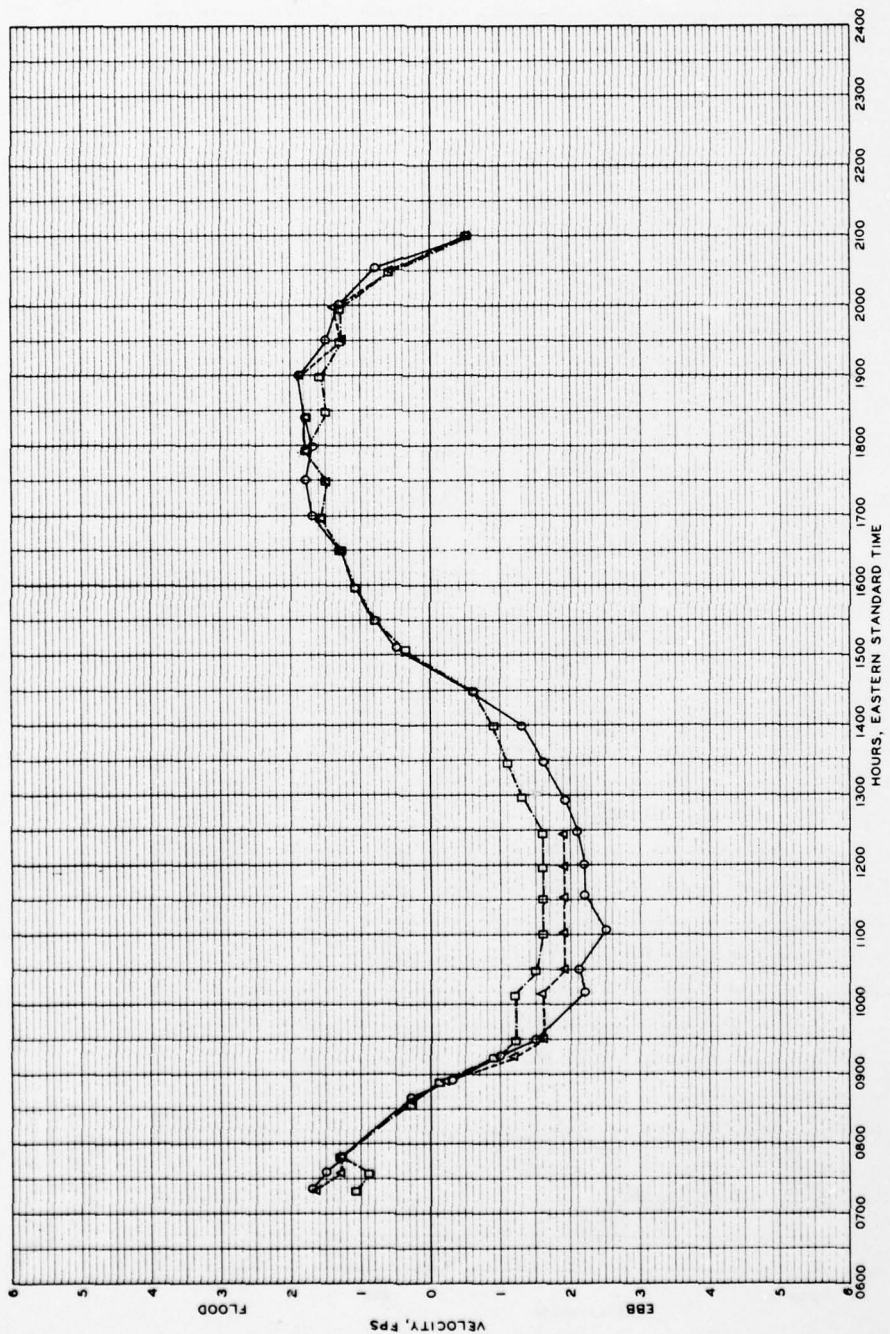
MASONBORO INLET
 PROTOTYPE VELOCITY 12 SEPT 1969
 RANGE 4 - STATION C (CENTER)

Incl 1 to App. A, p. 5 of 15 pp.



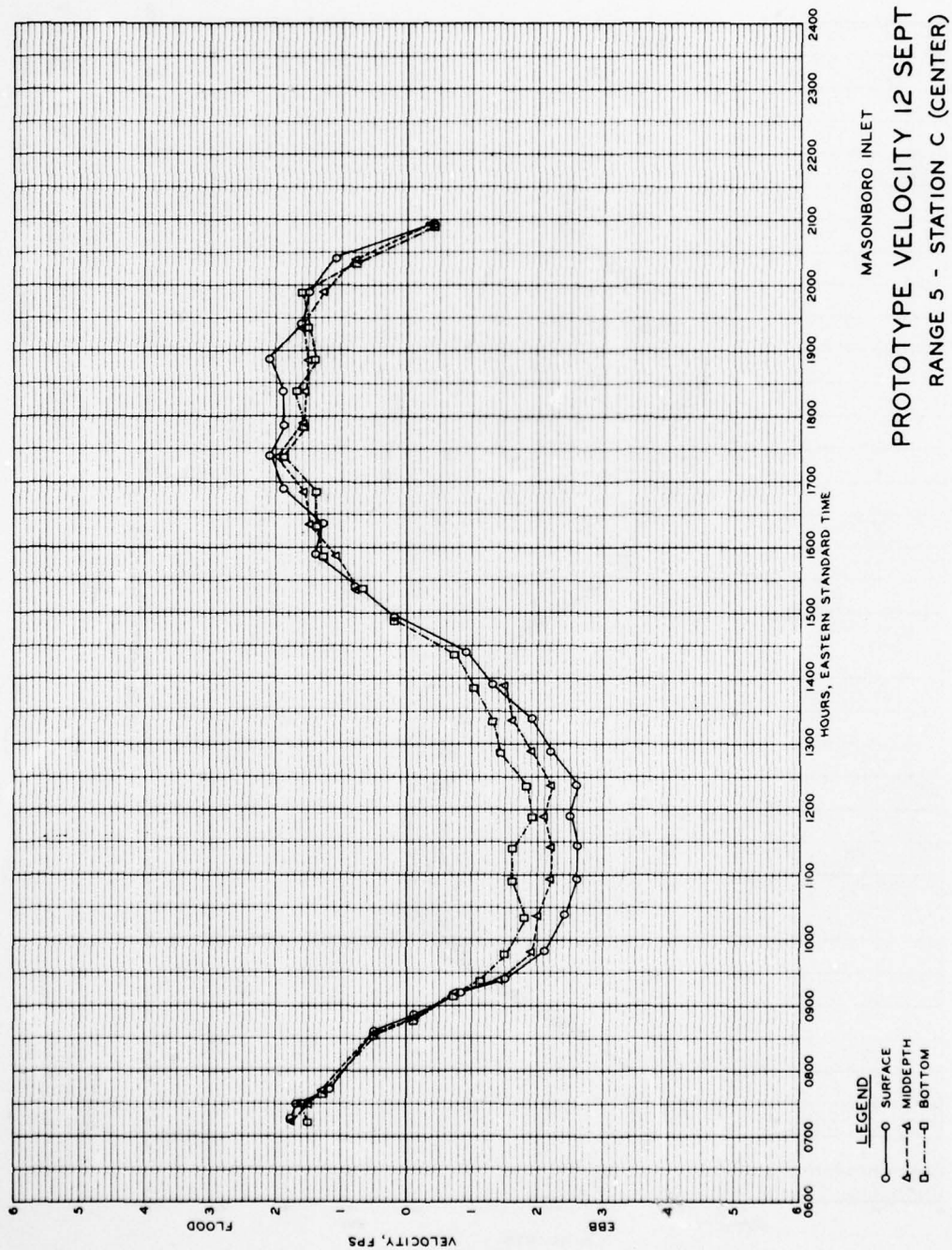
MASONBORO INLET
 PROTOTYPE VELOCITY 12 SEPT 1969
 RANGE 4 - STATION W (WEST)

Incl 1 to App. A, p. 6 of 15 pp.

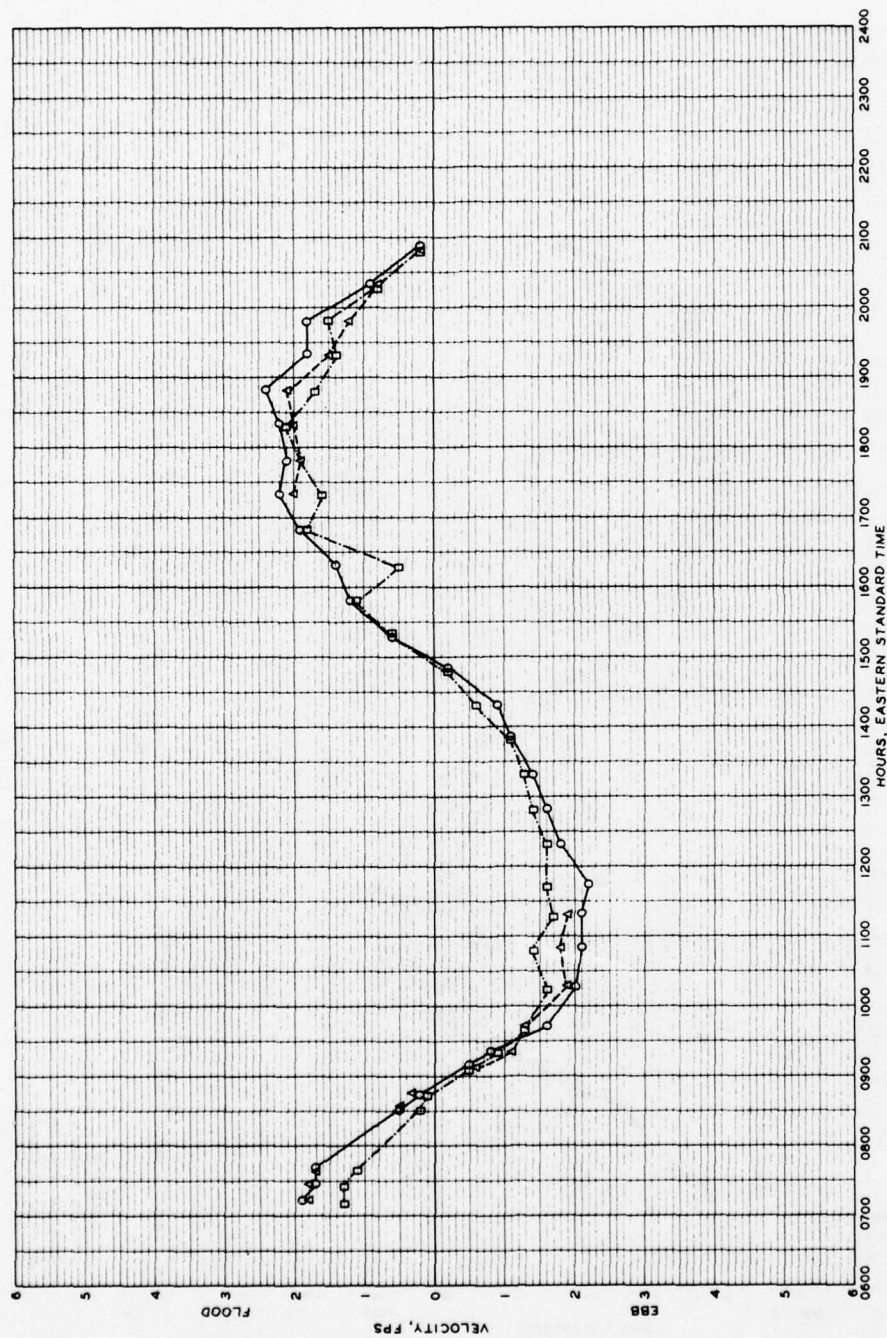


MASONBORO INLET
 PROTOTYPE VELOCITY 12 SEPT 1969
 RANGE 5 - STATION E (EAST)

Incl 1 to App. A, p. 7 of 15 pp.



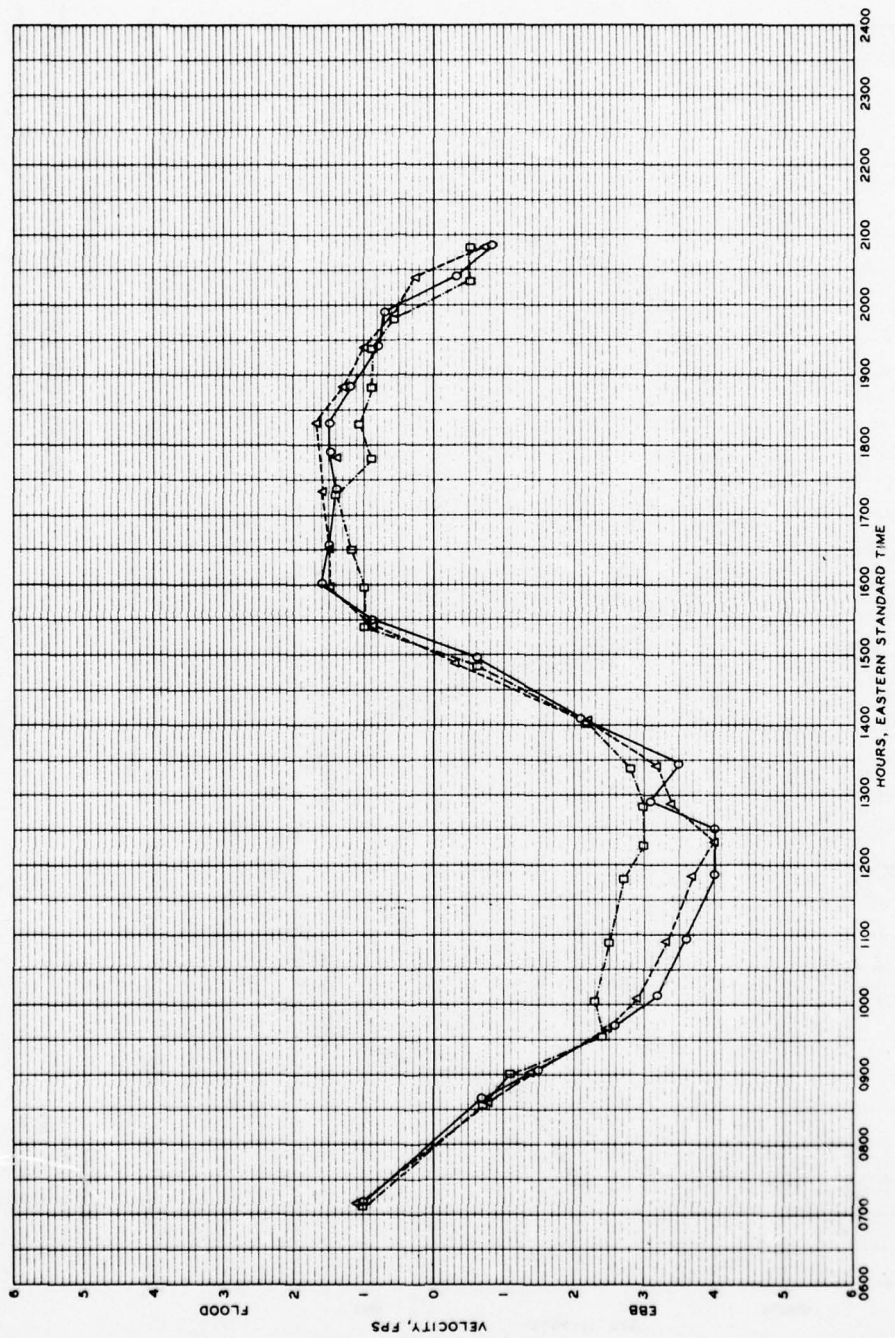
Incl 1 to App. A, p. 8 of 15 pp.



MASONBORO INLET
 PROTOTYPE VELOCITY 12 SEPT 1969
 RANGE 5 - STATION W (WEST)

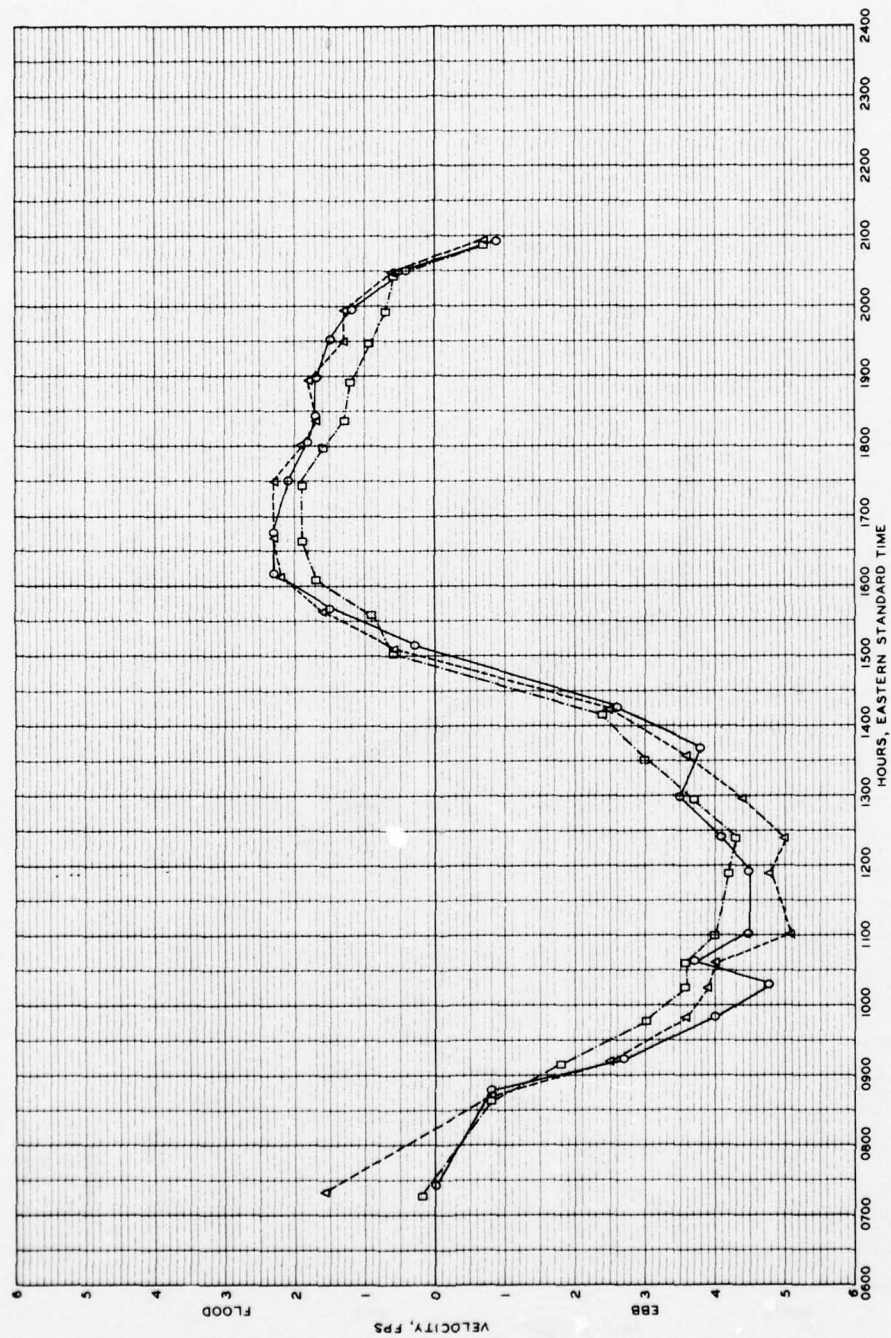
LEGEND
 O SURFACE
 Δ MIDDEPTH
 □ BOTTOM

Incl 1 to App. A, p. 9 of 15 pp.



MASONBORO INLET
 PROTOTYPE VELOCITY 12 SEPT 1969
 RANGE 1 - STATION N (NORTH)

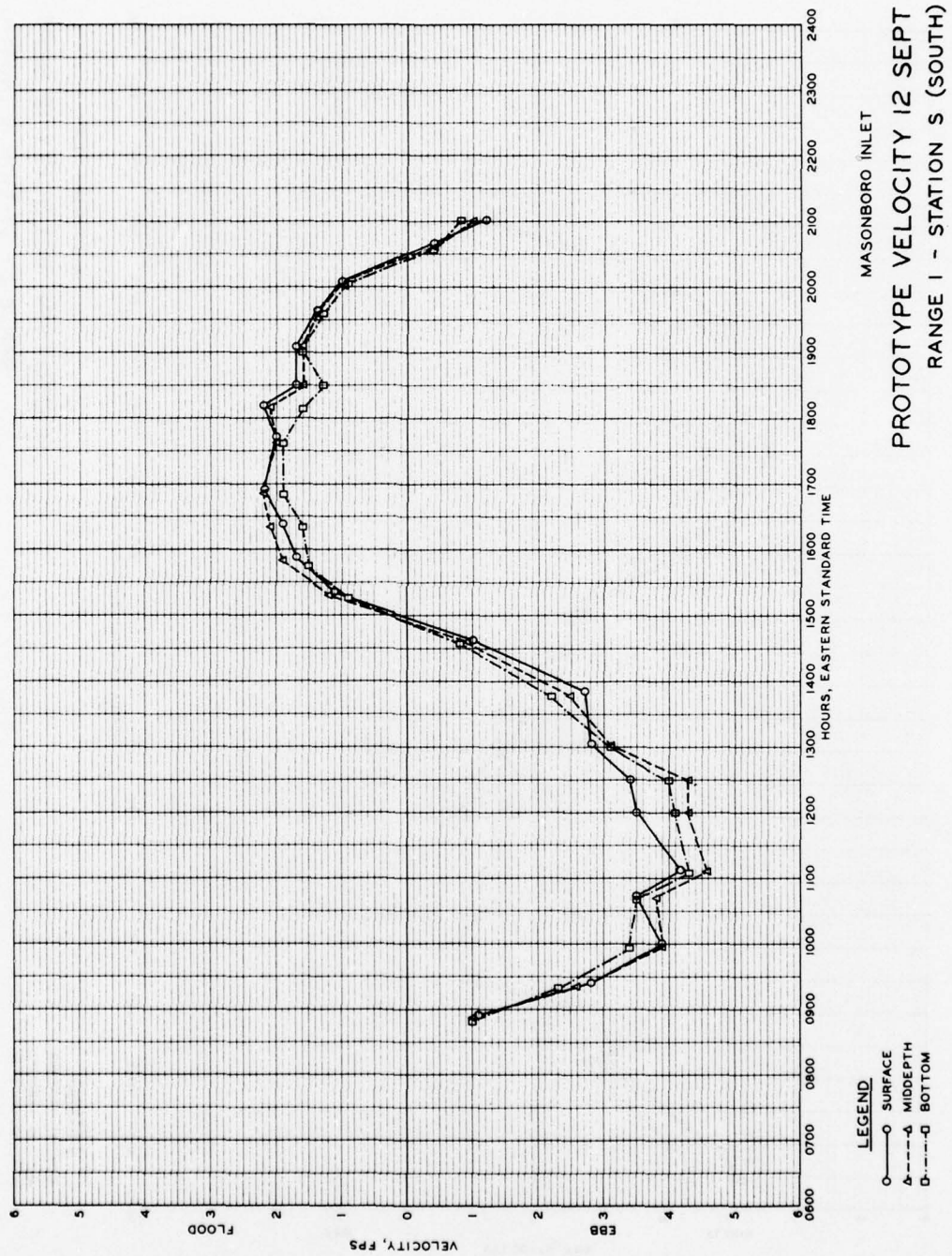
Incl 1 to App. A, p. 10 of 15 pp.



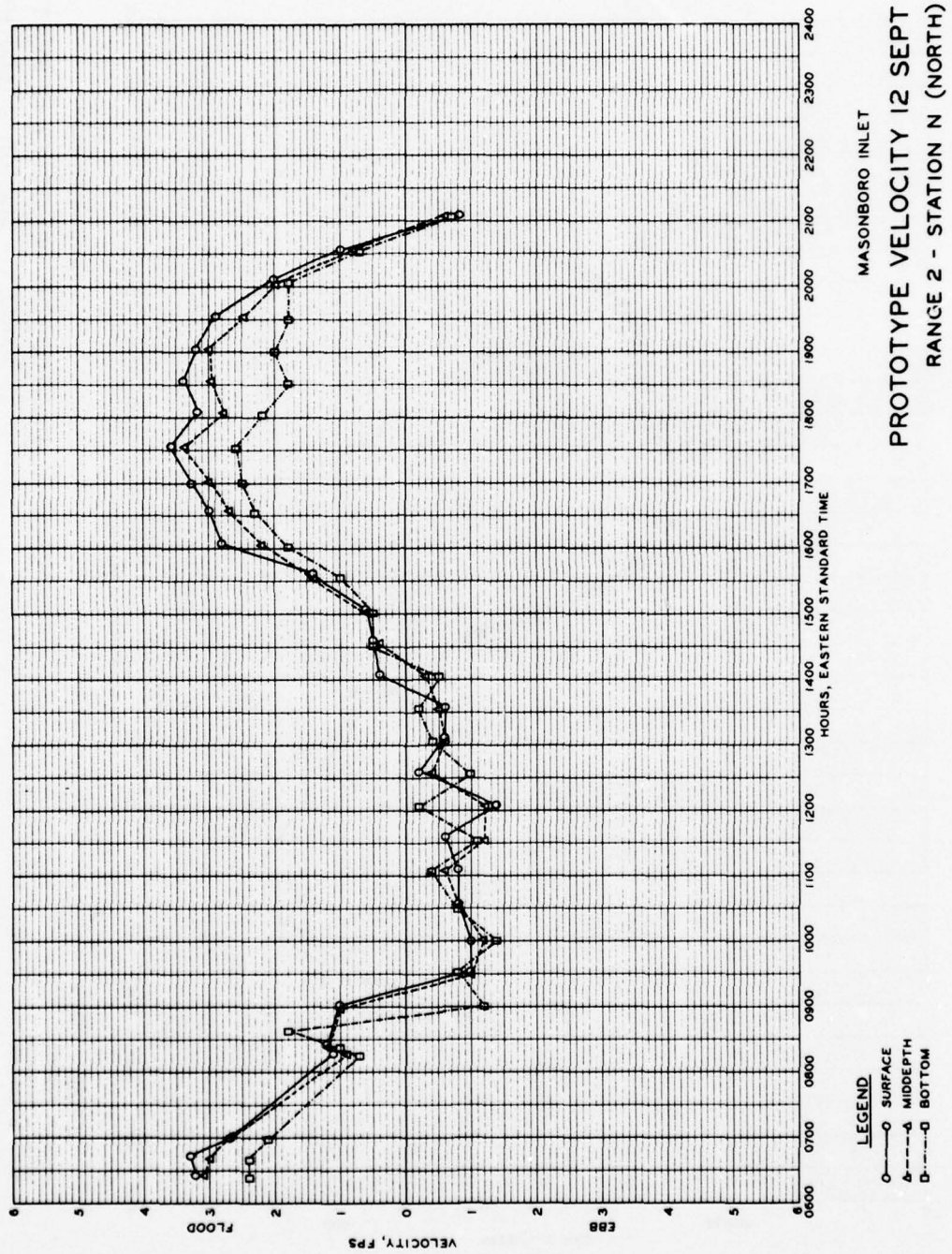
MASONBORO INLET
 PROTOTYPE VELOCITY 12 SEPT 1969
 RANGE 1 - STATION C (CENTER)

LEGEND
 O — SURFACE
 Δ — MIDDEPTH
 □ — BOTTOM

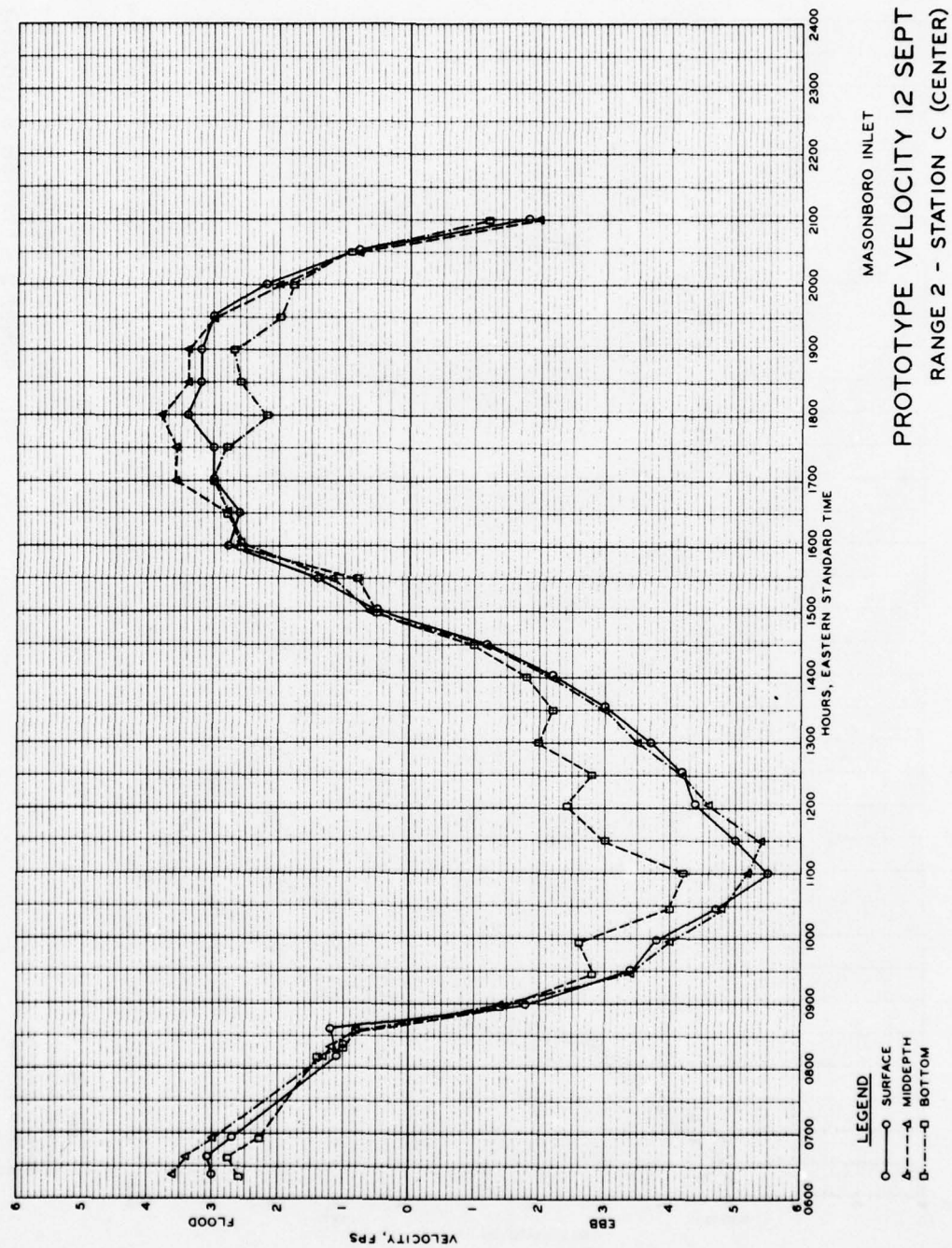
Incl 1 to App. A, p. 11 of 15 pp.



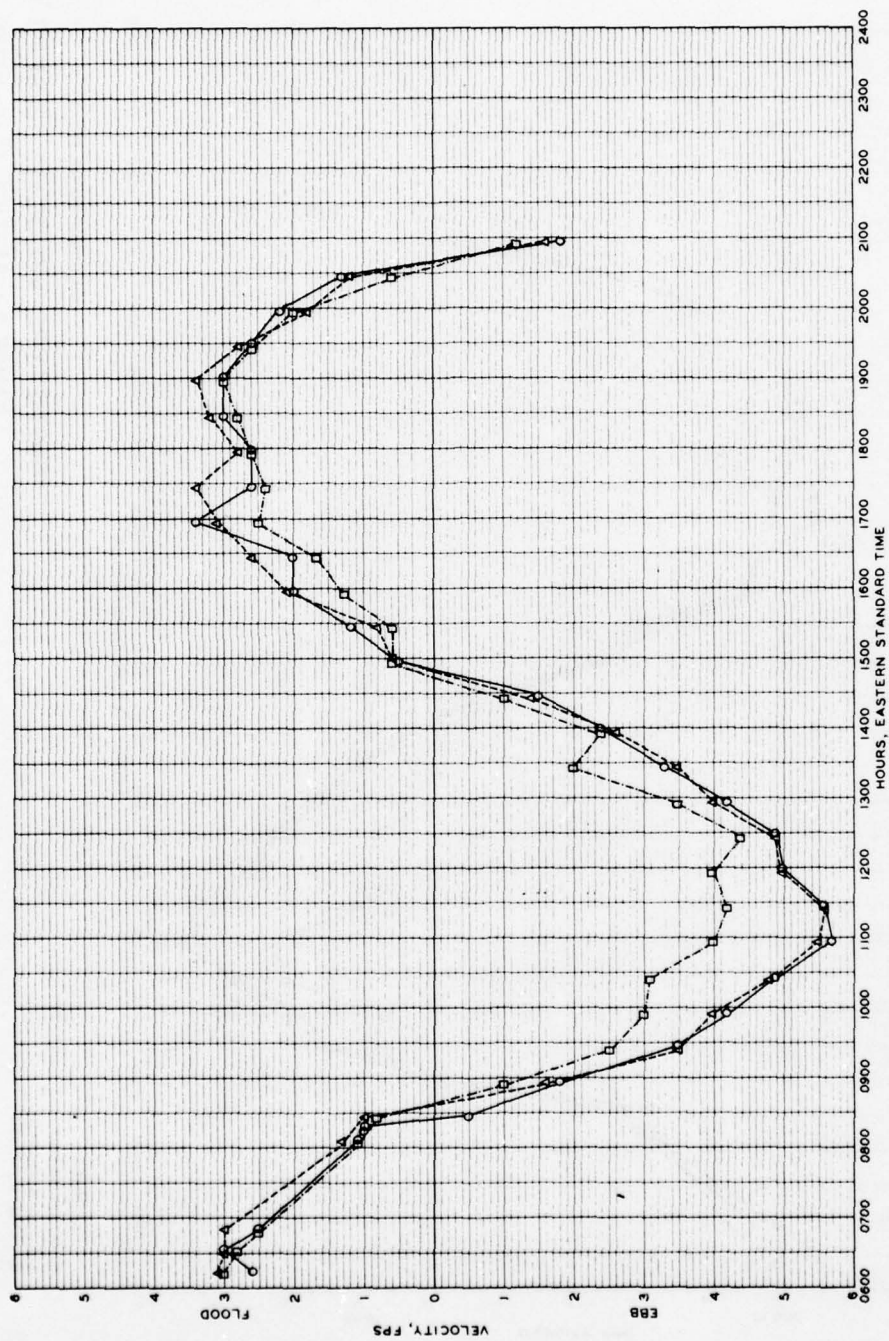
Incl 1 to App. A, p. 12 of 15 pp.



Incl 1 to App. A, p. 13 of 15 pp.

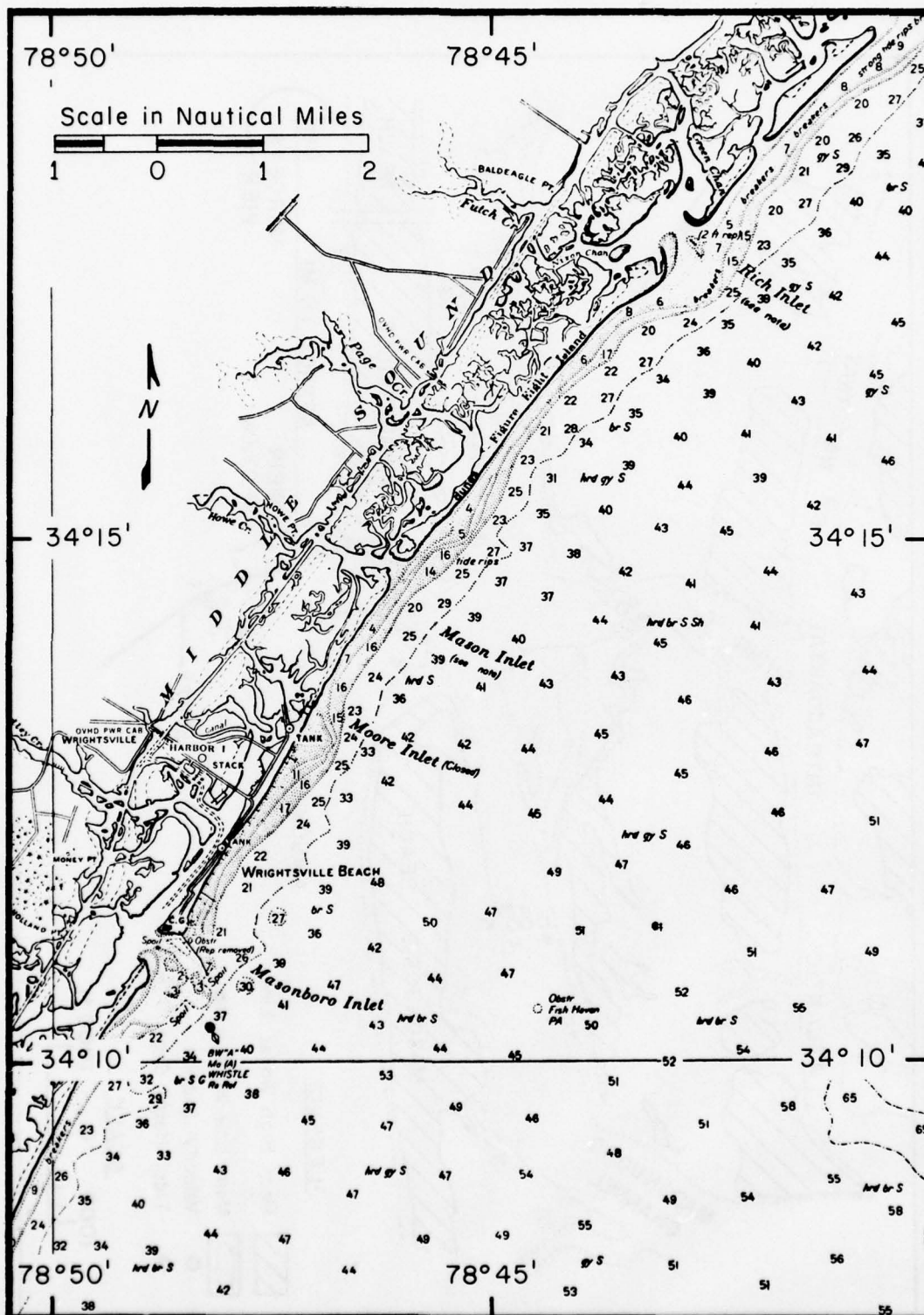


Incl 1 to App. A, p. 14 of 15 pp.

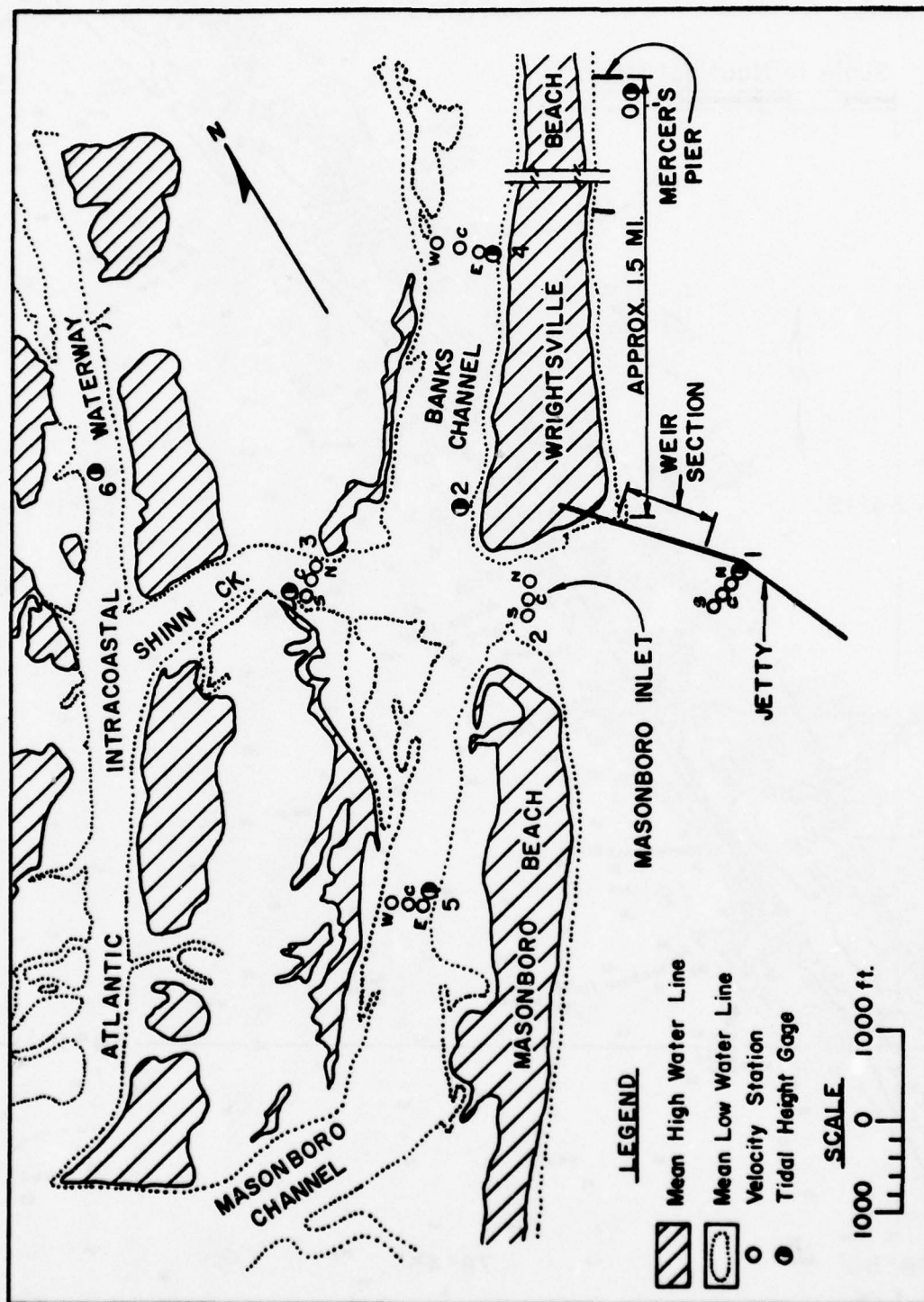


MASONBORO INLET
 PROTOTYPE VELOCITY 12 SEPT 1969
 RANGE 2 - STATION S (SOUTH)

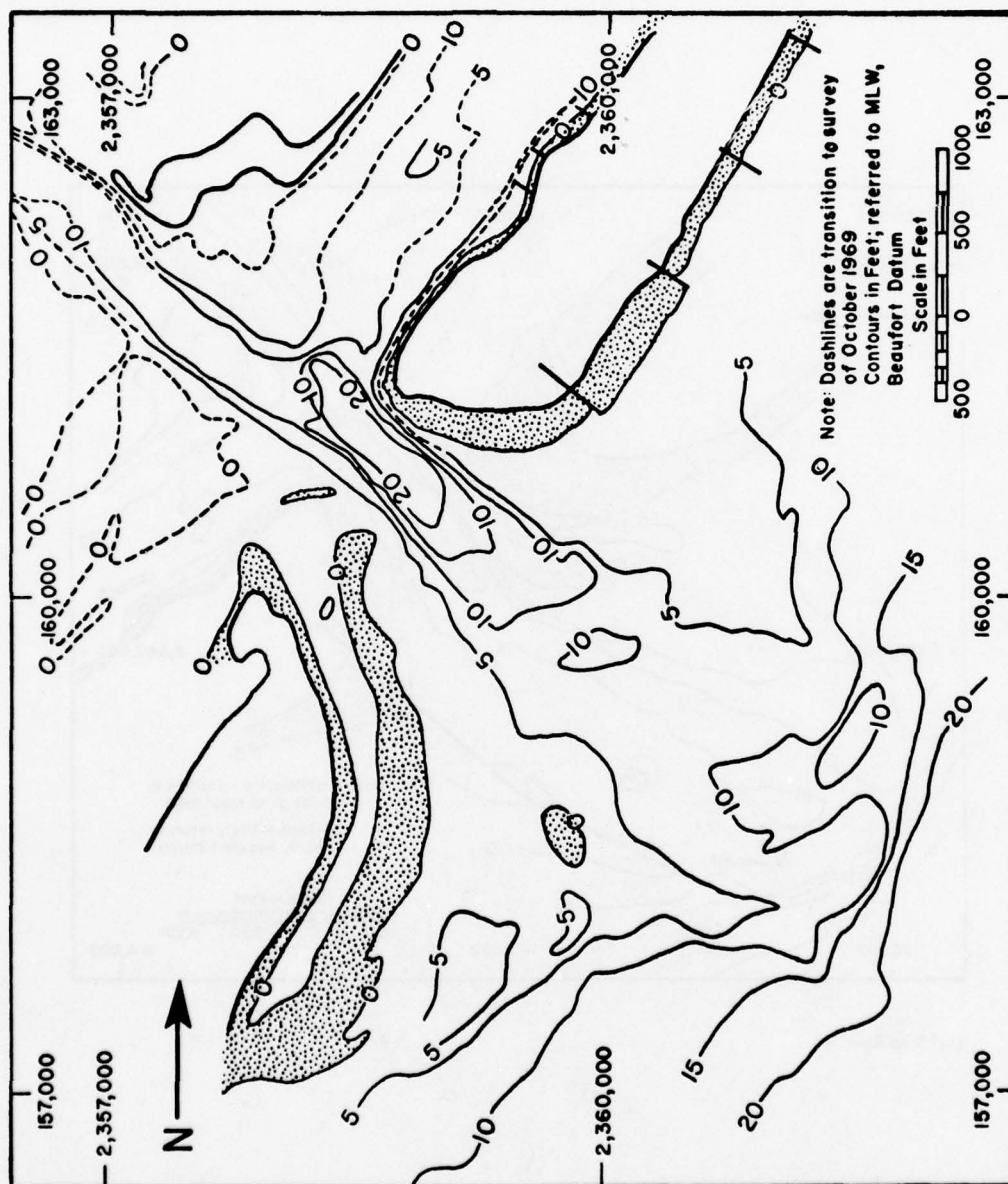
Incl 1 to App. A, p. 15 of 15 pp.



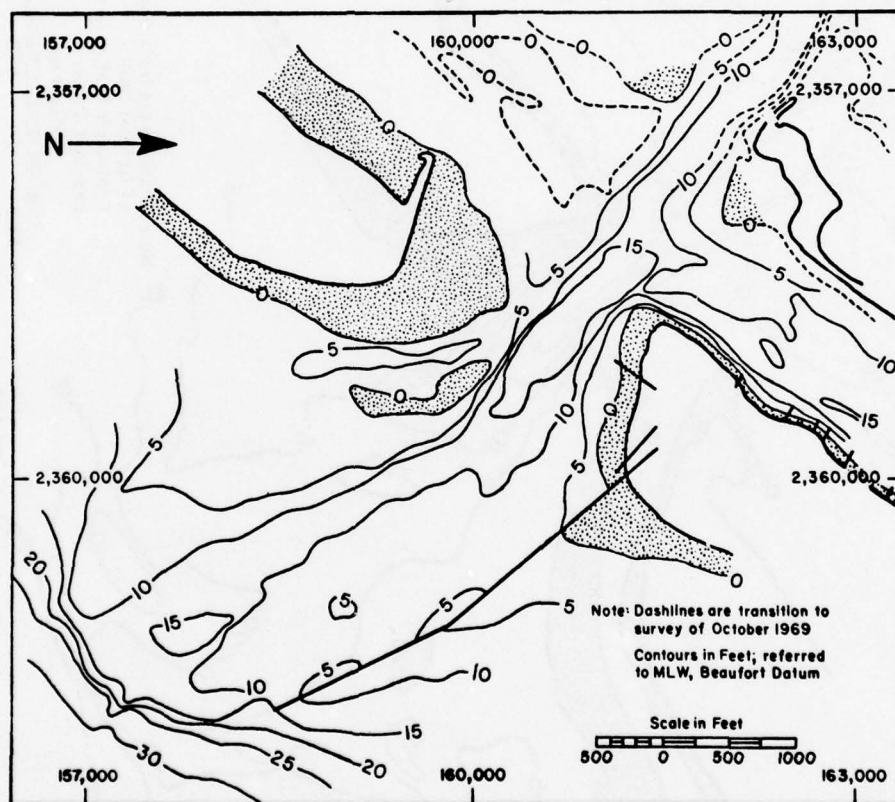
Incl 2 to App. A



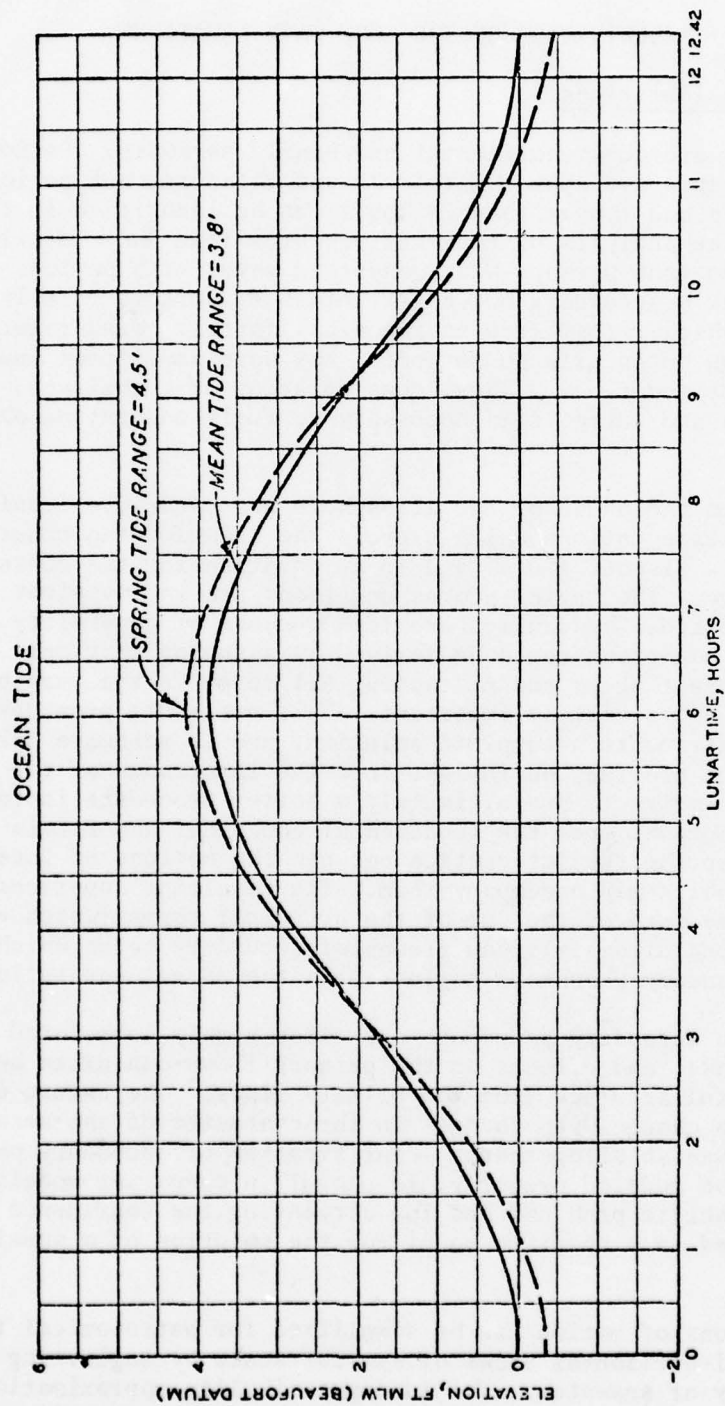
Incl 3 to App. A



Incl 4 to App. A



Incl 5 to App. A



MASONBORO INLET
MEAN AND SPRING TIDES

Incl 6 to App. A

APPENDIX B

A DERIVATION OF THE LONG WAVE EQUATIONS

1. General Considerations.

Tidal flows are quasi-horizontal and nearly periodic. Periods of greatest importance are approximately 12 and 24 hours, but periods as short as 3 hours and longer than 24 hours can be identified in tidal theory and in the analysis of the tidal records from many locations. Turbulent eddies, and perhaps wind-generated waves with periods measured in seconds, play a secondary but nevertheless measurable role in modifying the flows which result from astronomical forces. Wind-generated currents, though not nearly so periodic, may have amplitudes and durations similar to the tides. Thus, consideration of turbulence, wind-generated waves and currents is necessary to fully understand observed tidal flows.

All flows in the ocean or the atmosphere near sea level conform to the Navier-Stokes equations which express the laws for the conservation of momentum in a viscous fluid, and to an equation for the conservation of mass. However, the Navier-Stokes equations are inconvenient for a solution of the tidal hydraulics problems because of generality. A convenient set of equations could be derived by assuming that only the motions of interest occur and discarding all terms in the complete equations that are not obviously important. This procedure provides the first approximations to a complete solution, and is adequate for many applications but provides no insight into the importance of the neglected phenomena. An indirect, but ultimately a better procedure is to filter the undesired motions from the fundamental equations and retain the terms which describe the interaction between the motions of interest and other motions which may accompany them. The resulting equations may be expressed in the form of the sum of the principal terms (which could have been derived directly), and groups of secondary terms which describe the secondary phenomena neglected in the direct derivation.

Some of the secondary phenomena are often highly correlated with the primary flows, and effects on the primary flows can often be estimated with useful accuracy from the primary flows. The nature of this correlation can change with changes in the character of the secondary flow, and may vanish altogether. Identification of secondary phenomena, which may not be modeled properly, is useful in comparing models for the solution of specific problems and for estimating the confidence which should be placed in a specific model for the solution of a specific problem.

The equations of motion can be simplified for astronomical tides and other quasi-horizontal flows of similar scale by neglecting the compressibility of seawater. The incompressibility approximation is especially useful when numerical models are considered (see Sec. IV). The compressibility of seawater does not have a significant effect on

water velocities that are less than the speed of sound, or on water densities unless large vertical displacements occur. Since tidal velocities are low and the flow is quasi-horizontal, the seawater is assumed incompressible in this derivation.

Separation of tidal flows from small-scale flows, such as turbulence and wind-generated waves, is more difficult. This separation is accomplished, at least approximately, by defining a "large-scale flow" which is the average of the total flow over some element of space and time, and a "perturbation flow" which is the difference between the total flow and the large-scale flow. Numerical models can only deal effectively with the average flow where large averaging volumes and times are used (see Sec. IV). Recognizing the difference in the effective averaging implied by different models is essential to the proper interpretation of the results.

The equations may be simplified by suppressing details of the vertical structure of the flow by integration of each term in each equation from the bottom to the top of an identifiable fluid layer.

The filtering techniques described here are widely used in the field of hydrodynamics. The development given below is an outgrowth of the derivations by Fortak (1962) and Harris (1967).

2. The Primitive Equations.

The equations for the conservation of mass and momentum in an incompressible fluid on a rotating earth may be stated as:

$$\frac{\partial u}{\partial x} + \frac{\partial v}{\partial y} + \frac{\partial w}{\partial z} = 0, \quad (B1)$$

$$\begin{aligned} \rho \left[\frac{\partial u}{\partial t} + u \frac{\partial u}{\partial x} + v \frac{\partial u}{\partial y} + w \frac{\partial u}{\partial z} - f v + f_2 w \cos \Psi \right] &= \frac{\partial}{\partial x} \tau_{xx} + \frac{\partial}{\partial y} \tau_{yx} + \frac{\partial}{\partial z} \tau_{zx}, \\ \rho \left[\frac{\partial v}{\partial t} + u \frac{\partial v}{\partial x} + v \frac{\partial v}{\partial y} + w \frac{\partial v}{\partial z} + f u - f_2 w \sin \Psi \right] &= \frac{\partial}{\partial x} \tau_{xy} + \frac{\partial}{\partial y} \tau_{yy} + \frac{\partial}{\partial z} \tau_{zy}, \end{aligned} \quad (B2)$$

$$\begin{aligned} \rho \left[\frac{\partial w}{\partial t} + u \frac{\partial w}{\partial x} + v \frac{\partial w}{\partial y} + w \frac{\partial w}{\partial z} + g - f_2 (u \cos \Psi - v \sin \Psi) \right] \\ = \frac{\partial}{\partial x} \tau_{xz} + \frac{\partial}{\partial y} \tau_{yz} + \frac{\partial}{\partial z} \tau_{zz}, \end{aligned} \quad (B3)$$

where

u, v, w = components of velocity parallel to the x -, y -, and z -axes

z = positive upward

f = Coriolis parameter = $2 \Omega \sin \phi$

$f_2 = 2 \Omega \cos \phi$, a second Coriolis parameter

Ω = angular velocity of the earth = 7.292×10^{-5} radians per second

ϕ = latitude

Ψ = angle between the x-axis and the east direction

g = acceleration of gravity

ρ = fluid density

The components of the stress tensor are given by:

$$\begin{aligned}\tau_{xx} &= \mu \frac{\partial u}{\partial x} - p, & \tau_{yx} &= \mu \frac{\partial u}{\partial y}, & \tau_{zx} &= \mu \frac{\partial u}{\partial z}, \\ \tau_{xy} &= \mu \frac{\partial v}{\partial x}, & \tau_{yy} &= \mu \frac{\partial v}{\partial y} - p, & \tau_{zy} &= \mu \frac{\partial v}{\partial z}, \\ \tau_{xz} &= \mu \frac{\partial w}{\partial x}, & \tau_{yz} &= \mu \frac{\partial w}{\partial y}, & \tau_{zz} &= \mu \frac{\partial w}{\partial z} - p,\end{aligned}\quad (B4)$$

where μ is the coefficient of molecular viscosity, and p is the pressure. It is necessary to consider the earth's rotation in these equations because the period of rotation is of the same order of magnitude as the period of the astronomical tides. The Coriolis terms involving w are generally omitted because of the quasi-horizontal character of large-scale geophysical flows. These terms are always small relative to the acceleration of gravity, g , and are omitted in this appendix.

Treatment of the nonlinear terms in the momentum equations is simplified by adding the product of u , v , and w , and ρ times equation (B1) to equation (B2) to obtain:

$$\rho \left[\frac{\partial u}{\partial t} + \frac{\partial}{\partial x} u^2 + \frac{\partial}{\partial y} uv + \frac{\partial}{\partial z} uw - fv \right] = \frac{\partial}{\partial x} \tau_{xx} + \frac{\partial}{\partial y} \tau_{yx} + \frac{\partial}{\partial z} \tau_{zx} \quad (B5)$$

$$\rho \left[\frac{\partial v}{\partial t} + \frac{\partial}{\partial x} uv + \frac{\partial}{\partial y} v^2 + \frac{\partial}{\partial z} vw + fu \right] = \frac{\partial}{\partial x} \tau_{xy} + \frac{\partial}{\partial y} \tau_{yy} + \frac{\partial}{\partial z} \tau_{zy} \quad (B6)$$

$$\rho \left[\frac{\partial w}{\partial t} + \frac{\partial}{\partial x} uw + \frac{\partial}{\partial y} vw + \frac{\partial}{\partial z} w^2 + g \right] = \frac{\partial}{\partial x} \tau_{xz} + \frac{\partial}{\partial y} \tau_{yz} + \frac{\partial}{\partial z} \tau_{zz} \quad (B7)$$

3. Separation of Large- and Small-Scale Flows.

The unnecessary details of the small-scale flow may be eliminated from the equations by partitioning the total flow into a mean value, indicated by an overbar ($\bar{}$), and perturbations around this mean value. When the upper boundary of the flow being investigated is exposed to the wind, two types of perturbations must be recognized: (a) a generally

organized flow due to the wind-generated waves and indicated by a tilde (\sim); and (b) a generally random flow developed in response to velocity gradients produced by either the mean flow or the waves. This random perturbation is called *turbulence* and is indicated by a prime ($'$). Thus, each of the primary variables is partitioned into three components:

$$\begin{aligned} u &= \bar{u} + \tilde{u} + u' , & v &= \bar{v} + \tilde{v} + v' , \\ w &= \bar{w} + \tilde{w} + w' , & p &= \bar{p} + \tilde{p} + p' . \end{aligned} \quad (B8)$$

The mean values are defined for an elemental area or volume and time interval large enough to eliminate the variability due directly to the unwanted small-scale features caused by waves and turbulence, but not large enough to interfere with the description of the flow of primary interest.

Substitution from equation (B8) into equations (B1) and (B5) to (B7) and averaging over the same elemental space and time interval will eliminate linear terms in the perturbation quantities, but may leave products of perturbation variables. These products of perturbation quantities reveal interaction between large- and small-scale flows. The visible wave on the water surface is a result of the velocity perturbations due to waves; thus, it is necessary to carry out the vertical integration of the equations before carrying out the second averaging operation to describe the complete interaction between the waves and the mean flow. The perturbations resulting from turbulence do not have such an identifiable effect on the elevation of the water surface and the physics of the process is clearly revealed by completing the averaging process for the turbulence terms before carrying out the vertical integration. This procedure requires a certain lack of rigor because the characteristic periods of waves and turbulence overlap, and no completely rigorous means of distinguishing between the periods have been established. This lack of mathematical rigor is believed to permit a more reliable description of nature than could be obtained by neglecting the most prominent features of either waves or turbulence to obtain mathematical rigor.

When surface waves are omitted, the simple form of equations (B1) and (B5) to (B7) may be recovered by combining the products of turbulence terms with the definitions of the stresses given by equation (B4). When treated in this manner, the products of the turbulence terms are generally called "Reynolds stresses", after the British hydrodynamicist who first suggested the partitioning process. The following equations combine the Reynolds stresses with the molecular stresses, and the pressure term is expressed on the left side of the equations, as for inviscid fluids. The primitive equations (B1) and (B6) to (B8), when modified by the separation of scales of motion and prepared for vertical integration, give:

$$\frac{\partial}{\partial x}(\bar{u} + \tilde{u}) + \frac{\partial}{\partial y}(\bar{v} + \tilde{v}) + \frac{\partial}{\partial z}(\bar{w} + \tilde{w}) = 0 \quad (B9)$$

$$\begin{aligned} \frac{\partial}{\partial t}(\bar{u} + \bar{u}) + \frac{\partial}{\partial x}(\bar{u} + \bar{u})^2 + \frac{\partial}{\partial y}(\bar{v} + \bar{v})(\bar{u} + \bar{u}) + \frac{\partial}{\partial z}(\bar{w} + \bar{w})(\bar{u} + \bar{u}) \\ + \frac{1}{\rho} \frac{\partial}{\partial x}(\bar{p} + \bar{p}) - f(\bar{v} + \bar{v}) = \frac{1}{\rho} \left[\frac{\partial}{\partial x} \frac{\partial}{\partial t} \bar{u} \bar{u} + \frac{\partial}{\partial y} \frac{\partial}{\partial t} \bar{u} \bar{v} + \frac{\partial}{\partial z} \frac{\partial}{\partial t} \bar{u} \bar{w} \right] \end{aligned} \quad (B10)$$

$$\begin{aligned} \frac{\partial}{\partial t}(\bar{v} + \bar{v}) + \frac{\partial}{\partial x}(\bar{u} + \bar{u})(\bar{v} + \bar{v}) + \frac{\partial}{\partial y}(\bar{v} + \bar{v})^2 + \frac{\partial}{\partial z}(\bar{w} + \bar{w})(\bar{v} + \bar{v}) \\ + \frac{1}{\rho} \frac{\partial}{\partial y}(\bar{p} + \bar{p}) + f(\bar{u} + \bar{u}) = \frac{1}{\rho} \left[\frac{\partial}{\partial y} \frac{\partial}{\partial t} \bar{u} \bar{u} + \frac{\partial}{\partial y} \frac{\partial}{\partial t} \bar{v} \bar{v} + \frac{\partial}{\partial z} \frac{\partial}{\partial t} \bar{v} \bar{w} \right] \end{aligned} \quad (B11)$$

$$\begin{aligned} \frac{\partial}{\partial t}(\bar{w} + \bar{w}) + \frac{\partial}{\partial x}(\bar{u} + \bar{u})(\bar{w} + \bar{w}) + \frac{\partial}{\partial y}(\bar{v} + \bar{v})(\bar{w} + \bar{w}) + \frac{\partial}{\partial z}(\bar{w} + \bar{w})^2 \\ + \frac{1}{\rho} \frac{\partial}{\partial z}(\bar{p} + \bar{p}) + g = \frac{1}{\rho} \left[\frac{\partial}{\partial x} \frac{\partial}{\partial t} \bar{u} \bar{w} + \frac{\partial}{\partial y} \frac{\partial}{\partial t} \bar{v} \bar{w} + \frac{\partial}{\partial z} \frac{\partial}{\partial t} \bar{w} \bar{w} \right], \end{aligned} \quad (B12)$$

where

$$\begin{aligned} \frac{1}{\rho} \frac{\partial}{\partial x} \frac{\partial}{\partial t} \bar{u} \bar{u} &= \frac{\partial}{\partial x} \left[v \frac{\partial \bar{u}}{\partial x} - \overline{u' u'} \right], \quad \frac{1}{\rho} \frac{\partial}{\partial y} \frac{\partial}{\partial t} \bar{u} \bar{v} = \frac{\partial}{\partial y} \left[v \frac{\partial \bar{u}}{\partial y} - \overline{v' u'} \right], \\ \frac{1}{\rho} \frac{\partial}{\partial z} \frac{\partial}{\partial t} \bar{u} \bar{w} &= \frac{\partial}{\partial z} \left[v \frac{\partial \bar{u}}{\partial z} - \overline{w' u'} \right], \quad \frac{1}{\rho} \frac{\partial}{\partial x} \frac{\partial}{\partial t} \bar{v} \bar{v} = \frac{\partial}{\partial x} \left[v \frac{\partial \bar{v}}{\partial x} - \overline{u' v'} \right], \\ \frac{1}{\rho} \frac{\partial}{\partial y} \frac{\partial}{\partial t} \bar{v} \bar{v} &= \frac{\partial}{\partial y} \left[v \frac{\partial \bar{v}}{\partial y} - \overline{v' v'} \right], \quad \frac{1}{\rho} \frac{\partial}{\partial z} \frac{\partial}{\partial t} \bar{v} \bar{w} = \frac{\partial}{\partial z} \left[v \frac{\partial \bar{v}}{\partial z} - \overline{w' v'} \right], \\ \frac{1}{\rho} \frac{\partial}{\partial x} \frac{\partial}{\partial t} \bar{w} \bar{w} &= \frac{\partial}{\partial x} \left[v \frac{\partial \bar{w}}{\partial x} - \overline{u' w'} \right], \quad \frac{1}{\rho} \frac{\partial}{\partial y} \frac{\partial}{\partial t} \bar{w} \bar{w} = \frac{\partial}{\partial y} \left[v \frac{\partial \bar{w}}{\partial y} - \overline{v' w'} \right], \\ \frac{1}{\rho} \frac{\partial}{\partial z} \frac{\partial}{\partial t} \bar{w} \bar{w} &= \frac{\partial}{\partial z} \left[v \frac{\partial \bar{w}}{\partial z} - \overline{w' w'} \right], \end{aligned} \quad (B13)$$

where $v = \mu/\rho$ and is assumed to be constant.

Each term in equations (B9) to (B12) must be integrated from the bottom of the fluid layer, $z = Z(x, y, t)$, to the top of the layer, $z = h(x, y, t)$. In a well-mixed estuary, the bottom of the fluid layer is the seabed and the top is the free surface. In a stratified estuary, at least two fluid layers must be considered, and the bottom of one layer is the top of the next. Although this analysis is completed only for a single fluid layer, the general form is used here because it provides symmetry to the development without adding any complications.

If no fluid passes through the lower and upper boundaries of the fluid, the boundary conditions for the vertical integration are given by:

$$w_z = \frac{\partial Z}{\partial t} + u_z \frac{\partial Z}{\partial x} + v_z \frac{\partial Z}{\partial y}, \quad (B14)$$

and

$$w_h = \frac{\partial h}{\partial t} + u_h \frac{\partial h}{\partial x} + v_h \frac{\partial h}{\partial y}, \quad (\text{B15})$$

where the subscript Z or h indicates that the variable is evaluated at $z = Z$ or h . An overbar is used when needed to show that an average value of h is implied. Z is assumed constant with respect to the averaging process and no fluid passes through the upper or lower boundaries.

When any variable, ψ , is expressed in the form $\psi = \bar{\psi} + \tilde{\psi}$, the average of the vertical integral may be expressed as:

$$\overline{\int_{z_1}^h \psi dz} = \int_{z_1}^{\bar{h}} \bar{\psi} dz + \int_{\bar{h}}^h \bar{\psi} dz + \int_{z_1}^{\bar{h}} \tilde{\psi} dz, \quad (\text{B16})$$

where $z_1 \leq \bar{h}$. The averaging operator may be taken inside the first integral on the right in equation (B16) because the limit of integration is constant with respect to the averaging operation. This is not correct for the second and third integrals where the upper limit has not been submitted to the averaging operation. The second overbar in the first integral may be omitted because $\bar{\psi}$ is a constant with respect to the averaging operation. Generally, the second overbar is not used.

The Leibnitz rule for differentiation of an integral is essential to the formal integration of equations (B9) to (B12), and may be stated as:

$$\int_Z^h \left(\frac{\partial \psi}{\partial s} \right) dz = \frac{\partial}{\partial s} \int_Z^h \psi dz - \psi(h) \frac{\partial h}{\partial s} + \psi(Z) \frac{\partial Z}{\partial s}. \quad (\text{B17})$$

Application of equations (B14) to (B17) to the continuity equation (B9) yields:

$$\begin{aligned} \frac{\partial}{\partial t}(\bar{h} - Z) + \frac{\partial}{\partial x} \bar{U} + \frac{\partial}{\partial y} \bar{V} + \int_Z^h \left[\frac{\partial \tilde{u}}{\partial x} + \frac{\partial \tilde{v}}{\partial y} + \frac{\partial \tilde{w}}{\partial z} \right] dz \\ + \int_{\bar{h}}^h \left[\frac{\partial \bar{u}}{\partial x} + \frac{\partial \bar{v}}{\partial y} + \frac{\partial \bar{w}}{\partial z} \right] dz = 0, \end{aligned} \quad (\text{B18})$$

where

$$\bar{U} = \int_Z^{\bar{h}} \bar{u} dz, \quad \bar{V} = \int_Z^{\bar{h}} \bar{v} dz. \quad (\text{B19})$$

U and V are vertically averaged fluid transports parallel to the x- and y-axes.

The first integral in equation (B18) may be expanded to form:

$$\overline{\int_{\bar{z}}^{\bar{h}} \left[\frac{\partial \tilde{u}}{\partial x} + \frac{\partial \tilde{v}}{\partial y} + \frac{\partial \tilde{w}}{\partial z} \right] dz} + \overline{\int_{\bar{h}}^h \left[\frac{\partial \tilde{u}}{\partial x} + \frac{\partial \tilde{v}}{\partial y} + \frac{\partial \tilde{w}}{\partial z} \right] dz}. \quad (\text{B20})$$

The average value of the first integral in equation (B20) vanishes because the upper limit is a constant with respect to the averaging process and each term in the integral is linear in a perturbation quantity. The second integral in equation (B20) may be evaluated by the Leibnitz rule, equation (B17), to obtain:

$$\frac{\partial}{\partial t}(\bar{h} - \bar{h}) + \frac{\partial}{\partial x} \overline{\int_{\bar{h}}^h \tilde{u} dz} + \frac{\partial}{\partial y} \overline{\int_{\bar{h}}^h \tilde{v} dz}. \quad (\text{B21})$$

The first term in equation (B21) vanishes because it is the mean value of a linear perturbational quantity. The second and third integrals may be evaluated by expansion as a Taylor series about $z = \bar{h}$. Thus, these integrals take the form:

$$\begin{aligned} & \frac{\partial}{\partial x} \left[\overline{\tilde{u}_{\bar{h}} \bar{h}} + \frac{1}{2}(\bar{h})^2 \frac{\partial \tilde{u}_{\bar{h}}}{\partial z} + \frac{1}{3!}(\bar{h})^3 \frac{\partial^2 \tilde{u}_{\bar{h}}}{\partial z^2} + \dots \right] \\ & + \frac{\partial}{\partial y} \left[\overline{\tilde{v}_{\bar{h}} \bar{h}} + \frac{1}{2}(\bar{h})^2 \frac{\partial \tilde{v}_{\bar{h}}}{\partial z} + \frac{1}{3!}(\bar{h})^3 \frac{\partial^2 \tilde{v}_{\bar{h}}}{\partial z^2} + \dots \right], \end{aligned}$$

where the subscript \bar{h} indicates that the variables are evaluated at $z = \bar{h}$. Note that $\tilde{h} = h - \bar{h}$, $\tilde{u}_{\bar{h}}$, $\tilde{v}_{\bar{h}}$, and their derivatives are also perturbation quantities, and the mean value of terms of odd order tends to vanish. The first terms are generally much larger than the third. Thus, with good approximation, equation (B21) is given by:

$$\frac{\partial}{\partial x} \overline{\tilde{u}_{\bar{h}} \bar{h}} + \frac{\partial}{\partial y} \overline{\tilde{v}_{\bar{h}} \bar{h}}. \quad (\text{B22})$$

The second integral in equation (B20) has a nonzero value, even though the integrand has the form of a continuity equation which is expected to vanish everywhere within the fluid, because the limit of integration in variable z is highly correlated with the integrand.

The third integral in equation (B18) may be integrated by expanding each term as a Taylor series about $z = \bar{h}$, where $h - \bar{h} = \tilde{h}$. The average value of the resulting integral is:

$$\frac{1}{2} \left[\frac{\partial}{\partial x} \overline{\tilde{h}^2} \frac{\partial \tilde{u}(\bar{h})}{\partial z} + \frac{\partial}{\partial y} \overline{\tilde{h}^2} \frac{\partial \tilde{v}(\bar{h})}{\partial z} + \overline{\tilde{h}^2} \frac{\partial^2 \tilde{w}(\bar{h})}{\partial z^2} \right] + \text{smaller terms.}$$

All terms in the above expression are negligibly small under most conditions and are not considered further.

Equation (B18) has been derived on the assumption that no fluid enters or leaves the system through horizontal boundaries. If fluid is added at the surface through precipitation or condensation or removed through evaporation, or if there is seepage through the bottom, the net effects of these changes must be accounted for through a source-sink term. This is indicated by R , on the assumption that the maximum values of the source-sink term will result from rainfall. Thus, the continuity equation may be expressed as:

$$\frac{\partial}{\partial t}(\bar{h} - Z) + \frac{\partial}{\partial x}U + \frac{\partial}{\partial y}V = R + E, \quad (B23)$$

where

$$E = - \left[\frac{\partial}{\partial x} \overline{\tilde{u}_h \tilde{h}} + \frac{\partial}{\partial y} \overline{\tilde{v}_h \tilde{h}} \right]. \quad (B24)$$

E can be rewritten as:

$$E = - \frac{\partial}{\partial s} \overline{\tilde{q}_h \tilde{h}}, \quad (B25)$$

where s is distance along a wave ray in the direction of wave travel and \tilde{q}_h is the velocity in the direction of wave travel at $z = \bar{h}$, due to the wave. It results from the correlation between the displacement of free surface and the horizontal fluid velocity associated with the wave. This transport contributes significantly to the horizontal divergence only in regions where the wave amplitude changes rapidly in the direction of wave propagation, such as the shoaling and surf zones, or in regions, such as inlets, where the waves are modulated by the convergence or divergence of the mean flow.

Formal integration of the equations for the conservation of horizontal momentum from the bottom to the top of a fluid layer may be accomplished through application of equation (B14) to (B17) to obtain:

$$\begin{aligned} \frac{\partial U}{\partial t} + \frac{\partial}{\partial x} \overline{\frac{U^2}{D}} + \frac{\partial}{\partial y} \overline{\frac{UV}{D}} - fV + \frac{\partial}{\partial x} \int_Z^{\bar{h}} \overline{(u'')^2} dz \\ + \frac{\partial}{\partial y} \int_Z^{\bar{h}} \overline{v''u''} dz + \int_Z^{\bar{h}} \left(\frac{1}{\rho} \right) \frac{\partial}{\partial x} \overline{p} dz + \frac{\partial}{\partial t} \int_Z^{\bar{h}} \overline{\tilde{u}} dz \end{aligned}$$

$$\begin{aligned}
& + \frac{\partial}{\partial x} \int_Z^{\bar{h}} (\tilde{u})^2 dz + \frac{\partial}{\partial y} \int_Z^{\bar{h}} \tilde{u}\tilde{v} dz + \int_Z^{\bar{h}} \left(\frac{1}{\rho}\right) \frac{\partial \tilde{p}}{\partial x} dz - f \int_Z^{\bar{h}} \tilde{v} dz \\
& + \frac{\partial}{\partial t} \int_{\bar{h}}^{\bar{h}} \bar{u} dz + \frac{\partial}{\partial x} \int_{\bar{h}}^{\bar{h}} \bar{u}^2 dz + \frac{\partial}{\partial y} \int_{\bar{h}}^{\bar{h}} \bar{u}\bar{v} dz - f \int_{\bar{h}}^{\bar{h}} \bar{v} dz \\
& + \int_{\bar{h}}^{\bar{h}} \frac{1}{\rho} \frac{\partial p}{\partial x} dz = \int_Z^{\bar{h}} \left(\frac{1}{\rho}\right) \left[\frac{\partial}{\partial x} \frac{\partial}{\partial t} xx + \frac{\partial}{\partial y} \frac{\partial}{\partial t} yx + \frac{\partial}{\partial z} \frac{\partial}{\partial t} zx \right] dz ; \tag{B26}
\end{aligned}$$

$$\begin{aligned}
& \frac{\partial V}{\partial t} + \frac{\partial}{\partial x} UV + \frac{\partial}{\partial y} V^2 + fU + \frac{\partial}{\partial x} \int_Z^{\bar{h}} u''v'' dz \\
& + \frac{\partial}{\partial y} \int_Z^{\bar{h}} (v'')^2 dz + \int_Z^{\bar{h}} \left(\frac{1}{\rho}\right) \frac{\partial p}{\partial y} dz + \frac{\partial}{\partial t} \int_Z^{\bar{h}} \tilde{v} dz \\
& + \frac{\partial}{\partial x} \int_Z^{\bar{h}} \tilde{u}\tilde{v} dz + \frac{\partial}{\partial y} \int_Z^{\bar{h}} (\tilde{v})^2 dz + \int_Z^{\bar{h}} \left(\frac{1}{\rho}\right) \frac{\partial \tilde{p}}{\partial y} + f \int_Z^{\bar{h}} \tilde{u} dz \\
& + \frac{\partial}{\partial t} \int_{\bar{h}}^{\bar{h}} \bar{v} dz + \frac{\partial}{\partial x} \int_{\bar{h}}^{\bar{h}} \bar{u}\bar{v} dz + \frac{\partial}{\partial y} \int_{\bar{h}}^{\bar{h}} \bar{v}^2 dz + f \int_{\bar{h}}^{\bar{h}} \bar{u} dz \\
& + \int_{\bar{h}}^{\bar{h}} \left(\frac{1}{\rho}\right) \frac{\partial p}{\partial y} dz = \int_Z^{\bar{h}} \left(\frac{1}{\rho}\right) \left[\frac{\partial}{\partial x} \frac{\partial}{\partial t} xy + \frac{\partial}{\partial y} \frac{\partial}{\partial t} yy + \frac{\partial}{\partial z} \frac{\partial}{\partial t} zy \right] dz , \tag{B27}
\end{aligned}$$

where

$$\begin{aligned}
u'' &= \bar{u} - \frac{U}{D} , \\
v'' &= \bar{v} - \frac{V}{D} , \\
D &= \bar{h} - Z = \text{total depth.} \tag{B28}
\end{aligned}$$

Evaluation of equations (B26) and (B27) requires the vertical integral of the products $(1/\rho) \partial \bar{p}/\partial x$ and $(1/\rho) \partial \bar{p}/\partial y$, where ρ may be a function of z and, as yet, p is undefined. An expression of $\bar{p}(z)$ may be obtained by integrating the equation for the conservation of vertical momentum from an arbitrary value of z to the top of the layer. The possible variation of density with z may be accounted for approximately by means of the identity,

$$\frac{1}{\rho} = \left(\frac{1}{\bar{\rho}}\right) \left(1 - \frac{\rho''}{\bar{\rho}} + \left(\frac{\rho'''}{\bar{\rho}}\right)^2 - \dots\right), \quad (\text{B29})$$

where

$$\bar{\rho} = \frac{1}{D} \int_z^h \rho \, dz,$$

and

$$\rho'' = \rho - \bar{\rho}.$$

Since a well-mixed fluid layer is assumed, it is permissible to neglect $(\rho'')^2/\bar{\rho}^3$, and $\rho''/\bar{\rho}^2$ may be neglected in a first approximation. Since the error term is retained, a later correction can possibly be estimated if needed.

In developing an expression for the mean pressure through integration of the equation for vertical momentum, it is permissible to neglect all expressions involving the mean vertical velocity because of the quasi-horizontal nature of the mean flow. By combining equation (B29) with equations (B14) to (B17) and neglecting the mean vertical velocity, equation (B12) may be integrated to obtain:

$$\begin{aligned} & \frac{\partial}{\partial t} \int_z^h \bar{w} \, dz + \frac{\partial}{\partial x} \int_z^h \bar{u}\bar{w} \, dz + \frac{\partial}{\partial y} \int_z^h \bar{v}\bar{w} \, dz - \overline{(\bar{w})^2}_z + \left(\frac{1}{\bar{\rho}}\right) (\bar{p}_h - p) \\ & + g(\bar{h} - z) = \int_z^h \left(\frac{1}{\bar{\rho}}\right) \left[\frac{\partial}{\partial x} \frac{\rho}{\bar{\rho}} xz + \frac{\partial}{\partial y} \frac{\rho}{\bar{\rho}} yz + \frac{\partial}{\partial z} \frac{\rho}{\bar{\rho}} z^2 \right] dz \\ & - \int_z^h \frac{\rho''}{\bar{\rho}^2} \frac{\partial}{\partial z} p \, dz; \quad z \leq \bar{h}. \end{aligned} \quad (\text{B30})$$

By rearranging terms in equation (B30) and applying the averaging operator, the desired expression for the mean pressure may be obtained in the form:

$$\left(\frac{1}{\bar{\rho}}\right) \bar{p} = g(\bar{h}-z) + \left(\frac{1}{\bar{\rho}}\right) p_h - \overline{(\tilde{w})^2} + E_z, \quad (\text{B31})$$

where

$$E_z = \frac{\partial}{\partial t} \int_z^{\bar{h}} \tilde{w} dz + \frac{\partial}{\partial x} \int_z^{\bar{h}} \tilde{u}\tilde{w} dz + \frac{\partial}{\partial y} \int_z^{\bar{h}} \tilde{v}\tilde{w} dz + \int_z^{\bar{h}} \left(\frac{\rho''}{\bar{\rho}^2}\right) \frac{\partial \bar{p}}{\partial z} dz + \int_z^{\bar{h}} \left[\frac{\partial}{\partial x} \tau_{xz} + \frac{\partial}{\partial y} \tau_{yz} + \frac{\partial}{\partial z} \tau_{zz} \right] dz. \quad (\text{B32})$$

The first term on the right in equation (B31) is the familiar hydrostatic equation due to the weight of the water above z ; the second term is the atmospheric pressure. The third term is a negative dynamic term due to the vertical velocity at height, z , resulting from wave motion, and the fourth term, E_z , represents closure terms which can be neglected almost everywhere.

It is sufficient to consider the first integral in equation (B32) only for the interval, \bar{h} to h , because it is a linear perturbation term and the average value within fixed limits of integration vanishes. The development of equation (B25) shows that the integral can be obtained from the first terms in a Taylor series expansion in the form $\overline{\tilde{h}\tilde{w}}$. This term vanishes almost everywhere because of the usual 90° phase shift between the vertical displacement of the free surface and the vertical velocity due to gravity waves. The mean values of the second and third integrals vanish almost everywhere because of the usual 90° phase shift between the horizontal and vertical velocity components due to gravity waves. The fourth integral is always small because of the assumption of a well-mixed fluid layer.

In considering the final integral, a substitution for the stress terms from equation (B13) will be necessary. When the mean component of the vertical velocity is neglected, the required expression has the form:

$$\int_z^{\bar{h}} \left(\frac{\partial}{\partial x} \overline{u'w'} + \frac{\partial}{\partial y} \overline{v'w'} \right) dz + \overline{(w')^2}_h - \overline{(w')^2}_z. \quad (\text{B33})$$

The integrand in equation (B33) represents the gradient of the turbulent Reynolds stress terms involving vertical velocity and the

horizontal velocity in the direction of flow. These Reynolds stresses are generated by the vertical shear in the horizontal mean flow. Significant values of this gradient can occur only with large values of the curvature in the mean flow, such as at sharp bends in a channel. The term, $\overline{(w')^2}_h$, represents the effect of that part of the roughness of the free surface that is generated by turbulence in the water. Significant values rarely occur. The final term is the vertical component of the turbulent velocity at the seabed, and can also be neglected almost everywhere. Since the pressure enters equations (B26) and (B27) only in the form of horizontal gradients, and all terms in equation (B32) have been shown to be small, equation (B31) is taken as an adequate expression for p in the further consideration of equations (B26) and (B27). Substitution of the vertically averaged density $\bar{\rho}$ for ρ in equations (B26) and (B27) permits the application of equation (B16) to be vertical integration of the pressure gradient terms. Thus,

$$\overline{\int_Z^h \left(\frac{1}{\rho}\right) \frac{\partial p}{\partial x} dz} \approx \left(\frac{1}{\bar{\rho}}\right) \frac{\partial}{\partial x} \overline{\int_Z^h p dz} + p_Z \frac{\partial Z}{\partial x} - p_h \frac{\partial h}{\partial x}, \quad (B34)$$

$$\overline{\int_Z^h \left(\frac{1}{\rho}\right) \frac{\partial p}{\partial y} dz} \approx \left(\frac{1}{\bar{\rho}}\right) \frac{\partial}{\partial y} \overline{\int_Z^h p dz} + p_Z \frac{\partial Z}{\partial y} - p_h \frac{\partial h}{\partial y}. \quad (B35)$$

The vertical integral of the pressure may be computed from equation (B31) as:

$$\begin{aligned} \left(\frac{1}{\bar{\rho}}\right) \overline{\int_Z^h p dz} &= \left(\frac{1}{2}\right) g [\overline{D^2} + \overline{h^2}] + \left(\frac{1}{\bar{\rho}}\right) \overline{p_h D} - \int_Z^h \overline{w^2} dz \\ &= \left(\frac{1}{2}\right) g D^2 + \left(\frac{1}{2}\right) \overline{gh^2} + \left(\frac{1}{\bar{\rho}}\right) \overline{p_h D} - \int_Z^{\bar{h}} \overline{w^2} dz, \end{aligned} \quad (B36)$$

where terms which vanish in the mean have been eliminated. Terms in the perturbation of the atmospheric pressure, p' , due to the weight of the air column between the wave trough and the wave crest, are not given, because the ratio of air and water densities is so low as to make the perturbation of the atmospheric pressure at the water surface trivial.

By combining equation (B36) with equations (B34) and (B35), the mean vertically integrated pressure gradient terms are obtained in the form:

$$\overline{\int_Z^h \left(\frac{1}{\rho} \right) \frac{\partial p}{\partial x} dz} \approx gD \frac{\partial \bar{h}}{\partial x} + \left(\frac{1}{\bar{\rho}} \right) D \frac{\partial \bar{p}_h}{\partial x} + \left(\frac{1}{2} \right) g \frac{\partial \overline{h^2}}{\partial x} - \frac{\partial}{\partial x} \int_Z^h \overline{w^2} dz - \overline{w^2} D \frac{\partial Z}{\partial y}, \quad (\text{B37})$$

$$\overline{\int_Z^h \left(\frac{1}{\rho} \right) \frac{\partial p}{\partial y} dz} \approx gD \frac{\partial \bar{h}}{\partial y} + \left(\frac{1}{\bar{\rho}} \right) D \frac{\partial \bar{p}_h}{\partial y} + \left(\frac{1}{2} \right) g \frac{\partial \overline{h^2}}{\partial y} - \frac{\partial}{\partial y} \int_Z^h \overline{w^2} dz - \overline{w^2} \frac{\partial Z}{\partial y}. \quad (\text{B38})$$

In equations (B26) and (B27), the linear perturbation terms contribute to the vertical integral only from the region \bar{h} to h , and the quadratic terms contribute only from the region Z to \bar{h} as in the derivation of equation (B25). All integrals from \bar{h} to h may be carried out through Taylor series expansions as with equation (B25). By considering these principles and using equations (B37) and (B38), the horizontal transport equations may be expressed as:

$$\frac{\partial U}{\partial t} + \frac{\partial}{\partial x} \frac{U^2}{D} + \frac{\partial}{\partial y} \frac{UV}{D} - fV + gD \frac{\partial \bar{h}}{\partial x} + \left(\frac{1}{\bar{\rho}} \right) D \frac{\partial \bar{p}_h}{\partial x} = \left(\frac{1}{\bar{\rho}} \right) \left[\left(\overline{\tau_{zx}} \right)_h - \left(\overline{\tau_{zx}} \right)_Z \right] + S_{xt} - S_{xw} - S_{xo} - S_{xv}, \quad (\text{B39})$$

$$\frac{\partial V}{\partial y} + \frac{\partial}{\partial x} \frac{UV}{D} + \frac{\partial}{\partial y} \frac{V^2}{D} + fU + gD \frac{\partial \bar{h}}{\partial y} + \left(\frac{1}{\bar{\rho}} \right) D \frac{\partial \bar{p}_h}{\partial y} = \left(\frac{1}{\bar{\rho}} \right) \left[\left(\overline{\tau_{zy}} \right)_h - \left(\overline{\tau_{zy}} \right)_D \right] + S_{yt} - S_{yw} - S_{yo} - S_{yv}, \quad (\text{B40})$$

where $\left(\overline{\tau_{zx}} \right)_h$ and $\left(\overline{\tau_{zy}} \right)_h$ are the mean horizontal stresses parallel to the x- and y-axes in the upper boundary of the fluid, $\left(\overline{\tau_{zx}} \right)_h$ and $\left(\overline{\tau_{zy}} \right)_h$ are normally taken as the wind stress on the water and are evaluated as functions of the wind velocity, and $\left(\overline{\tau_{zx}} \right)_Z$ and $\left(\overline{\tau_{zy}} \right)_Z$ are the mean horizontal stresses parallel to the x- and y-axes at the bottom of the

fluid layer. These stresses are normally taken as the friction between the water and the seabed, and are usually evaluated as functions of the mean flow velocity.

S_{xt} and S_{yt} are the molecular and turbulent stresses experienced by the interior of the fluid layer, where

$$S_{xt} = \int_z^{\bar{h}} \left[\left(\frac{1}{\rho} \right) \frac{\partial}{\partial x} \mu \frac{\partial \bar{u}}{\partial x} - \frac{\partial}{\partial x} \overline{(u')^2} + \left(\frac{1}{\rho} \right) \frac{\partial}{\partial y} \mu \frac{\partial \bar{u}}{\partial y} - \frac{\partial}{\partial y} \overline{u'v'} \right] dz, \quad (B41)$$

$$S_{yt} = \int_z^{\bar{h}} \left[\left(\frac{1}{\rho} \right) \frac{\partial}{\partial x} \mu \frac{\partial \bar{v}}{\partial x} - \frac{\partial}{\partial x} \overline{u'v'} + \left(\frac{1}{\rho} \right) \frac{\partial}{\partial y} \mu \frac{\partial \bar{v}}{\partial y} - \frac{\partial}{\partial y} \overline{(v')^2} \right] dz. \quad (B42)$$

The molecular stresses may dominate in equations (B41) and (B42) within a few millimeters of a solid surface. The turbulent stresses are dominant in the interior of the fluid, and act to smooth the flow in a horizontal plane in the above equations. Velocity shears due either to the mean flow or waves contribute to the development of turbulence.

S_{xx} and S_{yy} , given by:

$$S_{xx} = \frac{\partial}{\partial x} \int_z^{\bar{h}} \overline{(u')^2} - \overline{(w')^2} dz + \left(\frac{1}{2} \right) g \frac{\partial}{\partial x} \overline{(\bar{h})^2} + \frac{\partial}{\partial y} \int_z^{\bar{h}} \bar{u} \bar{v} dz, \quad (B43)$$

$$S_{yy} = \frac{\partial}{\partial y} \int_z^{\bar{h}} \overline{(v')^2} - \overline{(w')^2} dz + \left(\frac{1}{2} \right) g \frac{\partial}{\partial y} \overline{(\bar{h})^2} + \frac{\partial}{\partial x} \int_z^{\bar{h}} \bar{u} \bar{v} dz, \quad (B44)$$

have been called radiation stresses by Longuet-Higgins and Stewart (1962, 1963, 1964), and are due entirely to the Reynolds stresses generated by gravity waves.

The terms,

$$\begin{aligned} S_{xx} = & \frac{\partial}{\partial t} \left[\overline{\bar{h}u} + \overline{\bar{h}^2 \frac{\partial \bar{u}}{\partial z}} \right] + \frac{\partial}{\partial z} \left[\frac{\partial}{\partial x} \overline{\bar{h}^2 u^2} + \frac{\partial}{\partial y} \overline{\bar{h}^2 v u} \right] - f \left[\overline{\bar{h}v} + \overline{\bar{h}^2 \frac{\partial \bar{v}}{\partial z}} \right] \\ & + \overline{\bar{w}^2 \frac{\partial \bar{z}}{\partial x}} + \left(\frac{1}{\rho} \right) \left[\overline{\bar{h} \frac{\partial p}{\partial x}} + \overline{(\bar{h})^2 \frac{\partial}{\partial z} \frac{\partial \bar{p}}{\partial x}} \right] + \frac{\partial}{\partial x} \overline{\bar{h}^2} (\bar{u} + u'') \frac{\partial u''}{\partial z} \\ & + \frac{\partial}{\partial y} \overline{\bar{h}^2} \left[(\bar{u} + u'') \frac{\partial v''}{\partial z} + (\bar{v} + v'') \frac{\partial u''}{\partial z} \right], \end{aligned} \quad (B45)$$

$$\begin{aligned}
S_{yo} = & \frac{\partial}{\partial t} \left[\overline{\tilde{h}\tilde{v}} + \overline{\tilde{h}^2 \frac{\partial \tilde{v}}{\partial z}} \right] + \frac{\partial}{\partial z} \left[\frac{\partial}{\partial y} \overline{\tilde{h}^2 \tilde{v}\tilde{u}} + \frac{\partial}{\partial y} \overline{\tilde{h}^2 \tilde{v}^2} \right] \\
& + f \left[\overline{\tilde{h}\tilde{u}} + \overline{\tilde{h}^2 \frac{\partial \tilde{u}}{\partial z}} \right] + \overline{\tilde{w}_z^2} \frac{\partial \tilde{z}}{\partial y} + \left(\frac{1}{\rho} \right) \left[\overline{\tilde{h} \frac{\partial \tilde{p}}{\partial y}} + \overline{\tilde{h}^2 \frac{\partial}{\partial z} \frac{\partial p_h}{\partial y}} \right] \\
& + \frac{\partial}{\partial x} \overline{\tilde{h}^2} \left[(\tilde{u} + u'') \frac{\partial v''}{\partial z} + (\tilde{v} + v'') \frac{\partial u''}{\partial z} \right] + \frac{\partial}{\partial y} \overline{\tilde{h}^2} (\tilde{v} + v'') \frac{\partial v''}{\partial z} , \quad (B46)
\end{aligned}$$

are additional stresses resulting from waves that have not been studied in detail. Each of these stress terms is proportional to the wave amplitude squared. In general, a decrease in the wave amplitude with time or in the direction of wave propagation causes an increase in the momentum in the direction of wave propagation. These groups of perturbation terms are generally smaller than the radiation stresses, and can generally be neglected relative to the uncertainties in the radiation and turbulence stresses. However, unrecognized existence of these terms could lead to poor reproduction of radiation stresses in experimental studies. The final term in each equation can be neglected because of the small pressure difference in the atmosphere between wave crest and trough, and because of the 90° phase shift between the displacement of the free surface and the horizontal gradient of the wave-induced pressure.

S_{xv} and S_{yv} are given by:

$$S_{xv} = \frac{\partial}{\partial x} \int_z^{\tilde{h}} (u'')^2 dz + \frac{\partial}{\partial y} \int_z^{\tilde{h}} u''v'' dz , \quad (B47)$$

$$S_{yv} = \frac{\partial}{\partial x} \int_z^{\tilde{h}} u''v'' dz + \frac{\partial}{\partial y} \int_z^{\tilde{h}} (v'')^2 dz . \quad (B48)$$

These terms arise because the advective terms given by equations (B39) and (B40) represent only the contribution from the vertically averaged velocity. In reality, the horizontal velocity is a function of z . The current speed generally increases with distance from the bottom. The integrals of $(u'')^2$ and $(v'')^2$ act as stresses, similar to the wind, turbulence, and radiation stresses previously discussed. Since only the gradients of these stresses affect the momentum balance, these terms can play a significant role, only when the gradients are large. In general, these terms will become large only when the flow is constrained; e.g., when the current passes through a channel connecting two bodies of water. A tidal inlet is such a channel, and these terms make a significant contribution to the momentum balance at the entrance or exit of a tidal inlet, especially when the depth of the inlet is less than that of the ocean or the bay near the inlet. No measured data which could be used to determine the importance of this term are known.

AD-A052 795

COASTAL ENGINEERING RESEARCH CENTER FORT BELVOIR VA
COMPARISON OF NUMERICAL AND PHYSICAL HYDRAULIC MODELS, MASONBOR--ETC(U)
JUN 77 D L HARRIS, B R BODINE
CERC-6ITI-6

F/G 8/8

UNCLASSIFIED

NL

3 of 3

AD
A052795



END
DATE
FILMED

5-78

DOC

APPENDIX C

A DERIVATION OF THE ONE-DIMENSIONAL OR CHANNEL EQUATIONS

Equations governing the flow of quasi-steady currents or long waves in a channel may be formed by choosing the x-axis to parallel as closely as possible to the axis of the channel, and to integrate each term in the long wave equations (1) and (3), with respect to y to obtain equations governing the flow in a channel of variable cross section. Each term in the integrated equation must be a function of x and t only. Therefore, each term is integrated or averaged over the cross section for specific values of x and t . Closure terms, generally neglected when fundamental equations are built up from the minimum number of terms, are defined. The closure terms are negligible in many practical problems. Equations (1) and (B39) may be arranged and expressed as an integral in the form:

$$\begin{aligned} \int_{y_1}^{y_2} \left[\frac{\partial U}{\partial t} + \frac{\partial}{\partial x} \frac{\partial U^2}{\partial y} + \frac{\partial}{\partial y} \frac{UV}{D} \right] dy + g \int_{y_1}^{y_2} D \frac{\partial \bar{h}}{\partial x} dy \\ + \left(\frac{1}{\rho} \right) \int_{y_1}^{y_2} (\tau_{zx})_Z dy = f \int_{y_1}^{y_2} V dy \\ + \int_{y_1}^{y_2} \left[\frac{1}{\rho} (\tau_{zx})_{\bar{h}} - \left(\frac{1}{\rho} \right) D \frac{\partial p_{\bar{h}}}{\partial x} \right] dy \\ + \int_{y_1}^{y_2} [S_{xt} - S_{xw} - S_{xo} - S_{xv}] dy . \quad (C1) \end{aligned}$$

The Leibnitz rule for the differentiation of an integral (eq. B17) can be used to integrate the first integral in equation (C1) in the form:

$$\begin{aligned} \int_{y_1}^{y_2} \left[\frac{\partial U}{\partial t} + \frac{\partial}{\partial x} \frac{U^2}{D} + \frac{\partial}{\partial y} \frac{UV}{D} \right] dy = \frac{\partial}{\partial t} A_C \bar{u} + \frac{\partial}{\partial x} A_C \bar{u}^2 \\ + \frac{\partial}{\partial x} \int_{y_1}^{y_2} [\bar{D} u''^2 + 2\bar{u} D''' U'' + D''' (U'')^2] dy , \quad (C2) \end{aligned}$$

where

$$A_c(x,t) = \int_{y_1}^{y_2} D \, dy$$

is the cross-sectional area of the inlet at position x along the channel at time, t .

$$\bar{\bar{u}}(x,t) = A_c^{-1} \int_{y_1}^{y_2} U \, dy = A_c^{-1} \int_{y_1}^{y_2} \int_D^{\bar{h}} u \, dz \, dy ,$$

$$u''(x,y,z,t) = u(x,y,z,t) - \bar{\bar{u}}(x,t) .$$

A double overbar ($\bar{\bar{}}$) is used here to indicate a cross-sectional average. Double primes ($''$) are used to indicate deviations from the cross-sectional average of functions which vary with depth, or deviation from the cross-channel mean of functions independent of z . Closure terms are retained in compact form as, the goal of this development is to show a generalized, but relatively simple extension of the lumped parameter inlet model of Keulegan (1967).

The second integral in equation (C1) may be expressed as:

$$\int_{y_1}^{y_2} D \frac{\partial \bar{h}}{\partial x} \, dy = A_c \frac{\partial \bar{\bar{h}}}{\partial x} + \bar{\bar{D}} h''(y_1) \frac{\partial y_1}{\partial x} - h''(y_2) \frac{\partial y_2}{\partial x} + \int_{y_1}^{y_2} D'' \frac{\partial \bar{h}''}{\partial x} \, dy , \quad (C3)$$

where

$$\bar{\bar{h}} = b^{-1} \int_{y_1}^{y_2} \bar{h} \, dy, \quad \bar{\bar{D}} = \frac{A_c}{b} ,$$

$$\bar{h}'' = \bar{h} - \bar{\bar{h}} , \quad D'' = D - \bar{\bar{D}} ,$$

$$b = b(x) = y_2(x) - y_1(x) ,$$

and $y_1(x)$ and $y_2(x)$ are the sides of the channel.

The third integral in equation (C1) may be expressed as:

$$\left(\frac{1}{\bar{\rho}}\right) \int_{y_1}^{y_2} (\tau_{zx})_Z dy = b \left(\frac{1}{\bar{\rho}}\right) (\overline{\tau_{zx}})_Z, \quad (C4)$$

where

$$(\overline{\tau_{zx}})_Z = b^{-1} \int_{y_1}^{y_2} (\tau_{zx})_Z dy$$

is the average value of the bottom and internal stress for an assigned value of x and t .

The first integral on the right in equation (C1) may be expressed as:

$$f \int_{y_1}^{y_2} V dy = f A_c \bar{V}, \quad \bar{V} = A_c^{-1} \int_{y_1}^{y_2} V dy, \quad (C5)$$

where \bar{V} is the average cross-sectional value of the flow normal to the channel axis. This will vanish if the cross-channel flow is symmetric with respect to the centerline of the channel.

The second integral on the right expresses the contribution of the atmosphere to the momentum of the water. The variation of these forces across a typical inlet for the time periods of importance in tidal problems is so small that the point values may be treated as means, and the integral may be expressed as:

$$\int_{y_1}^{y_2} \frac{1}{\bar{\rho}} (\tau_{zx})_{\bar{h}} - \left(\frac{1}{\bar{\rho}}\right) D \frac{\partial p_h}{\partial x} dy = \left(\frac{1}{\bar{\rho}}\right) b (\tau_{zx})_{\bar{h}} - \frac{A_c}{\bar{\rho}} \frac{\partial p_h}{\partial x}. \quad (C6)$$

The first term on the right in equation (C6) expresses the wind stress. Although wind stress cannot be predicted long in advance and is usually neglected, it can be significant. The second term, the atmospheric pressure gradient, is nearly always negligibly small.

The third term on the right in equation (C1) is the cross-channel integral of the closure terms of the two-dimensional equations (see Sec. II and App. B).

When \bar{V} and the perturbation terms are neglected, and the relation between bottom stress and velocity is considered, the only remaining terms of potential significance in equation (2) and (B40) are

$$g D \frac{\partial \bar{h}}{\partial y} = \left(\frac{1}{\bar{\rho}}\right) (\tau_{zy})_{\bar{h}} - fU + S_{yt} - S_{yx} - S_{y0} - S_{yv}. \quad (C7)$$

Division by gD yields:

$$\frac{\partial \bar{h}}{\partial y} = \frac{(1/\bar{\rho})(\tau_{zy})\bar{h} - fU}{gD} + \frac{S_{yt} - S_{yx} - S_{y0} - S_{yv}}{gD} \quad (C8)$$

Equation (C8) expresses the cross-channel slope as a function of the cross-channel wind stress, the rotation of the earth, the water depth, and the closure terms. The equation is rarely used in investigations of channel flow where cross-sectional averages are considered. However, it may be useful in estimating the probable error in using point measurements of water surface elevations as estimates of the cross-channel mean surface elevation.

The continuity equation for channel flow, obtained by cross-channel integration of equations (3) and (B23), takes the form:

$$\frac{\partial A}{\partial t} + \frac{\partial A_c \bar{u}}{\partial x} = \int_{y_1}^{y_2} (R + E) dy \quad (C9)$$

The one-dimensional transport equation obtained by substitution from equations (C2) to (C6) into equation (C1) is:

$$\frac{\partial A_c \bar{u}}{\partial t} + \frac{\partial A_c \bar{u}^2}{\partial x} + gA_c \frac{\partial \bar{h}}{\partial x} + \int_{y_1}^{y_2} (\tau_{zx})_Z dy = R_c \quad (C10)$$

where

$$\begin{aligned} R_c = & \frac{\partial}{\partial x} \int_{y_1}^{y_2} \bar{D}(u'')^2 + 2\bar{u}D''u'' + D''(u'')^2 dy \\ & - \int_{y_1}^{y_2} D'' \frac{\partial h''}{\partial x} dy + \frac{1}{\bar{\rho}} \left[b(\tau_{zx})_h - A_c \frac{\partial \bar{\rho} \bar{h}}{\partial x} \right] \\ & \int_{y_1}^{y_2} [S_{xt} - S_{xx} - S_{x0} - S_{xv}] dy - \bar{D}h''(y_1) \frac{\partial y_1}{\partial x} - h''(y_2) \frac{\partial y_2}{\partial x} \quad (C11) \end{aligned}$$

The remainder term, R_c , contains all terms which appear when the one-dimensional equations are derived, without approximation, from the three-dimensional equations, but which are generally neglected in the one-dimensional momentum equation.

At times it is more convenient to work with the equations for the mean flow rather than the equations for total transport. The differential

equation for the mean flow in a channel may be obtained from equation (C10) by differentiation of the product terms to obtain:

$$A_c \frac{\partial \bar{u}}{\partial t} + A_c \bar{u} \frac{\partial \bar{u}}{\partial x} + g A_c \frac{\partial \bar{h}}{\partial x} + \int_{y_1}^{y_2} (\tau_{zx}) Z dy + \bar{u} \left[\frac{\partial A_c}{\partial t} + \frac{\partial}{\partial x} A_c \bar{u} \right] = R_c . \quad (C12)$$

The bracketed term in the above equation is identical with the left side of equation (C9). Thus, this term may be eliminated by subtracting \bar{u} times equation (C9) from equation (C12). Further division by A_c yields:

$$\frac{\partial \bar{u}}{\partial t} + \frac{1}{2} \frac{\partial}{\partial x} \bar{u}^2 + g \frac{\partial \bar{h}}{\partial x} + \frac{1}{A_c} \int_{y_1}^{y_2} (\tau_{zx}) Z dy = \frac{1}{A_c} \left[R_c - \bar{u} \int_{y_1}^{y_2} (R + E) dy \right]. \quad (C13)$$

The continuity equation in the proper form for computing the mean flow may be obtained by expressing A_c as $A_c = \bar{D}b$ in equation (C9), differentiating product terms and dividing each term by b , the width of the channel, to obtain:

$$\frac{\partial \bar{D}}{\partial t} + \frac{\partial \bar{D} \bar{u}}{\partial x} = b^{-1} \int_{y_1}^{y_2} (R + E) dy - \frac{\bar{D}}{b} \left[\frac{\partial b}{\partial t} + \bar{u} \frac{\partial b}{\partial x} \right]. \quad (C14)$$

In most applications, $\partial Z / \partial t = 0$, and the terms on the right are neglected. If also $\bar{h} \ll Z$, the equation may be linearized to obtain the more familiar form:

$$\frac{\partial \bar{h}}{\partial t} + \frac{\partial \bar{D} \bar{u}}{\partial x} = 0 , \quad (C15)$$

where \bar{D} in the case is the difference between Z and the mean water level.

In accordance with letter from DAEN-RDC, DAEN-ASI dated 22 July 1977, Subject: Facsimile Catalog Cards for Laboratory Technical Publications, a facsimile catalog card in Library of Congress MARC format is reproduced below.

Harris, D Lee

Comparison of numerical and physical hydraulic models, Masonboro Inlet, North Carolina / by D. Lee Harris and B. R. Bodine. Vicksburg, Miss. : U. S. Waterways Experiment Station ; Springfield, Va. : available from National Technical Information Service, 1977.

195 p. : ill. ; 27 cm. (GITI report - U. S. Army. Corps of Engineers ; 6)

General investigation of tidal inlets; a program of research conducted jointly by U. S. Army Coastal Engineering Research Center, Fort Belvoir, Virginia, and U. S. Army Engineer Waterways Experiment Station, Vicksburg, Mississippi.

Appendices 1-4 published separately.

Literature cited: p. 147-152.

1. Hydraulic models. 2. Masonboro Inlet, N. C. 3. Mathematical models. 4. Tidal inlets. I. Bodine, B. R., joint author. II. United States. Coastal Engineering Research Center. III. United States. Waterways Experiment Station, Vicksburg, Miss. IV. Series: United States. Army. Corps of Engineers. GITI report ; 6.

GB454.T5.U5 no.6